January 2009

Making Metal and Semiconductor Contacts on Alkanethiolate Self-assembled Monolayer Adsorbed on Au

Peng Lu
Washington University in St. Louis

WASHINGTON UNIVERSITY

Department of Chemistry

Dissertation Examination Committee
Amy V. Walker, Chair
Michael L. Gross, co-chair
Joseph J. H. Ackerman
William E. Buhro
Daniel Giammar
Cynthia S. Lo

MAKING METAL AND SEMICONDUCTOR CONTACTS ON ALKANETHIOLATE SELF-ASSEMBLED MONOLAYERS ADSORBED ON AU

by

Peng Lu

A dissertation presented to the
Graduate School of Arts and Sciences
of Washington University in
partial fulfillment of the
requirements of the degree
of Doctor of Philosophy

December 2009

St. Louis, Missouri

ABSTRACT OF THE DISSERTATION

Making Metal and Semiconductor Contacts on Alkanethiolate Self-assembled Monolayer Adsorbed on Au

by

Peng Lu

Doctor of Philosophy in Chemistry

Washington University in St. Louis, 2009

Professor Amy V. Walker, Chairperson

Understanding and controlling the interactions of metals and semiconductors with organic substrates is critical to many technological applications. The primary goal of the research described in this dissertation is to understand the metal/organic and semiconductor/organic interactions and to develop methods to fabricate stable and robust metallic and semiconducting contacts on organic thin layers.

Alkanethiolate self-assembled monolayers (SAMs) adsorbed on Au, which have highly organized structures with a uniform density of terminal organic functional groups, were employed as model organic systems. Chemical vapor deposition (CVD) was employed to deposit selectively aluminum and alumina on functionalized SAMs. Methods were also developed to make stable Cu overlayers on SAMs *via* electroless deposition (EL). Finally, chemical bath deposition (CBD) was employed to deposit ZnS and CdSe on functionalized SAMs. The resulting deposit structures and reaction

mechanisms involved were studied using time-of-flight secondary ion mass spectrometry (TOF SIMS), scanning electron microscope (SEM) and X-ray photoelectron spectroscopy (XPS).

ACKNOWLEDGEMENTS

I would like to extend my sincere gratitude to my advisor, Prof. Amy V. Walker for her guidance and encouragement throughout my graduate study. She is a great mentor for my research and personal development. Her intelligence, dedication to research and care for her students will always be my inspiration.

I am grateful to my dissertation committee members, Prof. Michael L. Gross, Prof. William E. Buhro, Prof. Joseph J. H. Ackerman, Prof. Cynthia S. Lo and Prof. Daniel Giammar, for their time and valuable comments on this dissertation.

I also would like to acknowledge and thank the following persons who have made the completion of this dissertation possible:

My group members and fellow graduate students, Chuanzhen Zhou, Jennifer Fitzgerald, Zhiwei Shi, Gabriella Nagy, Zicheng Li, Guorong Sun and Jun Ma, for their friendship and help for my research and dissertation.

Ed Hiss, Andre d'Avignon and many others in the departments.

Jian Li, Xiao Huang, Mike Deutsch, Junqiu Yang, Fangyun Chou and Ying Zhang for all the good times we had together.

The Shatoff family, for treating me like a family member and making my stay in St. Louis like home.

Finally, my parents and my girlfriend Li, for their everlasting support, encouragement and love. They are always my source of courage and happiness.

Table of Contents

List of Tables

List of Schemes

List of Figures

Abbreviations

SIMS:	secondary ion mass spectrometry
TOF SIMS:	time-of-flight secondary ion mass spectrometry
SEM:	scanning electron microscope
XPS:	x-ray photoelectron spectroscopy
LMIG:	liquid metal ion gun
LMIS:	liquid metal ion source
SAMs:	self-assembled monolayers
PVD:	physical vapor deposition
CVD:	chemical vapor deposition
EL:	electroless deposition
CBD:	chemical bath deposition
MHA:	16-mercaptohexadecanoic acid
MHL:	16-mercaptohexadecanol
HDT:	hexadecanethiol
TMA:	trimethyl aluminum
EDTA:	ethylene-1-diamine tetraacetic acid
NTA:	nitrilotriacetic acid trisodium salt

Chapter 1

Introduction

1.1 Metal and Semiconductor Constructs on Organic Thin Films

Understanding and controlling the interaction of metals and semiconductors with organic substrates is critical to many technologies. Metallized polymers have many potential applications, including those in microelectronics,[1-3] polymer light emitting diodes (PLED)[4-6] and packaging.[7] Semiconductor constructs on organic thin layers are also employed in applications ranging from electroluminescence devices[8-12] to photodetectors.[13, 14] However, several issues must be addressed before these devices can be used in everyday applications.

In PLEDs, a metal (typically Al or Cu) layer is deposited on a conjugated polymer, forming the cathode.[4, 5] However, the metal often poorly adheres to the polymer, leading to unstable devices and short device lifetimes.[3, 15, 16] Previous studies have also observed that deposited Al[3, 16] and Ca[3, 15] diffuse through the polymer, forming an interfacial region. This also leads to unpredictable device performance.

Metallized organic monolayers are also promising building blocks for molecular electronic devices.[17-23] A wide range of devices have been demonstrated, including molecular rectifiers,[23, 24] diodes,[25] and transistors.[26] However, small changes in the metal/organic structure cause huge variations in their performance or even device failure.[27-30] Carpenter *et al.*[31] fabricated Au/octacanethiol/p^+-GaAs devices and measured

their electrical properties. They observed that 4 fold increase in the amount of Au penetration through the octadecanethiol monolayer led to ~200× decrease in the conductance of the device.

Similarly, for hybrid solar cells, the interaction between the semiconductor and organic layer greatly influences the charge transfer process in these devices and ultimately impacts the device performance.[17, 32-34] Huynh *et al*. [32-34] showed that high efficiency solar cells can be obtained by constructing CdSe or CdS nanocrystals on polymer films. A photovoltaic device consisting of CdSe nanorods and poly-3(hexylthiophene) achieved an external quantum efficiency of over 54%.[33] In contrast, photovoltaic devices assembled from CdSe and MEH-PPV poly(2-methoxy-5-(2'-ethyl-hexyloxy)-p-phenyl-enevinylene) only had an external quantum efficiency of 5%.[32]

However, it is very difficult to study the metal/organic and semiconductor/organic interactions on polymers, because polymer surfaces are not easy to control and modify systematically. To overcome this, self-assembled monolayers (SAMs) have been employed in these studies. SAMs have highly organized structures with a uniform density of terminal organic functional groups.[35, 36]

Many methods have been employed to deposit metal and semiconductor on organic thin layers, including physical vapor deposition (PVD),[37-39] chemical vapor deposition (CVD),[40-44] atomic layer deposition (ALD),[45-47] successive ionic layer adsorption and reaction (SILAR),[48, 49] chemical bath deposition (CBD)[50-52] and

electroless deposition.[53, 54] There are several experimental criteria required to form stable, robust metallic and semiconducting contacts on organic layers. First, the method must be compatible with the organic substrate, and so low deposition temperatures are required (≤ 50 °C).[35] Second, there should be no metal or semiconductor penetration through the substrate. Third, the deposit must be stable over time. Fourth, the deposition method should be chemically selective. In this thesis, the use of CVD, electroless deposition and CBD were investigated to deposit metals and semiconductors on SAMs.

1.2 Self-Assembled Monolayers on Au

Self-assembled monolayers (SAMs) are highly ordered two-dimensional molecular arrays that form spontaneously on a substrate by chemisorption of functionalized molecules.[35, 36] Many molecules can form SAMs, including alkanethiols, fatty acids, diphosphates, *etc*.[36] SAMs formed by alkanethiols adsorbed on Au have been thoroughly studied[55-58] and are employed in our studies.

An alkanethiol molecule consists of a thiol head group, a backbone of methylene groups, and a tail (terminal) group. To prepare alkanethiolate SAMs, a gold substrate is immersed into a 1 mM ethanolic solution of the corresponding alkanethiol at ambient temperature (21 ± 2 °C) for 24 h.[55, 58, 59] Figure 1.1 shows a schematic diagram for the formation of alkanethiolate SAMs on Au. After the immersion of the Au substrate, the thiol head groups rapidly adsorb on the substrate.[55] The alkane chains then undergo rearrangement over a longer time period to maximize the lateral interactions between the

chains to form a well-ordered SAM. In well-ordered SAMs, the alkanethiol chain are tilted approximately 30 degree from the surface normal.[60, 61] The surface properties of SAMs can be modified by varying the terminal groups (tail). For example, methyl terminated SAMs are hydrophobic, while hydroxyl terminated SAMs are hydrophilic.

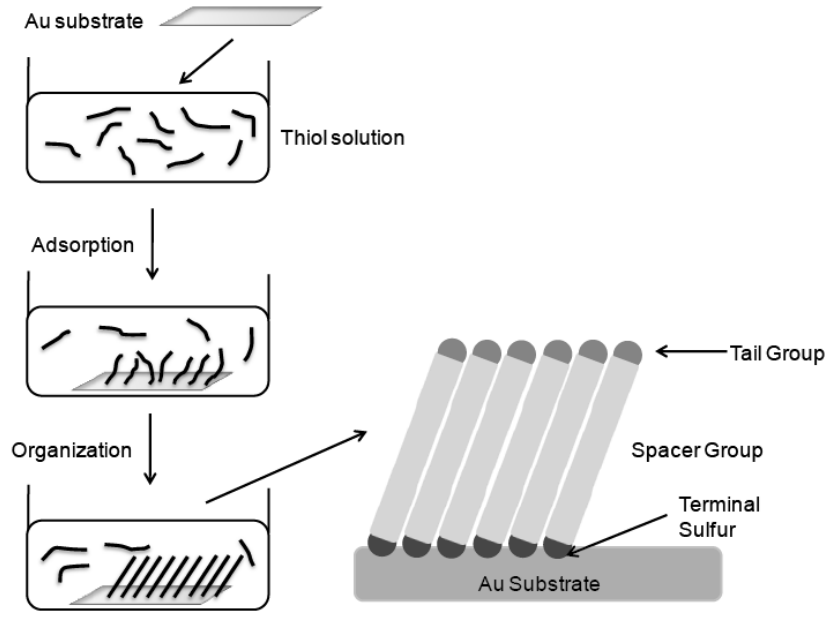

Figure 1.1 A Schematic diagram of the formation of an alkanethiolate SAM on Au surface.[62]

The structures and properties of alkanethiol SAMs adsorbed on Au have been studied using a number of techniques, including secondary ion mass spectrometry (SIMS),[63-66] infrared spectroscopy,[59, 67] ellipsometry[55, 67] and contact angle measurement.[55, 58, 59] Static SIMS can acquire detailed molecular information of SAMs. In the negative SIMS spectra, a rich variety of molecular secondary ions including

$(M\text{-}H)^-$, AuM^-, $AuSM^-$, $Au_2(M\text{-}H)^-$ and $Au(M\text{-}H)_2^-$ where M is the alkanethiol molecule have been observed.[65] Reflection adsorption infrared spectroscopy (RAIRS) is a convenient method to examine the order of a SAM structure. The asymmetric C-H stretching vibration of the alkyl chain is sensitive to the SAM packing density and the presence of gauche defects.[58] The C-H stretching vibration at 2918 cm^{-1} indicates a SAM with well-ordered structure, and the vibration at 2920 cm^{-1} is indicative of a less ordered SAM.[58, 68] Quantitative RAIRS measurements also indicate that well-ordered alkanethiolate SAMs have a tilt of 28^o.[68] Ellipsometry measures the thickness of SAMs adsorbed on Au substrate. By comparing the alkanethiol molecule length and SAM thickness, the ellipsometry studies confirm that the SAM molecules on Au tilt 30^o from the surface normal.[55] Contact angle measurements provide the surface roughness and wetting properties of the SAMs.[55, 58]

1.3 Techniques for Metal and Semiconductor Deposition on SAMs

1.3.1 Physical Vapor Deposition

In physical vapor deposition (PVD) a thin film is deposited on a substrate *via* the condensation of a vaporized material.[69] The material to be deposited (either a solid or a liquid) is vaporized by a number of methods, including thermal heating or sputtering. It is then transported under vacuum as a vapor to the substrate where the vapor recondenses to form the deposited film.[69, 70] PVD can be employed to deposit metals,[71] inorganic compounds[72] and organic thin films.[73]

To date, PVD has been extensively employed to deposit metals on polymers and SAMs.[37-39, 74-83] On SAMs, a wide range of behaviors have been observed: from metal-organic complex formation[39, 78] to metal penetration through the films[81, 84] and destruction of the monolayer caused by metal atoms.[39, 85] Table 1.1 summaries the results of previous studies of metal vapor deposition on -COOH,[38, 39, 75, 86-90] $-CO_2CH_3$,[38, 39, 77, 84, 87, 88, 91] -OH,[38, 39, 78, 86, 90, 92] $-OCH_3$[38, 39, 78, 80-82, 86] and $-CH_3$[38, 39, 84, 87-91, 93] terminated SAMs.

However, PVD is not the most suitable method to fabricate metal on organic thin layers because the outcome of the deposition reaction can not be precisely predicted.[39] For example, one may predict that Al will form Al-O bonds on $-OCH_3$ terminated SAMs from organometallic chemistry. However, experimentally vapor-deposited Al is observed to complex weakly with $-OCH_3$ terminal groups.[39, 78]

.

	-COOH	$-CO_2CH_3$	-OH	$-OCH_3$	$-CH_3$
Ca	React with SAMs and cause destruction of monolayer[39,82]				
Ti	React with SAMs and Cause Destruction of Monolayer[82,85,86,87]				
Mg	Insert into C-O bonds Penetration[39]	Insert into C-O bonds Penetration[39]	Insert into C-O bonds[39]	Insert into C-O bonds[39,80]	Penetration through monolayer[39]
Al	Insert into C-O bonds[39,76]	Insert into C-O bonds[39,77,84]	Insert into C-O bonds[39,78]	Weak Complex Penetration[39,78]	Penetration through monolayer[39,84]
Cu	Insert into C-O bonds Weak complex Penetration[39,40,75,90]	Insert into C-O bonds Weak complex Penetration[39,89,91]	Insert into C-O bonds Weak complex Penetration[90,92]	Weak complex Penetration[83]	Penetration through monolayer[90,91]
Au	Penetration through monolayer[81,88,93]				

Table 1.1 A summary of metal deposition behaviors on -COOH, $-CO_2CH_3$, -OH, $-OCH_3$ and $-CH_3$ terminated SAMs.

1.3.2 Chemical Vapor Deposition

Chemical vapor deposition (CVD) has been widely employed to deposit metals, oxides and compound thin films in the semiconductor industry and the metallurgical coating industry.[94-98] In a CVD, a substrate is exposed to one or more volatile precursors, typically organometallic compounds. The precursor then either decomposes on the substrate owing to pyrolysis, or chemically reacts with the substrate to produce the desired deposit.[95, 96, 99] CVD is more attractive than PVD to grow thin films on organic substrates because the reactions are potentially chemically selective. However, CVD usually requires high reaction temperatures ($T \geq 200$ °C),[95, 98] which are incompatible with most organic thin films.

1.3.3 Electroless Deposition

Electroless deposition is widely employed in metal coating and interconnects fabrication in microelectronics and metal coating.[100, 101] A variety of metals and alloys, including Ni, Zn, Cu, Au, Ag and Pt, can be deposited using this method.[101] In electroless deposition, metal deposition occurs via the chemically promoted reduction of metal ions without an externally applied potential.[100, 102] Electroless deposition is also a promising candidate to make metal contacts on organic thin layers. It can be performed at low temperature ($\leq$ 50 °C) and thus has the potential to make stable metal overlayers without damaging the organic substrate.[37, 53] Finally, as a solution-based technique, electroless deposition is convenient, inexpensive, and can be readily adapted to large area processing.

1.3.4 Chemical Bath Deposition

Chemical bath deposition (CBD) is a solution-based method that employs a controlled ion exchange reaction to deposit thin films on a substrate.[103] The basic reactions involved are conceptually simple: cations and anions are slowly released in the bath, and they react to form precipitates that deposit on the substrate.[104] CBD is a particularly interesting method to deposit compound semiconductor on organic thin layers, because it can be performed at low temperature and can be selective.[105, 106]

1.4 Research Objectives

In this thesis, methods to fabricate stable metal and semiconductor (aluminum, alumina, copper, ZnS and CdSe) thin films on functionalized SAMs were developed and the reaction pathways involved investigated in detail. Selective growth of metal and semiconductor films on functionalized SAMs was also demonstrated.

The organization of the thesis is as follows. Chapter 2 gives an introduction to TOF SIMS, including its applications, working principles and the instrument used in our studies.

Chapter 3 presents a description of the chamber employed in trimethyl aluminum (TMA) chemical vapor deposition (CVD). The chamber was built to perform UV activated CVD during these studies..

Chapter 4 describes the investigation of room temperature CVD of aluminum and alumina on functionalized SAMs. Using trimethyl aluminum (TMA) as a precursor,

aluminum and alumina can be deposited on functionalized SAMs. TMA reacted with -OH and -COOH terminal groups to form dimethyl aluminum complexes. No reaction was observed with $-CH_3$ terminated SAMs. In a nitrogen-purged glove box, alumina was deposited on -OH, -COOH and $-CH_3$ terminated SAMs. The deposited alumina was strongly bound to -OH and -COOH terminated SAMs, but did not adhere to $-CH_3$ terminated SAMs and so could be removed by rinsing with organic solvents. In a high vacuum deposition chamber (base pressure $\leq 2 \times 10^{-8}$ Torr), metallic aluminum was deposited on -OH and -COOH terminated SAMs. UV light activated CVD was also demonstrated, which led to an increase in the deposition rate of Al on -OH and -COOH terminated SAMs. Selective deposition of aluminum and alumina on the -COOH regions of a patterned -COOH/$-CH_3$ SAM was also demonstrated.

The mechanism of copper electroless deposition on functionalized SAMs is discussed in Chapter 5. Copper was observed to deposit on -COOH and $-CH_3$ terminated SAMs. On -COOH terminated SAMs, Cu^{2+}-carboxylate complexes formed, and they provided the nucleation sites for Cu film formation. On $-CH_3$ terminated SAMs, no surface complex was formed. When the reaction temperature was raised from 22 °C to 45 °C, copper deposition was observed to continue on -COOH terminated SAMs as the deposited film was stabilized by the surface Cu^{2+}-carboxylate complex. On $-CH_3$ terminated SAMs, no copper deposition was observed at 45 °C. However, the deposited copper overlayer was not stable on both -COOH and $-CH_3$ terminated SAMs, and penetrated through the monolayer for at least 48 h after deposition ceased. Copper did not

deposit on -OH terminated SAMs, because the hydroxyl terminal groups reacted with formaldehyde to form acetals, which prevented Cu^{2+} ions adsorption to -OH terminated SAMs.

In Chapter 6, a new copper electroless method was developed to selectively deposit stable copper overlayers on SAMs without copper penetration. A "seeding" step was introduced, and this step greatly increased the copper deposition rate on -COOH terminated SAMs. However, copper penetration was still observed. To prevent copper penetration, an organic additive, adenine, was added to the bath. With electroless deposition, copper overlayers were selectively deposited in the -COOH terminated SAM regions of a patterned -COOH/-CH_3 SAM surface.

In Chapter 7, chemical bath deposition was employed to deposit ZnS on SAMs and the reaction pathways were investigated. On -COOH terminated SAMs, two types of ZnS nanocrystallites were observed to form via different pathways: larger crystallites formed *via* cluster-by-cluster deposition, and smaller nanoflowers formed *via* ion-by-ion growth. On -CH_3 and -OH terminated SAMs, ZnS deposited via the cluster-by-cluster mechanism and only larger crystallites were formed. When the deposition was performed on a patterned -COOH/-CH_3 SAM, ZnS nanoflowers were selectively deposited in the -COOH terminated SAM areas of the patterned SAM surface, forming "nanoflowerbeds".

Chapter 8 gives another example of the deposition of a semiconductor, CdSe, on SAMs using CBD. In this case, CdSe nanoparticles with narrow size distributions were observed. On -COOH terminated SAMs, CdSe CBD followed a mixed ion-by-ion and

cluster-by-cluster mechanism. On -OH and -CH_3 terminated SAMs, CdSe nanoparticles only formed *via* cluster-by-cluster deposition. Selective deposition of CdSe was also achieved on patterned -COOH/-CH_3 SAM.

Chapter 9 summarizes the conclusions to the work performed and also discusses possible future work to be performed.

1.5 References

1. Sacher, E., *Metallization of Polymers 2*. Kluwer Academic/Plenum Publishers: New York, 2002.

2. Sacher, E.; Pireaux, J.-J.; Kowalczyk, S. P., *Metallization of Polymers*. American Chemical Society: Washington, DC, 1990; Vol. 440.

3. Birgerson, J.; Fahlman, M.; Broms, P.; Salaneck, W. R., Conjugated Polymer Surfaces and Interfaces: A Mini-Review and Some New Results. *Synth. Met.* **1996,** 80, 125-130.

4. Friend, R.; Burroughes, J.; Shimoda, T., Polymer Diodes. *Phys. World* **1999,** June, 35-40.

5. Friend, R. H.; Gymer, R. W.; Holmes, A. B.; Burroughes, J. H.; Marks, R. N.; Taliani, C.; Bradley, D. D. C.; Dos Santos, D. A.; Bredas, J. L.; Logdlund, M.; Salaneck, W. R., Electroluminescence in Conjugated Polymers. *Nature* **1999,** 397, 121-128.

6. Halls, J. J. M.; Walsh, C. A.; Greenham, N. C.; Marseglia, E. A.; Friend, R. H.; Moratti, S. C.; Holmes, A. B., Electroluminescence in Conjugated Polymers. *Nature* **1995,**

397, 121-128.

7. Mittal, K. L., *Metallized Plastics: Fundamentals and Applications*. Marcel Dekker: New York, 1997.

8. Colvin, V. L.; Schlamp, M. C.; Alivisatos, A. P., Light-Emitting Diodes Made from Cadmium Selenide Nanocrystals and a Semiconducting Polymer. *Nature* **1994,** 370, 354-357.

9. Huang, J. M.; Yang, Y.; Yang, B.; Liu, S. Y.; Shen, J. C., Assembly and Applications of the Inorganic Nanocrystals in Polymer Networks. *Thin Solid Films* **1998,** 327-329, 536-540.

10. Lee, J.; Sundar, V. C.; Heine, J. R.; Bawendi, M. G.; Jensen, K. F., Full Color Emission from II-VI Semiconductor Quantum Dot-Polymer Composites. *Adv. Mater.* **2000,** 12, 1102-1105.

11. Que, W.; Zhou, Y.; Lam, Y. L.; Chan, Y. C.; Kam, C. H.; Liu, B. W.; Gan, L. M.; Chew, C. H.; Xu, G. Q.; Chua, S. J.; al., e., Photoluminescence and Electroluminescence from Copper Doped Zinc Sulphide Nanocrystals/Polymer Composite. *Appl. Phys. Lett.* **1998,** 73, 2727-2729.

12. Schlamp, M. C.; Peng, X.; Alivisatos, A. P., Improved Efficiencies in Light Emitting Diodes Made with CdSe(CdS) Core/Shell Type Nanocrystals and a Semiconducting Polymer. *J. Appl. Phys.* **1997,** 82, 5837-5842.

13. Amos, F. F.; Morin, S. A.; Streifer, J. A.; Hamers, R. J.; Jin, S., Photodetector Arrays Directly Assembled onto Polymer Substrates from Aqueous Solution. *J. AM. CHEM.*

SOC. **2007,** 129, 14296-14302.

14. Ghosh, P. K.; Mitra, M. K.; Chattopadhyay, K. K., ZnS Nanobelts Grown in a Polymer Matrix by Chemical Bath Deposition. *Nanotechnology* **2005,** 16, 107-112.

15. Dannetun, P.; Fahlman, M.; Fauquet, C.; Kaerijama, K.; Sonoda, Y.; Lazzaroni, R.; Bredas, J. L.; Salaneck, W. R., Interface Formation Between Poly(2,5-diheptyl-p-phenylenevinylene) and Calcium - Implications for Light-Emitting Diodes. *Synth. Metal.* **1994,** 67, 133-136.

16. Logdlund, M.; Bredas, J. L., Theoretical Studies of the Interaction between Aluminum and Poly(p-phenylenevinylene) and Derivatives. *J. Chem. Phys.* **1994,** 101, 4357-4364.

17. Chen, J.; Reed, M. A., Electronic Transport of Molecular Systems. *Chem. Phys.* **2002,** 281, 127-145.

18. Chen, J.; Reed, M. A.; Rawlett, A. M.; Tour, J. M., Large On-Off Ratios and Negative Differential Resistance in a Molecular Electronic Device *Science* **1999,** 286, 1550-1552.

19. Reed, M. A., Molecular-Scale Electronics. *Proc. IEEE* **1999,** 87, 652-658.

20. Reinerth, W. A. J., L., II; Burgin, T. P.; Zhou, C.-w.; Muller,; C. J.; Deshpande, M. R. R., M. A.; Tour, J. M., Molecular Scale Electronics: Syntheses and Testing *Nanotechnology* **1998,** 9, 246-250.

21. Zhou, C.; Nagy, G.; Walker, A. V., Towards Molecular Electronic Circuitry: Selective Deposition of Metals on Patterned Self-Assembled Monolayer Surfaces. *J. Am. Chem.*

Soc. **2005,** 127, 12160-12161.

22. Aswal, D. K.; Lenfant, S.; Guerin, D.; Yakhmi, J. V.; Vuillaume, D., Self Assembled Monolayers on Silicon for Molecular Electronics. *Ana. Chem. Acta.* **2006,** 568, 84-108.

23. Metzger, R. M., Unimolecular Electrical Rectifiers. *Chem. Rev.* **2003,** 103, 3803-3834.

24. Isoda, S.; Miyamoto, M.; Inatomi, K.-i.; Ueyama, S., A Self-Assembled Molecular Rectifier: Two-Dimensional Crystals of Cytochrome c Formed on a Flavolipid Monolayer. *Thin Solid Films* **2004,** 468, 255-261.

25. Austin, M. D.; Chou, S. Y., Fabrication of a Molecular Self-Assembled Monolayer Diode Using Nanoimprint Lithography. *Nano. Lett.* **2003,** 3, 1687-1690.

26. Collet, J.; Vuillaume, D., Nano-Field Effect Transistor with an Organic Self-Assembled Monolayer as Gate Insulator. *Appl. Phys. Lett.* **1998**, 2681-2683.

27. Janes, D. B.; Lee, T.; Liu, J.; Batisuta, M.; Chen, N.-P.; Walsh, B. L.; Andres, R. P.; Chen, E.-H.; Melloch, M. R.; Woodall, J. M.; Reifenberger, R., Self-Assembled Metal/Molecule/Semiconductor Nanostructures for Electronic Device and Contact Applications *J. Electron. Mater.* **2000,** 29, 565-569.

28. Lodha, S.; Carpenter, P.; Janes, D. B., Effect of Contact Properties on Current Transport in Metal/Molecule/GaAs Devices *J. Appl. Phys.* **2006,** 99.

29. Hsu, J. W. P.; Loo, Y. L.; Lang, D. V.; Rogers, J. A., Nature of Electrical Contacts in a Metal-Molecule-Semiconductor System. *J. Vac. Sci. Technol. B* **2003,** 21, 1928-1935.

30. Stewart, D. R.; Ohlberg, D. A. A.; Beck, P. A.; Chen, Y.; Williams, R. S.; Jeppesen, J.

O.; Nielsen, K. A.; Stoddart, J. F., Molecule-Independent Electrical Switching in Pt/Organic Monolayer/Ti Devices. *Nano. Lett.* **2004,** 4, 133-136.

31. Carpenter, P. D.; Lodha, S.; Janes, D. B.; Walker, A. V., Characterization of Gold contacts in GaAs-based Molecular Devices: Relating Structure to Electrical Properties. *Chem. Phys. Lett.* **2009,** 472, 220-223.

32. Greenham, N. C.; Peng, X. G.; Alivisatos, A. P., Charge Separation and Transport in Conjugated-Polymer/Semiconductor-Nanocrystal Composites Studied by Photoluminescence Quenching and Photoconductivity. *Phys. ReV. B* **1996,** 54, 17628-17637.

33. Huynh, W. U.; Dittmer, J. J.; Alivisatos, A. P., Hybrid Nanorod-Polymer Solar Cells. *Science* **2002,** 295, 2425-2427.

34. Huynh, W. U.; Peng, X. G.; Alivisatos, A. P., CdSe Nanocrystal Rods/Poly(3-hexylthiophene) Composite Photovoltaic Devices. *Adv. Mater.* **1999,** 11, 923-927.

35. Schreiber, F., Structure and Growth of Self-Assembling Monolayers. *Prog. Surf. Sci.* **2000,** 65, 151-256.

36. Ulman, A., Formation and Structure of Self-Assembled Monolayers. *Chem. Rev.* **1996,** 96, 1533-1554.

37. Dake, L. S.; King, D. E.; Czanderna, A. W., Ion Scattering and X-Ray Photoelectron Spectroscopy of Copper Overlayers Vacuum Deposited onto Mercaptohexadecanoic Acid Self-Assembled Monolayers. *Solid State Sci.* **2002,** 2, 781-789.

38. Nagy, G.; Walker, A. V., Dynamics of the Interaction of Vapor-Deposited Copper with Alkanethiolate Monolayers: Bond Insertion, Complexation, and Penetration Pathways. *J. Phys. Chem. B* **2006,** 110, 12543-12554.

39. Nagy, G.; Walker, A. V., Dynamics of Reactive Metal Adsorption on Organic Thin Films. *J. Phys. Chem. C* **2007,** 111, 8543-8556.

40. Aliganga, A. K. A.; Wang, Z.; Mittler, S., Chemical Vapor Deposition of Mercury on Alkanedithiolate Self-Assembled Monolayers. *J. Phys. Chem. B* **2004,** 108, 10949-10954.

41. Jeon, N. L.; Nuzzo, R. G., Patterned Self-Assembled Monolayers Formed by Microcontact Printing Direct Selective Metalization by Chemical Vapor Deposition on Planar and Nonplanar Substrates. *Langmuir* **1995,** 11, 3024-3026.

42. Weiβ, J.; Himmel, H. J.; Fischer, R. A.; Woll, C., Self-Terminated CVD-Functionalization of Organic Self-Assembled Monolayers (SAMs) with Trimethylamine Alane (TMAA). *Chem. Vap. Deposition* **1998,** 4, (1), 17–21.

43. Wohlfart, P.; Weiss, J.; Kashammer, J.; Kreiter, M.; Winter, C.; Fischer, R. A.; Mittler-Neher, S., MOCVD of Aluminum Oxide/Hydroxide onto Organic Self-Assembled Monolayers. *Chem. Vap. Deposition* **1999,** 5, 165-170.

44. Wohlfart, P.; Weiss, J.; Kashammer, J.; Winter, C.; Scheumann, V.; Fischer, R. A.; Mittler-Neher, S., Selective Ultrathin Gold Deposition by Organometallic Chemical Vapor Deposition onto Organic Self-Assembled Monolayers (SAMs). *Thin Solid Films* **1999,** 340, 274-279.

45. George, S. M.; Ott, A. W.; Klaus, J. W., Surface Chemistry for Atomic Layer Growth.

J. Phys. Chem. **1996,** 100, 13121-13131.

46. Lim, B. S.; Rahtu, A.; Gordon, R. G., Atomic Layer Deposition of Transition Metals. *Nat. Mater.* **2003,** 2, 749-754.

47. Matero, R.; Rahtu, A.; Ritala, M.; Leskela, M.; Sajavaara, T., Effect of Water Dose on the Atomic Layer Deposition Rate of Oxide Thin Films. *Thin Solid Films* **2000,** 368, 1-7.

48. Kale, R. B.; Sartale, S. D.; Chougule, B. K.; Lokhande, C. D., Growth and Characterization of Nanocrystalline CdSe Thin Films Deposited by the Successive Ionic Layer Adsorption and Reaction Method. *Semicond. Sci. Technol.* **2004,** 19, 980-986.

49. Pathan, H. M.; Sankapal, B. R.; Desai, J. D.; Lokhande, C. D., Preparation and Characterization of Nanocrystalline CdSe Thin Films Deposited by SILAR Method. *Mater. Chem. Phys.* **2003,** 78, 11-14.

50. Flatha, J.; Meldrumb, F. C.; Knolla, W., Nucleation and Growth of Semiconductor Particles on Self-Assembled Monolayers by Chemical Solution Deposition. *Thin Solid Films* **1998,** 327-329, 506-509.

51. Meldrum, F. C.; Flath, J.; Knoll, W., Chemical Deposition of PbS on Self-Assembled Monolayers of 16-Mercaptohexadecanoic Acid. *Langmuir* **1997,** 13, 2033-2049.

52. Meldrum, F. C.; Flatha, J.; Knoll, W., Formation of Patterned PbS and ZnS Films on Self-Assembled Monolayers. *Thin Solid Films* **1999,** 348, 188-195.

53. Zangmeister, C. D.; van Zee, R. D., Electroless Deposition of Copper onto 4-Mercaptobenzoic Acid Self-Assembled on Gold. *Langmuir* **2003,** 19, 8065-8068.

54. Zhu, P.; Masuda, Y.; Koumoto, K., Seedless Micropatterning of Copper by Electroless Deposition on Self-Assembled Monolayers. *J. Mater. Chem* **2004,** 14, 976-981.

55. Bain, C. D.; Troughton, E. B.; Tao, Y.-T.; Evall, J.; Whitesides, G. M.; Nuzzo, R. G., Formation of Monolayer Films by the Spontaneous Assembly of Organic Thiols from Solution onto Gold. *J. Am. Chem. Soc.* **1989,** 111, 321-335.

56. Bensebaa, F.; Ellis, T. H.; Badia, A.; Lennox, R. B., Probing the Different Phases of Self-Assembled Monolayers on Metal Surfaces: Temperature Dependence of the C–H Stretching Modes *J. Vac. Sci. Technol., A* **1995,** 13, 1331-1336.

57. Delamarche, E.; Michel, B.; Kang, H.; Gerber, C., Thermal Stability of Self-Assembled Monolayers. *Langmuir* **1994,** 10, 4103–4108.

58. Nuzzo, R. G.; Dubios, L. H.; L., A. D., Fundamental Studies of Microscopic Wetting on Organic Surfaces. 1. Formation and Structural Characterization of a Self-Consistent Series of Polyfunctional Organic Monolayers. *J. Am. Chem. Soc.* **1990,** 112, 558-569.

59. Dubios, L. H.; Zegarski, B. R.; Nuzzo, R. G., Fundamental Studies of Microscopic Wetting on Organic Surfaces. 2. Interaction of Secondary Adsorbates with Chemically Textured Organic Monolayers. *J. Am. Chem. Soc.* **1990,** 112, 570-579.

60. Dubois, L. H.; Nuzzo, R. G., Synthesis, Structure, and Properties of Model Organic Surfaces. *Ann. Rev. Phys. Chem.* **1992,** 43, 437-463.

61. Bain, C. D.; Whitesides, G. M., Formation of Monolayers by the Coadsorption of Thiols on Gold: Variation in The Length of the Alkyl Chain. *J. Am. Chem. Soc.* **1989,** 111,

7164-7175.

62. http://www.ifm.liu.se/applphys/ftir/sams.html, accessed Oct 7th, 2009.

63. Offord, D. A.; John, C. M.; Linford, M. R.; Griffin, J. H., Contact Angle Goniometry, Ellipsometry, and Time-of-Flight Secondary Ion Mass Spectrometry of Gold Supported, Mixed Self-Assembled Monolayers Formed from Alkyl Mercaptans. *Langmuir* **1994,** 10, 883-889.

64. Pan, S.; Belu, A. M.; Ratner, B. D., Self Assembly of 16-Mercapto-1-Hexadecanol on Gold: Surface Characterization and Kinetics. *Mater. Sci. Eng. C* **1999,** 7, 51-58.

65. Tarlov, M. J.; Newman, J. G., Static Secondary Ion Mass Spectrometry of Self-Assembled Alkanethiol Monolayers on Gold. *Langmuir* **1992,** 8, 1398-1405.

66. Wolf, K. V.; Cole, D. A.; Bernasek, S. L., High-Resolution TOF-SIMS Study of Varying Chain Length Self-Assembled Monolayer Surfaces. *Anal. Chem.* **2002,** 74, 5009-5016.

67. Porter, M. D.; Bright, T. B.; Allara, D. L.; Chidsey, C. E. D., Spontaneously Organized Molecular Assemblies. 4. Structural Characterization of n-Alkyl Thiol Monolayers on Gold by Optical Ellipsometry, Infrared Spectroscopy, and Electrochemistry. *J. Am. Chem. Soc.* **1987,** 109, 3559-3568.

68. Laibinis, P. E.; Whitesides, G. M.; Allara, D. L.; Tao, Y. T.; Parikh, A. N.; Nuzzo, R. G., Comparsion of the Structures and Wetting Properties of Self-Assembled Monolayers of n-Alkanethiols on the Coinage Metal-Surfaces, Copper, Silver and Gold. *J. Am. Chem. Soc.* **1991,** 113, 7152-7167.

69. Reichelt, K.; Jiang, X., The Preparation of Thin Films by Physical Vapor Deposition. *Thin Solid Films* **1990,** 191, 91-126.

70. Mattox, D. M., *Handbook of Physical Vapor Deposition (PVD) Processing*. William Andrew Publishing: Noyes, 1998.

71. Rauf, S.; Ventzek, P. L. G.; Arunachalam, V., Ionized Physical Vapor Deposition of Cu on 300 mm Wafers: A Modeling Study. *J. Appl. Phys.* **2001,** 89, 2525-2534.

72. Kong, Y. C.; Yu, D. P.; Zhang, B.; Fang, W.; Feng, S. Q., Ultraviolet-Emitting ZnO Nanowires Synthesized by a Physical Vapor Deposition Approach. *Appl. Phys. Lett.* **2001,** 78, 407-409.

73. Xiao, R. F.; Ho, W. C.; Chow, L. Y.; Fung, K. K.; Zheng, J. Q., Physical Vapor Deposition of Highly Oriented Fullerene C_{60} Films on Amorphous Substrates. *J. Appl. Phys.* **1995,** 77, (3572-3574).

74. Cooper, E.; Leggett, G. J., Influence of Tail-Group Hydrogen Bonding on the Stabilities of Self-Assembled Monolayers of Alkylthiols on Gold. *Langmuir* **1999,** 15, 1024-1032.

75. Czanderna, A. W.; King, D. E.; Spaulding, D., Metal Overlayers on Organic Functional Groups of Self-Organized Molecular Assemblies. 1. X-Ray Photoelectron Spectroscopy of Interactions of Cu/COOH on 11-Mercaptoundecanoic Acid *J. Vac. Sci. Technol., A* **1991,** 9, 2607-2613.

76. Fisher, G. L.; Hooper, A. E.; Opila, R. L.; Allara, D. L.; Winograd, N., The Interaction of Vapor-Deposited Al Atoms with CO_2H Groups at the Surface of a

Self-Assembled Alkanethiolate Monolayer on Gold. *J. Phys. Chem. B* **2000,** 104, 3267-3273.

77. Fisher, G. L.; Hooper, A. E.; Opila, R. L.; Jung, D. R.; Allara, D. L.; Winograd, N., The Interaction between Vapor-Deposited Al Atoms and Methylester-Terminated Self-Assembled Monolayers Studied by Time-of-Flight Secondary Ion Mass Spectrometry, X-Ray Photoelectron Spectroscopy and Infrared Reflectance Spectroscopy. *J. Electron Spectrosc. Relat. Phenom.* **1998,** 98-99, 139-148.

78. Fisher, G. L.; Walker, A. V.; Hooper, A. E.; Tighe, T. B.; Bahnck, K. B.; Skriba, H. T.; Reinard, M. D.; Haynie, B. C.; Opila, R. L.; Winograd, N.; Allara, D. L., Bond Insertion, Complexation, and Penetration Pathways of Vapor-Deposited Aluminum Atoms with HO- and CH_3O-Terminated Organic Monolayers. *J. Am. Chem. Soc.* **2002,** 124, 5528-5541.

79. Walker, A. V.; Fisher, G. L.; Hooper, A. E.; Tighe, T.; Opila, R. L.; Winograd, N.; Allara, D. L., Nucleation and Growth of Vapor-Deposited Metal Films on Self-Assembled Monolayers Studied by Multiple Characterization Probes. In *Metallization of Polymers 2*, Sacher, E., Ed. Kluwer Academic/Plenum: New York,, 2002; pp 117-126.

80. Walker, A. V.; Tighe, T. B.; Cabarcos, O.; Haynie, B. C.; Allara, D. L.; Winograd, N., Dynamics of Interaction of Magnesium Atoms on Methoxy-Terminated Self-Assembled Monolayers: An Example of a Reactive Metal with a Low Sticking Probability. *J. Phys. Chem. C* **2007,** 111, 765-772.

81. Walker, A. V.; Tighe, T. B.; Cabarcos, O. M.; Reinard, M. D.; Haynie, B. C.; Uppili, S.; Winograd, N.; Allara, D. L., The Dynamics of Noble Metal Atom Penetration through Methoxy-Terminated Alkanethiolate Monolayers. *J. Am. Chem. Soc.* **2004,** 126, 3954-3963.

82. Walker, A. V.; Tighe, T. B.; Haynie, B. C.; Uppili, S.; Allara, D. L.; Winograd, N., Chemical Pathways in the Interactions of Reactive Metal Atoms with Organic Surfaces: Vapor Deposition of Ca and Ti on a Methoxy-Terminated Alkanethiolate Monolayer on Au. *J. Phys. Chem. B* **2005,** 109, 11263-11272.

83. Walker, A. V.; Tighe, T. B.; Reinard, M. D.; Haynie, B. C.; Allara, D. L.; Winograd, N., Solvation of Zero-Valent Metals in Organic Thin Films. *Chemcal Physics Letters* **2003,** 369, 615-620.

84. Hooper, A. E.; Fisher, G. L.; Konstadinidis, K.; Jung, D. R.; Nguyen, H.; Opila, R. L.; Collins, R. W.; Winograd, N.; Allara, D. L., Chemical Effects of Methyl and Methyl Ester Groups on the Nucleation and Growth of Vapor-Deposited Aluminum Films. *J. Am. Chem. Soc.* **1999,** 121, (35), 8052−8064.

85. Tighe, T. B.; Daniel, T. A.; Zhu, Z.; Uppili, S.; Winograd, N.; Allara, D. L., Evolution of the Interface and Metal Film Morphology in the Vapor Deposition of Ti on Hexadecanethiolate Hydrocarbon Monolayers on Au. *J. Phys. Chem. B* **2005,** 109, 21006-21014.

86. Konstadinidis, K.; Zhang, P.; Opila, R. L.; Allara, D. L., An in-situ X-ray Photoelectron Study of the Interaction between Vapor-Deposited Ti Atoms and Functional

Groups at the Surfaces of Self-Assembled Monolayers. *Surf. Sci.* **1995,** 338, 300-312.

87. Zhu, Z.; Allara, D. L.; Winograd, N., Chemistry of Metal Atoms Reacting with Alkanethiol Self-assembled Monolayers. *Appl. Surf. Sci.* **2006,** 252, 6686-6688.

88. Zhu, Z.; Daniel, T. A.; Maitani, M.; Cabarcos, O. M.; Allara, D. L.; Winograd, N., Controlling Gold Atom Penetration through Alkanethiolate Self-Assembled Monolayers on Au{111} by Adjusting Terminal Group Intermolecular Interactions. *J. Am. Chem. Soc.* **2006,** 128, 13710-13719.

89. Herdt, G. C.; Jung, D. R.; Czanderna, A. W., Weak Interactions between Deposited Metal Overlayers and Organic Functional Groups of Self-Assembled Monolayers. *Prog. Surf. Sci.* **1995,** 50, 103-129.

90. Herdt, G. C.; Jung, D. R.; Czanderna, A. W., Penetration of Deposited Ag and Cu Overlayers Through Alkanethiol Self-Assembled Monolayers on Gold. *J. Adhesion.* **1997,** 60, 197-22.

91. Herdt, G. C.; Czanderna, A. W., Metal Overlayers on Organic Functional Groups of Self-Organized Molecular Assemblies: VII. Ion Scattering Spectroscopy and X-Ray Photoelectron Spectroscopy of Cu/CH_3 and $Cu/COOCH_3$. *J. Vac. Sci. Technol., A* **1997,** 15, 513-519.

92. Jung, D. R.; King, D. E.; Czanderna, A. W., XPS of Organized Molecular Assembly/Copper Interfaces: $HS(CH_2)_{11}OH/Cu$. *Appl. Surf. Sci.* **1993,** 70/71, 127-132.

93. Ohgi, T.; Sheng, H. Y.; Dong, Z. C.; Nejoh, H., Observation of Au Deposited Self-Assembled Monolayers of Octanethiol by Scanning Tunneling Microscopy. *Surf. Sci.*

1999, 442, (277-282).

94. Dapkus, P. D., Metalorganic Chemical Vapor Deposition. *Ann. Rev. Mater. Sci.* **1982,** 12, 243-269.

95. Dobkin, D. M.; Zuraw, M. K., *Principles of Chemical Vapor Deposition*. Kluwer Academic Publishers: Dordrecht, The Netherlands, 2003.

96. Hampden-Smith, M. J.; Kodas, T. T., Chemical Vapor Deposition of Metals: Part 1. An Overview of CVD Processes. *Chem. Vap. Deposition.* **1995,** 1, 8-23.

97. Jaraith, R.; Jain, A.; Tolles, R. D.; Hampden-Smith, M. J.; T. T. Kodas, *The Chemistry of Metal CVD*. VCH, Weinheim: 1994.

98. Pierson, H. O., *Handbook of Chemical Vapor Deposition (CVD) - Principles, Technology and Applications*. 2 ed.; William Andrew Publishing: Noyes 1999.

99. Herman, I. P., Laser-Assisted Deposition of Thin Films from Gas-Phase and Surface-Adsorbed Molecules. *Chem. Rev.* **1989,** 89, 1323-1357.

100. Vaskelis, A. S., M., Electroless Plating. In *Plastics Finishing and Decorating*, Satas, D., Ed. Van Nostrand Reinhold Company: New York, 1986; pp 287-319.

101. Mallory, G. O.; Hajdu, J. B., *Electroless Plating - Fundamentals and Applications*. William Andrew Publishing: Noyes 1990.

102. Yanagimoto, H.; Deki, S.; Akamatsu, K.; Gotoh, K., Selective Electroless Copper Deposition on Aluminum Nitride Substrate with Patterned Copper Seed Layer *Thin Solid Films* **2005,** 491, 18-22.

103. O'Brien, P.; McAleese, J., Developing and Understanding of the Processes

Controlling the Chemical Bath Deposition of ZnS and CdS. *J. Mater. Chem.* **1998,** 8, (11), 2309-2314.

104. Hodes, G., Mechanisms of Chemical Deposition. In *Chemical Solution Deposition Of Semiconductor Films*, Marcel Dekker, Inc.: New York, 2002.

105. Flath, J.; Meldrum, F. C.; Knoll, W., Nucleation and Growth of Semiconductor Particles on Self-Assembled Monolayers by Chemical Solution Deposition. *Thin Solid Films* **1998,** 327-329, 506-509.

106. Meldrum, F. C.; Flath, J.; Knoll, W., Formation of Patterned PbS and ZnS Films on Self-Assembled Monolayers. *Thin Solid Films* **1999,** 348, 188-195.

Chapter 2

Time-of-Flight Secondary Ion Mass Spectrometry

2.1 Introduction

Time-of-flight secondary ion mass spectrometry (TOF SIMS) is a highly sensitive surface analysis technique.[1-3] It is widely used in the analysis of organic thin films,[4, 5] biomaterials[6] and polymers.[7, 8] TOF SIMS employs a pulsed primary ion beam to desorb and ionize species ("secondary" species) from a sample surface. The desorbed secondary ions are analyzed using a time-of-flight (TOF) mass analyzer. TOF SIMS has many advantages, including high surface sensitivity, high mass resolution, parallel mass detection, and imaging and depth profiling abilities.[9-11]

The history of secondary ion mass spectrometry (SIMS) goes back to the mid 19th century when sample sputtering by gaseous ions was first discovered. Herzog and Vieboeck[12] studied the fundamentals of SIMS and developed the first instrument to have an electron primary ion source in 1949. In the 1960s, Herzog, Liebl and coworkers[13] built the first commercial SIMS instruments for the analysis of extraterrestrial materials. In the 1970s, Benninghoven and co-workers[14-18] developed single ion counting techniques, which allowed for the development for static SIMS. Initially, magnetic sector and quadrupole mass analyzers were employed in SIMS, then TOF analyzers was developed for modern SIMS systems,[1, 19] however magnetic sectors instruments are still widely used. In recent years, the development of cluster primary ions beams has lead to the

development of high lateral resolution molecular 2D and 3D imaging.[20-23]

SIMS can be operated in two different modes: static and dynamic. For static SIMS, the primary ion dose is less than 10^{13} ions cm^{-2} (i.e. less than 1% of the number of surface atoms, 10^{15} ions cm^{-2}).[9] The low ion beam dose is important to maintain the sensitivity to the uppermost monolayers of the sample. The desorbed secondary species can be ions, neutrals or electrons. Static SIMS is normally used to obtain high mass resolution spectra, as well as SIMS images. In this case the sample surface is divided into a series of pixels, and a mass spectrum is obtained at every pixel by rastering the primary ion beam across the surface. Using a computer allows one to analyze the data, providing a mass spectrometric image. [23-25] Dynamic SIMS is used primarily for depth profiling and uses an ion dose > 10^{13} cm^{-2}. In dynamic SIMS, the analyzed surface is damaged and eroded away owing to sputtering. The generated secondary ions are analyzed as a function of depth (depth profiling).[26-28]

In a SIMS experiment, the primary ions collide with sample surface atoms and transfer their energy to the sample surface, leading to a collision cascade within the sample (Figure 2.1).[1, 9] This leads to the ejection of electrons, ions and neutrals from the surface.[9] These secondary species are characteristic of the atoms and molecules present in the surface region. The secondary ion current is given by:

$$I_m^{\pm} = I_p \times Y_m \times \eta^{\pm} \times \alpha^{\pm} \times \theta_m \quad (1)$$

where $I_m^{\pm}$ is the secondary ion intensity of a species m; I_p is the primary ion beam current (number of primary ions × charge per ion / time); Y_m is the sputtering yield (number of

secondary ions generated per primary ion); $\eta^{\pm}$ is the ion transmission efficiency for positive (+) or negative ions (-). $\alpha^{\pm}$ is the ionization probability of the sputtered species, and θ_m is coverage (surface concentration) of species m in the analyzed areas.[29]

Most of the ejected secondary species are neutrals (~ 95%). Secondary ions comprise ~ 5% of the sputtered species.[9] The secondary ions are then extracted to a time-of-flight mass spectrometer for analysis.

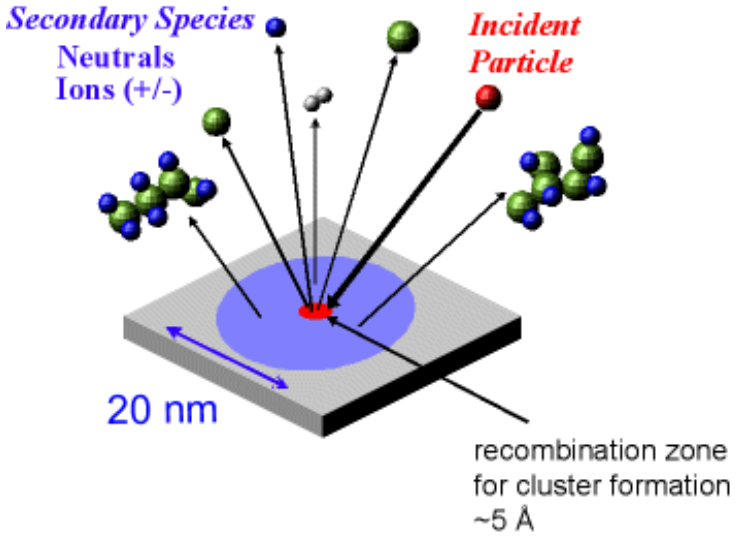

Figure 2.1 Primary ion sputtering and secondary species generation in TOF SIMS. The incident particles are ions, and are referred to as primary ions. Emitted secondary species are atomic and molecular fragments, which are characteristic of the surface chemistry.[30]

2.2 TOF SIMS Instrument

In these studies, an ION TOF IV spectrometer (ION TOF Inc., Chestnut Hill, NY) equipped with a Bi_n^{m+} (n = 1 - 6, m = 1, 2) liquid metal ion gun was employed. Typically, Bi^+ ions with kinetic energy of 25 keV were used as the primary ions contained within a ~100 nm diameter probe beam. The primary ion beam was rastered over the sample to obtain SIMS spectra and acquire MS images. The secondary ions were extracted into a time-of-flight mass spectrometer with a 2000 V potential and were reaccelerated to 10 keV before reaching the detector. The mass resolution (m/Δm) was typically 5000 at *m/z* 29. The instrument was also equipped with an electron flood gun for charge compensation.

2.2.1 Vacuum System

The ION TOF IV consisted of a load lock (airlock) for sample introduction, a preparation chamber and an analysis chamber, separated by gate valves. The vacuum system was computer controlled. Figure 2.2 shows a schematic diagram for the vacuum system. The airlock chamber was pumped with a turbomolecular pump (Pfeiffer, 240 l s^{-1}) and was maintained at < 10^{-6} mbar when transferring the sample. The preparation chamber and main chamber were pumped with turbomolecular pumps (Leybold, 460 l s^{-1}) and were kept at < 5×10^{-9} mbar. The turbo pumps were backed by a turbo drag pump (Pfeiffer, 60 l s^{-1}) and a diaphragm pump (Vacuubrandt, 1 l s^{-1}).

Vacuum gauges were used to monitor the chamber pressure. G-Airlock, G-Prep were all range gauges monitoring the airlock chamber and the preparation chamber

pressures, and G-Main was a cold cathode ion gauge for the main chamber. Venting valves were employed to vent to chambers. VV-Airlock, VV-Prep and VV-Main stand for the venting valves for these chambers, respectively. The buffer pressure was monitored by a pirani gauge.

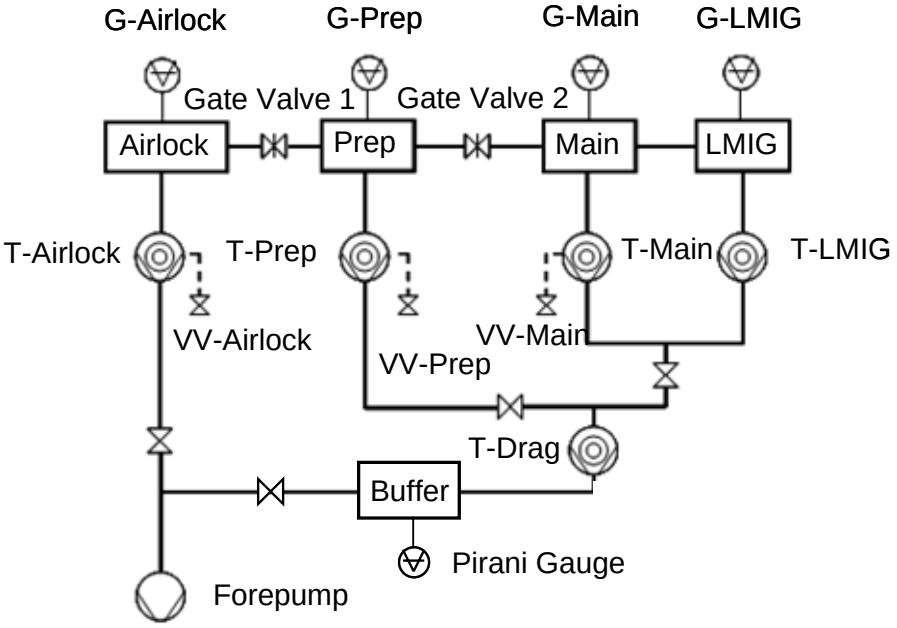

Figure 2.2 A Schematic Diagram of ION TOF IV vacuum system.[31]

2.2.2 Liquid Metal Ion Gun

A liquid metal ion gun (LMIG) was used to generate pulsed high energy ion beam and focus the beam to a small spot size for sample bombardment. The LMIG can be separated into five different units: liquid metal ion source (LMIS), blanker/chopper, buncher, mass selection unit and primary focusing unit.

The LMIS operates with metals (e.g. Ga) or metal alloys (e.g. Au), which were easily liquidized.[1, 9, 11] It consisted of an emitter, a suppressor, and an extractor. In the ion emitter, a tungsten tip with a small tip radius was wetted by a metal or alloy supplied from a reservoir. At the same time, a strong electric field was applied to the emitter through an extraction electrode in front of the tip. The electric field forced the liquid metal to the needle tip, and a cone shape (Taylor cone) was formed.[32] Field evaporation occurred in the Taylor cone owing to the extremely high electric field strength, and metal ions were emitted from a very small area with a radius in the nm range[33] (Figure 2.3). The emission current was controlled by the potential difference between the emitter and the extraction electrode, and can be fine-tuned by the suppressor that surrounded the emitter. Typically, emission currents from a Bi LMIS at 25 keV were ~ 1 μA.[33]

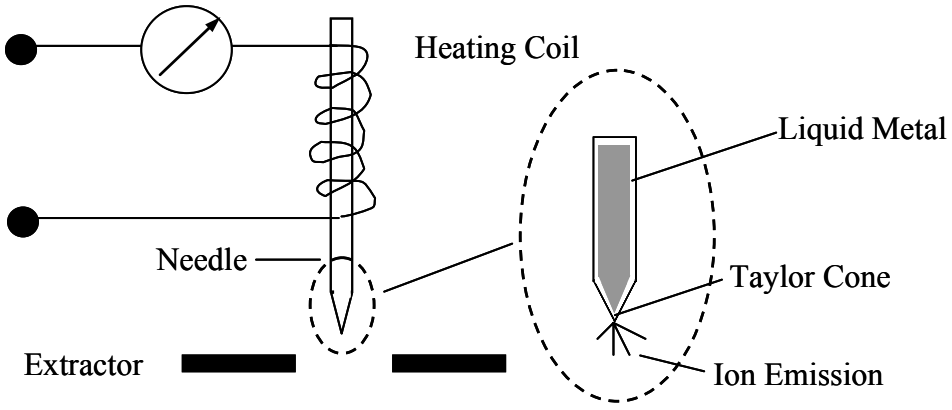

Figure 2.3 A schematic diagram of a liquid metal ion gun source.[9]

After leaving the emitter, the primary ion beam was focused by ion optics before reaching the sample surface. The focusing optics consisted of three lenses (Lens Source, Lens Magnification and Lens Target) and two apertures.

To be compatible with the TOF analyzer, the continuous primary ion beam generated from the LMIS must be pulsed. In the LMIS, a high performance beam blanker was employed for high speed motionless beam blanking. To select desired mass in a primary ion pulse, a mass selection unit was employed (Figure 2.4). When there was no voltage applied, primary ions were able to traverse through the aperture and thus were selected. After the voltage was turned on, primary ions were deflected by the electric field to the voltage plates and so could not arrive at the sample surface.

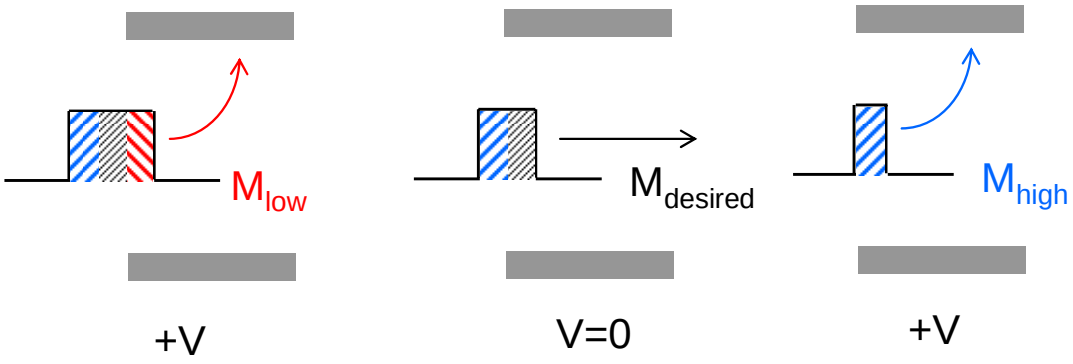

Figure 2.4 A Schematic diagram of the mass selection unit. When lighter primary ions ($M_{low} < M_{desired}$) arrived at the aperture, voltage was applied and ions were deflected to the voltage plates. Then the voltage decreased to 0 and primary ions with desired mass traversed through the aperture and were selected. Then the voltage was applied again to filter heavier primary ions ($M_{high} > M_{desired}$).

To obtain high mass resolution spectra, it is important that the primary ions in the pulse arrive at the sample surface simultaneously. To achieve this, bunching was employed. Bunching accelerated the ions within a pulse to different energies so that the primary ions arrived at the sample surface at the same time. However, after bunching the primary ion beam energy spread increased to several hundreds of electron volts, and this led to lower spatial resolutions and so bunching was not employed for imaging applications.

2.2.3 Electron Flood Gun

A low energy electron flood gun (~ 18 eV) was equipped in the ION TOF IV instrument for charge compensation. When analyzing electrically insulating samples, charge will quickly build up on the sample surface. These localized surface charges substantially decreased the secondary ion signals. The electron flood gun compensated for the surface charges by neutralizing the positive charge on the surface with electrons.

2.2.4 Time-of-Flight Analyzer

A time-of-flight analyzer was used to detect the secondary ions. When a primary ion pulse hit the sample, secondary ions were extracted to the analyzer and accelerated by an electric field to the detector. All ions left the sample surface at the same time because the ion pulse was very short (< 1 ns), and traveled the same distance to the detector. Under an electric field of known strength, each ion was accelerated to certain velocity that was determined by the mass-to-charge (*m/z*) ratio. Thus, the ions arrived at the detector at different times, and the ion travel times could be used to calculate the *m/z* ratios of the

emitted ions.

The TOF analyzer employed in our studies consisted of an Einzel lens to focus the ion beam onto the detector, a deflection unit to align the beam, a reflectron (ion mirror), a postacceleration unit and a detector.

When secondary ions were ejected from the sample, they had a kinetic energy spread about 10-15 eV. To compensate for this, a reflectron TOF geometry was employed (Figure 2.5).[33, 34] When the secondary ions penetrated into the reflectron electric field, they were reversed in direction towards a detector. If the acceleration/deceleration voltages were properly configured, the more energetic ions penetrated deeper into the retarding field, traveled a slightly longer distance, and arrived at the detector at the same time as the less energetic ions. In a reflectron TOF, the flight time is given by,

$$t = t_{drift1} + t_{drift2} + t_{accel/deccel} = \sqrt{m/2eV}(L_1 + L_2 + 4d) \qquad (2)$$

where t_{drift1} is the flight time through L_1, t_{drift2} is the flight time through L_2, $t_{accel/deccel}$ is the flight time in the reflectron electric field. Since the ions of the same *m/z* have the same flight time after going through the reflectron, the mass resolution is improved.

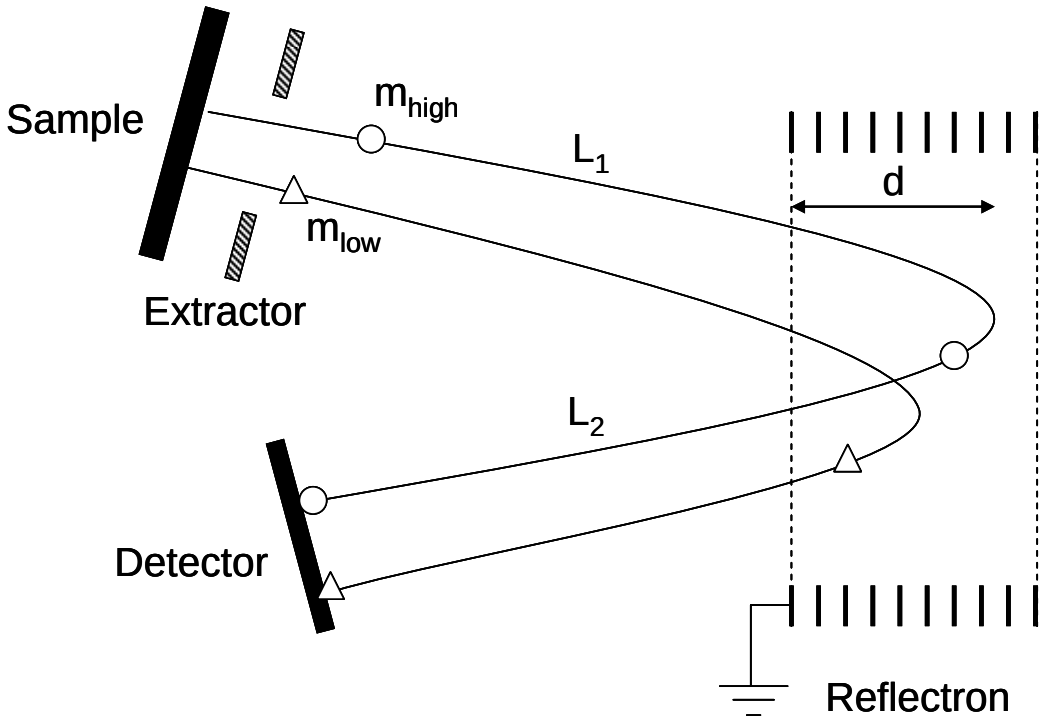

Figure 2.5 A Schematic diagram of a reflectron TOF. m_{high} and m_{low} are the same ions with different initial kinetic energies. m_{high} refers to faster ions with higher kinetic energy and m_{low} refers to slower ions with lower energy.

After leaving the reflectron, the secondary ions pass through the postacceleration optics and arrive at the secondary ion detector. The postacceleration voltage is 10 kV, which ensures that heavy ions can be more efficiently detected. The detector consists of a multichannel plate to convert ions to electrons, a scintillator to convert electrons to photons, and a photomultiplier to amplify the photon signal.

2.3 References

1. Benninghoven, A.; Rudenauer, F. G.; Werner, H. W., *Secondary Ion Mass Spectrometry: Basic Concepts, Instrumental Aspects, Applications and Trends*. John Wiley & Sons: New York, NY, 1987.

2. Vaeck, L. V.; Adriaens, A.; Gijbels, R., Static Secondary Ion Mass Spectrometry: (S-SIMS) Part 1. Methodology and Structural Interpretation. *Mass. Spec. Rev.* **1999,** 18, 1-47.

3. Vaeck, L. V.; Adriaens, A.; Gijbels, R., Static Secondary Ion Mass Spectrometry: (S-SIMS) Part 2. Material Science and Applications. *Mass. Spec. Rev.* **1999,** 18, 48-81.

4. Cooper, E.; Leggett, G. J., Static Secondary Ion Mass Spectrometry Studies of Self-Assembled Monolayers: Influence of Adsorbate Chain Length and Terminal Functional Group on Rates of Photooxidation of Alkanethiols on Gold. *Langmuir* **1998,** 14, 4795-4801.

5. Gillen, G.; Bennett, J.; Tarlov, M. J.; Burgess, D. R. F., Molecular Imaging Secondary Ion Mass Spectrometry for the Characterization of Patterned Self-Assembled Monolayers on Silver and Gold. *Anal. Chem.* **1994,** 66, 2170-2174.

6. Belu, A. M.; Graham, D. J.; Castner, D. G., Time-of-Flight Secondary Ion Mass Spectrometry: Techniques and Applications for the Characterization of Biomaterial Surfaces. *Biomaterials* **2003,** 24, 3635-3653.

7. Eynde, X. V.; Bertrand, P., ToF-SIMS Quantification of Polystyrene Spectra based on Principal Component Analysis (PCA). *Surf. Interface Anal.* **1997,** 25, 878-888.

8. Galuska, A. A., ToF-SIMS Determination of Molecular Weights from Polymeric Surfaces and Microscopic Phases. *Surf. Interface Anal.* **1997,** 25, 790-798.

9. Vickerman, J. C., *ToF SIMS: Surface Analysis by Mass Spectrometry*. IM Publications and Surface Spectra Limited: Chichester and Manchester, UK, 2001; p 1-40.

10. Winograd, N.; Postawa, Z.; Cheng, J.; Szakal, C.; Kozole, J.; Garrison, B. J., Improvements in SIMS continue: Is the end in sight? *Appl. Surf. Sci.* 252, 6836-6843.

11. Williams, P., Secondary Ion Mass Spectrometry. *Ann. Rev. Mater. Sci.* **1985,** 15, 517-548.

12. Herzog, R. F. K.; Viehbeock, F. P., Ion Source for Mass Spectrography. *Phys. Rev.* **1949,** 76, 855-856.

13. Liebl, H. J.; Herzog, R. F. K., Sputtering Ion Source for Solids. *J. Appl. Phys.* **1963,** 34, 2893-2896.

14. Benninghoven, A., The Analysis of Monomolecular Layers of Solids by Secondary Ion Emission. *Z. Phys.* **1970,** 230, 403-417.

15. Benninghoven, A., Surface Investigation of Solids by the Statistical Method of Secondary Ion Mass Spectrocopy (SIMS). *Surf. Sci.* **1973,** 35, 427-457.

16. Benninghoven, A., Developments in Secondary Ion Mass Spectroscopy and Applications to Surface Studies. *Surf. Sci.* **1975,** 53, 596-625.

17. Benninghoven, A., Chemical Analysis of Inorganic and Organic Surfaces and Thin Films by Static Time-of-Flight Secondary Ion Mass Spectrometry (TOF-SIMS). *Angew. Chem. Int. Ed.* **1994,** 33, 1023-1043.

18. Benninghoven, A.; Sichtermann, W. K., Detection, Identification, and Structural Investigation of Biologically Important Compounds by Secondary Ion Mass Spectrometry. *Anal. Chem.* **1978,** 50, 1180-1184.

19. Schueler, B., Microscopic Imaging by Time-of-Flight Secondary Ion Mass Spectrometry. *Microsc. Microanal. Microstruct.* **1992,** 3, 119-139.

20. Belu, A. M.; Davies, M. C.; Newton, J. M.; Patel, N., TOF-SIMS Characterization and Imaging of Controlled-Release Drug Delivery Systems. *Anal. Chem.* **2000,** 72, 5625-5638.

21. Colliver, T. L.; Brummel, C. L.; Pacholski, M. L.; Swanek, F. D.; Ewing, A. G.; Winograd, N., Atomic and Molecular Imaging at the Single-Cell Level with TOF-SIMS. *Anal. Chem.* **1997,** 69, 2225-2231.

22. Winograd, N., Prospects for Imaging TOF-SIMS: From Fundamentals to Biotechnology. *Appl. Surf. Sci.* **2003,** 203-204, 13-19.

23. Johansson, B., ToF-SIMS imaging of lipids in cell membranes *Surf. Interface Anal.* **2006,** 38, (1401-1412).

24. Microbiology Application Note NanoSIMS 50 *Cameca Application Notes* **2008**.

25. Stevie, F. A.; Downey, S. W.; Brown, S. R.; Shofner, T. L.; Decker, M. A.; Dingle, T.; Christman, L., Nanoscale Elemental Imaging of Semiconductor Materials using Focused Ion Beam Secondary Ion Mass Spectrometry. *J. Vac. Sci. Tech. B* **1999,** 17, 2476-2482.

26. Brison, J.; Houssiau, L., On the Understanding and the Optimization of ToF-SIMS Depth Profiles by Cosputtering Cesium and Xenon. *Surf. Interface Anal.* **2006,** 38,

1715-1719.

27. Cheng, J.; Winograd, N., Depth Profiling of Peptide Films with TOF-SIMS and a C_{60} Probe *Anal. Chem.* **2005,** 77, 3651-3659.

28. Hinder, S. J.; Lowe, C.; Watts, J. F., ToF-SIMS Depth Profiling of a Complex Polymeric Coating Employing a C_{60} Sputter Source *Surf. Interface Anal.* **2007,** 39, 467-475.

29. Desorption Ionization by Particle Bombardment. In *The encyclopedia of mass spectrometry*, Gross, M. L.; Caprioli, R. M.; Armentrout, P. B., Eds. Elsevier: 2007; Vol. 6.

30. Revised from http://nxw.chem.psu.edu/nxw/research.asp, accessed September, 17th.

31. Revised from TOF SIMS IV - *users' guide*, ION-TOF GmbH, Münster, Germany.

32. Taylor, G., Disintegration of Water Drops in an Electric Field. *Proc. R. Soc. London, A* **1964,** 280, 383-397.

33. TOF SIMS IV - users' guide, ION-TOF GmbH, Münster, Germany.

34. Wollnik, H., Time-of-Flight Analyzer. *Mass. Spec. Rev.* **1993,** 12, 89-114.

Chapter 3

Construction of High Vacuum Chamber for UV Activated Chemical Vapor Deposition

3.1 Introduction

Chemical vapor deposition is a widely used technique to grow oxides, metals, semiconductors and compound thin-film materials,[1-3] and is employed in a broad range of commercial applications.[1-6]

In a typical chemical vapor deposition, a substrate is exposed to one or more volatile precursors. The precursor either decomposes on the substrate owing to pyrolysis, or chemically reacts with the substrate to produce the desired deposit. In Chapter 4, an area selective chemical vapor deposition of aluminum and alumina was demonstrated using trimethyl aluminum (TMA) as precursor. It was shown that the deposition chamber base pressure was important to determine deposited species. When CVD was performed in a nitrogen-purged glove box, alumina was deposited. In contrast, when the deposition was carried out under high vacuum conditions (base pressure ~ 10^{-8} Torr) on -COOH and -OH terminated SAMs, metallic aluminum was formed.

To improve further the Al CVD process, a high vacuum chamber was designed for CVD on SAMs. First, the chamber was designed so that its base pressure is 10^{-8} Torr, but the pressure can be easily controlled from 10^{-4} Torr to 10^{-8} Torr. This pressure range is needed for exposing SAMs to several to 1×10^{6} Langmuir (1 Langmuir = 10^{-6} Torr · s)

precursor for investigation of the reaction pathways involved. Second, it was observed that the Al CVD process was very slow. To accelerate the reaction, it has been demonstrated that UV activation can be employed.[7-11] Thus, the chamber was designed so that UV light could be introduced without photooxidation of the SAM. Third, the chamber must provide a suitable interface to attach to the TOF SIMS system described in Chapter 2. This allows immediate sample transfer in vacuum after CVD to minimize sample oxidation or contamination during the transfer process.

In this chapter, the design and construct of a CVD chamber satisfying the above requirements are described in details. The chamber was employed for UV photo activated Al CVD using TMA. However, it has not been connected to the TOF SIMS yet.

3.2 Overview

The CVD deposition system consisted of a deposition chamber, a chamber stand, a gas line, a bypass line, and a UV light activation source equipped with a deuterium lamp (Figure 3.1). The whole system was pumped with a turbomolecular pump (Leybold, TMP 151, 145 l s^{-1}) backed by a rotary pump (Alcatel 2015, 298 l min^{-1}). Pressure of the chamber was monitored by a cold cathode ionization gauge (Kert J. Lesker, Series 423) and a Pirani gauge (Kert J. Lesker, Series 345). A second Pirani gauge and a Bourdon gauge were used to monitor the gas line pressure. In a typical CVD experiment, the TMA precursor was introduced from the gas line through a precision ultrahigh vacuum leak valve (MDC, ULV-150), which had an adjustable leak rate (range: 1×10^{-10} Torr l s^{-1} to 1

× 10^{-2} Torr). During the deposition, the butterfly valve was closed to protect the turbomolecular pump. After each deposition, the chamber was pumped *via* the bypass line until the pressure is sufficiently low(~ 10^{-4} Torr) to open the butterfly valve.

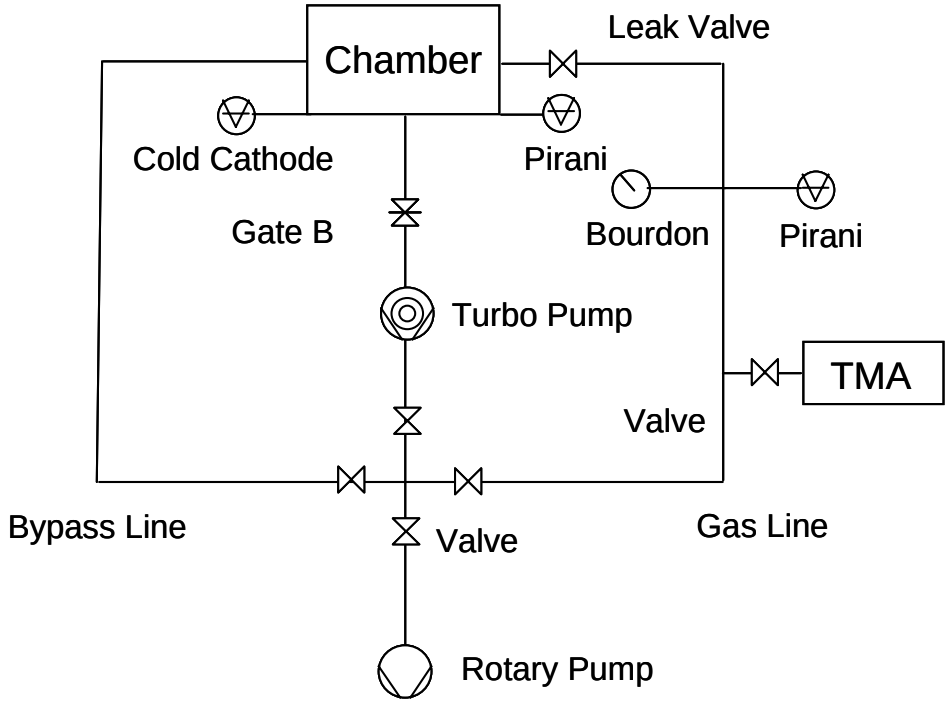

Figure 3.1 A schematic diagram of the vacuum system for the high vacuum CVD chamber.

3.2.1 CVD Chamber

The CVD chamber was constructed using a 6-way 6” CF cross cube (Figure 3.2). To the six sides of the chamber, the following parts were attached: a gate valve which will be employed to attach the chamber to the TOF SIMS preparation chamber, a butterfly valve separating the chamber from the turbo pump, a cluster flange connecting the gas line, the

bypass line and the cold cathode gauge, a sample transfer arm, a glass observation window, and a calcium fluoride window for UV light transmission. The gate valve and magnetic transfer arm were designed to interface with the TOF SIMS system. Sample transfer will be achieved under vacuum between the CVD chamber and TOF SIMS by using the transfer arm. To align the transfer arm with the TOF SIMS sample transfer system, a port aligner (MDC) was employed.

A butterfly valve separated the turbomolecular pump from the CVD chamber and protected the turbo pump from exposure to high pressures during CVD. CVD precursors are generally reactive and may damage (corrode) the turbo pump. For high dose TMA CVD (chamber pressure > 10^{-5} Torr), the butterfly valve was kept closed and the turbo pump was separated from the deposition environment.

The cluster flange had three $2\frac{3}{4}"$ CF ports, which connected to the gas line, the bypass line, and the cold cathode ionization gauge to the chamber. The leak valve controlled the CVD precursor pressure in the CVD chamber. The bypass line directly connected to the rotary pump, and was used for pumping out the chamber after CVD deposition. A cold cathode ionization gauge was attached to the third port and monitored the CVD chamber pressure.

A $4\frac{1}{2}"$ CF window was used for sample alignment and observation in the chamber. A $2\frac{3}{4}"$ CF CaF_2 window was used to transmit UV light into the CVD chamber. .

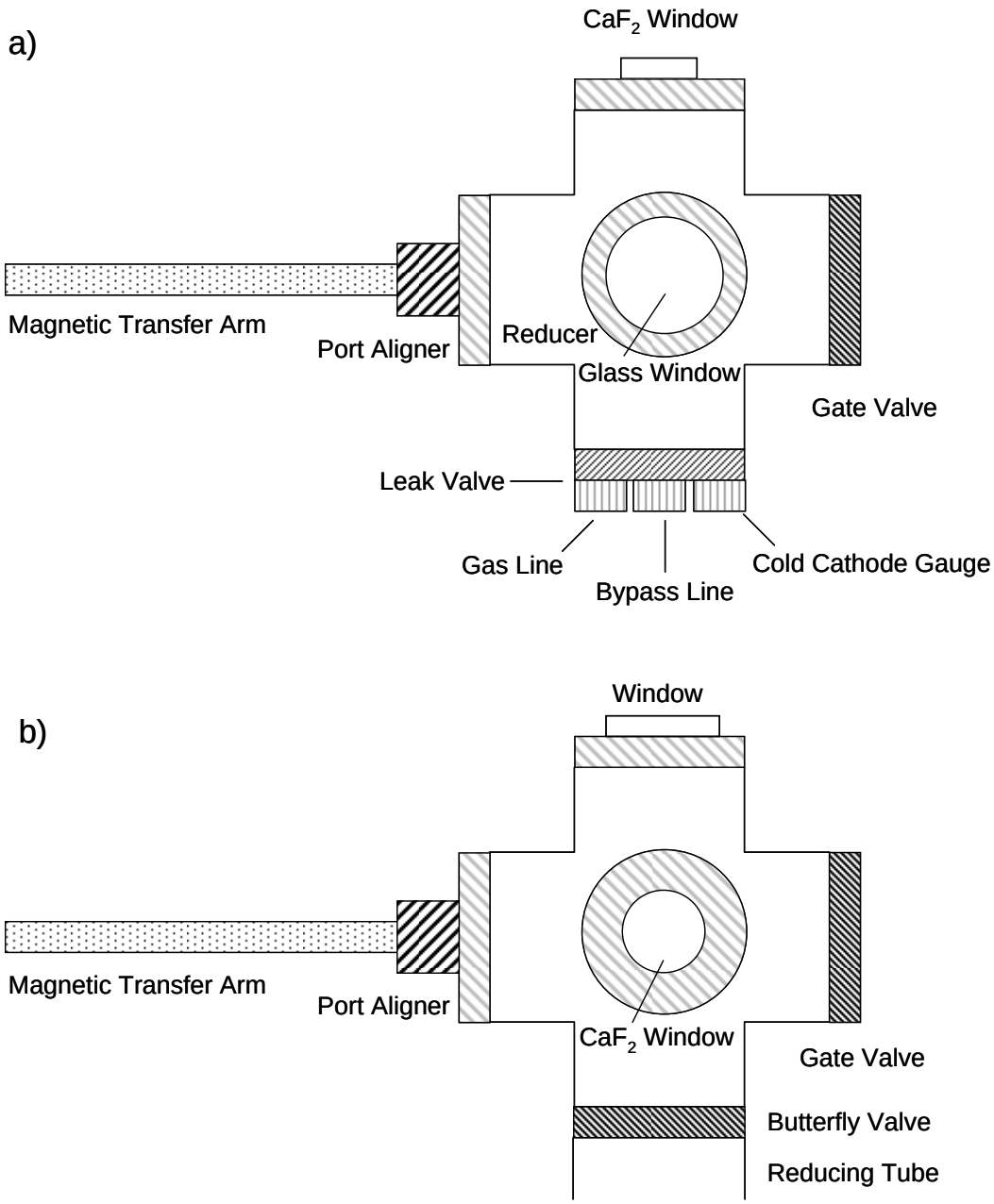

Figure 3.2 A schematic diagram of the high vacuum CVD chamber (a) Top view. The butterfly valve separating the chamber and turbomolecular pump was on the opposite side of the glass window and not shown in this graph. (b) Side view. The cluster flange was on the opposite side of the CaF_2 window and not shown in this graph.

3.2.2 CVD Gas Line

The gas line on the CVD system delivered the gaseous precursor from the precursor container vessel to the CVD chamber for reaction. One end of the gas line connected to the CVD chamber *via* a leak valve which precisely controlled deposition pressure, and the other end was attached to a NW16 4 way cross that linked the gas line, the bypass line, and the turbo pump to the rotary backing pump. The gas line pressure was monitored by a Pirani gauge and a Bourdon gauge (see Figure 3.3 for a schematic diagram).

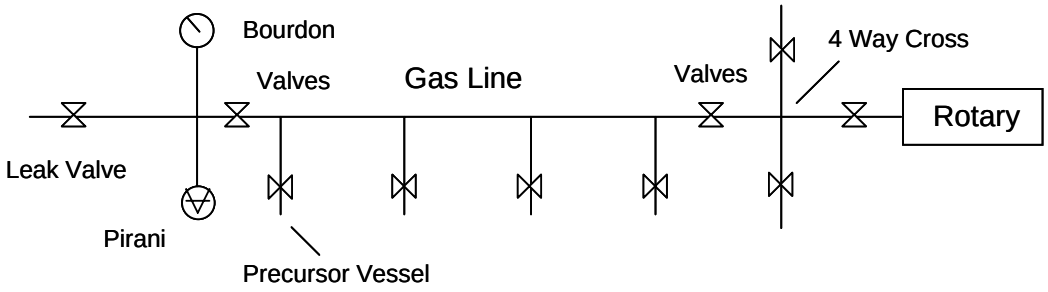

Figure 3.3 A schematic diagram of the gas line on the CVD chamber.

3.2.3 UV Lamp

A Series Q Deuterium Source System (New Port Stratford, Inc. Stratford, CT) was employed to provide UV illumination during the deposition. This system was equipped with a deuterium lamp (30 W, high uniformity, 1 mm arc diameter) which had a spectrum output from 160 nm to 500 nm.[12] Previous studies showed that trimethyl aluminum photodissociated at 193 nm, 248 nm, and 308 nm,[7, 9, 11] and thus the UV source was suitable for TMA CVD activation. The output beam went into the CVD chamber through

a CaF_2 window (CeramTec Corporation), which was able to transmit light at wavelengths below 200 nm.[13] During the deposition, the UV beam was parallel to the sample surface to minimize sample damage caused by UV radiation.

3.2.4 CVD Chamber Holder and Stand

The CVD chamber was mounted on a chamber holder attached to an aluminum stand. The holder and stand ensured that the chamber was at the same height as the TOF SIMS preparation chamber, and thus the CVD chamber could be coupled to the TOF SIMS.

Appendix: Design drawings of the holder and the stand can be found in Appendix Figures A3.1 - A3.3.

3.3 References

1. Dobkin, D. M.; Zuraw, M. K., *Principles of Chemical Vapor Deposition*. Kluwer Academic Publishers: Dordrecht, The Netherlands, 2003.

2. Galasso, F. S., *Chemical Vapor Deposited Materials*. CRC Press: 1991.

3. Sherman, A., *Chemical Vapor Deposition for Microelectronics*. Noyes Publications: Park Ridge, NJ, 1987.

4. Jaraith, R.; Jain, A.; Tolles, R. D.; Hampden-Smith, M. J.; T. T. Kodas, *The Chemistry of Metal CVD*. VCH, Weinheim: 1994.

5. Jensen, R., *Microelectronics Processing*. American Chemical Society: Washington, DC, 1989.

6. Dapkus, P. D., Metalorganic Chemical Vapor Deposition. *Ann. Rev. Mater. Sci.* **1982,** 12, 243-269.

7. Beuermann, T.; Stuke, M., Photolysis of Group III (Al, Ga, In) Trimethyl Compounds: Detection of Organic Photofragments CH_3 and C_2H_6 by Picosecond Laser Mass Spectrometry. *Chem. Phys. Lett.* **1991,** 178, 197-203.

8. Herman, I. P., Laser-Assisted Deposition of Thin Films from Gas-Phase and Surface-Adsorbed Molecules. *Chem. Rev.* **1989,** 89, 1323-1357.

9. Kobayashi, M.; Sato, A.; Tanaka, Y.; Shinohara, H.; Sato, H., Photodissociation of Multiayered Trimethylaluminum Adsorbed on a Cryogenic Substrate: a Time-of-Flight Mass-Spectrometry Study. *Appl. Organometal. Chem.* **1993,** 7, 303-309.

10. Motooka, T.; Gorbatkin, S.; Lake, R. E., UV-Laser Photolysis of Trimethylaluminum for Al Film Growth. *J. Appl. Phys.* **1985,** 58, 4397-4401.

11. Zhang, Y.; Stuke, M., UV Excimer Laser Photoproducts from Absorbing and Transparent Surfaces Covered by Aluminum Alkyl Adsorbates. *J. Phys. Chem.* **1989,** 93, 4503-4507.

12. Newport Coorperation, Oriel Deuterium Lamp Catalogue.

13. CerameTec Cooperation Online Source, Optical Transmission Curves, http://www2.ceramtec.com/part_intro/intro_viewport.cfm, accessed September 23th, 2009.

Chapter 4

Chemical Vapor Deposition of Aluminum and Alumina on Alkanethiolate Self-Assembled Monolayers Adsorbed on Gold

[Portions of this work have been published previously by Peng Lu, Korhan Demirkan, Robert L. Opila, and Amy V. Walker, *J. Phys. Chem. C*, 2008, *112*, 2091-2098. Korhan Demirkan performed the XPS studies described here in the group of R. L. Opila. A description of these is included for completeness.]

Abstract: The reaction of trimethylaluminum (TMA) with -COOH, -OH and -CH_3 terminated self-assembled monlayers (SAMs) adsorbed on gold was investigated with time-of-flight secondary ion mass spectrometry (TOF SIMS) and X-ray photoelectron spectroscopy (XPS). It is demonstrated that TMA can be employed to deposit both alumina and aluminum on functionalized SAMs at room temperature. The reaction was influenced by both the level of H_2O and O_2 present in the environment and the SAM terminal groups. In a nitrogen-purged glovebox, alumina was deposited on -COOH, -OH, and -CH_3 terminated SAMs. TMA reacted with -OH and -COOH terminal groups to form dimethyl aluminum complexes, which then reacted with H_2O and O_2 to deposit alumina. Alumina deposited on -COOH and -OH terminated SAMs was strongly adherent. TMA did not react with -CH_3 terminated SAMs, and the alumina deposited was formed by TMA reaction with H_2O and O_2 in the environment and could be removed by rinsing with

an organic solvent. In a deposition chamber with a base pressure $\leq 10^{-8}$ Torr, aluminum was deposited only on -COOH and -OH terminated SAMs but not on $-CH_3$ terminated SAMs. UV light can be employed to increase the Al deposition rate on -COOH and -OH terminated SAMs. Using CVD, aluminum and alumina could be selectively deposited in the -COOH terminated SAM areas of a patterned -COOH/$-CH_3$ SAM depending on the reaction conditions.

4.1 Introduction

Metalized organic thin films have many important applications in molecular electronics, polymer light-emitting diodes, and other electroluminescent devices.[1-5] Therefore, it is important to control and understand metal atom deposition on organic thin films. However, it is difficult to study the reaction mechanisms on most organic films because their surface properties are not well defined. To overcome this, self-assembled monolayers (SAMs), which have a highly ordered structure and a uniform surface density, have been employed as model systems for understanding the metal-molecule interactions.[6-12]

Most previous studies on the interactions of metals with organic thin films employed physical vapor deposition (PVD).[9-29] These studies showed that the interactions of vapor deposited metal with organic thin films could be very complicated. A wide range of behaviors were observed, from metal-organic complex formation,[11, 12, 15] to metal atom penetration through the film,[27] to destruction of monolayer caused by metal atoms.[25] The mechanism of interaction depends on the properties of both the metal and the organic thin film, and the outcome of the interaction can not be easily predicted.[23]

Aluminum is of particular interest in this study because it is widely employed as a metallic contact material in many organic electronic devices.[30, 31] Many studies have been reported on the physical vapor deposition (PVD) of aluminum on polymers and SAM. Birgerson *et al.*[32-35] studied Al vapor deposition on polymer surfaces, and Al was observed to form covalent bonds with the polymer backbones and oxygen-containing

groups prior to forming a metallic overlayer. Raman spectroscopy[36] and XPS[37] studies also confirmed that aluminum could undergo covalent addition to polymers and react with methoxy groups to form an oxycarbide species. Reaction of vapor deposited Al with functionalized SAMs has also been investigated extensively.[9-12, 15, 27] It was observed that Al inserted into the C-O bonds of the terminal groups on -OH,[11] -COOH,[15] and $-CO_2CH_3$[10, 12] terminated SAMs. On $-OCH_3$ terminated SAMs, Al weakly interacted with the $-OCH_3$ terminal group and penetrated through the monolayer to the Au/S interface.[9, 11, 27] Vapor deposited Al did not react with $-CH_3$ terminated SAMs, and penetrate through the SAMs. After the deposited Al reached a ~1:1 ratio with Au, metallic Al overlayers started to form at the SAM/vacuum interface.[12]

However, there are some concerns in PVD. Metal penetration through the SAMs is usually a problem, and one can not predict the reaction outcome in PVD. Other deposition techniques can be used to deposit metal and other materials, including electroless deposition,[38-40] atomic layer deposition (ALD),[41-43] and chemical vapor deposition (CVD).[44-46] CVD is an attractive method to grow thin films on organic substrates, because the reactions are chemically selective, the thickness of the film can be easily controlled, and a variety of materials can be deposited using this technique.

To date there have only been a few studies of CVD on organic thin films. [47-54] This is because most CVD processes require high temperatures (≥ 200 °C) which are incompatible with organic thin films. Alkanethiolate SAMs adsorbed on Au are thermally sensitive and undergo a phase transaction to a liquid-like state at temperatures above

~120 °C.[6] The density of defects within the monolayer increases when SAM surface temperature increases above room temperature, and defects created above 70 °C are irreversible even upon sample cooling.[55]

Several studies have demonstrated the feasibility of CVD to deposit metals on functionalized SAMs. Wohlfart *et al.*[52] employed trimethylamine alane (TMAA) to deposit alumina and aluminum hydroxide on -OH and -COOH terminated SAMs. Fischer *et al.*[51, 53] also deposited gold on thiol terminated SAMs using a methyltrimethylphospane gold (I) precursor. However, the reaction temperature was 70 °C, which may have led to damage of the monolayer.

A second issue is that deposition rates using CVD are often very low on organic thin films.[52, 53, 56] Unlike in PVD where the deposition rate is determined by the pressure of the metal vapor, CVD rate is limited by the rates of precursor adsorption and reaction with the substrate.[56] To improve the deposition rate, a UV source can be used to decompose the precursor prior to adsorption on the substrate, leading to an activated CVD process.[57-60] During the activation, the UV light may interact with the precursors in gas phase and adsorbed on the substrate, as well as the substrates.[56]

In this chapter, Al CVD using trimethyl aluminum (TMA) on functionalized SAMs at room temperature is demonstrated. When the deposition was performed in a N_2-purged glovebox, alumina formed on -OH, -COOH, and -CH_3 terminated SAMs. The deposited alumina film strongly adhered to -OH and -COOH terminated SAMs but could be easily removed from the -CH_3 terminated SAMs by rinsing with organic solvent. In

contrast, metallic Al was deposited on -OH and -COOH terminated SAMs in a deposition chamber with a base pressure $\leq 10^{-8}$ Torr. No reaction was observed on -CH_3 terminated SAMs. UV photoactivation of TMA improved the deposition rate on -OH and -COOH terminated SAMs but had no effect on -CH_3 terminated SAMs. It is also demonstrated that alumina and aluminum can be selectively deposited in the -COOH SAM terminated regions of a patterned -COOH/-CH_3 SAMs using appropriate experimental conditions.

4.2 Experimental

4.2.1 Materials

Chromium and gold (99.995%) were purchased from Alfa Aesar Inc. (Wardhill, MA). Trimethylaluminum (97%) (TMA) was obtained from Sigma Aldrich (St. Louis, MO) and transferred into glass vials inside a nitrogen-purged glove box (Model 855AC, Plas Labs Inc, Lansing, MI). TMA was purified prior to use by repeated freeze-pump-thaw cycles. Silicon wafers (<111> orientation) were purchased from Addison Technologies (San Jose, CA) and etched using piranha etch (H_2SO_4:H_2O_2 = 3:1) before use. Hexadecanethiol (98%) and mercaptohexadecanoic acid (98%) were also obtained from Sigma Aldrich (St. Louis, MO). Mercaptohexadecanol and ^{18}O-labeled mercaptohexadecanol were synthesized according to the procedure described by Walker *et al.*.[11]

4.2.2 SAM Preparation

The preparation and characterization of SAMs adsorbed on Au used in this study have been described in detail previously.[11, 12, 15, 61, 62] Briefly, Cr (~ 50 Å) and then Au (~1000

Å) were thermally deposited onto freshly etched Si native oxide wafers. Well-organized self-assembled monolayers were formed by placing the prepared Au substrates in a 1 mM ethanolic solution of the relevant alkanethiol molecule (with $-CH_3$, -OH or -COOH terminal functional groups) for 24 h at ambient temperature (21 ± 2 °C). To ensure that the prepared SAMs were well-ordered and free from significant chemical contamination, a sample from each batch (~1 cm^2) was characterized using time-of-flight secondary ion mass spectrometry (TOF SIMS) and single wavelength ellipsometry (Gaertner Inc., Stamford, CT) prior to the CVD experiment.

4.2.3 Chemical Vapor Deposition

TMA CVD was performed under several different experimental conditions. SAMs were exposed to TMA vapor (vapor pressure 8.4 Torr at 20 °C)[63] in (a) a nitrogen-purged glove box; (b) a vacuum chamber with a base pressure of 2.2×10^{-7} Torr; (c) a vacuum chamber with a base pressure of 2.7×10^{-8} Torr, and (d) an ultra high vacuum (UHV) chamber with a base pressure ~ 1×10^{-9} Torr (TOF SIMS preparation chamber). All reactions were carried out at room temperature, 21 ± 2 °C.

To photoactivate TMA, it was exposed to UV light from a Deuterium Lamp (30 W, Newport, Stratford, CT) in a specifically designed vacuum chamber (See Chapter 3).

After reaction with TMA, the samples were immediately transferred to the TOF SIMS for analysis.

4.2.4 UV Photopatterning of SAMs

UV Photopatterning of SAMs was performed as follows. A mask (a copper TEM grid, Electron Microscopy Inc. Hatfield, PA) was placed on top of the SAM to be patterned (SAM#1). The SAM with mask was then placed 50 mm from a 500 W Hg arc lamp and exposed to the UV light for 2 h to ensure that photooxidation was complete. The UV photopatterned SAM#1 was then immersed in a freshly-made 1 mM ethanolic solution of the second alkanethiol (SAM#2) for 24 h. In the areas exposed to UV light, the photooxidized SAM#1 was displaced by SAM#2. A SAM#1/SAM#2 patterned surface was then obtained. The patterned surfaces were rinsed copiously with degassed ethanol and dried with N_2 gas.

4.2.5 Time-of-Flight Secondary Ion Mass Spectrometry (TOF SIMS)

TOF SIMS analyses were performed using an ION TOF IV spectrometer (ION TOF, Inc., Chestnut Hill NY) equipped with a Bi_n^{m+} (n = 1 - 6, m = 1 - 2) liquid metal ion gun. The instrument consisted of an air lock for sample introduction, a preparation chamber, and an analysis chamber, each separated by gate valves. The pressures of the analysis and preparation chambers were maintained at $< 5 \times 10^{-9}$ Torr. The Bi^+ primary ions were accelerated to 25 keV and contained within a ~100 nm diameter probe beam. The beam was rastered over a (100×100 μm^2) area during spectra acquisition and a (500×500 μm^2) area during image acquisition. The total ion dose was less than 10^{11} cm^{-2}, and all spectra were obtained within the static SIMS regime.[64] The secondary ions were extracted into a time-of-flight mass spectrometer using a potential of 2000 V and were reaccelerated to 10 keV before reaching the detector. The peak intensities were

reproducible to within ± 10 % from scan to scan and sample to sample. For each experiment, at least two samples were prepared, and three areas on each sample were examined. The data shown represent an average of all measurements.

4.2.6 X-ray Photoelectron Spectroscopy (XPS)

A Surface Science Laboratories SSX-100 spectrometer was employed to perform the ex-situ XPS analyses. The spectrometer was equipped with a monochromatic Al Kα (1486.6 eV) source and a hemispherical detector. Data were taken at a photoelectron takeoff angle of 45° from the sample surface, with a band pass energy of 55.87 eV and an energy step of 0.1 eV. The full width at half-maximum (FWHM) for Au 4f is 1.18 eV. The resulting spectra were fit with Gaussians. FWHM of 1.2 eV (metallic aluminum) and 1.9 eV (oxidized aluminum) was used to fit the Al 2p peaks.

4.3 Results and Discussion

4.3.1 Reaction of TMA with -CH_3, -OH, and -COOH terminated SAMs: TOF SIMS Study

After TMA exposure, Al-containing ions were observed in the positive and negative ion TOF SIMS mass spectra, indicating that TMA has reacted with the SAMs (Figure 4.1). Al-containing fragment ions observed in the mass spectra are summarized in Table 4.1. No ions of the form of $AlSH_2^+$, AlS_x^-, or $Al_xAu_yS_z^-$ were observed, indicating that Al did not penetrate through the SAMs the Au/S interface.[11, 12, 15] Further, there was no evidence that aluminum carbide formed in the deposited films; no $Al_xC_y^-$ ions were observed.[23, 65]

On -OH and -COOH terminated SAMs, AlO^- and $AlO(CH_2)_x^{\pm}$ ions were observed in the TOF SIMS spectra, suggesting that Al has inserted into the C-O bonds of the terminal groups to form metal-organic complexes.[11, 15] Al^+ and AlO^- ions were also observed on $-CH_3$ terminated SAMs, indicating that TMA has also reacted with water and oxygen present in the reaction chamber. The intensities of the ions decreased as the vacuum in the deposition chamber was improved (Figure 4.1). These data suggest that TMA reacted with H_2O and O_2 present in the deposition environment and formed alumina. As the amount of H_2O and O_2 in the deposition chamber decreased under high vacuum conditions, the reaction to form alumina on $-CH_3$ terminated SAMs stopped, but TMA continued to react with -OH and -COOH terminated SAMs.

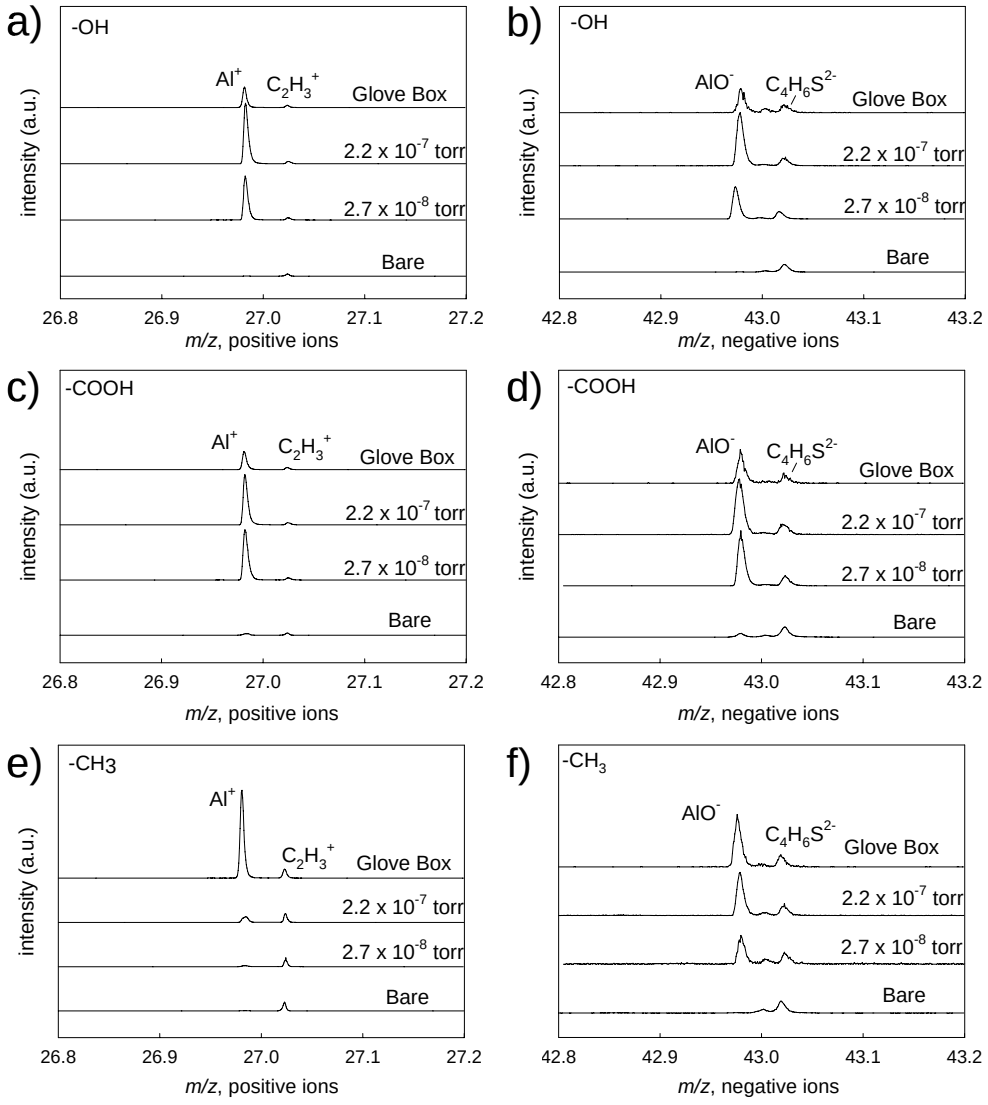

Figure 4.1 High resolution TOF SIMS spectra of Al^+ (nominal mass *m/z* 27) and AlO^- (nominal mass *m/z* 43) ions after (a,b) -OH, (c,d) -COOH and (e,f) -CH_3 terminated SAMs have been exposed to TMA for 15 minutes under different reaction conditions: a nitrogen-purged glove box, a reaction chamber with a base pressure of 2.2×10^{-7} Torr and a reaction chamber with a base pressure of 2.7×10^{-8} Torr.

SAM	Ions	
	Positive	**Negative**
$-CH_3$	Al^+	AlO^-, AlO_2^-, $Al_2O_3H^-$
-OH	Al_x^+, $AlOC^+$, $AlO(CH_2)_x^+$, $AlO(CH)_x(CH_2)_y^+$	AlO^-, AlO_2^-, $Al_2O_3H^-$, $AlO(CH_2)_x^-$, $AlO(CH)_x(CH_2)_y^-$
-COOH	Al_x^+, $AlOC^+$, $AlO(CH_2)_x^+$, $AlOOC(CH_2)_x^+$	AlO^-, AlO_2^-, $Al_2O_3H^-$, $AlO(CH_2)_x^-$, $AlOOC(CH_2)_x^-$

Table 4.1: Fragment ions observed in the TOF SIMS spectra upon reaction of TMA with $-CH_3$, -OH and -COOH terminated SAMs.

The positive ion mass spectra of $-CH_3$, -OH and -COOH terminated SAMs prior to and after TMA CVD in a deposition chamber with a base pressure of 2.7×10^{-8} Torr are shown in Figure 4.2. After TMA exposure, in the positive ion mass spectra, Al^+ ion is the most prominent ion for the -OH and -COOH terminated SAMs, indicating that the SAMs were covered by an Al overlayer. In contrast, on $-CH_3$ terminated SAMs, no distinct Al^+ peak was observed and the high mass ions intensities were similar to those prior to deposition. This suggests that an overlayer does not form on $-CH_3$ terminated SAMs (Figure 4.2). The negative ion mass spectra also support that an overlayer has formed on -OH and -COOH terminated SAMs but not on $-CH_3$ terminated SAMs (data not shown).

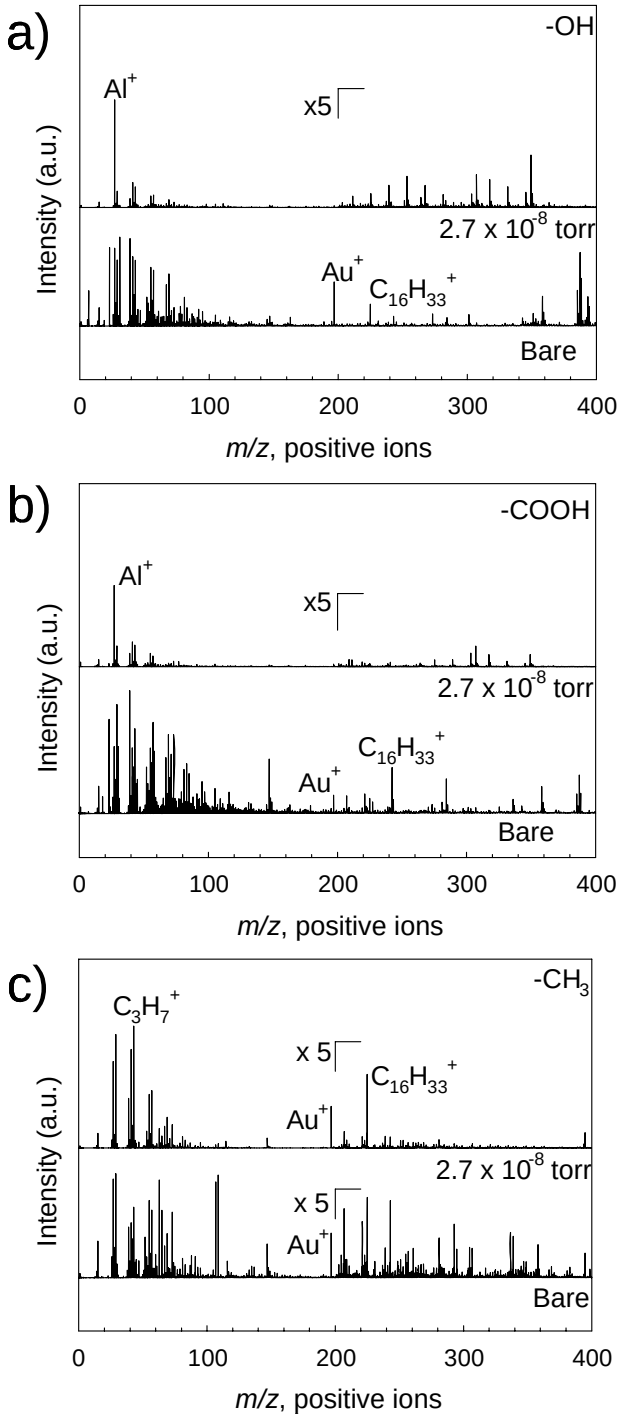

Figure 4.2 High resolution positive ion TOF SIMS spectra (*m/z* 0 - 400) of (a) -OH, (b) -COOH and (c) $-CH_3$ terminated SAMs before and after exposure to TMA for 15 minutes in a reaction chamber with a base pressure of 2.7×10^{-8} Torr.

To confirm that -OH and -COOH terminated SAMs reacted with TMA, the following three experiments were performed. First, TMA CVD was carried out in a nitrogen-purged glove box for 15 min, and after deposition the samples were rinsed with hexane. For $-CH_3$ terminated SAMs, the intensities of signals for Al-containing ions decreased significantly upon rinsing, indicating that the Al-containing species did not strongly bind to the SAM surface. In contrast, the intensities of these ion signals remained approximately constant prior to and after rinsing on -OH and -COOH terminated SAMs, suggesting that these monolayers have reacted and formed strong bonds with TMA (Figure 4.3). In the second experiment, TMA CVD was performed under UHV conditions (chamber base pressure ~ 10^{-9} Torr). After exposure to 9 L and 90 L of TMA, Al-containing ions such as Al^+ and AlO^- were observed on -OH and -COOH terminated SAMs but not on $-CH_3$ terminated SAMs. This observation indicates that TMA has reacted with the -OH and -COOH terminal groups but not with the $-CH_3$ terminal group (Figure 4.4). [11, 12, 15] In the third experiment, TMA CVD was performed on ^{18}O-labeled mercaptohexadecanol (-OH terminated) SAMs in a nitrogen-purged glovebox and under ultra high vacuum (uhv) conditions. After exposure to TMA, $Al^{18}OCH_2^-$ ions were observed on -OH terminated SAMs. Since the only source for ^{18}O is the -OH terminal groups on the SAMs, these ions confirm that TMA reacted with the -OH terminal group. In addition, Al and ^{16}O containing ions such as $Al^{16}O_2^-$ were also observed after deposition in the glovebox, indicating that TMA also reacted with H_2O and O_2 present in the environment (Figure 4.5).

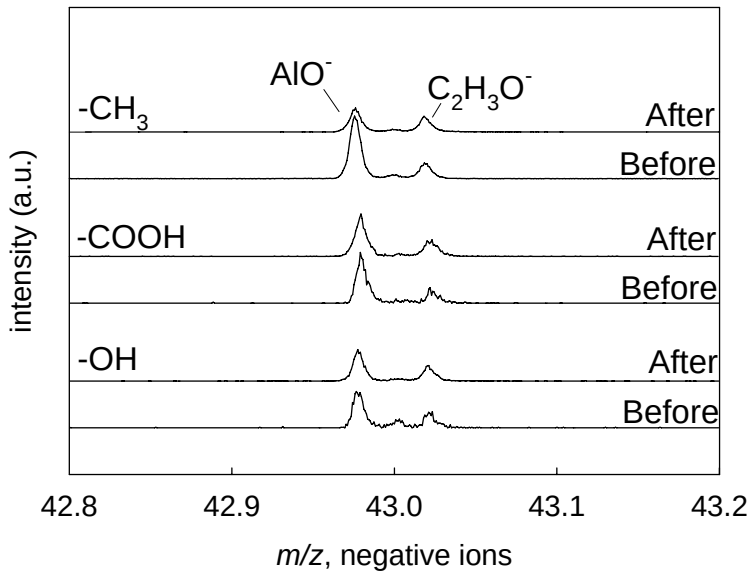

Figure 4.3 High resolution negative ion mass spectra of AlO^- ion (nominal mass *m/z* 43) of $-CH_3$, -COOH and -OH terminated SAMs exposed to TMA vapor for 15 min in a nitrogen-purged glove box.

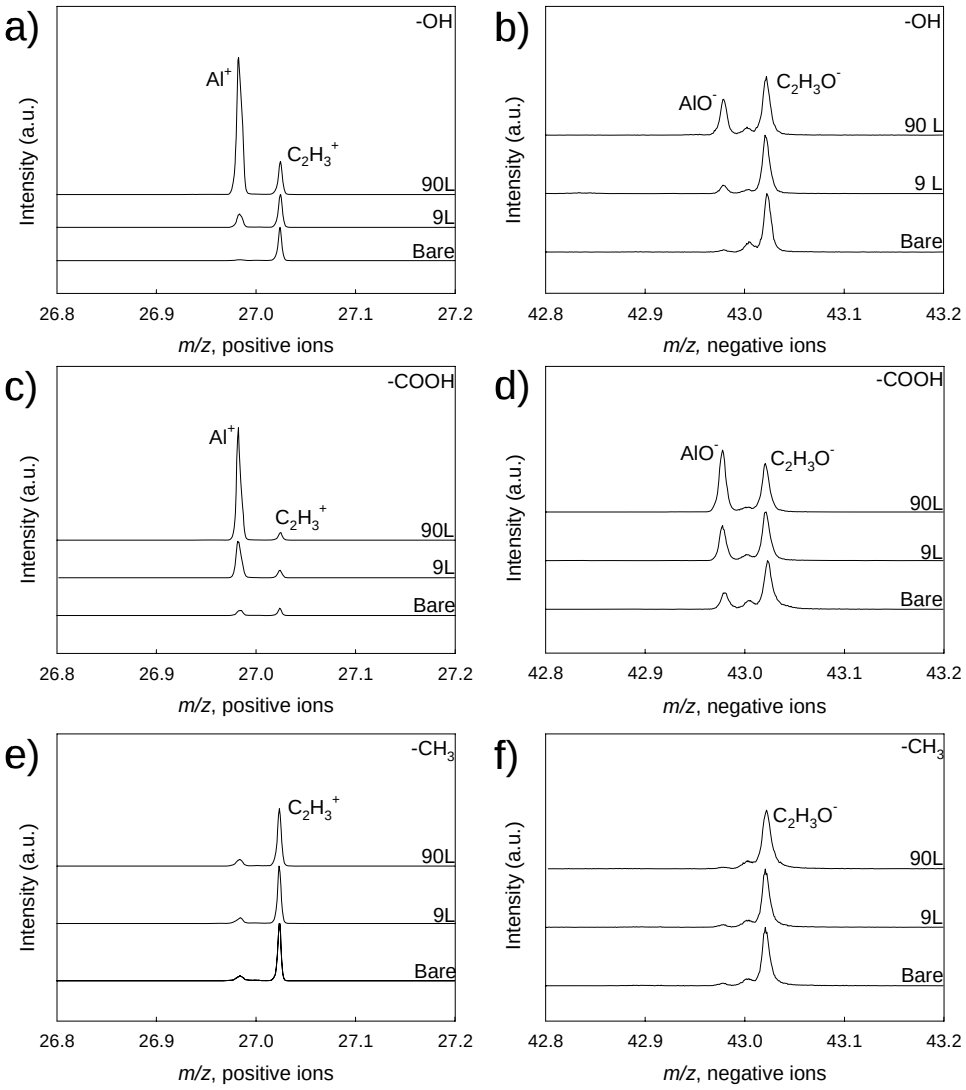

Figure 4.4 High resolution TOF SIMS spectra of Al^+ (nominal mass *m/z* 27) and AlO^- (nominal mass *m/z* 43) ions after (a,b) -OH, (c,d) -COOH and (e,f) $-CH_3$ terminated SAMs were exposed to TMA for 15 min in a reaction chamber with a base pressure below 10^{-9} Torr.

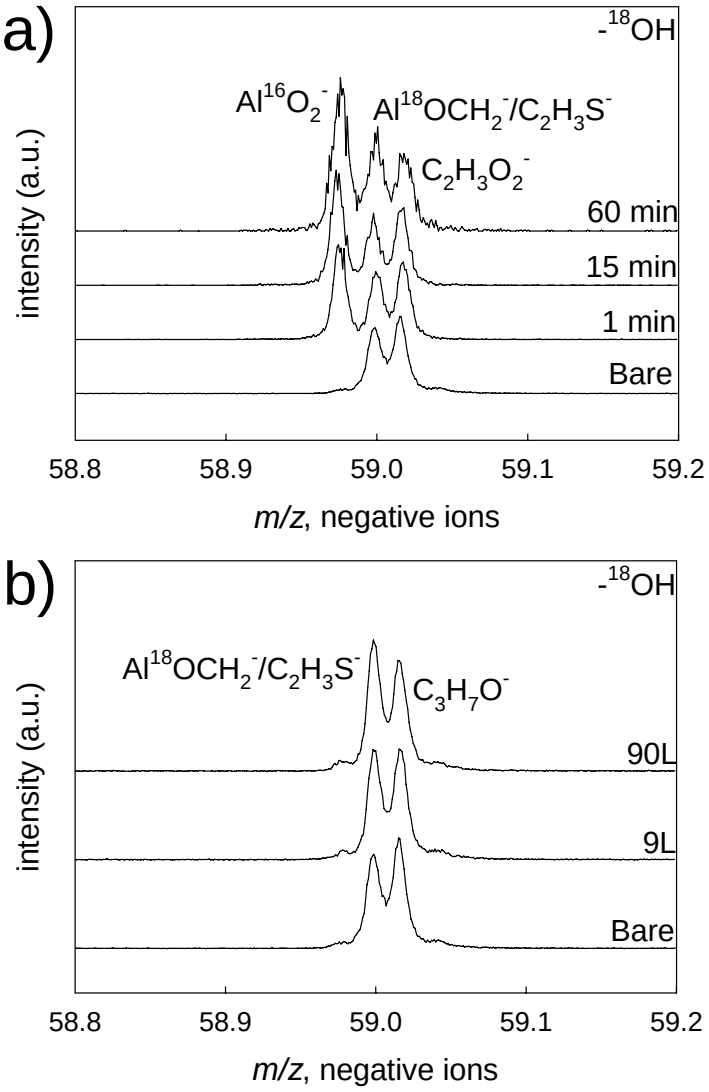

Figure 4.5 High resolution negative ion TOF SIMS spectra of AlO^- ion (nominal mass *m/z* 43) of $-^{18}OH$ terminated SAMs exposed to TMA for (a) between 1 and 60 min in a nitrogen-purged glove box and (b) for 9 L and 90 L (1 L = 10^{-6} Torr·s) in a reaction chamber with a base pressure below 10^{-9} Torr.

4.3.2 Reaction of TMA with -CH_3, -OH, and -COOH terminated SAMs: XPS Study

Ex situ XPS measurements were also performed on -CH_3, -OH and -COOH terminated SAMs prior to and after TMA CVD. The XPS data are consistent with the TOF SIMS observations. Briefly, the C 1s spectra indicate that TMA reacted with -OH and -COOH terminated SAMs to form Al-organic complexes, but did not react with -CH_3 terminated SAMs. The data also show that alumina was deposited on -OH and -COOH terminated SAMs under glovebox conditions. As the base pressure of the deposition chamber decreased, the Al(0) peak intensity increased, indicating that Al(0) was deposited. For -CH_3 terminated SAMs, the Al 2p and O 1s data suggest that nonstoichiometric aluminum oxide film (AlO_x) has deposited. The XPS data also indicate that no aluminum carbide (C 1s 282 eV) has formed on any of the SAMs.

4.3.2.1 XPS Spectra of the Bare Monolayers

Consistent with previous studies,[11, 12, 15] the core-level XPS spectra of the bare -CH_3-, -OH- and -COOH terminated SAMs show the following peaks. For -CH_3 terminated SAMs, a peak at 285 eV was observed in the C 1s spectrum. The C 1s spectrum of the -OH terminated SAM displays two peaks, at 285.2 eV and 287.0 eV, and were assigned to -$\underline{C}H_2$- and -$\underline{C}H_2OH$, respectively. A single peak in the O 1s spectrum at ~533 eV corresponded to the -$CH_2\underline{O}H$ functional group. For -COOH terminated SAMs, peaks at 285.2 eV and 289.2 eV were observed in the C 1s spectrum and were assigned to -$\underline{C}H_2$-

and -COO. A single broad peak at ~532 eV in the O 1s spectrum could be assigned to the -COOH oxygens (Figure 4.6).

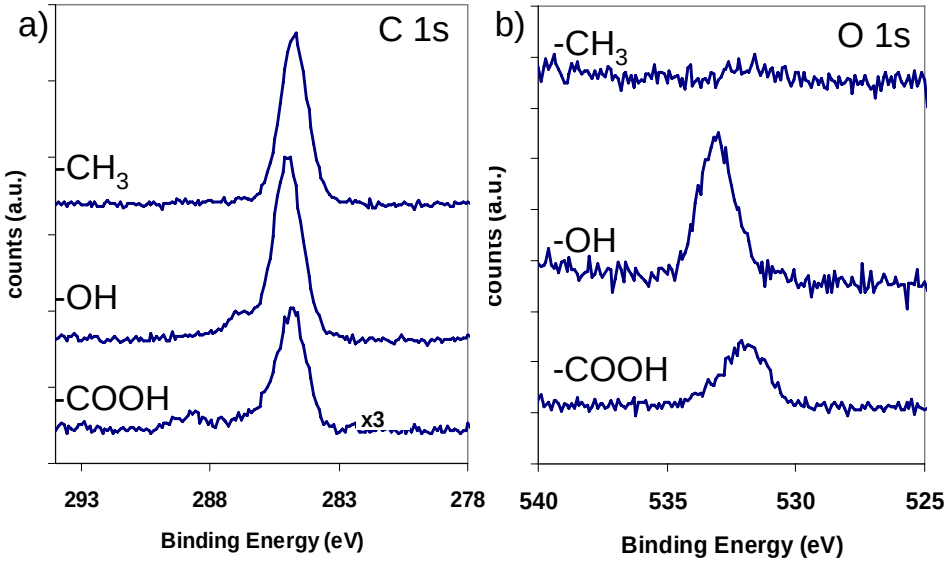

Figure 4.6 Core-level XPS spectra of the bare -CH_3, -OH and -COOH terminated SAMs adsorbed on gold. (a) The C 1s core level spectrum. (b) The O 1s core level spectrum.

4.3.2.2 XPS Spectra of -CH_3 terminated SAMs after TMA CVD

In agreement with the TOF SIMS data, the C 1s core-level XPS spectra show that TMA did not react with -CH_3 terminated SAMs. No new peaks were observed in the C 1s spectra after TMA deposition. Two O 1s peaks of varying relative ratios were observed at ~531.5 eV and ~533 eV, and could be assigned to oxygen in alumina, Al_2O_3 and AlO_x (or $Al(OH)_x$), respectively. The Al 2p data could be fit to two peaks at ~75 eV and ~73 eV which were assigned to aluminum in Al_2O_3 and Al(0), respectively. A FWHM of 1.9 eV was assumed for the oxidized aluminum species in the fitting process. However, Al peak

width for an amorphous aluminum oxide species may be higher (e.g. 2.1 eV) owing to the presence of a surface oxide.[66] This may explain the broad Al 2p peak (Figure 4.7).

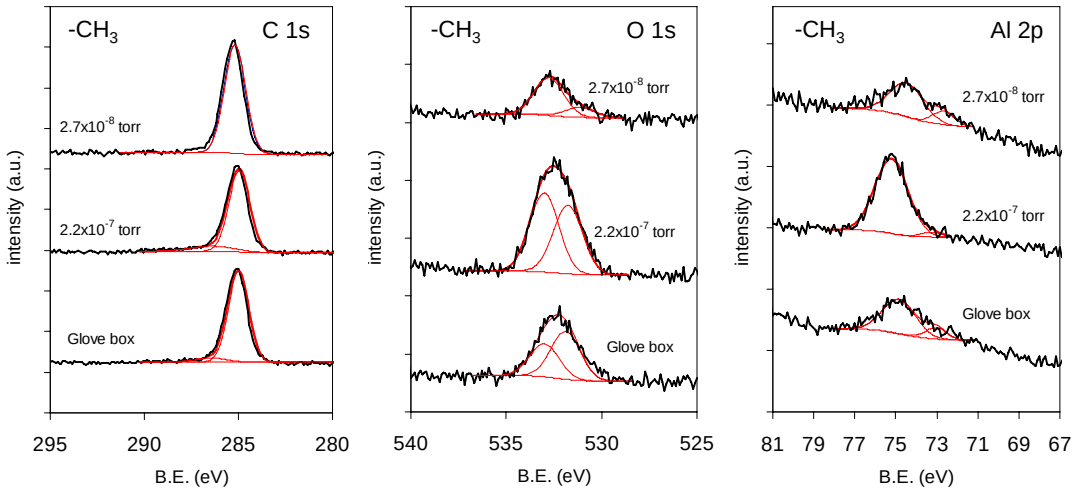

Figure 4.7 Core-level C 1s, O 1s and Al 2p XPS spectra of -CH_3 terminated SAMs after exposure to TMA vapor for 15 min in a nitrogen-purged glove box, a reaction chamber with a base pressure of 2.2 × 10^{-7} Torr and a reaction chamber with a base pressure of 2.7 × 10^{-8} Torr. The fits to the data are shown in red.

4.3.2.3 XPS Spectra of -OH terminated SAMs after TMA CVD

XPS spectra confirm that TMA reacted with -OH terminated SAMs. After TMA CVD, notable changes were observed in the C 1s spectra. The -$\underline{C}H_2$ 1s peak broadened considerably on the high binding energy side and a second peak appeared at ~290 eV, indicating that TMA has reacted with the -OH terminated SAM. In addition, there was no evidence that aluminum carbide (282.3 eV) had formed after deposition. The O 1s peak

could be fit to two separate oxygen-containing species with binding energies of 531.8 eV and ~533 eV, which were assigned to oxygen in alumina and oxygen in the hydroxyl group respectively. The decrease in the binding energy indicates an increased electron density on the hydroxyl group atoms, suggesting that TMA reacted with the -OH terminal group to form an aluminum-organic complex. Two peaks at 72.9 eV and 75.5 eV were present in the Al 2p spectra, and were assigned to Al (0) and $\underline{Al}_2O_3$. Notably, the intensity Al (0) peak increased as the base pressure of the reaction decreased, suggesting that metallic aluminum was deposited. This is also consistent with the TOF SIMS data (Figure 4.8).

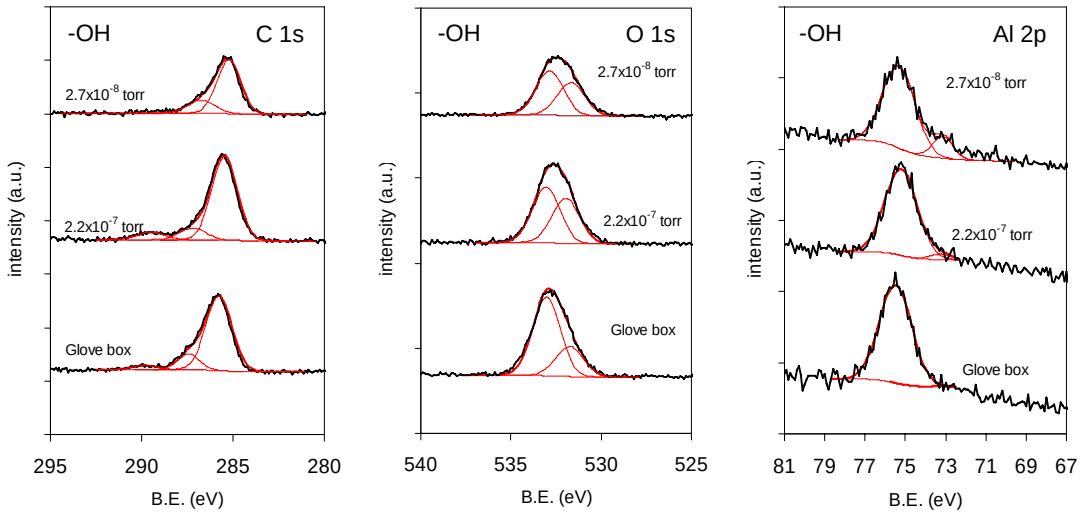

Figure 4.8 Core-level C 1s, O 1s and Al 2p XPS spectra of -OH terminated SAMs after exposure to TMA vapor for 15 min in a nitrogen-purged glove box, a reaction chamber with a base pressure of 2.2×10^{-7} Torr and a reaction chamber with a base pressure of 2.7×10^{-8} Torr. The fits to the data are shown in red.

4.3.2.4 XPS Spectra of -COOH terminated SAMs after TMA CVD

XPS data suggest that TMA also reacted with -COOH terminated SAMs. Similar as on -OH terminated SAMs, the -$\underline{C}H_2$ C 1s peak broadened on the high binding energy side and a second peak also appeared at a binding energy of ~289 eV after TMA deposition on -COOH terminated SAMs. These observations suggest that the TMA reacted with -OH and -COOH to form similar metal-organic complexes. No evidence of aluminum carbide (282.3 eV) was observed. The O 1s peak could be fit to 531.9 eV peak for oxygen in alumina and 533.0 eV peak for carboxyl oxygens which have reacted with TMA to form metal-organic complexes. In the Al 2p spectra, two peaks at 72.8 eV and 75 eV were observed and were assign to Al (0) and Al_2O_3 respectively. In agreement with the TOF SIMS data, the intensity of Al(0) peak increased as the base pressure of the reaction decreased, suggesting that metallic aluminum was deposited (Figure 4.9).

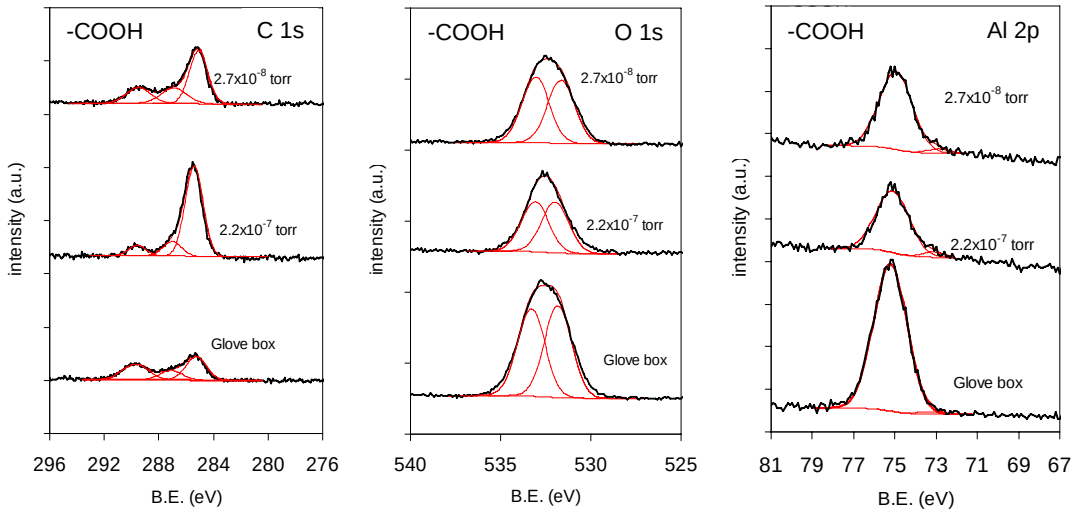

Figure 4.9 Core-level C 1s, O 1s and Al 2p XPS spectra of -COOH terminated SAMs after exposure to TMA vapor for 15 min in a nitrogen-purged glove box, a reaction chamber with a base pressure of 2.2×10^{-7} Torr and a reaction chamber with a base pressure of 2.7×10^{-8} Torr. The fits to the data are shown in red.

4.3.3 UV Photoassisted Al CVD on -OH, -COOH, and -CH_3 terminated SAMs

UV photoassisted Al CVD was also performed by exposing TMA to a deuterium lamp (160 nm - 500 nm). The UV light was maintained parallel to the SAMs surface in the deposition process so that the photooxidation of the SAMs was minimized. Figure 4.10 shows the negative ion TOF SIMS spectra of the -OH, -COOH, and -CH_3 terminated SAMs after 90s and 15 min UV irradiation. The MSO_3^- peaks in the spectra indicate that -COOH terminated SAMs were not oxidized, and the -OH and -CH_3 terminated SAMs were slightly oxidized (Figure 4.10).

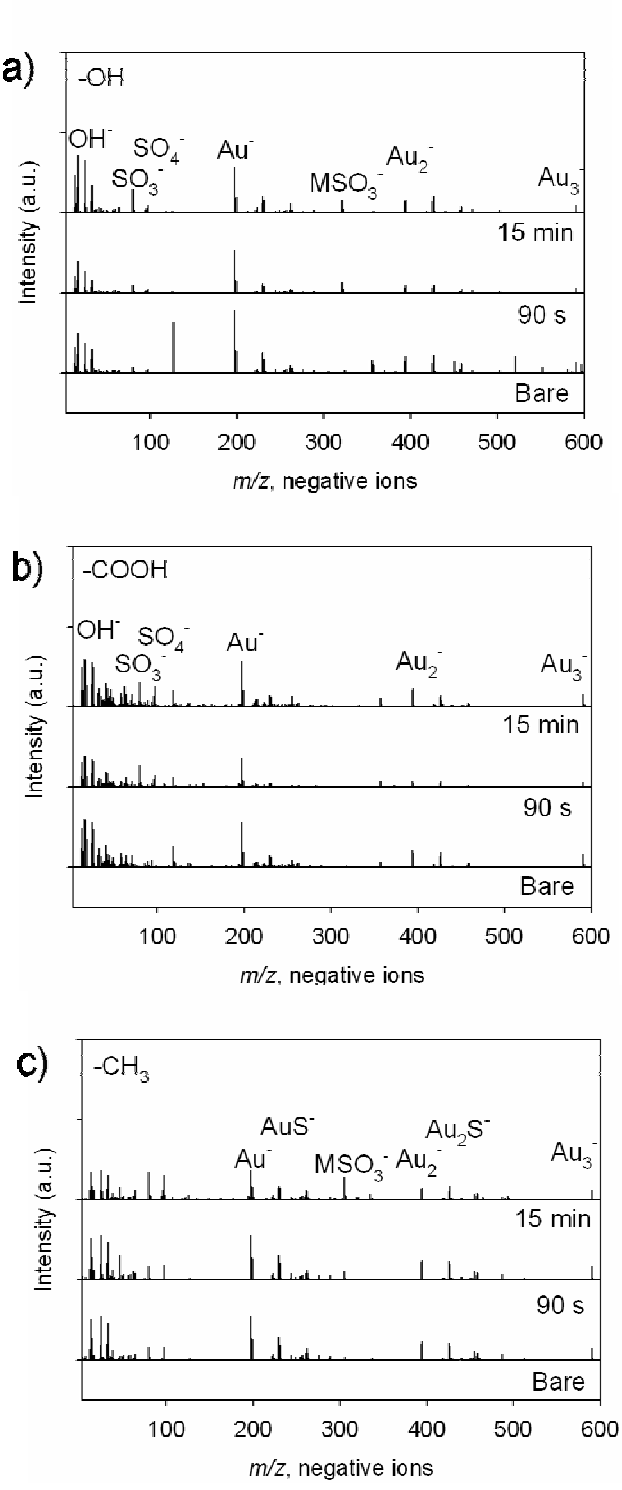

Figure 4.10 High resolution negative ion TOF SIMS spectra (*m/z* 0 – 600) of (a) -OH, (b) -COOH and (c) -CH_3 terminated SAMs under parallel D_2 lamp irradiation for 90s and 15 minutes in a reaction chamber with a base pressure $\leq 2 \times 10^{-8}$ Torr.

The use of UV light significantly increased the deposition rates on -OH and -COOH terminated SAMs, but had no effect on the deposition rate on $-CH_3$ terminated SAMs (Figure 4.11). Under UV activation, the intensity of Al^+ peak was 4 and 6 times larger on -OH and -COOH terminated SAMs, respectively, than after TMA exposure without UV light (Figure 4.11a, c) The AlO^- peak intensity also increased significantly (Figure 4.11b,d). In contrast, no evidence of TMA deposition was observed on $-CH_3$ terminated SAMs: no Al^+ or AlO^- ions were observed (Figure 4.11e, f). In agreement with our previous observations, TMA reacted with -OH and -COOH terminated SAMs but did not react with the $-CH_3$ terminated SAMs. Further, the increase in the Al^+ peak intensity (4 to 6 times) was significantly higher than the increase in the intensity of AlO^- peak, suggesting that Al was the dominant product.

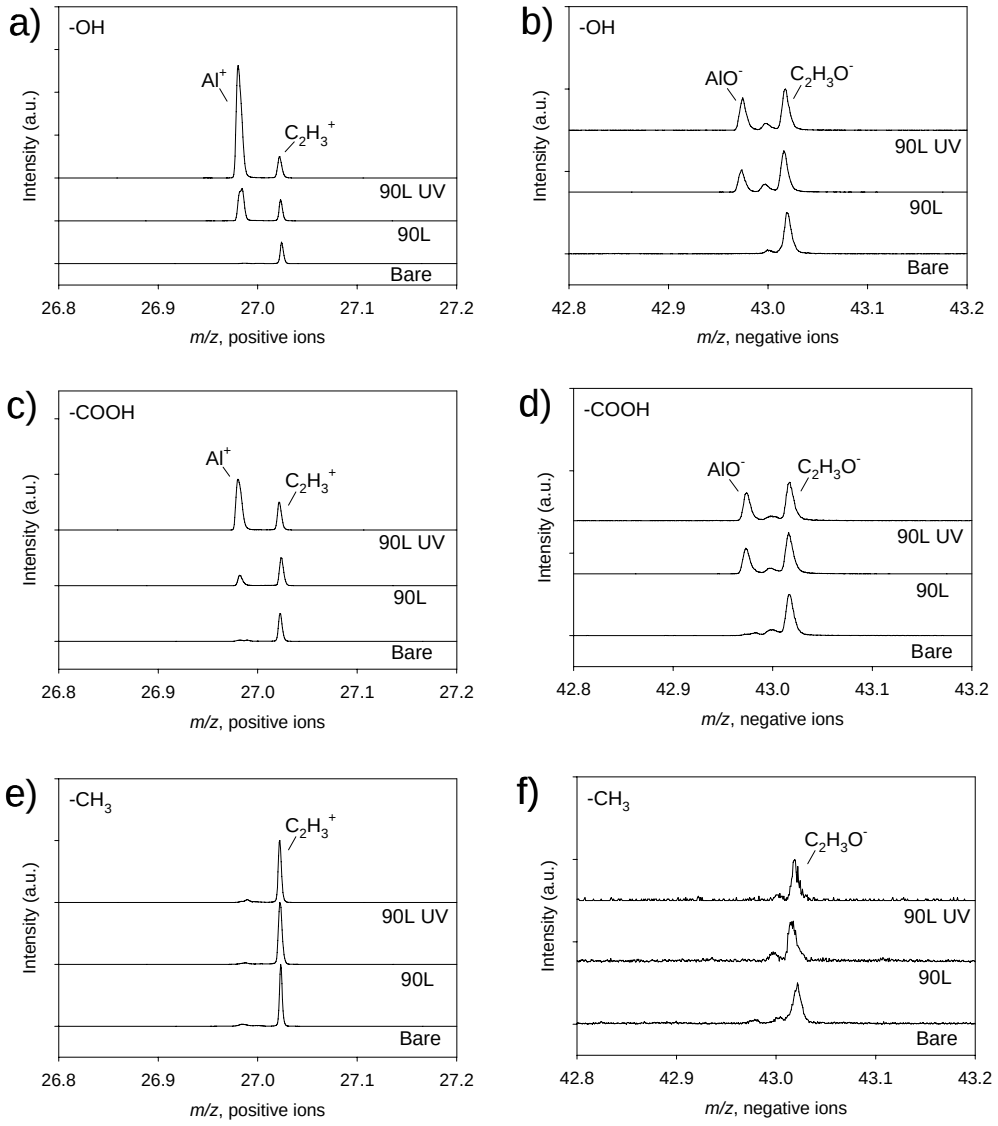

Figure 4.11 High resolution TOF SIMS spectra of Al^+ (nominal mass *m/z* 27) and AlO^- (nominal mass *m/z* 43) ions after (a,b) -OH, (c,d) -COOH and (e,f) -CH_3 terminated SAMs were exposed to TMA for 90 L dose under D_2 lamp irradiation in a reaction chamber with a base pressure $\leq 2 \times 10^{-8}$ Torr.

4.3.4 Reaction Pathways of TMA CVD on Functionalized SAMs

4.3.4.1 TMA Reaction with -OH and -COOH terminated SAMs

The TOF SIMS and XPS data indicate that TMA reacted with -OH and -COOH terminated SAMs to form a surface-bound complex. Previous studies showed that TMA reacted with hydroxylated alumina *via* oxidative addition and the loss of methane gas.[63, 67, 68] A similar reaction mechanism is proposed here. The first step in the reaction is the oxidative insertion of TMA into the -OH and -COOH terminal groups to form a dimethyl aluminum complex (Scheme 4.1). Note the reaction is shown using a TMA dimer since it is know that gaseous TMA exists in this state at room temperature.[69] This mechanism is also supported by UV photoactivated Al CVD data. It is known that TMA undergoes photodissociation at 193 nm, 248 nm, and 308 nm to generate an excited $Al(CH_3)_2$ species.[56, 57, 70, 71] These species more readily react with the -OH and -COOH terminal groups, and thus the deposition rate increases (Figure 4.11).

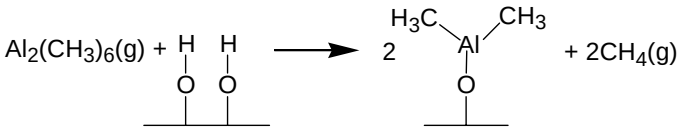

Scheme 4.1 Proposed oxidative insertion of trimethylaluminum dimer with -OH and -COOH terminated SAMs to form a dimethyl aluminum complex and methane.

4.3.4.2 Deposition of Alumina and Aluminum Oxide on Functionalized SAMs

Alumina was deposited on all SAMs studied when Al CVD was performed in a nitrogen-purged glovebox. In the initial stages of Al CVD, TMA is proposed to react with -OH and -COOH terminated SAMs to form dimethyl aluminum complexes (Scheme 4.1). The dimethyl aluminum complexes may react with H_2O and O_2 present in the glovebox to generate new Al-OH bonds (Scheme 4.2). These then react with gaseous TMA leading to formation of an alumina (Al_2O_3) overlayer. TMA can also react with O_2 to form an oxide layer with higher Al/O ratio than Al_2O_3.[72, 73]

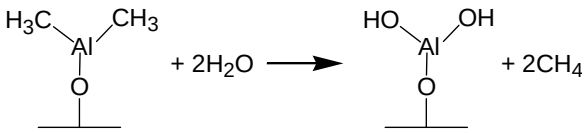

Scheme 4.2 Proposed reaction of a surface dimethyl aluminum complex with water to form a hydroxylated surface and methane gas.

In contrast, TMA did not react with -CH_3 terminated SAMs. No experimental evidence of TMA reaction with -CH_3 terminated SAMs was observed in the TOF SIMS and XPS data, which agreed with previous DFT calculations.[74] Since there was no reaction between TMA and the -CH_3 terminal group and there were no oxygen containing groups in the SAM, alumina and aluminum oxide were deposited *via* physical adsorption after gas-phase reaction of TMA with H_2O and O_2 present in the environment. These species did not strongly adhere to the SAM surface, and so could be easily removed by

rinsing with organic solvents (Figure 4.3).

4.3.4.3 Deposition of Aluminum on Functionalized SAMs

Under very high vacuum conditions, TMA continued to deposit on -OH and -COOH terminated SAMs but no aluminum-containing species was deposited on -CH_3 terminated SAMs. The deposition of Al(0) under high vacuum conditions is proposed to occur *via* the following process. Initially, TMA reacts with -OH and -COOH terminal groups to form a dimethyl aluminum species as in Scheme 4.1. The neighboring dimethyl aluminum complexes then react with each other to form a bridged dialuminum complex. Once formed, these dialuminum complexes rapidly disproportionate and lead to the deposition of Al(0). As the reaction continues, aluminum deposits *via* the dissociative adsorption of TMA on the surface and the evolution of ethane (Scheme 4.3).[63, 68, 75] Since Al(0) is only observed when the H_2O/O_2 residual pressure in the deposition chamber is very low, this process must be much slower than the reaction of dimethyl aluminum with H_2O as in Scheme 4.2.

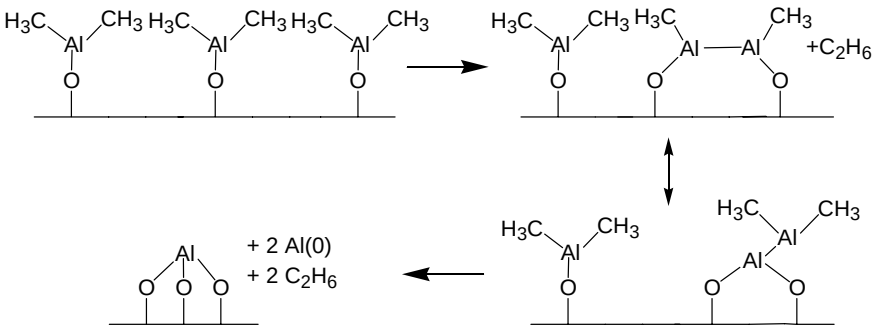

Scheme 4.3 Proposed reaction of surface dimethyl aluminum complexes to produce Al(0)

4.3.5 Selective CVD on Patterned SAMs

TMA can be employed to deposit selectively aluminum or alumina on the -COOH regions of -COOH/-CH_3 patterned SAMs. When a patterned -COOH (bar area) / -CH_3 (square area) SAM was exposed to TMA vapor in a nitrogen-purged glovebox, alumina was selectively deposited in the -COOH terminated SAM areas but not on the -CH_3 terminated SAM areas (Figure 4.12). The Al^+ ion signal intensity indicates that alumina has deposited on the -COOH terminated SAM but not on the -CH_3 terminated SAM areas. The OH^- ion intensity is indicative of the -COOH terminated SAM. However, if the deposition was performed using UV photoactivation of TMA at pressures $\leq 2 \times 10^{-8}$ Torr, selective deposition of aluminum was achieved (Figure 4.13). The Al^+ ion intensity indicates that Al(0) has deposited on the -COOH terminated SAM but not on the -CH_3 terminated SAM areas. The OH^- ion intensity is indicative of -COOH terminated SAMs, and the molecular ion (AuA_2^-, $A = S(CH_2)_{15}CH_3$) is indicative of -CH_3 teminated SAMs.

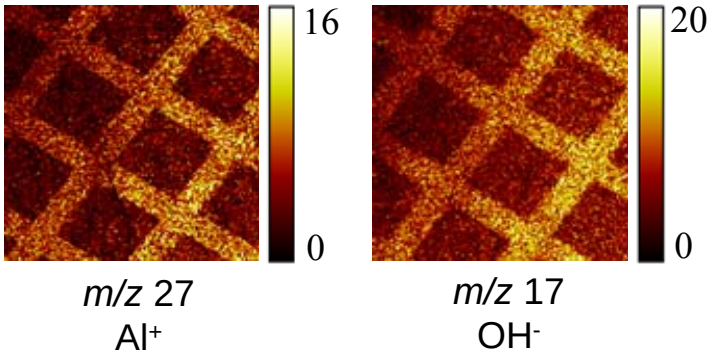

Figure 4.12 TOF SIMS images of Al^+ (*m/z* = 27) and OH^- (*m/z* = 17) after a patterned -COOH/-CH_3 terminated SAM was exposed to TMA for 3 min in a nitrogen-purged glove box followed by rinsing in hexane. Area of analysis: 500 × 500 μm^2; 128 × 128 $pixels^2$. Intensity scale represents maximum ion count.

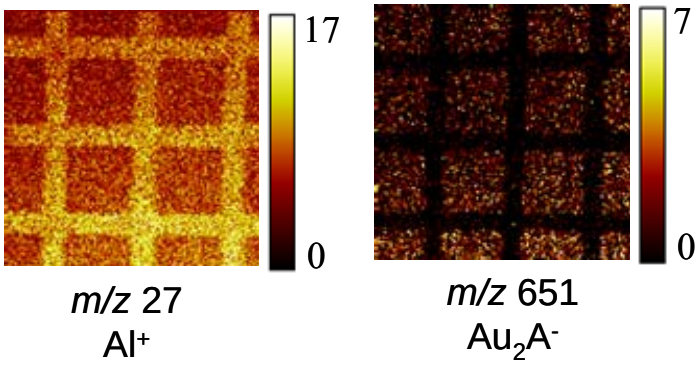

Figure 4.13 TOF SIMS images of Al^+ (*m/z* = 27), OH^- (*m/z* 17) and -CH_3 terminated SAMs molecular ion Au_2A^-(A = $S(CH_2)_{15}CH_3$, *m/z* 651) after a patterned -COOH/-CH_3 terminated SAM was exposed to TMA for 3min in a deposition chamber (base pressure ≤ 2×10^{-8} Torr) with D_2 lamp irradiation. Area of analysis: 500 × 500 μm^2; 128 × 128 $pixels^2$. Intensity scale represents maximum ion count.

4.4 Conclusions

In summary, alumina and aluminum can be deposited on functionalized SAMs at room temperature using chemical vapor deposition. In a nitrogen-purged glovebox where ppm level H_2O and O_2 existed, alumina was deposited on -CH_3, -OH and -COOH terminated SAMs. TMA reacted with -OH and -COOH terminated SAMs to form a dimethyl aluminum complex, and this surface-bound complex reacted with H_2O and O_2 to form alumina. There was no reaction between TMA and -CH_3 terminated SAMs, and the deposited alumina could be removed from the surface by rinsing with hexane. In a deposition chamber with a pressure < 10^{-8} Torr, an Al overlayer was deposited on -OH and -COOH terminated SAMs, and no aluminum containing species deposited on -CH_3 terminated SAMs. UV light can be employed to increase the Al deposition rate on -OH and -COOH terminated SAMs. When a patterned -COOH/-CH_3 SAM was exposed to TMA, alumina or aluminum can be selectively deposited in the -COOH terminated SAM regions. .

Chemical vapor deposition can be employed to fabricate stable metal, metal oxide or semiconductor thin films on functionalized SAMs. By controlling the surface functionalities and reaction conditions, these reactions can be selective.

Appendix: High resolution negative ion TOF SIMS spectra *m/z* = 0 - 900 of -OH, -COOH and -CH_3 terminated SAMs before and after exposure to TMA for 15 minutes in a reaction chamber with a base pressure of 2.7 × 10^{-8} torr；NMR spectra of

16-bromohexadecanoic acid, 16-bromohexadecanol, 16-bromohexadecyl acetate ($^{18}O_2$), 16-thioacetyl hexadecyl acetate ($^{18}O_2$) and 16-mercaptohexadecanol (^{18}O); IR spectrum of 16-mercaptohexadecanol (^{18}O); These spectra can be found in the Appendix Figure A4.1 - A.7.

4.5 References

1. Jung, D. R.; Czanderna, A. W., Chemical and Physical Interactions at Metal/Self-Assembled Organic Monolayer Interfaces *Crit. Rev. Solid State Mater. Sci.* **1994,** 19, 1-54.

2. Jung, D. R.; Czanderna, A. W.; Herdt, G. C., Bonding at Metal/Self-Assembled Organic Monolayer Interfaces. In *Polymer Surfaces and Interfaces: Characterization, Modification and Application*, Mittal, K. L.; Lee, K.-W., Eds. VSP: 1997.

3. Mittal, K. L., *Metallized Plastics: Fundamentals and Applications*. Marcel Dekker: New York, 1997.

4. Sacher, E., *Metallization of Polymers 2*. Kluwer Academic/Plenum Publishers: New York, 2002.

5. Sacher, E.; Pireaux, J.-J.; Kowalczyk, S. P., *Metallization of Polymers*. American Chemical Society: Washington, DC, 1990; Vol. 440.

6. Schreiber, F., Structure and Growth of Self-Assembling Monolayers. *Prog. Surf. Sci.* **2000,** 65, 151-256.

7. Ulman, A., Formation and Structure of Self-Assembled Monolayers. *Chem. Rev.*

1996, 96, 1533-1554.

8. Ulman, A., *An Introduction to Ultrathin Organic Films: From Langmuir-Blodgett to Self-Assembly*. Academic Press: New York, 1991; p 237-304.

9. Walker, A. V.; Tighe, T. B.; Reinard, M. D.; Haynie, B. C.; Allara, D. L.; Winograd, N., Solvation of Zero-Valent Metals in Organic Thin Films. *Chemcal Physics Letters* **2003,** 369, 615-620.

10. Fisher, G. L.; Hooper, A. E.; Opila, R. L.; Jung, D. R.; Allara, D. L.; Winograd, N., The Interaction between Vapor-Deposited Al Atoms and Methylester-Terminated Self-Assembled Monolayers Studied by Time-of-Flight Secondary Ion Mass Spectrometry, X-Ray Photoelectron Spectroscopy and Infrared Reflectance Spectroscopy. *J. Electron Spectrosc. Relat. Phenom.* **1998,** 98-99, 139-148.

11. Fisher, G. L.; Walker, A. V.; Hooper, A. E.; Tighe, T. B.; Bahnck, K. B.; Skriba, H. T.; Reinard, M. D.; Haynie, B. C.; Opila, R. L.; Winograd, N.; Allara, D. L., Bond Insertion, Complexation, and Penetration Pathways of Vapor-Deposited Aluminum Atoms with HO- and CH_3O-Terminated Organic Monolayers. *J. Am. Chem. Soc.* **2002,** 124, 5528-5541.

12. Hooper, A. E.; Fisher, G. L.; Konstadinidis, K.; Jung, D. R.; Nguyen, H.; Opila, R. L.; Collins, R. W.; Winograd, N.; Allara, D. L., Chemical Effects of Methyl and Methyl Ester Groups on the Nucleation and Growth of Vapor-Deposited Aluminum Films. *J. Am. Chem. Soc.* **1999,** 121, (35), 8052–8064.

13. Czanderna, A. W.; King, D. E.; Spaulding, D., Metal Overlayers on Organic

Functional Groups of Self-Organized Molecular Assemblies. 1. X-Ray Photoelectron Spectroscopy of Interactions of Cu/COOH on 11-Mercaptoundecanoic Acid *J. Vac. Sci. Technol., A* **1991,** 9, 2607-2613.

14. Dake, L. S.; King, D. E.; Czanderna, A. W., Ion Scattering and X-Ray Photoelectron Spectroscopy of Copper Overlayers Vacuum Deposited onto Mercaptohexadecanoic Acid Self-Assembled Monolayers. *Solid State Sci.* **2002,** 2, 781-789.

15. Fisher, G. L.; Hooper, A. E.; Opila, R. L.; Allara, D. L.; Winograd, N., The Interaction of Vapor-Deposited Al Atoms with CO_2H Groups at the Surface of a Self-Assembled Alkanethiolate Monolayer on Gold. *J. Phys. Chem. B* **2000,** 104, 3267-3273.

16. Herdt, G. C.; Czanderna, A. W., Metal Overlayers on Organic Functional Groups of Self-assembled Monolayers: VIII. X-Ray Photoelectron Spectroscopy of the Ni/COOH Interface *J. Vac. Sci. Technol., A* **1999,** 17, 3415-3418.

17. Herdt, G. C.; Czanderna, A. W., Metal Overlayers on Organic Functional Groups of Self-Organized Molecular Assemblies. V. Ion Scattering Spectroscopy and X-Ray Photoelectron Spectroscopy of Ag/COOH Interfaces *J. Vac. Sci. Technol., A* **1995,** 13, 1275-1280.

18. Herdt, G. C.; Czanderna, A. W., Metal Overlayers on Organic Functional Groups of Self-Organized Molecular Assemblies: VII. Ion Scattering Spectroscopy and X-Ray Photoelectron Spectroscopy of Cu/CH_3 and $Cu/COOCH_3$. *J. Vac. Sci. Technol., A* **1997,** 15, 513-519.

19. Herdt, G. C.; Jung, D. R.; Czanderna, A. W., Weak Interactions between Deposited Metal Overlayers and Organic Functional Groups of Self-Assembled Monolayers. *Prog. Surf. Sci.* **1995,** 50, 103-129.

20. Jung, D. R.; Czanderna, A. W., Metal Overlayers on Organic Functional Groups of Self-Assembled Monolayers. VI. X-Ray Photoelectron Spectroscopy of Cr/COOH on 16-Mercaptohexadecanoic Acid. *J. Vac. Sci. Technol., A* **1995,** 13, 1337-1344.

21. Jung, D. R.; Czanderna, A. W.; Herdt, G. C., Interactions and Penetration at Metal/Self-Assembled Organic Monolayer Interfaces *J. Vac. Sci. Technol., A* **1996,** 14, 1779-1781.

22. Jung, D. R.; King, D. E.; Czanderna, A. W., XPS of Organized Molecular Assembly/Copper Interfaces: $HS(CH_2)_{11}OH$/Cu. *Appl. Surf. Sci.* **1993,** 70/71, 127-132.

23. Nagy, G.; Walker, A. V., Dynamics of Reactive Metal Adsorption on Organic Thin Films. *J. Phys. Chem. C* **2007,** 111, 8543-8556.

24. Nagy, G.; Walker, A. V., Dynamics of the Interaction of Vapor-Deposited Copper with Alkanethiolate Monolayers: Bond Insertion, Complexation, and Penetration Pathways. *J. Phys. Chem. B* **2006,** 110, 12543-12554.

25. Tighe, T. B.; Daniel, T. A.; Zhu, Z.; Uppili, S.; Winograd, N.; Allara, D. L., Evolution of the Interface and Metal Film Morphology in the Vapor Deposition of Ti on Hexadecanethiolate Hydrocarbon Monolayers on Au. *J. Phys. Chem. B* **2005,** 109, 21006-21014.

26. Walker, A. V.; Fisher, G. L.; Hooper, A. E.; Tighe, T.; Opila, R. L.; Winograd, N.;

Allara, D. L., Nucleation and Growth of Vapor-Deposited Metal Films on Self-Assembled Monolayers Studied by Multiple Characterization Probes. In *Metallization of Polymers 2*, Sacher, E., Ed. Kluwer Academic/Plenum: New York,, 2002; pp 117-126.

27. Walker, A. V.; Tighe, T. B.; Cabarcos, O. M.; Reinard, M. D.; Haynie, B. C.; Uppili, S.; Winograd, N.; Allara, D. L., The Dynamics of Noble Metal Atom Penetration through Methoxy-Terminated Alkanethiolate Monolayers. *J. Am. Chem. Soc.* **2004,** 126, 3954-3963.

28. Walker, A. V.; Tighe, T. B.; Stapleton, J. J.; Haynie, B. C.; Allara, D. L.; Winograd, N., Interaction of Vapor-Deposited Ti and Au with Molecular Wires. *Appl. Phys. Lett.* **2004,** 84, 4008-4010.

29. Zhou, C.; Nagy, G.; Walker, A. V., Towards Molecular Electronic Circuitry: Selective Deposition of Metals on Patterned Self-Assembled Monolayer Surfaces. *J. Am. Chem. Soc.* **2005,** 127, 12160-12161.

30. Friend, R. H.; Gymer, R. W.; Holmes, A. B.; Burroughes, J. H.; Marks, R. N.; Taliani, C.; Bradley, D. D. C.; Dos Santos, D. A.; Bre´das, J. L.; Logdlund, M.; Salaneck, W. R., Electroluminescence in Conjugated Polymers. *Nature* **1999,** 397, 121-128.

31. Tsubouchi, K.; Masu, K., Selective Aluminum Chemical Vapor Deposition *J. Vac. Sci. Technol., A* **1992,** 10, 856-862.

32. Birgerson, J.; Fahlman, M.; Broms, P.; Salaneck, W. R., Conjugated Polymer Surfaces and Interfaces: A Mini-Review and Some New Results. *Synth. Met.* **1996,** 80,

125-130.

33. Dannetun, P.; Logdlund, M.; Fredriksson, C.; Fauquet, C.; Stafstrom, S.; Spangler, C. W.; Bredas, J. L.; Salaneck, W. R., Reactions of low work function metals Na, Al, and Ca on alpha,omega-diphenyltetradecaheptaene. Implications for metal/polymer interfaces. *J. Chem. Phys* **1994,** 100, 6765-6771.

34. Lazzaroni, R.; Logdlund, M.; Calderone, A.; Bredas, J. L.; Dannetun, P.; Fauquet, C.; Fredriksson, C.; Stafstrom, S.; Salaneck, W. R., Chemical and Electronic Aspects of Metal/Conjugated Polymer Interfaces. Implications for Electronic Devices. *Synth. Met.* **1995,** 71, 2159-2162.

35. Salaneck, W. R.; Bredas, J.-L., The Metal-on-Polymer Interface in Polymer Light Emitting Diodes. *AdV. Mater.* **1996,** 8, 48-52.

36. Hawkridge, A. M.; Pemberton, J. E., Model Aluminum−Poly(p-phenylenevinylene) Interfaces Studied by Surface Raman Spectroscopy. *J. Am. Chem. Soc.* **2003,** 125, 624-625.

37. Atreya, M.; Li, S.; Kang, E. T.; Neoh, K. G.; Ma, Z. H.; Tan, K. L., In Situ X-Ray Photoelectron Spectroscopy Studies of Interactions of Evaporated Metals with Poly(p-Phenylene Vinylene) and its Ring-Substituted Derivatives *J. Vac. Sci. Technol., A* **1999,** 17, 853-861.

38. Shacham-Diamand, Y.; Dubin, V.; Angyal, M., Electroless Copper Deposition for ULSI. *Thin Solid Films* **1995,** 262, (1995), 93-103.

39. Zangmeister, C. D.; van Zee, R. D., Electroless Deposition of Copper onto

4-Mercaptobenzoic Acid Self-Assembled on Gold. *Langmuir* **2003,** 19, 8065-8068.

40. Zhu, P.; Masuda, Y.; Koumoto, K., Seedless Micropatterning of Copper by Electroless Deposition on Self-Assembled Monolayers. *J. Mater. Chem* **2004,** 14, 976-981.

41. George, S. M.; Ott, A. W.; Klaus, J. W., Surface Chemistry for Atomic Layer Growth. *J. Phys. Chem.* **1996,** 100, 13121-13131.

42. Lim, B. S.; Rahtu, A.; Gordon, R. G., Atomic Layer Deposition of Transition Metals. *Nat. Mater.* **2003,** 2, 749-754.

43. Matero, R.; Rahtu, A.; Ritala, M.; Leskela, M.; Sajavaara, T., Effect of Water Dose on the Atomic Layer Deposition Rate of Oxide Thin Films. *Thin Solid Films* **2000,** 368, 1-7.

44. Dobkin, D. M.; Zuraw, M. K., *Principles of Chemical Vapor Deposition*. Kluwer Academic Publishers: Dordrecht, The Netherlands, 2003.

45. Galasso, F. S., *Chemical Vapor Deposited Materials*. CRC Press: 1991.

46. Sherman, A., *Chemical Vapor Deposition for Microelectronics*. Noyes Publications: Park Ridge, NJ, 1987.

47. Jeon, N. L.; Clem, P. G.; Payne, D. A.; Nuzzo, R. G., A Monolayer-Based Lift-Off Process for Patterning Chemical Vapor Deposition Copper Thin Films. *Langmuir* **1996,** 11, 5350–5355.

48. Jeon, N. L.; Nuzzo, R. G., Patterned Self-Assembled Monolayers Formed by Microcontact Printing Direct Selective Metalization by Chemical Vapor Deposition on

Planar and Nonplanar Substrates. *Langmuir* **1995,** 11, 3024-3026.

49. Weckenmann, U.; Mittler, S.; Kramer, S.; Aliganga, A. K. A.; Fischer, R. A., A Study on the Selective Organometallic Vapor Deposition of Palladium onto Self-assembled Monolayers of 4,4‘-Biphenyldithiol, 4-Biphenylthiol, and 11-Mercaptoundecanol on Polycrystalline Silver. *Chem. Mater.* **2004,** 16, 621-628.

50. Weiβ, J.; Himmel, H. J.; Fischer, R. A.; Woll, C., Self-Terminated CVD-Functionalization of Organic Self-Assembled Monolayers (SAMs) with Trimethylamine Alane (TMAA). *Chem. Vap. Deposition* **1998,** 4, (1), 17–21.

51. Winter, C.; Weckenmann, U.; Fischer, R. A.; Kashammer, J.; Scheumann, V.; Mittler, S., Selective Nucleation and Area-Selective OMCVD of Gold on Patterned Self-Assembled Organic Monolayers Studied by AFM and XPS: A Comparison of OMCVD and PVD. *Chem. Vap. Deposition* **2000,** 6, 199-205.

52. Wohlfart, P.; Weiss, J.; Kashammer, J.; Kreiter, M.; Winter, C.; Fischer, R. A.; Mittler-Neher, S., MOCVD of Aluminum Oxide/Hydroxide onto Organic Self-Assembled Monolayers. *Chem. Vap. Deposition* **1999,** 5, 165-170.

53. Wohlfart, P.; Weiss, J.; Kashammer, J.; Winter, C.; Scheumann, V.; Fischer, R. A.; Mittler-Neher, S., Selective Ultrathin Gold Deposition by Organometallic Chemical Vapor Deposition onto Organic Self-Assembled Monolayers (SAMs). *Thin Solid Films* **1999,** 340, 274-279.

54. Aliganga, A. K. A.; Wang, Z.; Mittler, S., Chemical Vapor Deposition of Mercury on Alkanedithiolate Self-Assembled Monolayers. *J. Phys. Chem. B* **2004,** 108, 10949-10954.

55. Bensebaa, F.; Ellis, T. H.; Badia, A.; Lennox, R. B., Probing the Different Phases of Self-Assembled Monolayers on Metal Surfaces: Temperature Dependence of the C–H Stretching Modes *J. Vac. Sci. Technol., A* **1995,** 13, 1331-1336.

56. Herman, I. P., Laser-Assisted Deposition of Thin Films from Gas-Phase and Surface-Adsorbed Molecules. *Chem. Rev.* **1989,** 89, 1323-1357.

57. Beuermann, T.; Stuke, M., Photolysis of Group III (Al, Ga, In) Trimethyl Compounds: Detection of Organic Photofragments CH_3 and C_2H_6 by Picosecond Laser Mass Spectrometry. *Chem. Phys. Lett.* **1991,** 178, 197-203.

58. Beuermann, T.; Stuke, M., Tunable UV Laser Photolysis of Organometallics with Product Detection by Laser Mass Spectrometry: Trimethylaluminum. *Appl. Phys. B* **1989,** 49, 145-148.

59. Motooka, T.; Gorbatkin, S.; Lake, R. E., UV-Laser Photolysis of Trimethylaluminum for Al Film Growth. *J. Appl. Phys.* **1985,** 58, 4397-4401.

60. Motooka, T.; Gorbatkin, S.; Lubben, D.; Eres, D.; Greene, J. E., Mechanisms of Al Film Growth by Ultraviolet Laser Photolysis. *J. Vac. Sci. Technol. A* **1986,** 4, 3146-3152.

61. Bain, C. D.; Troughton, E. B.; Tao, Y.-T.; Evall, J.; Whitesides, G. M.; Nuzzo, R. G., Formation of Monolayer Films by the Spontaneous Assembly of Organic Thiols from Solution onto Gold. *J. Am. Chem. Soc.* **1989,** 111, 321-335.

62. Nuzzo, R. G.; Dubios, L. H.; L., A. D., Fundamental Studies of Microscopic Wetting on Organic Surfaces. 1. Formation and Structural Characterization of a Self-Consistent Series of Polyfunctional Organic Monolayers. *J. Am. Chem. Soc.* **1990,** 112, 558-569.

63. Soto, C.; Tysoe, W. T., The Reaction Pathway for Growth of Alumina on High Surface Area Alumina and In Unltrahigh Vacuum by a Reaction between Trimethylaluminum and Water. *JOURNAL OF Vacuum Science and Technology, A* **1991,** 9, 2686-2695.

64. Vickerman, J. C., *ToF SIMS: Surface Analysis by Mass Spectrometry.* IM Publications and Surface Spectra Limited: Chichester and Manchester, UK, 2001; p 1-40.

65. Walker, A. V.; Tighe, T. B.; Haynie, B. C.; Uppili, S.; Allara, D. L.; Winograd, N., Chemical Pathways in the Interactions of Reactive Metal Atoms with Organic Surfaces: Vapor Deposition of Ca and Ti on a Methoxy-Terminated Alkanethiolate Monolayer on Au. *J. Phys. Chem. B* **2005,** 109, 11263-11272.

66. van den Brand, J.; Snijders, P. C.; Sloof, W. G.; Terryn, H.; de Wit, J. H. W., *J. Phys. Chem. B* **2004,** 108, 6017-6024.

67. Lewinski, J.; Zachara, J.; Justyniak, I., Structural Aspects of the Aluminum-Carboxylate Interaction. Molecular Structure of the Tetranuclear $[(AlMe_2)_2(\mu\text{-}O_2C)_2\text{-}1,2\text{-}C_6H_4]_2$ Adduct. *Inorg. Chem* **1998,** 37, 2575-2577.

68. Soto, C.; Wu, R.; Bennett, D. W.; Tysoe, W. T., Infrared Spectroscopy of Trimethylaluminum and Dimethylaluminum chloride Adsorbed on Alumina. *Chem. Mater.* **1994,** 6, 1705-1711.

69. Parker, J. K.; Nelson, H. H., Kinetics and Thermodynamics of the Al + Trimethylaluminum Reaction. *Chem. Phys. Lett.* **2002,** 360, 313-319.

70. Kobayashi, M.; Sato, A.; Tanaka, Y.; Shinohara, H.; Sato, H., Photodissociation of

Multiayered Trimethylaluminum Adsorbed on a Cryogenic Substrate: a Time-of-Flight Mass-Spectrometry Study. *Appl. Organometal. Chem.* **1993,** 7, 303-309.

71. Zhang, Y.; Terrill, R. H.; Tanzer, T. A.; Bohn, P. W., Ozonolysis Is the Primary Cause of UV Photooxidation of Alkanethiolate Monolayers at Low Irradiance. *J. Am. Chem. Soc.* **1998,** 120, 2654-2655.

72. Chowdhuri, A. R.; Takoudisa, C. G., Metalorganic Chemical Vapor Deposition of Aluminum Oxide on Si: Evidence of Interface SiO_2 Formation. *Appl. Phys. Lett.* **2002,** 80, 4241-4243.

73. Ault, B. S., Matrix Isolation Investigation of the Reaction of $(CH_3)_3Al$ with O_2. *J. Organomet. Chem.* **1999,** 572, 169-175.

74. Xu, Y.; Musgrave, C. B., A DFT Study of the Al2O3 Atomic Layer Deposition on SAMs: Effect of SAM Termination. *Chem. Mater.* **2004,** 16, 646-653.

75. Strongin, D. R.; Comita, P. B., Surface Chemistry of Dlmethylalumlnum Hydride and Trimethylaluminum on Polycrystalline Aluminum. *J. Phys. Chem.* **1991,** 95, 1329-1333.

Chapter 5

Electroless Deposition of Copper on Functionalized Alkanethiolate Self-Assembled Monolayers

[Portions of this work have been published previously by Peng Lu and Amy V. Walker, *Langmuir*, **2007**, 2*3*, 12577-12582]

Abstract: The reaction pathways involved in the electroless deposition of copper on -COOH, -CH_3 and -OH terminated SAMs were investigated using time-of-flight secondary ion mass spectrometry (TOF SIMS) and scanning electron microscopy (SEM). Cu^{2+} ions formed Cu^{2+}-carboxylate complexes on -COOH terminated SAMs. Copper was deposited on -COOH terminated SAMs at 22 °C and 45 °C from the reduction of Cu^{2+}-carboxylate complexes. However, deposited Cu was not stabilized on -COOH terminated SAMs, and continued to penetrate to the Au/S interface after deposition. On -CH_3 terminated SAMs, Cu^{2+} containing ions only weakly adsorbed on the SAM surface. Copper was deposited on -CH_3 terminated SAMs at 22 °C but not at 45 °C because Cu^{2+} containing ions were not adsorbed stably on the SAM surface at 45 °C. Copper did not deposit on -OH terminated SAMs, because the hydroxyl terminal groups on the SAMs reacted with the reducing agent formaldehyde in plating solution to form acetals which prevented Cu deposition.

5.1 Introduction

Since the mid 1990s, copper has been used as interconnects in microchips and for wiring.[1-4] Copper is therefore of great interest to make metalized organic layers for applications in molecular/organic electronics[5-18] and other polymeric structures. However, it is difficult to understand and control the interaction of copper with polymers because the polymer surface can not be systematically controlled.[19-21] Self-assembled monolayers (SAMs) have highly organized structures with a uniform surface density of terminal groups.[22-25] They are thus ideal model systems for studying the interaction of copper with organic substrates.

Physical vapor deposition (PVD) is usually employed to deposit metals on polymers and SAMs.[26-46] The interactions between vapor-deposited copper and functionalized SAMs with -COOH,[26, 27, 40, 47, 48] -CO_2CH_3,[31, 35, 40] -OH,[33, 38, 40] -OCH_3,[40, 44, 45] and -CH_3[31, 40, 49] terminal groups have been studied. On -COOH, -OH, and -CO_2CH_3 terminated SAMs, there is a competition between Cu insertion into the C-O bonds of the terminal groups, stabilization at the SAM/vacuum interface via the formation of weak complexes, and penetration to the Au/S interface.[40] On -OCH_3 terminated SAMs, copper interacts weakly with the terminal groups and simultaneously penetrates through the SAM to the Au/S interface.[40, 44, 46] Copper penetrates through the -CH_3 terminated SAMs but does not interact with the terminal methyl group.[31, 40, 49] On polymer surfaces, Cu also only weakly interacts with polymers, leading to poor interfacial adhesion and penetration of copper into the polymer film.[19, 40, 50]

Compared to PVD, electroless deposition is a soft deposition technique and thus has several potential advantages. First, electroless deposition can be performed at low temperatures (≤ 50 °C) and thus has the potential to reduce or eliminate copper penetration through SAMs.[51, 52] Second, as a solution phase technique, electroless deposition is convenient, inexpensive, and can be easily adapted to large area processing.

Several studies of copper electroless deposition on SAMs were reported.[51-53] Zangmeister and van Zee[52] observed that copper was deposited on 4-mercaptobenzoic acid SAMs but not on octadecanethiolate or 3-mercaptobenzoic SAMs. They proposed that Cu^{2+} ions complexed with the deprotonated -COOH groups on the 4-mercapbenzoic acid SAM surface, but were sterically hindered from forming complexes with the carboxylic groups on the 3-mercapbenzoic acid SAM. Once the surface copper complex had formed, it was reduced by formaldehyde to deposit copper metal on the SAMs. Garno *et al.*[51] also observed that copper could be deposited on -COOH terminated SAMs. They also noted that small amount of copper was deposited on $-CH_3$ terminated SAMs but no copper was deposited on -OH terminated SAMs.

In this chapter, the electroless deposition of copper on functionalized SAMs was investigated. In agreement with previous studies,[51] we observed that copper deposited on both $-CH_3$ and -COOH terminated SAMs but not on -OH terminated SAMs. However, copper was observed to penetrate both $-CH_3$ and -COOH terminated SAMs, indicating that the use of electroless deposition did not prevent copper penetration as previously suggested.[51, 52] In addition, deposited copper was not stabilized on the SAMs, and copper

continued to penetrate through the SAMs after removal from the plating solution. Finally, we have shown that formaldehyde reacted with the hydroxyl groups on the -OH terminated SAMs to form acetals. The acetals prevented the formation of stable Cu^{2+}-SAM complexes, so no copper was deposited on the -OH terminated SAMs.

5.2 Experimental

5.2.1 Materials

Copper sulfate (≥ 99%), ethylene-1-diamine tetraacetic acid (EDTA) disodium salt dehydrate (≥ 99.0%), formaldehyde (37 wt% in water) and sodium hydroxide (≥ 98%, pellets) were purchased from Sigma Aldrich (Saint Louis, MO). Gold and chromium were obtained from Alfa Aesar Inc. and were of 99.995% purity. Hexadecanethiol (HDT) (99%), 16-mercaptohexadecanoic acid (MHA) (99%), and mercaptohexadecanol (MHL) (99%) were purchased from Asemblon, Inc. (Redmond, WA). Anhydrous ethanol (A.C.S. grade) was obtained from Aaper Alchohol (Shelbyville, KY). Native silicon oxide wafers (<111> orientation) were purchased from Addison Technologies, Inc. (Pottstown, PA) and were cleaned with piranha etch (H_2SO_4:H_2O_2 = 3:1) before use. All chemicals were used as-received and without further purification.

5.2.2 SAMs Preparation

Alkanethiolate SAMs adsorbed on gold substrates were prepared using previously published methods.[54-56] Briefly, first Cr (~ 5 nm) and then Au (~ 100 nm) were thermally deposited onto clean Si native oxide wafers. The prepared Au substrates were then

immersed into a 1 mM ethanolic solution of the relevant alkanethiolate molecule for 24 h at ambient temperature (21 ± 2 °C) to prepare well-organized SAMs. For each batch, one sample (~ 1 cm × 1 cm) was taken and characterized using single-wavelength ellipsometry (Gaertner Scientific Corp., Skokie, IL) and TOF SIMS (ION TOF Inc., Chestnut Hill, NY) prior to electroless deposition to ensure that the SAMs were free of significant chemical contamination.

5.2.3 Copper Electroless Deposition

The plating solution was prepared using 4 mM $CuSO_4$, 10 mM EDTA disodium salt, and 10 mM formaldehyde. Before the addition of formaldehyde, the pH of the solution was adjusted to 12.8 with sodium hydroxide. It was used immediately after preparation. After addition of formaldehyde, samples were immersed in the plating solution for 60 min at 22 °C and 45 °C. After removed from the solution, samples were rinsed thoroughly with copious deionized water and absolute ethanol, and dried with nitrogen gas. Samples were then immediately transferred to TOF SIMS or SEM for analysis.

To study the interaction between the plating solution and hydroxyl terminated SAMs, samples were immersed in four different solutions containing one component from the plating solution at 22 °C for 60 min. The solutions were 4 mM $CuSO_4$, 10 mM EDTA disodium salt, 10 mM formaldehyde, and NaOH. The pH of each solution is adjusted to 12.8 with NaOH to mimic the plating conditions.

5.2.4 Time-of-Flight Secondary Ion Mass Spectrometry (TOF SIMS)

An ION TOF IV spectrometer (ION TOF Inc., Chestnut Hill, NY) equipped with a Bi

liquid metal ion gun was employed. Briefly, this instrument consists of an air lock, a preparation chamber and an analysis chamber, each separated by gate valves. The pressure of the preparation and analysis chambers were maintained at $\leq 3.8 \times 10^{-9}$ mbar. The primary ions used in the analysis were Bi^{+} ions, which were accelerated to 25 keV and contained within a ~100 nm diameter probe beam. The analysis area was (100 × 100) μm^2. The total accumulated primary ion dose was less than 10^{11} ions cm^{-2} and so all the spectra were acquired within the static regime.[57] The ejected secondary ions were extracted into a time-of-flight mass spectrometer with a 2000V potential and were reaccelerated to 10 keV before reaching the detector. Peak intensities were reproducible to within ± 10% from scan to scan and from sample to sample. For each electroless deposition experiment, at least two samples were prepared and three areas on each sample were examined. Each presented data point is an average over at least six measurements.

A video camera (ExwaveHAD, Sony) mounted in the TOF SIMS analysis chamber was employed to obtain optical images.

5.2.5 Scanning Electron Microscopy (SEM)

SEM measurements were conducted on a Field Emission Scanning Electron Microscope (Hitachi s-4500) equipped with a NORAN Instruments energy dispersive x-ray (EDX) microanalysis system, a back scattering detector and a mechanical straining stage.

5.3 Results

5.3.1 Copper Electroless Deposition on -COOH and -CH_3 Terminated SAMs

After 60 min deposition at 22 °C, SEM and optical images showed that copper was deposited on both -COOH and -CH_3 terminated SAMs (Figure 5.1). In agreement with previous studies,[52] copper crystallites of several micrometers in diameter were observed on the -COOH and -CH_3 terminated SAM surfaces. In the TOF SIMS spectra, Cu-containing ions, including Cu_x^+ (x = 1-3), were observed, indicating that copper has deposited on these SAMs (Figure 5.2). For -COOH terminated SAMs, $CuCOO(CH_2)_x^+$ ions were observed in the positive ion TOF SIMS spectra, suggesting that copper weakly interacted with carboxylic terminal groups (Figure 5.3). No $Cu_xO_y^{\pm}$ ions were observed, indicating that copper did not form a strong complex with the -COOH group by insertion into the C-O bond. There was no evidence that copper interacted with the -CH_3 terminal groups: no $Cu(CH)_x(CH_2)_y^{\pm}$ ions were observed.

When the deposition was performed at 45 °C, the intensities of copper ions (Cu^+) and copper-containing ions ($CuCOO(CH_2)_x^+$) increased for -COOH terminated SAMs, suggesting that more copper has deposited on the surface (Figure 5.2, Figure 5.3, Appendix A5.3). No Cu_x^+ (x = 1-3) ions were observed on -CH_3 terminated SAMs, indicating that copper has not deposited on the SAM at this temperature (Figure 5.2, Appendix A5.1).

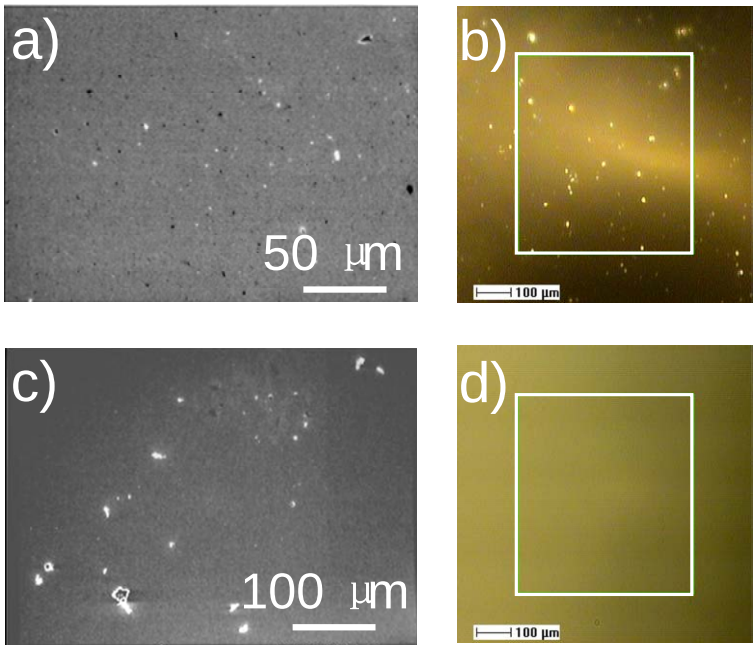

Figure 5.1 (a, c) SEM and (b, d) optical images after copper electroless deposition at 22 °C for 1h on (a, b) -COOH and (c, d) -CH_3 terminated SAMs. The white patches in the SEM images indicate that copper crystallites have formed. In the optical images the size of the white box is 500 × 500 μm^2.

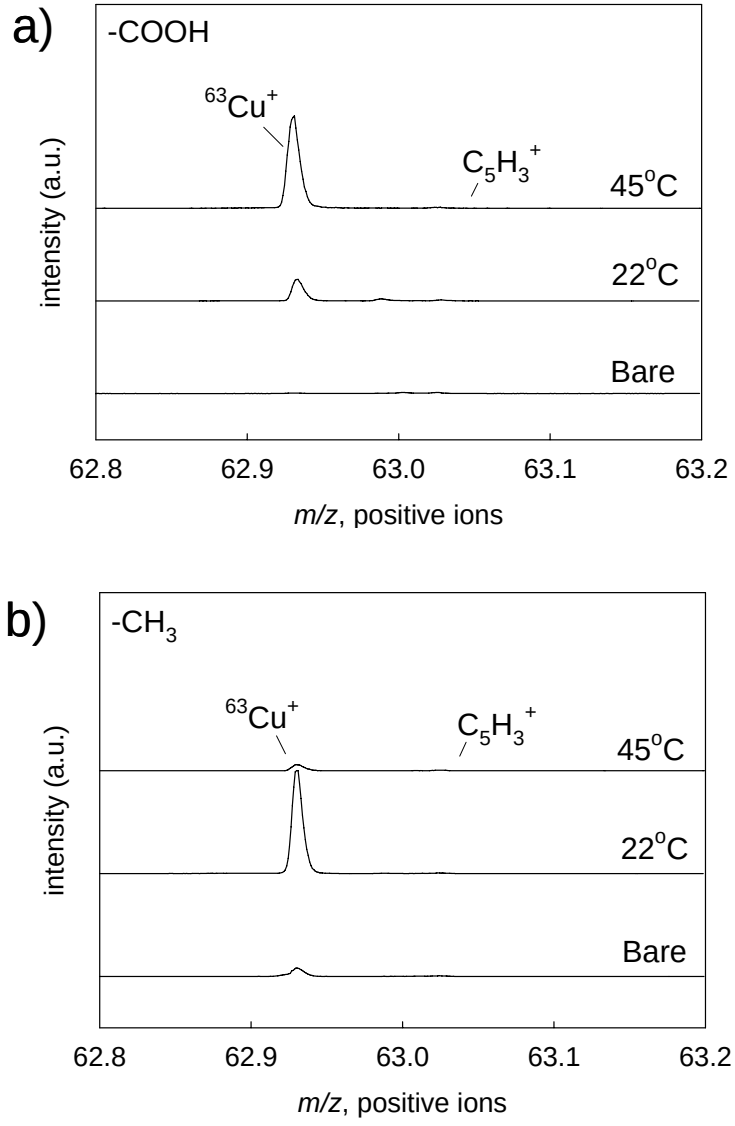

Figure 5.2 High mass resolution positive ion TOF SIMS spectra of $^{63}Cu^+$ (nominal mass *m/z* 63), on -COOH and -CH_3 terminated SAMs prior to and after Cu electroless depositions for 1 h at 22 °C and 45 °C. The mass spectra were normalized to the intensity of the $C_5H_3^+$ ion signal to make clear the changes in the mass spectra upon Cu deposition.

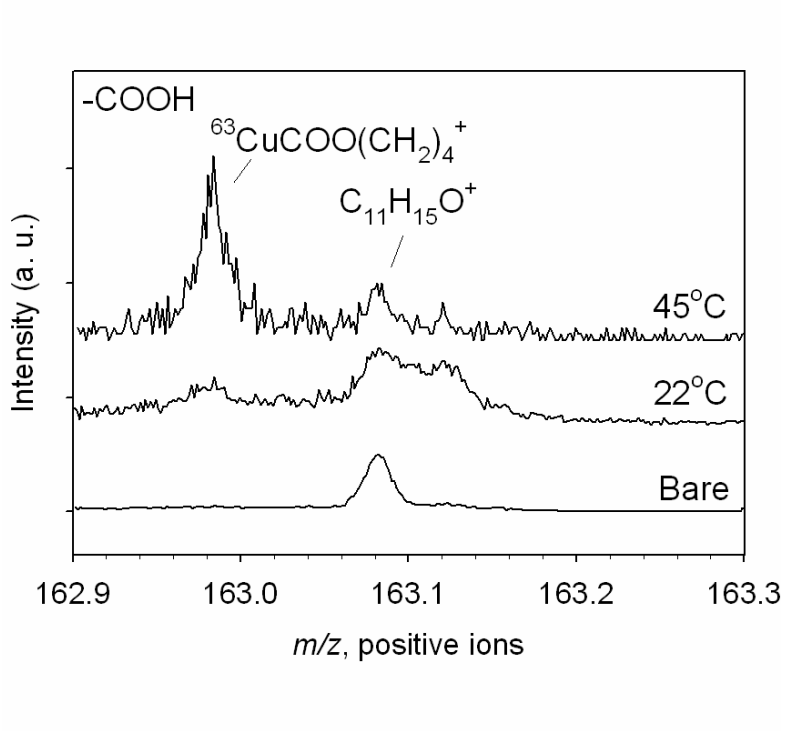

Figure 5.3 High mass resolution positive ion TOF SIMS spectra of $^{63}CuCOO(CH_2)_4^+$ (nominal mass *m/z* 163), on -COOH terminated SAMs prior to and after Cu electroless depositions for 1 h at 22 °C and 45 °C. The ions were assigned based on accurate mass and fragmentation mechanism, and they were not structurally characterized. The mass spectra were normalized to the intensity of the $C_{11}H_{15}O^+$ ion signal to make clear the changes in the mass spectra upon Cu deposition.

Similar to the vapor deposition of Cu on SAMs, copper was also observed to penetrate through the monolayer to the Au/S interface after electroless deposition. In the positive ion mass spectra, $CuSH_2^+$ ions were observed after 60 min deposition at 22 °C and 45 °C on both -COOH and -CH_3 terminated SAMs (Figure 5.4). For -COOH terminated SAMs, the $CuSH_2^+$ ion signal intensity greatly increased at 45 °C compared to 22 °C, indicating that more copper penetrated to the Au/S interface. For -CH_3 terminated SAMs, the intensity of $CuSH_2^+$ ion signal after 45 °C deposition was negligible, confirming that Cu did not deposit on the -CH_3 terminated SAMs.

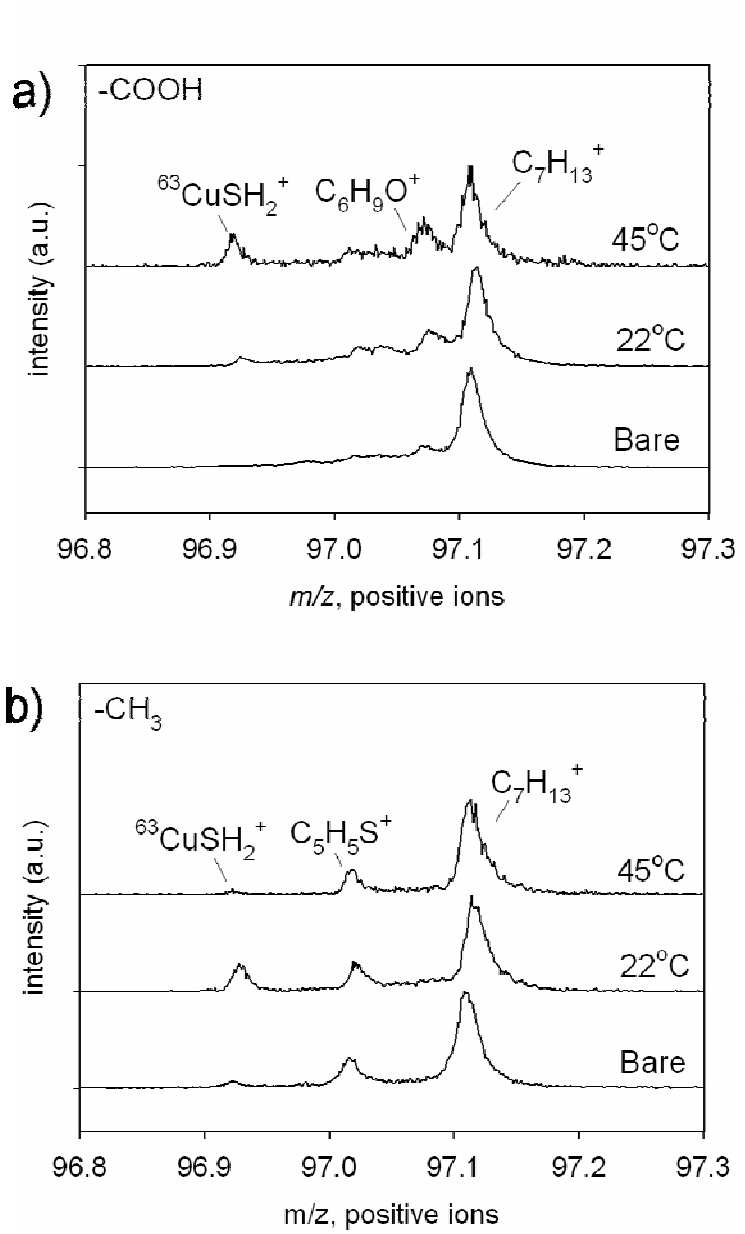

Figure 5.4 High mass resolution positive ion TOF SIMS spectra of $^{63}CuSH_2^+$ (nominal mass *m/z* 97) for (a) -COOH and (b) -CH_3 terminated SAMs prior to and after Cu electroless depositions for 1h at 22 °C and at 45 °C. The ion intensities were normalized to the intensity of $C_7H_{13}^+$ to make clear the changes in the mass spectra upon Cu deposition.

5.3.2 Stability of Cu Deposited on -COOH Terminated SAMs

If the copper is stabilized at the SAM/vacuum (air) interface, it is expected that the intensities of the ions characteristic of the Cu-carboxylate interaction would remain approximately constant with time. In contrast, if the fragment ion intensities change significantly over time, it indicates that copper is not stabilized at the SAM terminal group and is diffusing to the Au/S interface. After deposition, the intensity of $CuCOO(CH_2)_4^+$ ion, which is indicative of copper interaction with -COOH terminal groups, decreased significantly with time (Figure 5.5 a). For samples plated at 22 °C and 45 °C, the intensities of the $CuCOO(CH_2)_4^+$ ion were ~50% and ~60%, respectively, after 2800 min (48 h) of deposition (Figure 5.5 a). At the same time, the intensity of $CuSH_2^+$ ion, which is characteristic of Cu penetration, increased with time (Figure 5.5 b). The ion intensity of $CuSH_2^+$ increased approximately 200% over 48 h when deposition was performed at 45 °C, and slightly increased after deposition at 22 °C (Figure 5.5 b). These observations suggest that the deposited copper was not stabilized on the -COOH terminated SAMs but slowly penetrated through the SAMs to the Au/S interface after deposition.

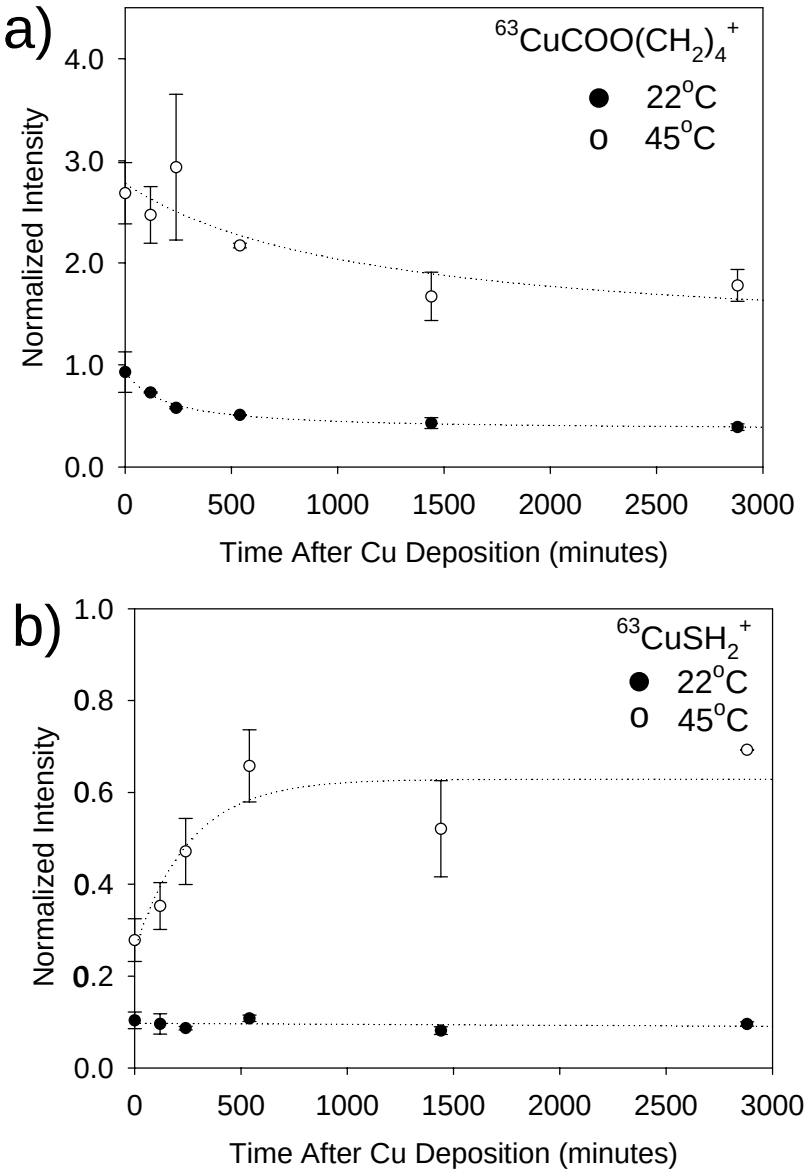

Figure 5.5 Integrated SIMS ion peak intensities of (a) $^{63}CuCOO(CH_2)_4^+$ and (b) $^{63}CuSH_2^+$ plotted versus time after Cu electroless depositions for 1h at 22 °C and 45 °C. The intensities of the $^{63}CuCOO(CH_2)_4^+$ and $^{63}CuSH_2^+$ were normalized to $C_{11}H_{15}O^+$ and $C_7H_{13}^+$ respectively to make clear the changes in the SIMS spectra upon Cu electroless deposition. The dotted lines are drawn to guide the eyes.

5.3.3 Copper Electroless Deposition on -OH terminated SAMs

In agreement with previous studies,[51] copper did not deposit on -OH terminated SAMs after electroless deposition. After 60 min deposition at 22 °C and 45 °C, no evidence of copper deposition on -OH terminated SAMs was observed in the TOF SIMS spectra: Cu_x^+ (x = 1-3), or other copper containing ions, were not observed (Figure 5.7). In addition, the SEM and optical images show that after electroless deposition, there were speckled areas on the SAM, suggesting that the -OH terminated SAM has been damaged (Figure 5.6). Together, these observations indicate that -OH terminated SAMs reacted with the plating solution, and the reaction prevented copper deposition.

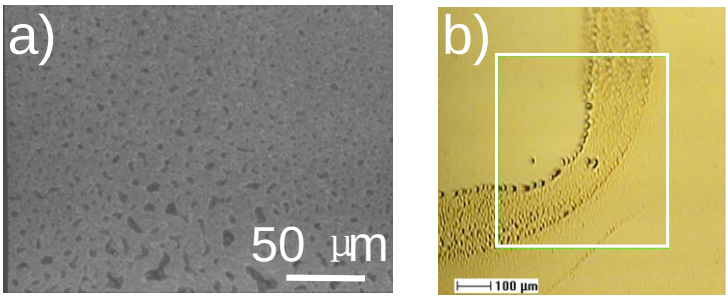

Figure 5.6 (a) SEM and (b) optical images after copper electroless deposition at 22 °C for 1h on -OH terminated SAMs. In the optical images the size of the white box is 500 × 500 μm^2.

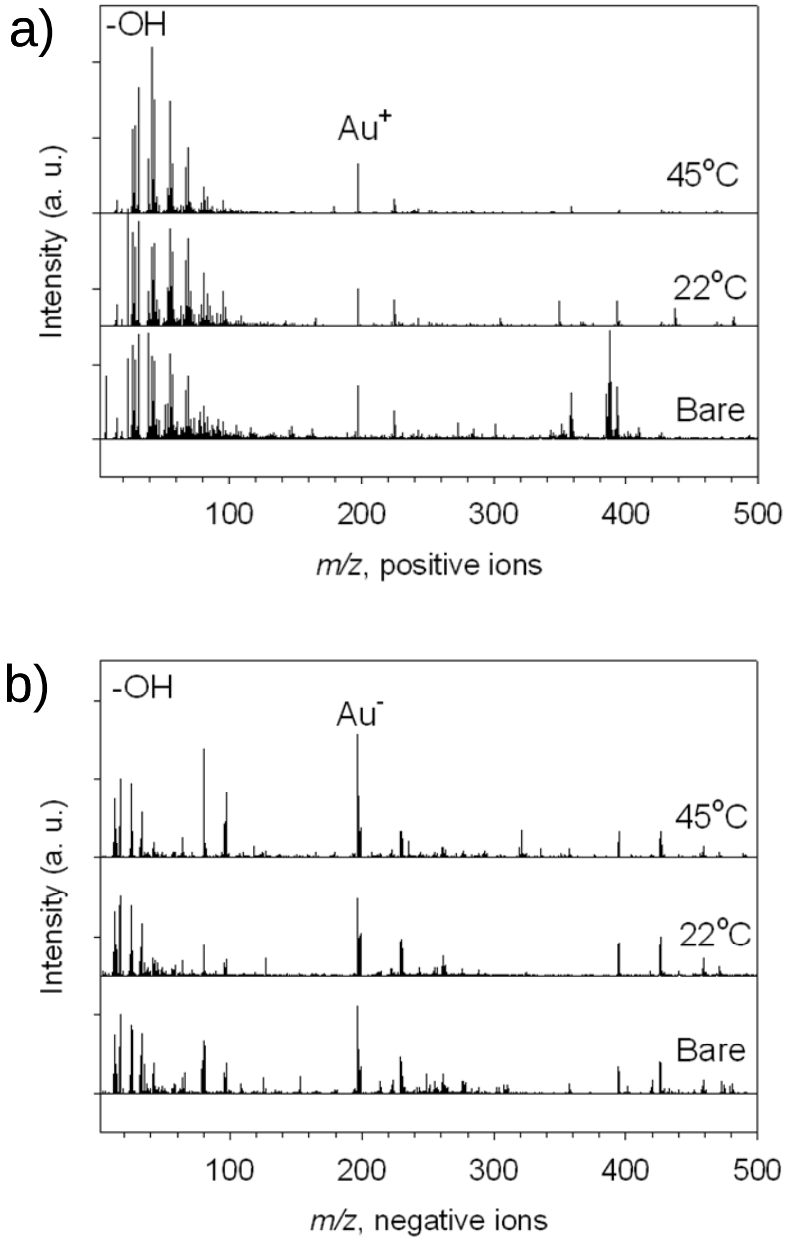

Figure 5.7 (a) Positive, (b) Negative ion TOF SIMS spectra (*m/z* 2-500) for -OH terminated SAMs prior to and after Cu electroless depositions at 22 °C and at 45 °C for 1 h.

To investigate the interactions between -OH terminated SAMs and the plating solution, SAM samples were immersed in solutions containing the individual components of the deposition bath for 1 h at 22 °C. The solutions tested were 4 mM $CuSO_4$, 10 mM EDTA disodium, 10 mM formaldehyde, and 100mM NaOH. The pH of each solution was kept at 12.8 to mimic the plating conditions. After immersion in the copper sulfate solution, the positive TOF SIMS spectra indicate that Cu^{2+} ions had adsorbed on -OH terminated SAMs. This suggests that it was not the adsorption of Cu ions on the -OH terminated SAMs which prevented the electroless deposition of Cu. No reaction was observed between -OH terminated SAMs and either EDTA or NaOH solutions (data not shown). However, the data indicate that formaldehyde reacted with -OH terminated SAMs. In the positive ion mass spectra, ions of the form of $[(CH_2)_xO\text{-}(CH_2)\text{-}O(CH_2)_x]^+$ were observed, indicating that acetals had formed on the SAM surface (Figure 5.8). It is likely that this reaction prevented the deposition of copper on -OH terminated SAMs.

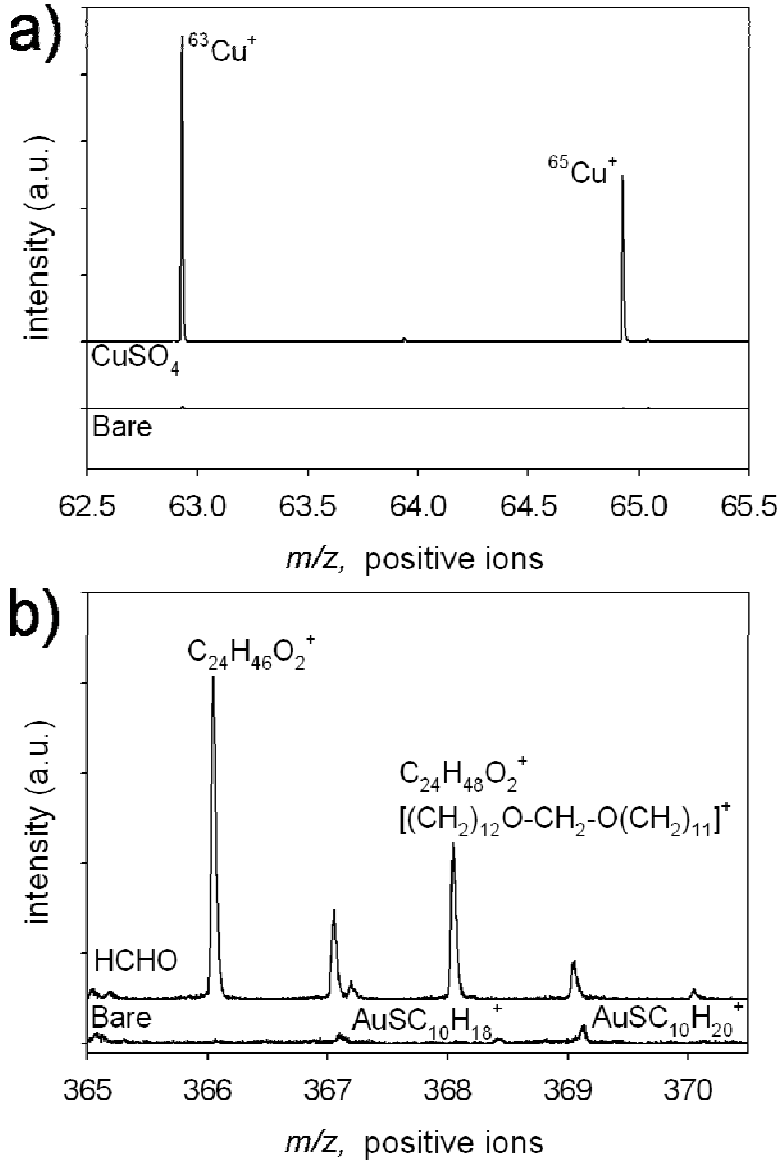

Figure 5.8 High resolution positive ion TOF SIMS spectra of (a) Cu^+ (nominal masses *m/z* 63, 65) and (b) $[(CH_2)_{12}O\text{-}CH_2\text{-}O(CH_2)_{11}]^+$ (nominal mass *m/z* 368) after immersion of -OH terminated SAMs in $CuSO_4$ and HCHO solutions, respectively, at 22 °C for 1h. The ions were assigned based on accurate mass and fragmentation mechanism, and they were not structurally characterized.

5.4 Discussion

In general, copper electroless deposition on semiconductors and metals is believed to proceed *via* two half-cell reactions in the presence of formaldehyde:

$$2HCHO + 4OH^- \rightarrow 2HCOO^- + H_2 + 2\,H_2O + 2e^-$$

$$CuEDTA^{2-} + 2e^- \rightarrow Cu + EDTA^{4-}$$

While there have been many studies on the electroless deposition of copper, no definitive mechanism has been established.[58-60]

In the studies by Zangmeister and van Zee,[52] a mechanism involving the reduction of a copper-SAM complex by formaldehyde was proposed. Based on this mechanism, we propose the following reaction pathways for copper electroless deposition on functionalized SAMs. Upon immersion in the plating solution, Cu^{2+} ions form complexes with -COOH terminal groups (Figure 5.3). Cu^{2+} ions only weakly adsorb on -CH_3 terminated SAMs. A Cu^{2+}-SAM complex can not form on -OH terminated SAMs because the -OH terminal groups react with formaldehyde to form acetals, which prevent Cu^{2+} ions complexing with the -OH terminated SAMs (Figure 5.8). The pH of the plating solution (~12.8) is higher than the pKa of hexadecanoic acid films (~8.5 - 8.8),[61] and thus it is likely that many of the -COOH groups on the SAM have deprotonated and complexed with Cu^{2+} ions. Once formed, the Cu^{2+}-carboxylate complexes are reduced to copper by formaldehyde (Scheme 5.1). Additional Cu^{2+} ions can then adsorb on the copper surface and be reduced.[58]

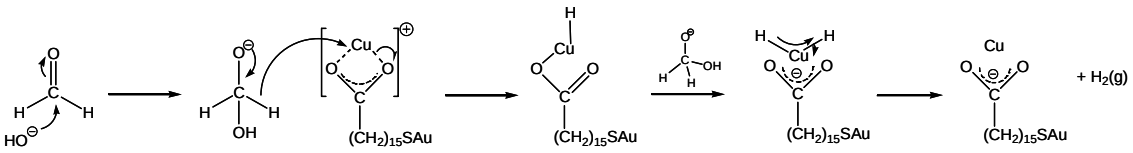

Scheme 5.1 Formaldehyde reduction of Cu^{2+} complexed to the terminal group of -COOH terminated SAMs.

This mechanism explains two experimental observations. First, copper crystallites rather than a smooth copper film were observed. The equilibrium constant between Cu^{2+} and carboxylic acid is very low (< 100)[62] compared with the binding constant of Cu^{2+} and EDTA (5×10^{18} at experimental conditions).[63] Given the large EDTA concentration in the plating solution, few Cu^{2+}-carboxylate complexes form and thus are sparsely distributed on the -COOH terminated SAM. These complexes provide nucleation sites for further copper deposition, and thus copper crystallites were observed to grow rather than a smooth copper film. Second, at 45 °C Cu^{2+} ions could still form complexes with -COOH terminated SAMs. However, the interaction between Cu^{2+} and $-CH_3$ terminal groups is very weak, and so Cu^{2+} ions are not stabilized on the SAM surface. Thus copper deposits on -COOH terminated SAMs but not on $-CH_3$ terminated SAMs at 45 °C.

Finally, the increase in the amount of Cu penetration through -COOH terminated SAMs at 45 °C can be explained in the following way. Self-assembled monolayers are able to diffuse on the surface, generating transient defects. In agreement with the hopping mechanism proposed by Walker, Allara, Winograd and co-workers,[29, 34, 44] as the

temperatures of the bath increases the diffusion rate of the SAM increases, creating more transient defects which lead to an increase in the Cu penetration through the monolayer.

5.5 Conclusions

In summary, the reaction pathways involved in the electroless deposition of Cu on functionalized alkanethiolate SAMs are as follows. Upon immersion in the plating solution, Cu^{2+} ions form weak complexes with $-CH_3$ and -COOH terminated SAMs, but not with -OH terminated SAMs. This is because -OH terminal groups react with formaldehyde in the plating solution to form acetals, which prevent Cu^{2+} adsorption. Once formed, the surface Cu complexes can be reduced to Cu^0 by formaldehyde. As the deposition proceeds, additional Cu^{2+} ions adsorb on the copper surface and are reduced. After electroless deposition, scattered copper crystallites form on $-CH_3$ and -COOH terminated SAMs. This is because the association constants of Cu^{2+} with the terminal groups are very low, and thus the Cu^{2+} surface complexes that act as copper nucleation sites are sparsely distributed on the SAM surface.

For a successful electroless deposition on SAMs, two requirements must be considered. First, the deposition should be selective. Our studies indicate that the selectivity of copper electroless deposition can be controlled by varying the SAMs terminal functionality and the reaction temperature. Second, the deposited copper layer should be stabilized at the SAM/air interface. In this study, copper was observed to penetrate through the monolayer to the Au/S interface during the deposition and

continued to penetrate through the SAM even after removal from the plating solution. In order to fabricate stable metal/SAM junctions for use in molecular architectures, an alternative copper electroless deposition process that leads to the formation of stable metal overlayers with negligible metal atom penetration must be developed. A potential solution is to speed up the reaction by adding organic additives and/or forming a catalyst seed layer. In this case the Cu penetration is decreased because the Cu-Cu interaction is so strong.[27]

Appendix: Positive and negative ion mass spectra (*m/z* = 2-500) of -CH_3 and -COOH, SAMs prior to and after Cu electroless deposition at 22 °C and 45°C: These figures can be found in Appendix Figures A5.1-A5.4.

5.6 References

1. Li, J.; Seidel, T. E.; Mayer, J. W., Copper Based Metallization in ULSI Structures 2. Is Cu Ahead of Its Time as an On-Chip Interconnect Material. *MES Bulletin* **1994,** 19, 15-18.

2. Lin, X. W.; Pramanik, D., Future Interconnect Technologies and Copper Metallization. *Solid State Tech.* **1998,** 41, 63-69.

3. Gutmanna, R. J.; Chow, T. P.; Kaloyeros, A. E.; Lanford, W. A.; Muraka, S. P., Thermal Stability of On-Chip Copper Interconnect Structures. *Thin Solid Films* **1995,** 262, 177-186.

4. Monteiro, O. R., Novel Metallization Technique for Filling 100-nm-Wide Trenches and Vias with Very High Aspect Ratio *J. Vac. Sci. Technol. B* **1999,** 17, 1094-1097.

5. Aviram, A., Molecules for Memory, Logic, and Amplification. *J. Am. Chem. Soc.* **1988,** 110, 5687-5692.

6. Avouris, P., Molecular Electronics with Carbon Nanotubes. *Acc. Chem. Res.* **2002,** 35, 1026-1034.

7. Chen, J.; Reed, M. A., Electronic Transport of Molecular Systems. *Chem. Phys.* **2002,** 281, 127-145.

8. Chen, J.; Reed, M. A.; Rawlett, A. M.; Tour, J. M., Large On-Off Ratios and Negative Differential Resistance in a Molecular Electronic Device. *Science* **1999,** 286, 1550-1552.

9. Chen, J.; Wang, W.; Reed, M. A.; Rawlett, A. M.; Price, D. W.; Tour, J. M., Room-Temperature Negative Differential Resistance in Nanoscale Molecular Junctions. *Appl. Phys. Lett.* **2000,** 77, 1224-1226.

10. Collier, C. P.; Mattersteig, G.; Wong, E. W.; Luo, Y.; Beverly, K.; Sampaio, J.; Raymo, F. M.; Stoddart, J. F.; Heath, J. R., A [2]Catenane-Based Solid State Electronically Reconfigurable Switch. *Science* **2000,** 289, 1172-1175.

11. Lau, C. N.; Stewart, D. R.; Williams, R. S.; Bockrath, M., Direct Observation of Nanoscale Switching Centers in Metal/Molecule/Metal Structures. *Nano Lett.* **2004,** 4, 569-572.

12. Metzger, R. M., Unimolecular Electrical Rectifiers. *Chem. ReV.* **2003,** 103,

3803-3834.

13. Metzger, R. M.; Chen, B.; Hopfner, U.; Lakshmikantham, M. V.; Vuillaume, D.; Kawai, T.; Wu, X.; Tachibana, H.; Hughes, T. V.; Sakurai, H.; Baldwin, J. W.; Hosch, C.; Cava, M. P.; Brehmer, L.; Ashwell, G. J., Unimolecular Electrical Rectification in Hexadecylquinolinium Tricyanoquinodimethanide. *J. Am. Chem. Soc.* **1997,** 119, 10455-10466.

14. Ratner, M. A.; Davis, B.; Kemp, M.; Mujica, V.; Roitberg, A.; Yaliraki, S., Molecular Wires: Charge Transport, Mechanisms, and Control. *Ann. N. Y. Acad. Sci.* **1998,** 852, 22-37.

15. Reed, M. A., Molecular-Scale Electronics. *Proc. IEEE* **1999,** 87, 652-658.

16. Reinerth, W. A.; Jones, L., II.; Burgin, T. P.; Zhou, C.-W.; Muller, C. J.; Deshpande, M. R.; Reed, M. A.; Tour, J. M., Molecular Scale Electronics: Syntheses and Testing *Nanotechnology* **1998,** 9, 246-250.

17. Tour, J. M.; Reinerth, W. A.; Jones, L., II.; Burgin, T. P.; Zhou, C.-W.; Muller, C. J.; Deshpande, M. R.; Reed, M. A., Recent Advances in Molecular Scale Electronics. *Ann. N. Y. Acad. Sci.* **1998,** 852, 197-205.

18. Metzger, R. M., Hexadecylquinolinium Tricyanoquinodimethanide, a Unimolecular Rectifier Between 370 and 105 K and its Spectroscopic Properties. *AdV. Mater. Opt. Electron.* **1999,** 9, 253-263.

19. Zaporojtchenko, V.; Strunksus, T.; Behnke, K.; von Bechtolsheim, C.; Kiene, M.; Faupel, F., Metal/Polymer Interfaces with Designed Morphologies *J. Adhes. Sci.*

Technol. **2000,** 14, 467-490.

20. Walker, A. V.; Fisher, G. L.; Hooper, A. E.; Tighe, T.; Opila, R. L.; Winograd, N.; Allara, D. L., Metallization of Polymers 2. **2002**, pp 117-126.

21. Prissanaroon, W.; Brack, N.; Pigram, P. J.; Liesegang, J., Electropolymerization of DBSA-Doped Polypyrrole Films on PTFE via an Electroless Copper Interlayer. *Surf. Interface Anal.* **2003,** 35, 974-983.

22. Schreiber, F., Structure and Growth of Self-Assembling Monolayers. *Prog. Surf. Sci.* **2000,** 65, 151-256.

23. Ulman, A., An Introduction to Ultrathin Organic Films: From Langmuir-Blodgett to Self-Assembly. *Academic Press: New York* **1991**, 237-304.

24. Ulman, A., Formation and Structure of Self-Assembled Monolayers. *Chem. Rev.* **1996,** 96, 1533-1554.

25. Dubios, L. H.; Nuzzo, R. G., *Annu. Rev. Phys. Chem.* **1992,** 43, 437-463.

26. Czanderna, A. W.; King, D. E.; Spaulding, D., Metal Overlayer on Organic Functional Group of Self-Organized Molecular Assemblies. 1. X-ray Photoelectron Spectroscopy of Interaction of Cu/COOH on 11-Mercaptoundecanoic Acid. *J. Vac. Sci. Technol., A* **1991,** 9, 2607-2613.

27. Dake, L. S.; King, D. E.; Czanderna, A. W., Ion Scattering and X-Ray Photoelectron Spectroscopy of Copper Overlayers Vacuum Deposited onto Mercaptohexadecanoic Acid Self-Assembled Monolayers. *Solid State Sci.* **2002,** 2, 781-789.

28. Fisher, G. L.; Hooper, A. E.; Opila, R. L.; Jung, D. R.; Allara, D. L.; Winograd, N.,

The Interaction between Vapor-Deposited Al Atoms and Methylester-Terminated Self-Assembled Monolayers Studied by Time-of-Flight Secondary Ion Mass Spectrometry, X-Ray Photoelectron Spectroscopy and Infrared Reflectance Spectroscopy. *J. Electron Spectrosc. Relat. Phenom.* **1998,** 98-99, 139-148.

29. Fisher, G. L.; Walker, A. V.; Hooper, A. E.; Tighe, T. B.; Bahnck, K. B.; Skriba, H. T.; Reinard, M. D.; Haynie, B. C.; Opila, R. L.; Winograd, N.; Allara, D. L., Bond Insertion, Complexation, and Penetration Pathways of Vapor-Deposited Aluminum Atoms with HO- and CH_3O-Terminated Organic Monolayers. *J. Am. Chem. Soc.* **2002,** 124, 5528-5541.

30. Herdt, G. C.; Czanderna, A. W., Metal Overlayers on Organic Functional Groups of Self-Organized Molecular Assemblies. V. Ion Scattering Spectroscopy and X-Ray Photoelectron Spectroscopy of Ag/COOH Interfaces *J. Vac. Sci. Technol., A* **1995,** 13, 1275-1280.

31. Herdt, G. C.; Czanderna, A. W., Metal Overlayers on Organic Functional Groups of Self-Organized Molecular Assemblies: VII. Ion Scattering Spectroscopy and X-Ray Photoelectron Spectroscopy of Cu/CH_3 and $Cu/COOCH_3$. *J. Vac. Sci. Technol., A* **1997,** 15, 513-519.

32. Herdt, G. C.; Czanderna, A. W., Metal Overlayers on Organic Functional Groups of Self-assembled Monolayers: VIII. X-Ray Photoelectron Spectroscopy of the Ni/COOH Interface *J. Vac. Sci. Technol., A* **1999,** 17, 3415-3418.

33. Herdt, G. C.; Jung, D. R.; Czanderna, A. W., Weak Interactions between Deposited

Metal Overlayers and Organic Functional Groups of Self-Assembled Monolayers. *Prog. Surf. Sci.* **1995,** 50, 103-129.

34. Hooper, A. E.; Fisher, G. L.; Konstadinidis, K.; Jung, D. R.; Nguyen, H.; Opila, R. L.; Collins, R. W.; Winograd, N.; Allara, D. L., Chemical Effects of Methyl and Methyl Ester Groups on the Nucleation and Growth of Vapor-Deposited Aluminum Films. *J. Am. Chem. Soc.* **1999,** 121, (35), 8052–8064.

35. Jung, D. R.; Czanderna, A. W., Chemical and Physical Interactions at Metal/Self-Assembled Organic Monolayer Interfaces *Crit. ReV. Solid State Mater. Sci.* **1994,** 19, 1-54.

36. Jung, D. R.; Czanderna, A. W., Metal Overlayers on Organic Functional Groups of Self-Assembled Monolayers. VI. X-ray Photoelectron Spectroscopy of Cr/COOH on 16-mercaptohexadecanoic acid *J. Vac. Sci. Technol. A* **1995,** 13, 1337-1344.

37. Jung, D. R.; Czanderna, A. W.; Herdt, G. C., Interactions and Penetration at Metal/Self-Assembled Organic Monolayer Interfaces *J. Vac. Sci. Technol., A* **1996,** 14, 1779-1781.

38. Jung, D. R.; King, D. E.; Czanderna, A. W., XPS of Organized Molecular Assembly/Copper Interfaces: $HS(CH2)_{11}OH$/Cu. *Appl. Surf. Sci.* **1993,** 70/71, 127-132.

39. King, D. E.; Czanderna, A. W., Oxidation Behavior of Thin Copper Films on a Mercaptoundecanoic Acid Organized Molecular Assembly. *Langmuir* **1994,** 10, 1630-1631.

40. Nagy, G.; Walker, A. V., Dynamics of the Interaction of Vapor-Deposited Copper

with Alkanethiolate Monolayers: Bond Insertion, Complexation, and Penetration Pathways. *J. Phys. Chem. B* **2006,** 110, 12543-12554.

41. Nagy, G.; Walker, A. V., Dynamics of Reactive Metal Adsorption on Organic Thin Films. *J. Phys. Chem. C* **2007,** 111, 8543-8556.

42. Tighe, T. B.; Daniel, T. A.; Zhu, Z.; Uppili, S.; Winograd, N.; Allara, D. L., Evolution of the Interface and Metal Film Morphology in the Vapor Deposition of Ti on Hexadecanethiolate Hydrocarbon Monolayers on Au. *J. Phys. Chem. B* **2005,** 109, 21006-21014.

43. Walker, A. V.; Tighe, T. B.; Cabarcos, O.; Haynie, B. C.; Allara, D. L.; Winograd, N., Dynamics of Interaction of Magnesium Atoms on Methoxy-Terminated Self-Assembled Monolayers: An Example of a Reactive Metal with a Low Sticking Probability. *J. Phys. Chem. C* **2007,** 111, 765-772.

44. Walker, A. V.; Tighe, T. B.; Cabarcos, O. M.; Reinard, M. D.; Haynie, B. C.; Uppili, S.; Winograd, N.; Allara, D. L., The Dynamics of Noble Metal Atom Penetration through Methoxy-Terminated Alkanethiolate Monolayers. *J. Am. Chem. Soc.* **2004,** 126, 3954-3963.

45. Walker, A. V.; Tighe, T. B.; Reinard, M. D.; Haynie, B. C.; Allara, D. L.; Winograd, N., Solvation of Zero-Valent Metals in Organic Thin Films. *Chem. Phys. Lett.* **2003,** 369, 615-620.

46. Walker, A. V.; Tighe, T. B.; Stapleton, J. J.; Haynie, B. C.; Allara, D. L.; Winograd, N., Interaction of Vapor-Deposited Ti and Au with Molecular Wires. *Appl. Phys. Lett.*

2004, 84, 4008-4010.

47. Jung, D. R.; Czanderna, A. W.; Herdt, G. C., Bonding at Metal/Self-Assembled Organic Monolayer Interfaces. In *Polymer Surfaces and Interfaces: Characterization, Modification and Application*, Mittal, K. L.; Lee, K.-W., Eds. VSP: Utrecht: The Netherlands, 1997.

48. Smith, E. L.; Alves, C. A.; Anderegg, J. W.; Porter, M. D.; Spierko, L. M., Deposition of Metal Overlayers at End-Group-Functionalized Thiolate Monolayers Adsorbed at Au. 1. Surface and Interfacial Chemical Characterization of Deposited Cu Overlayers at Carboxylic Acid-Terminated Structures. *Langmuir* **1992,** 8, 2707-2714.

49. Colavita, P. E.; Doescher, M. S.; Molliet, A.; Evans, U.; Reddic, J.; Zhou, J.; Chen, D.; Miney, P. G.; Myrick, M. L., Effects of Metal Coating on Self-Assembled Monolayers on Gold. 1. Copper on Dodecanethiol and Octadecanethiol. *Langmuir* **2002,** 18, 8503-8509.

50. Opila, R. L.; Eng, J., Jr., Thin Films and Interfaces in Microelectronics: Composition and Chemistry as Function of Depth. *Prog. Surf. Sci.* **2002,** 69, 125-163.

51. Garno, J. C.; Zangmeister, C. D.; Batteas, J. D., Directed Electroless Growth of Metal Nanostructures on Patterned Self-Assembled Monolayers. *Langmuir* **2007,** 23, 7874-7879.

52. Zangmeister, C. D.; van Zee, R. D., Electroless Deposition of Copper onto 4-Mercaptobenzoic Acid Self-Assembled on Gold. *Langmuir* **2003,** 19, 8065-8068.

53. Zhu, P.; Masuda, Y.; Koumoto, K., Seedless Micropatterning of Copper by

Electroless Deposition on Self-Assembled Monolayers. *J. Mater. Chem* **2004,** 14, 976-981.

54. Fisher, G. L.; Hooper, A. E.; Opila, R. L.; Allara, D. L.; Winograd, N., The Interaction of Vapor-Deposited Al Atoms with CO2H Groups at the Surface of a Self-Assembled Alkanethiolate Monolayer on Gold. *J. Phys. Chem. B* **2000,** 104, 3267-3273.

55. Nuzzo, R. G.; Allara, D. L., Adsorption of Bifunctional Organic Disulfides on Gold Surface. *J. Am. Chem. Soc.* **1983,** 105, 4481.

56. Nuzzo, R. G.; Dubios, L. H.; L., A. D., Fundamental Studies of Microscopic Wetting on Organic Surfaces. 1. Formation and Structural Characterization of a Self-Consistent Series of Polyfunctional Organic Monolayers. *J. Am. Chem. Soc.* **1990,** 112, 558-569.

57. Vickerman, J. C., *ToF SIMS: Surface Analysis by Mass Spectrometry*. IM Publications and Surface Spectra Limited: Chichester and Manchester, UK, 2001; p 1-40.

58. Dumesic, J.; Koutsky, J. A.; Chapman, T. W., The Rate of Electroless Copper Depositionby Formaldehyde Reduction. *J. Electrochem. Soc.* **1974,** 121, 1405-1412.

59. Mishra, K. G.; Paramguru, R. K., Kinetics and Mechanism of Electroless Deposition of Copper. *J. Electrochem. Soc.* **1996,** 143, 510-516.

60. Shacham-Diamand, Y.; Dubin, V.; Angyal, M., Electroless Copper Deposition for ULSI. *Thin Solid Films* **1995,** 262, (1995), 93-103.

61. Kanicky, J. R.; Shah, D. O., Effect of Degree, Type, and Position of Unsaturation on the pK_a of Long-Chain Fatty Acids. *J. Colloid Interface Sci.* **2002,** 256, 201-207.

62. Martell, A. E.; Smith, R. M., *Critical Stability Constants*. Plenum Press New York, 1974; Vol. 3, p 1-12.

63. Martell, A. E.; Smith, R. M., *Critical Stability Constants*. Plenum Press New York, 1974; Vol. 1, p 204-211.

Chapter 6

Preventing Metal Penetration and Selective Deposition of Copper on Functionalized Self-Assembled Monolayers

Abstract: The use of "seeding" and organic additives to increase the copper electroless deposition rate on -COOH terminated SAMs was investigated. In the "seeding" step, -COOH terminated SAMs were immersed in a plating solution containing Cu^{2+} ions for 15 min to form a Cu^{2+}-carboxylate catalyst layer, prior to the addition of the reducing agent formaldehyde. "Seeding" increased copper deposition rate dramatically, but did not prevent copper penetration through the SAMs. Organic additives, adenine and guanine, were also employed to improve the deposition rate. However, additives slowed down the deposition rate compared with "seeded" deposition. However, additives were observed to affect copper penetration through the SAMs to the Au/S interface. With adenine as additive, no copper penetration was observed on -COOH terminated SAMs after Cu electroless deposition. Using guanine as additive, copper penetration was also significantly reduced but not eliminated. Adenine and guanine formed large additive-SAM complexes, which affected Cu penetration, with -COOH terminated SAMs. When electroless deposition was performed under "seeded" conditions with adenine as additive at 45 °C, copper was selectively deposited in the -COOH terminated SAM regions of a patterned -COOH/-CH_3 SAM.

6.1 Introduction

In Chapter 5, we demonstrated that copper can be deposited on -CH_3 and -COOH terminated SAMs by using electroless deposition. However, the deposited copper poorly adhered to the SAM surfaces and penetrated through the monolayer to the Au/S interface for at least 48 h after deposition ceased.[1] This suggests that the previous electroless deposition conditions were not suitable to make stable metal/SAM/metal or metal/SAM/semiconductor junctions for use in molecular devices.[2, 3] Thus new electroless deposition processes are required to form stable metal overlayers on the SAMs.

Previous studies on vapor-deposited copper on SAMs showed that less copper penetration occurred when the deposition rate was faster.[4, 5] This is because the Cu-Cu interaction is very strong, and thus Cu-Cu binding is favored upon deposition over copper penetration through the SAM to the Au/S interface. For an electroless deposition, two approaches are generally employed to speed up a reaction. First, a seed layer of a catalyst, typically Sn or Pd, can be used.[6-12] Second, organic additives (e.g. adenine and guanine, Figure 6.1) have been employed to accelerate the copper electroless deposition, alter the film growth kinetics, and control the properties of the deposited films in copper electroless deposition.[13-15] For example, Paunovic *et al.*[14] demonstrated that adenine and guanine accelerated the rate of copper electroless deposition and suppressed metallic copper oxidation.

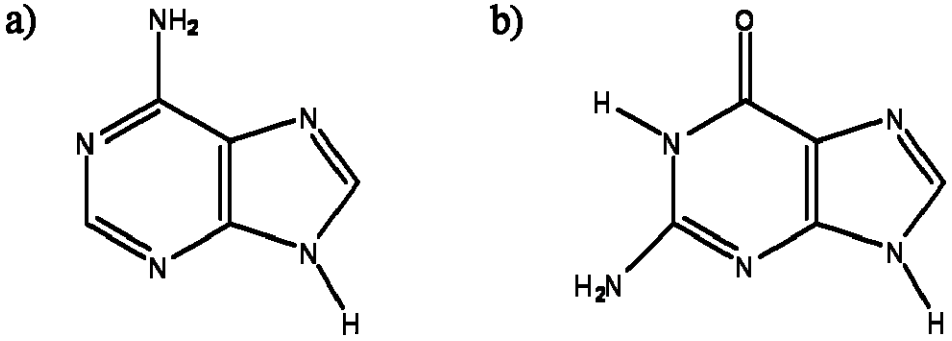

Figure 6.1 Structures of additives (a) adenine (b) guanine.

In the research reported in this chapter, we investigated the use of a seeding Cu layer and organic additives, adenine and guanine, in Cu electroless deposition -COOH terminated SAMs. Cu was employed as the seed layer rather than Pd or Sn since Cu(I), Cu(II) and Cu(0) are know to be catalytically active.[16-19] Seeding significantly increased the copper deposition rate, but copper still penetrated through the SAMs. Seeding and using the additives, adenine or guanine, led to a decreased deposition rate compared with seeding alone, but the rate was still higher than that in a seedless deposition. Adenine prevented copper penetration through the monolayer, but guanine only reduced the extent of copper penetration. Adenine and guanine complexed with -COOH terminal groups and provided a barrier for copper to penetrate through the monolayer. Selective copper deposition in -COOH terminated SAM regions of -COOH/-CH_3 patterned SAMs was also achieved by employing seeding and adenine.

6.2 Experimental

6.2.1 Materials

Copper sulfate (≥ 99%), ethylene-1-diamine tetraacetic acid (EDTA) disodium salt dehydrate (≥ 99.0%), formaldehyde (37 wt% in water), sodium hydroxide (≥ 98%, pellets), adenine (≥ 99%) and guanine (≥ 99%) were purchased from Sigma Aldrich (Saint Louis, MO). Gold and chromium were obtained from Alfa Aesar Inc. and were of 99.995% purity. Hexadecanethiol (HDT) (99%), 16-mercaptohexadecanoic acid (MHA) (99%), and mercaptohexadecanol (MHL) (99%) were purchased from Asemblon, Inc. (Redmond, WA). Anhydrous ethanol (A.C.S. grade) was obtained from Aaper Alchohol (Shelbyville, KY). Native silicon oxide wafers (<111> orientation) were purchased from Addison Technologies, Inc. (Pottstown, PA) and were cleaned with piranha etch (H_2SO_4:H_2O_2 = 3:1) before use. All chemicals were used as-received and without further purification.

6.2.2 SAM Preparation

Alkanethiolate SAMs adsorbed on gold substrates were prepared using previously published methods.[20-23] Briefly, first Cr (~ 5 nm) and then Au (~ 100 nm) were thermally deposited onto clean Si native oxide wafers. The prepared Au substrates were then immersed into a 1 mM ethanolic solution of the relevant alkanethiolate molecule for 24 h at ambient temperature (21 ± 2 °C) to prepare well-organized SAMs. For each batch, one sample (~ 1 cm × 1 cm) was taken and characterized using single-wavelength ellipsometry (Gaertner Scientific Corp., Skokie, IL) and TOF SIMS (ION TOF Inc.,

Chestnut Hill, NY) prior to electroless deposition to ensure that the SAMs were free of significant chemical contamination.

6.2.3 Copper Electroless Deposition

The plating solution was prepared using 4 mM $CuSO_4$, 10 mM EDTA disodium salt, and 10 mM formaldehyde. Before the addition of formaldehyde, the pH of the solution was adjusted to 12.8 with sodium hydroxide. It was used immediately after preparation. Two experimental conditions were employed. Under the "unseeded" conditions, samples were immersed in the plating solution after addition of formaldehyde. In contract, under the "seeded" conditions, samples were kept in the Cu^{2+} ion-containing solution for 15 min prior to addition of formaldehyde. This step is called "seeding". After addition of formaldehyde, samples were kept in the plating solution at 45 °C for 60 min. After removal from the solution, samples were rinsed thoroughly with copious deionized water and absolute ethanol, and dried with nitrogen gas. Samples were then immediately transferred to TOF SIMS or SEM for analysis.

Adenine and guanine were used as additives in a second series of electroless deposition experiments. The concentration of the additive in the plating solution was 0.04 mM. The samples were seeded in the plating solution containing either adenine or guanine for 15 min. Copper electroless deposition was performed at 45 °C for 60 min. After removal from the solution, samples were rinsed thoroughly with copious deionized water and absolute ethanol, and dried with N_2 before TOF SIMS and SEM characterization.

6.2.4 UV Photopatterning of SAMs

UV photopatterning was employed to prepare the patterned -COOH/-CH_3 SAM following the method of Zhou & Walker.[24-26] Briefly, a copper mask (Electron Microscopy, Inc. Hatfield, PA) was placed on the -COOH terminated SAM (MHA). The sample was placed approximately 50 mm away from a 500 W Hg arc lamp equipped with a dichroic mirror and a narrow-band-pass filter (280-400 nm) (Thermal Oriel, Spectra Physics Inc., Stratford, CT). The -COOH terminated SAM was then exposed to the UV light for 2 h photooxidation. After UV exposure, the photooxidized -COOH terminated SAM was immersed into a freshly made 1 mM -CH_3 terminated alkanethiol (HDT) ethanolic solution for 24 h. In the areas exposed to UV light, the -CH_3 terminated SAM was adsorbed, creating a HDT/MHA patterned surface. After removal from the HDT solution, the samples were rinsed thoroughly with copious degassed ethanol and dried with nitrogen before electroless deposition.

6.2.5 Time-of-Flight Secondary Ion Mass Spectrometry (TOF SIMS)

An ION TOF IV spectrometer (ION TOF Inc., Chestnut Hill, NY) equipped with a Bi liquid metal ion gun was employed. Briefly, this instrument consists of an air lock, a preparation chamber and an analysis chamber, each separated by gate valves. The pressure of the preparation and analysis chambers were maintained at $\leq 3.8 \times 10^{-9}$ mbar. The primary ions used in the analysis were Bi^+ ions, which were accelerated to 25 keV and contained within a ~100 nm diameter probe beam. The analysis area was (100 × 100) μm^2. Total accumulated primary ion dose was less than 10^{11} ions cm^{-2}, and so all the

spectra were acquired within the static regime.[27] The ejected secondary ions were extracted into a time-of-flight mass spectrometer with a 2000 V potential and were reaccelerated to 10 keV before reaching the detector. Peak intensities were reproducible to within ± 10% from scan to scan and from sample to sample. For each electroless deposition experiment, at least two samples were prepared and three areas on each sample were examined. Each presented data point is an average over at least six measurements, and the error bars show the standard deviations.

A video camera (ExwaveHAD, Sony) mounted in the TOF SIMS analysis chamber was employed to obtain optical images.

6.2.6 Scanning Electron Microscopy (SEM)

SEM measurements were conducted on a Field Emission Scanning Electron Microscope (Hitachi s-4500) equipped with a NORAN Instruments energy dispersive x-ray (EDX) microanalysis system, a back scattering detector and a mechanical straining stage.

6.3 Results and Discussion

6.3.1 Seeded Copper Electroless Deposition on -COOH and -CH_3 terminated SAMs

Immersion of the SAM into a bath containing Cu^{2+} ions, EDTA and sodium hydroxide for 15 min prior to addition of formaldehyde ("seeded" conditions) was observed to greatly enhance the rate of copper deposition on -COOH terminated SAMs (Figure 6.2). In contrast to the "unseeded" conditions (immediate immersion in a bath with Cu^{2+} ions and

formaldehyde), a densely packed layer of submicron copper crystallites was observed after 1 h reaction at 45 °C. The TOF SIMS spectra confirm that more copper was deposited: the intensity of Cu^+ ions on -COOH terminated SAMs significantly increased under the "seeded" conditions (Figure 6.3 a). Further, the Cu^+ ions intensity remained approximately constant after sonication of the sample, indicating that the deposited copper layer formed under "seeded" conditions strongly adhered to -COOH terminated SAMs (Figure 6.3 b).

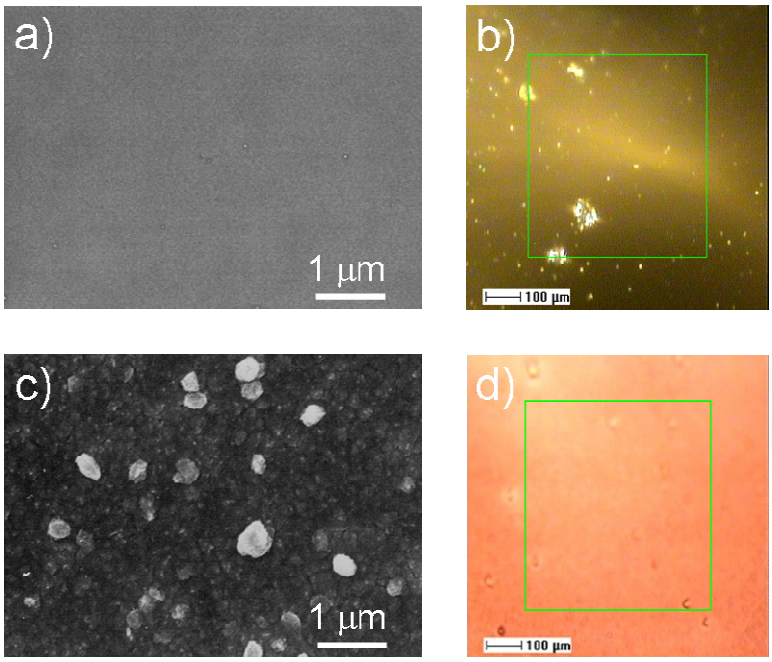

Figure 6.2 (a, c) SEM and (b, d) optical images after copper electroless deposition at 45 °C for 1 h on -COOH terminated SAMs under (a, b) unseeded conditions, and (c, d) seeded conditions. In the optical images the size of the square box is 500 × 500 μm^2.

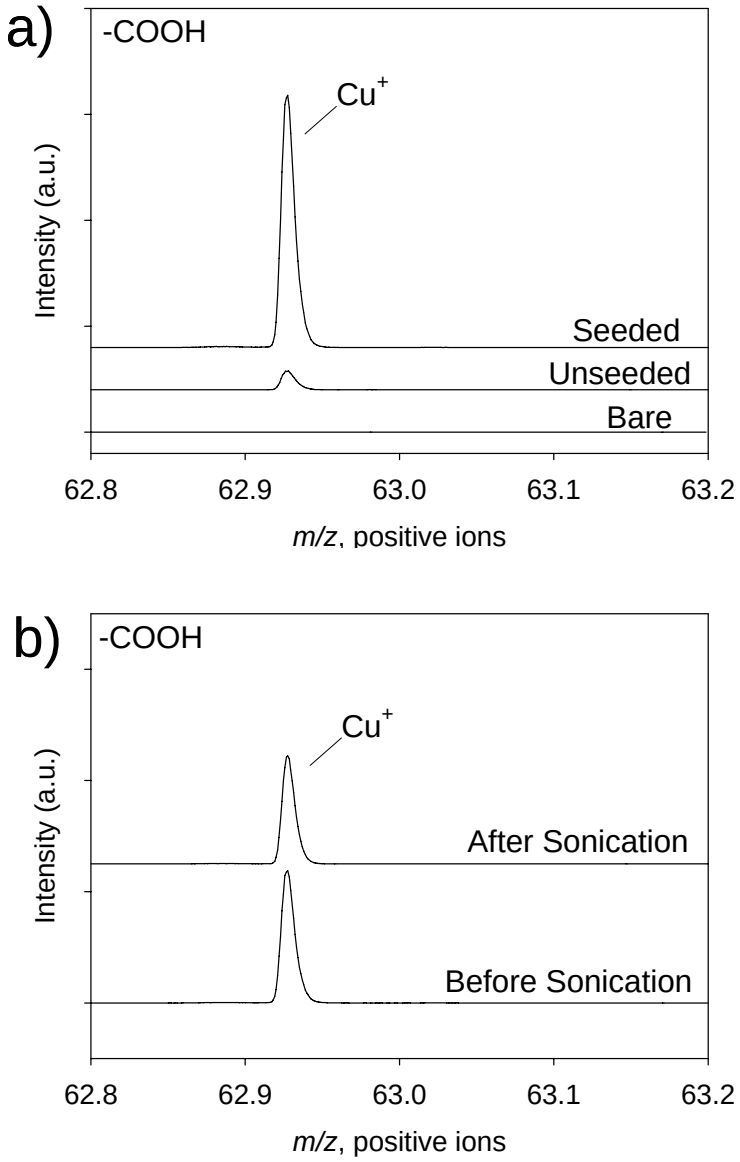

Figure 6.3 High mass resolution positive ion TOF SIMS spectra of $^{63}Cu^{+}$ ion (nominal mass *m/z* 63) on -COOH terminated SAMs after 1 h Cu electroless deposition at 45 °C (a) under unseeded and seeded conditions, (b) seeded sample prior to and after sonication in deionized water for 3 min

The SIMS mass spectra also show that seeding leads to an increase in the number of Cu^{2+}-carboxylate ions present on the surface. In Figure 6.4, it can be seen that the ion intensity of $Cu(COO)(CH_2)_4^+$, a characteristic ion of the Cu^{2+}-carboxylate surface complex, was greatly increased using seeded deposition. These observations suggest that the increase in the deposition rate is caused by the increase in the number of Cu^{2+}-carboxylate surface complexes present on the surface, which serve as nuclei for the subsequent Cu deposition.[28]

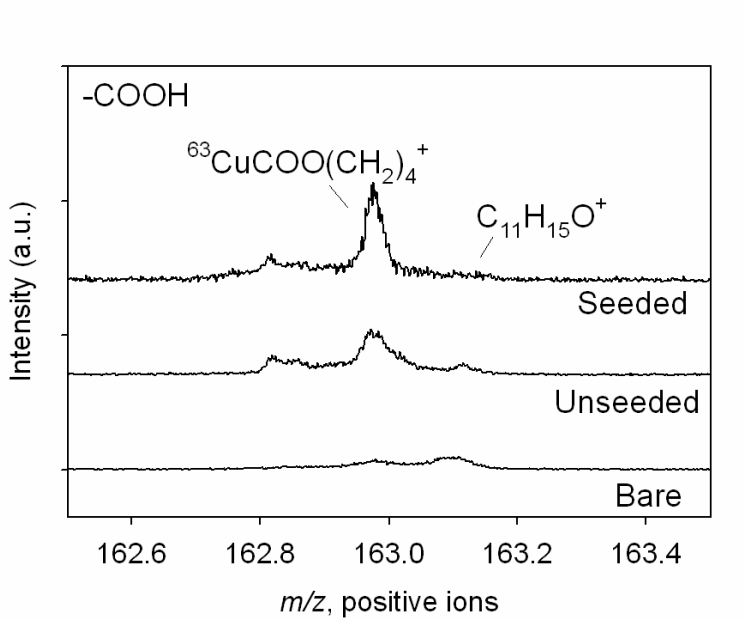

Figure 6.4 High mass resolution positive ion TOF SIMS spectra of $CuCOO(CH_2)_4^+$ ion (nominal mass *m/z* 163) on -COOH terminated SAMs after Cu electroless depositions for 1h at 45 °C under unseeded and seeded conditions. The ions were assigned based on accurate mass and fragmentation mechanism, and were not structurally characterized. The ion intensities were normalized to the intensity of $C_{11}H_{15}O^+$ ions to make clear the changes in the mass spectra upon Cu deposition.

However, seeding did not prevent copper penetration through the -COOH terminated SAM to the Au/S interface. Using "seeded" and "unseeded" deposition conditions, $CuSH_2^+$ ions were observed in the positive ions mass spectra, indicating that Cu had penetrated through the monolayer.

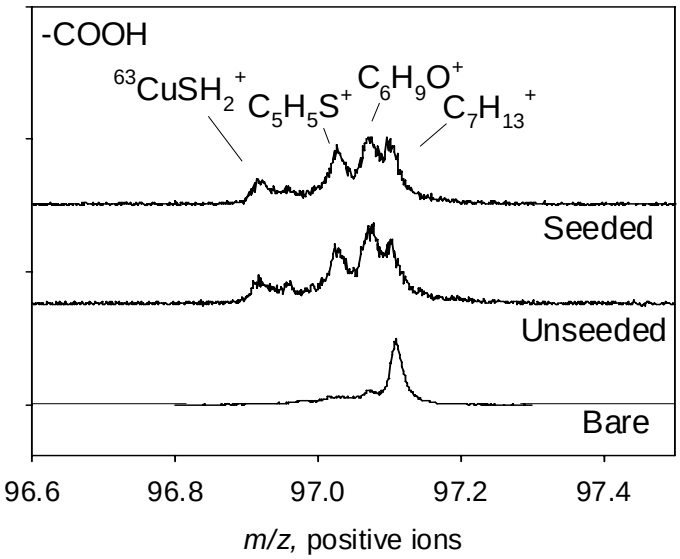

Figure 6.5 High mass resolution positive ion TOF SIMS spectra of $CuSH_2^+$ ion (nominal mass *m/z* 97) on -COOH terminated SAMs after Cu electroless depositions for 1h at 45 °C under unseeded and seeded conditions. The ion intensities were normalized to the intensity of $C_7H_{13}^+$ ions to make clear the changes in the mass spectra upon Cu deposition.

Finally, it is noted that the seeding step also increased the copper deposition rate on -CH_3 terminated SAMs. Under the "unseeded" conditions, no Cu_x^+ ions were observed in the TOF SIMS spectra, indicating that there was little/no copper deposition on the surface. In contrast, under the "seeded" conditions, signals for Cu_x^+ ions had a high intensity, suggesting that Cu was deposited on -CH_3 terminated SAMs (Figure 6.6 a). However, the deposited copper only weakly adhered to the -CH_3 terminated SAM surface and could easily be removed using sonication (Figure 6.6 b).

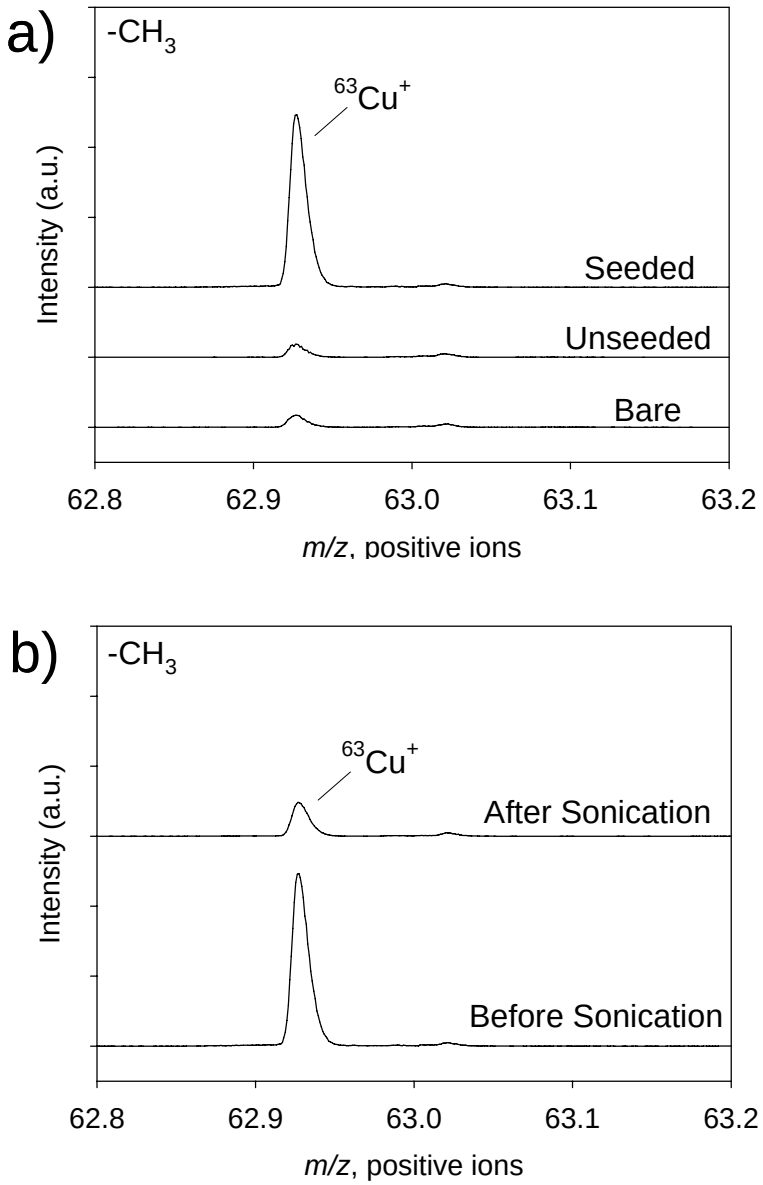

Figure 6.6 High mass resolution positive ion TOF SIMS spectra of $^{63}Cu^+$ ion (nominal mass *m/z* 63) on -CH_3 terminated SAMs after 1 h Cu electroless deposition at 45 °C (a) under unseeded and seeded conditions, (b) seeded sample prior to and after sonication in deionized water for 3 min. The ion intensities were normalized to the intensity of $C_5H_3^+$ ions to make clear the changes in the mass spectra upon Cu deposition.

6.3.2 Copper Electroless Deposition on -COOH terminated SAMs Using Organic Additives

Additives, such as adenine or guanine, were demonstrated to increase the rate of copper electroless deposition.[14] However, it was observed in the TOF SIMS spectra that under "seeded" conditions, the amount of copper decreased when adenine or guanine was added to the bath (Figure 6.7), suggesting that the additives impeded copper deposition under these conditions. Finally, it is noted that the deposition rate was still larger than under "unseeded" conditions. The most likely reason for the reduction in the deposition rate is that the number of Cu^{2+}-carboxylate complexes has been reduced. In the TOF SIMS spectra, $CuCOO(CH_2)_4^+$ ion intensity decreased significantly after addition of guanine, and was approximately zero after addition of adenine (Figure 6.8).

The TOF SIMS data also indicate that after adding adenine or guanine to the bath, copper penetration through the -COOH terminated SAMs was significantly reduced. After addition of adenine, the ion intensity of $CuSH_2^+$, a characteristic ion of Cu penetration through the layer, was reduced to zero in the TOF SIMS spectra. Using guanine as additive, the $CuSH_2^+$ ion intensity also decreased to ~1/3 of the intensity observed under seeded or unseeded conditions (Figure 6.9).

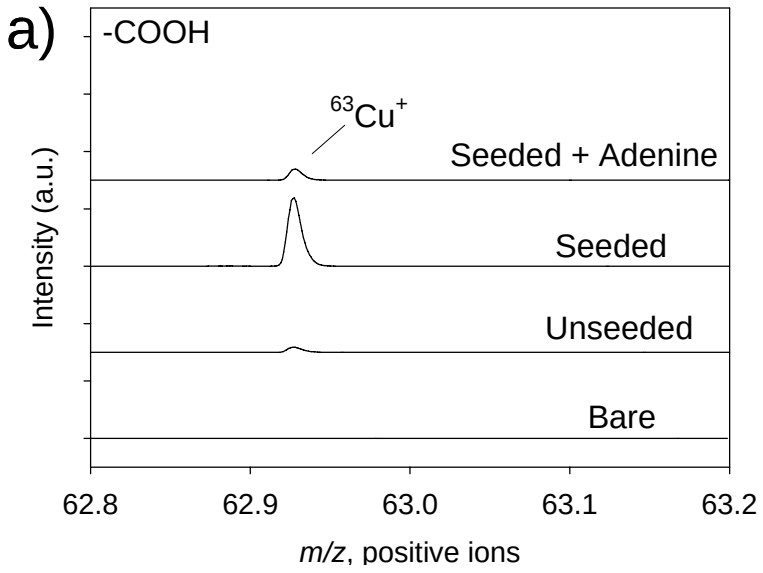

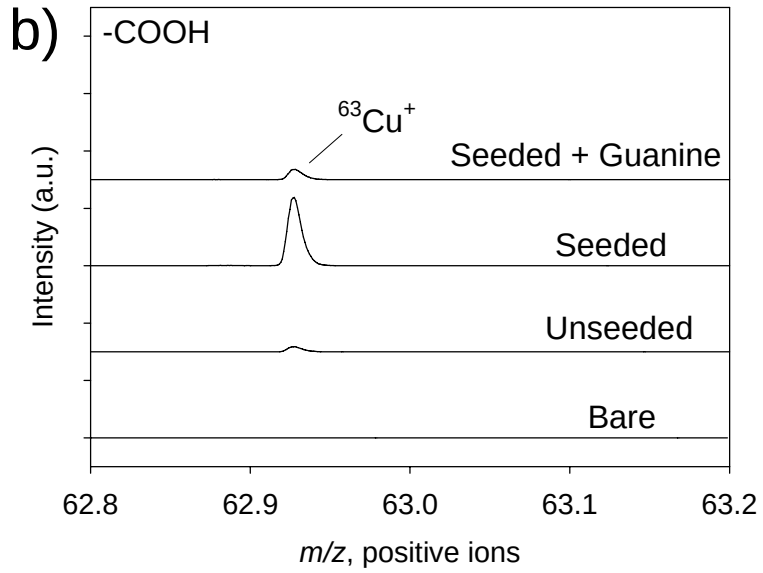

Figure 6.7 High mass resolution positive ion TOF SIMS spectra of $^{63}Cu^+$ ion (nominal mass *m/z* 63) on -COOH terminated SAMs prior to and after Cu electroless depositions at 45 °C for 1 h with (a) adenine, (b) guanine as additive. The ion intensities were normalized to the intensity of $C_5H_3^+$ ions to make clear the changes in the mass spectra upon Cu deposition.

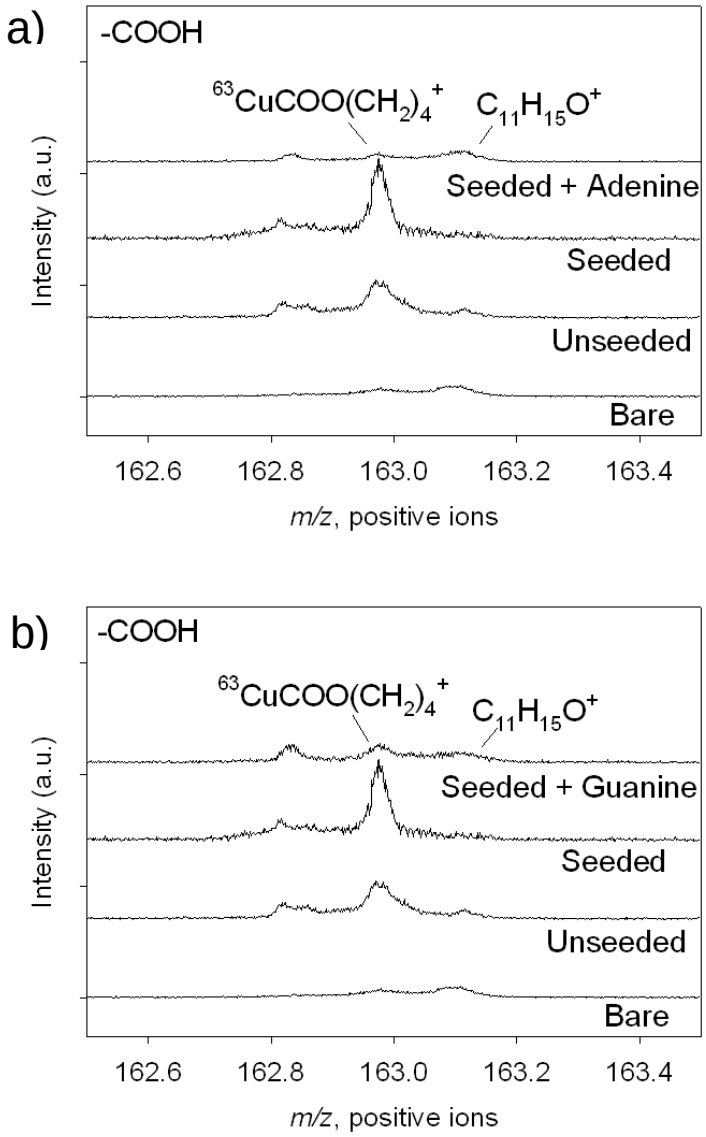

Figure 6.8 High mass resolution positive ion TOF SIMS spectra of $^{63}CuCOO(CH_2)_4^+$ ion (nominal mass *m/z* 163) on -COOH terminated SAMs prior to and after Cu electroless depositions at 45 °C for 1h with (a) adenine, (b) guanine as additive. The ion intensities were normalized to the intensity of $C_{11}H_{15}O^+$ to make clear the changes in the mass spectra upon Cu deposition.

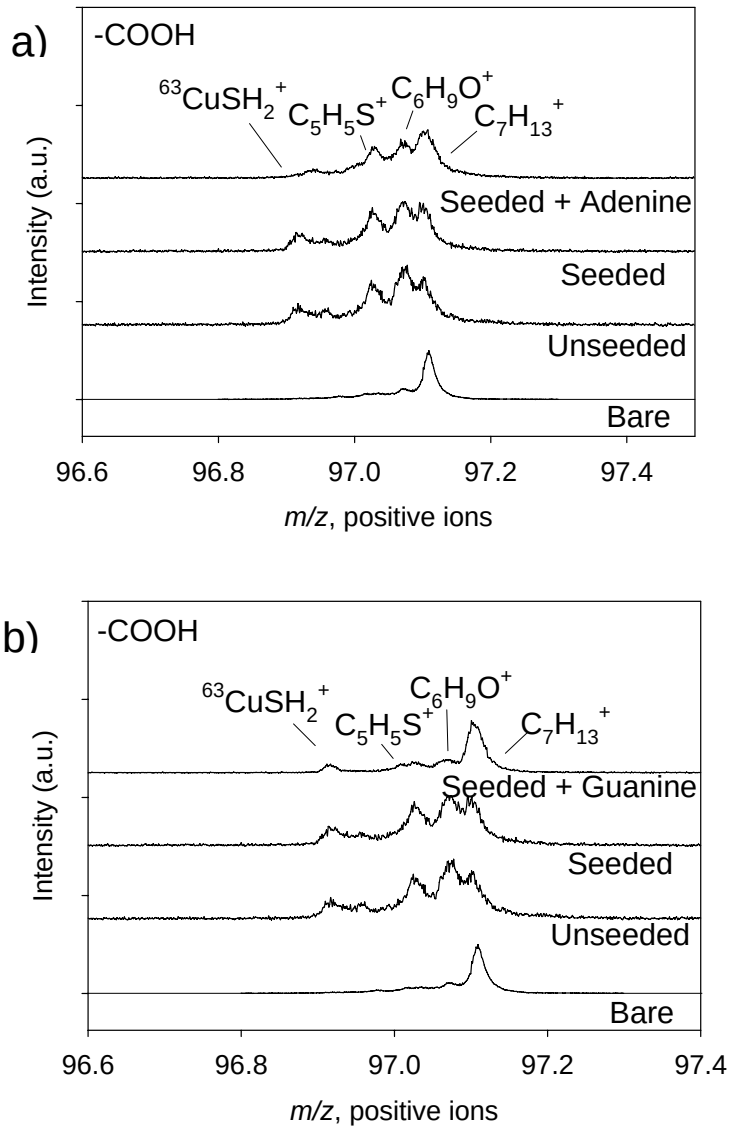

Figure 6.9 High mass resolution positive ion TOF SIMS spectra of $^{63}CuSH_2^+$ ion (nominal mass *m/z* 97) on -COOH terminated SAMs prior to and after Cu electroless depositions at 45 °C for 1h with (a) adenine, (b) guanine as additive. The ion intensities were normalized to the intensity of $C_7H_{13}^+$ to make clear the changes in the mass spectra upon Cu deposition.

There are two possible ways that the addition of adenine and guanine reduced the amount of copper penetration: a) they may form large Cu^{2+}-adenine or Cu^{2+}-guanine complexes that can not diffuse through the SAM layer;[29-32] and b) the carboxylate SAM terminal groups interact with adenine or guanine which prevents copper penetration.

To test whether the formation of large Cu^{2+}-adenine or Cu^{2+}-guanine complexes was responsible for the observed decrease/elimination of Cu penetration, the following experiment was performed. Adenine (or guanine) was added to the bath containing Cu^{2+} ions, EDTA and NaOH and allowed to stand 15 min prior to addition of formaldehyde and the sample. If the formation of large Cu^{2+} complexes was responsible for the decrease in Cu penetration, it is expected that there would be a decrease in the $CuSH_2^+$ ion intensity.

In the TOF SIMS spectra, it was observed that the $CuSH_2^+$ ion intensity was significantly higher than under standard conditions (seeded conditions in which the organic additives are added to the bath along with the sample), indicating that more copper penetrated through the SAMs (Figure 6.10). These observations suggest that the formation of larger Cu^{2+} complexes was not responsible for the observed decrease in copper penetration.

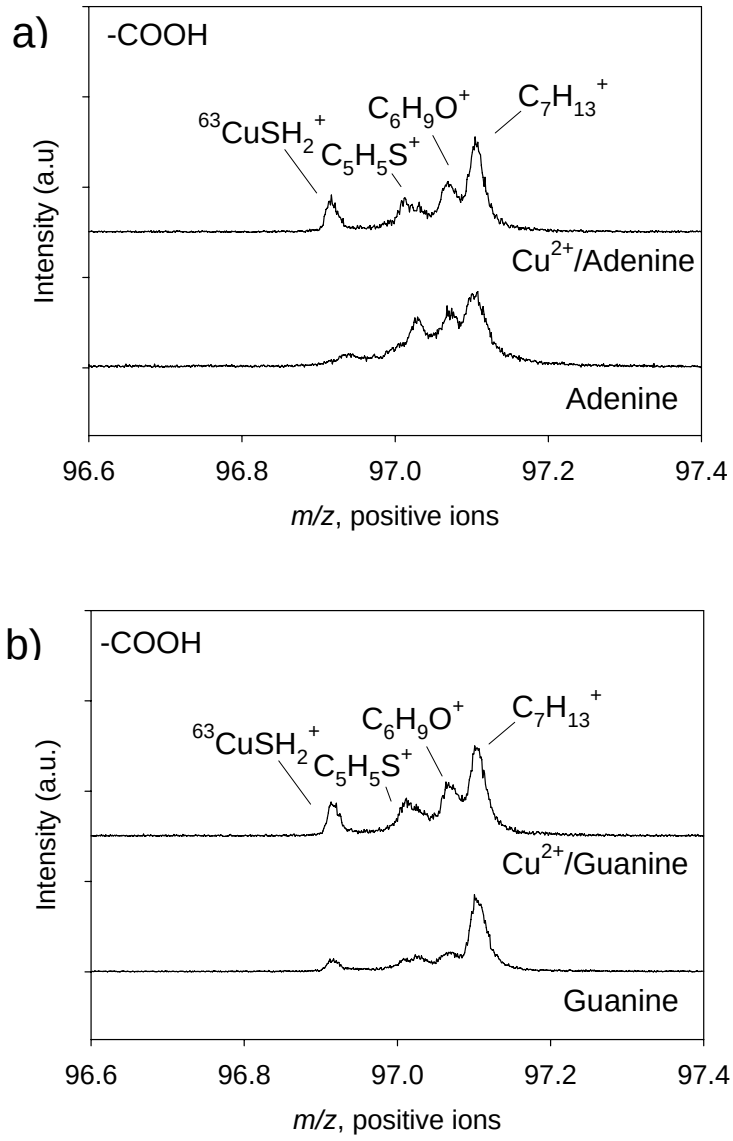

Figure 6.10 High mass resolution positive ion TOF SIMS spectra of $^{63}CuSH_2^+$ ion (nominal mass *m/z* 97) on -COOH terminated SAMs after Cu electroless depositions at 45 °C for 1 h. (a) with adenine as additive under standard and Cu^{2+}-adenine complex formation conditions; (b) with guanine as additive under standard and Cu^{2+}-guanine complex formation conditions. The ion intensities were normalized to the intensity of $C_7H_{13}^+$.

Rather, the TOF SIMS spectra suggest that the formation of adenine- or guanine-terminal group complexes was responsible for the observed decrease in the copper penetration. A series of ions of the form adenine-$(COO)_2(CH_2)_x(CH)_y^+$ and guanine-$(COO)_2(CH_2)_x(CH)_y^+$ were observed in the TOF SIMS spectra, indicating that adenine and guanine complexed with the -COOH terminated SAM surface (Figure 6.11). These ions were assigned based on accurate mass and were not structurally characterized. The low ion intensity of the guanine complexes suggest that fewer guanine-terminal group complexes formed compared to adenine. Further, these complexes were weakly bound to the SAM and could be removed *via* sonication in deionized water (Figure 6.11).

To test whether these surface complexes aid in the prevention of Cu penetration to the Au/S interface, the adenine (or) guanine was added to the bath solution at the same time as the reducing agent, formaldehyde. This minimized the time for additive surface complexes to form. The TOF SIMS data show that the adenine (or guanine) surface complexes were significantly reduced: the intensities of adenine-$(COO)_2(CH_2)_{19}(CH)_6^+$ and guanine-$(COO)_2(CH_2)_{15}(CH)_8^+$ ions were greatly decreased (Figure 6.12).

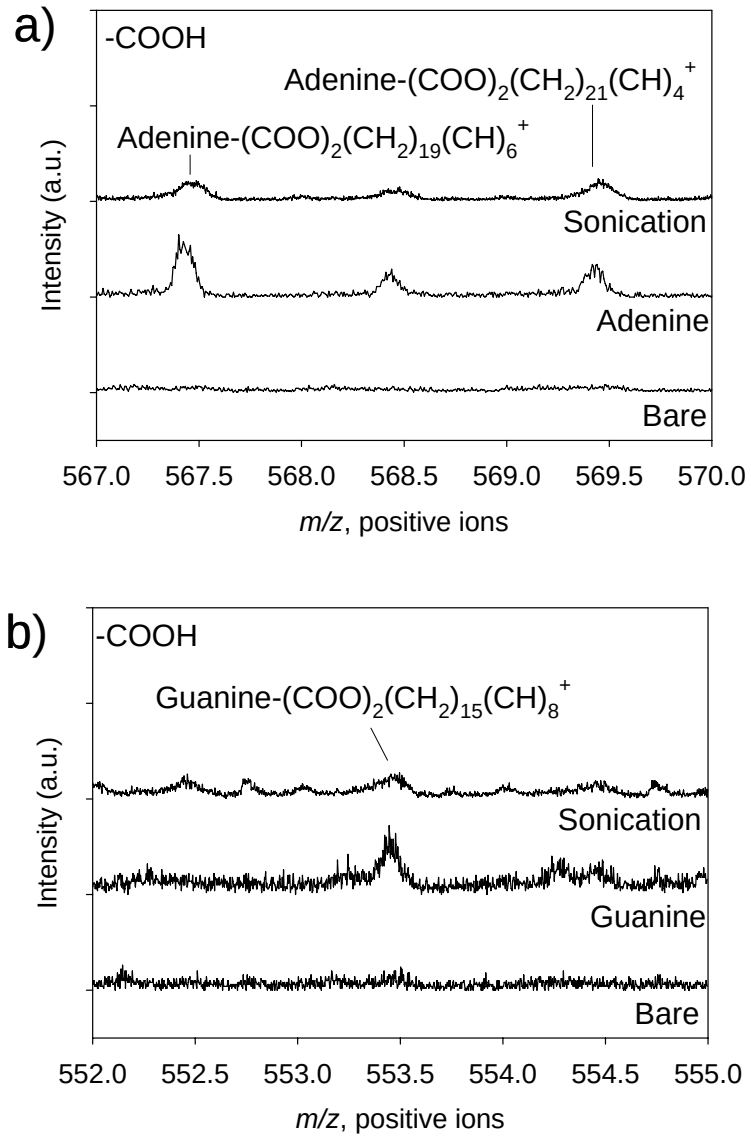

Figure 6.11 High mass resolution positive ion TOF SIMS spectra of (a) adenine-surface complex ions and (b) guanine-surface complex ions on -COOH terminated SAMs prior to and after 3 min sonication in deionized water. The ions were assigned based on accurate mass and were not structurally characterized. The deposition was performed under standard seeded conditions at 45 °C for 1 h with (a) adenine and (b) guanine as additive.

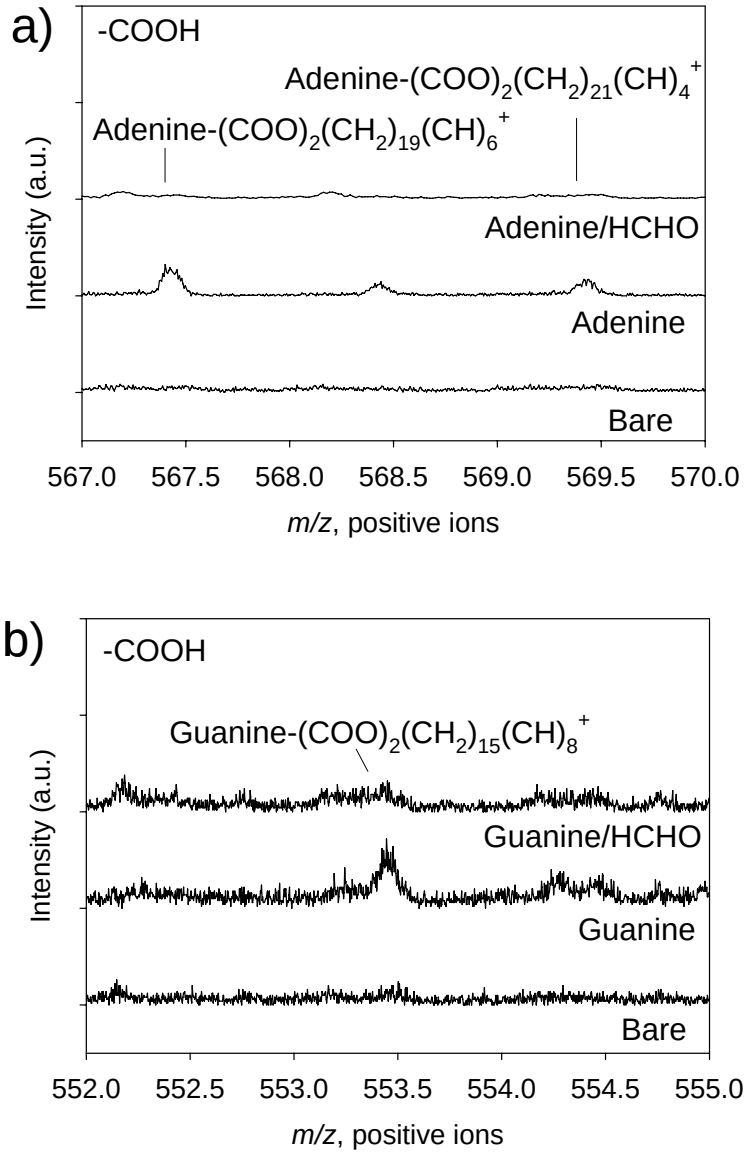

Figure 6.12 High mass resolution positive ion TOF SIMS spectra of (a) adenine-surface complex ions and (b) guanine-surface complex ions on -COOH terminated SAMs after Cu electroless deposition at 45 °C for 1 h. The ions were assigned based on accurate mass and were not structurally characterized. “Adenine” and “Guanine” indicate the deposition was under standard seeded conditions, and “Adeine/HCHO” and “Guanine/HCHO” indicate that additives were added together with formaldehyde.

Consistent with the reduction in the intensities of adenine (or guanine) surface complex ions, there was an increase in the $Cu(COO)(CH_2)_4^+$ ion intensity, which is characteristic of the Cu^{2+}-carboxylate terminal group interaction (Figure 6.13). Further, in the TOF SIMS spectra, the ion intensity for the $CuSH_2^+$ ions was also observed to increase when the organic additive and formaldehyde were added to the plating solution simultaneously (Figure 6.14). These observations suggest that the formation of additive-surface complexes mediate the Cu^{2+} surface interaction, and so aid in the prevention of Cu penetration through the monolayer.

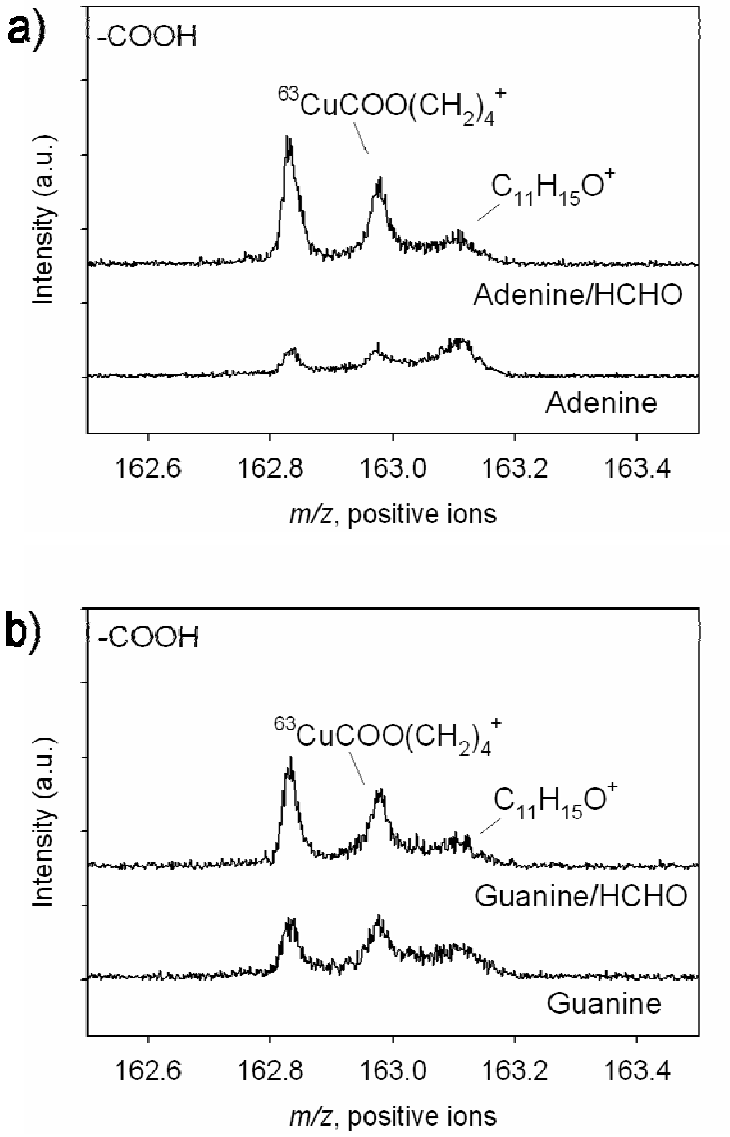

Figure 6.13 High mass resolution positive ion TOF SIMS spectra of $^{63}CuCOO(CH_2)_4^+$ ion (nominal mass *m/z* 163) on -COOH terminated SAMs after Cu electroless depositions at 45 °C for 1h with (a) adenine (b) guanine as additive. "Adenine" and "Guanine" indicate the deposition was under standard seeded conditions, and "Adeine/HCHO" and "Guanine/HCHO" indicate that additives were added together with formaldehyde. The ion intensities were normalized to the intensity of $C_{11}H_{15}O^+$.

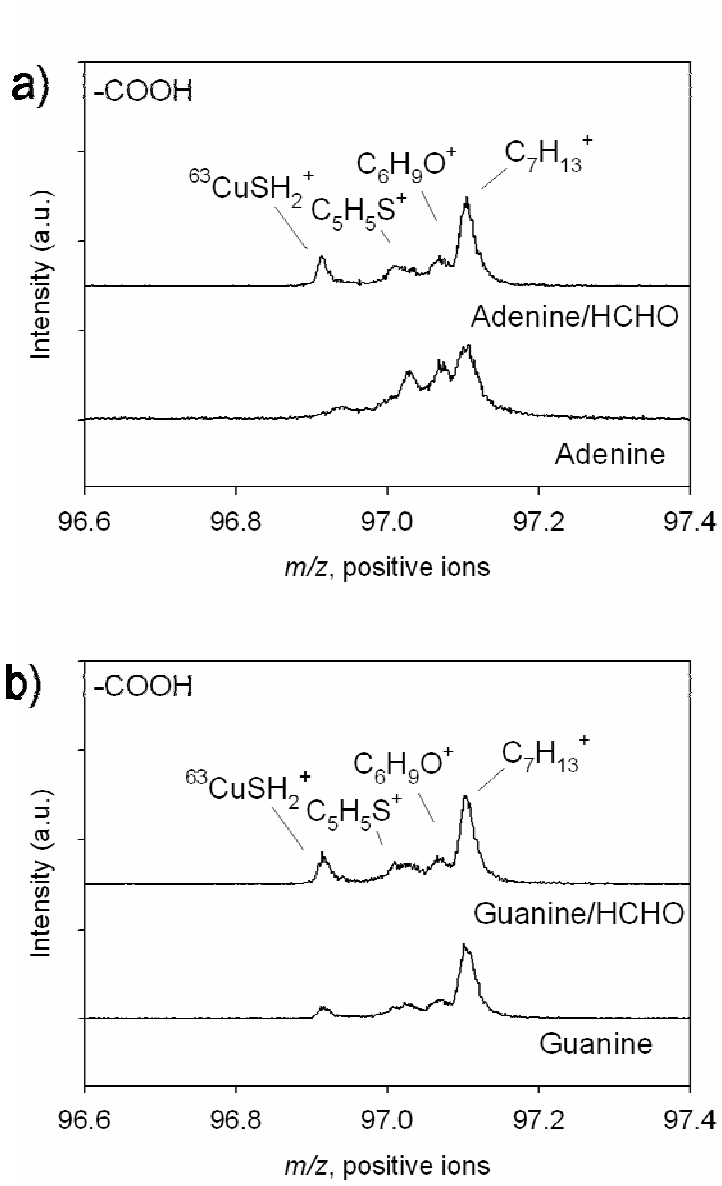

Figure 6.14 High mass resolution positive ion TOF SIMS spectra of $^{63}CuSH_2^+$ ion (nominal mass *m/z* 97) on -COOH terminated SAMs after Cu electroless depositions at 45 °C for 1h with (a) adenine (b) guanine as additive. "Adenine" and "Guanine" indicate the deposition was under standard seeded conditions, and "Adeine/HCHO" and "Guanine/HCHO" indicate that additives were added together with formaldehyde. The ion intensities were normalized to the intensity of $C_7H_{13}O^+$.

6.3.3 Reaction Pathways Involved in Copper Electroless Deposition

In Chapter 5, copper electroless deposition on functionalized SAMs was proposed to occur as follows. Upon immersion in the plating solution, Cu^{2+} ions form weak Cu^{2+}-carboxylate complexes with -COOH terminated SAMs. Once formed, these complexes are reduced to Cu(0) by formaldehyde. On $-CH_3$ terminated SAMs, there is no specific Cu^{2+}-surface interaction. However, at 22 °C, Cu is deposited on $-CH_3$ terminated SAMs; the Cu nucleates at the Cu^{2+} ions trapped on the surface. At high temperature (45°C), Cu^{2+} ions are no longer stabilized on $-CH_3$ terminated SAMs and thus no copper can be deposited.

The above studies support this mechanism. First, seeding increased copper deposition on -COOH terminated SAMs. This is because the number of Cu^{2+}-surface complexes, which were the nucleation sites for copper deposition, was increased under "seeded" condition. Second, the organic additives, adenine and guanine, were observed to reduce significantly Cu penetration through the monolayer, and indeed prevent it in the case of adenine. The most likely reason for this is that adenine and guanine formed bulky additive-surface complexes that mediated the Cu^{2+}-surface interaction. There were fewer Cu nucleation sites on the surface since the Cu^{2+}-carboxylate interaction was reduced. Thus, copper was more likely to nucleate at one of these points or in solution, rather than penetrate through the monolayer. The data suggest that more adenine-carboxylate complexes were formed than guanine-carboxylate complexes. Thus, adenine is a more effective additive to prevent Cu penetration in agreement with the experiment.

6.3.4 Selective Copper Electroless Deposition on Patterned SAMs

The data indicate that selective deposition of copper can be achieved on -COOH/-CH_3 terminated SAMs under the following conditions:

a) bath temperature 45 °C. At this temperature, the amount of deposited copper on -CH_3 terminated SAMs is greatly reduced (negligible);

b) seeded conditions with adenine. Under these conditions, the Cu deposition rate is greatly increased, and the penetration of Cu through the monolayer is eliminated.

Figure 6.15 shows an example of the data obtained: optical, SEM and TOF SIMS images of a patterned -COOH/-CH_3 SAM after Cu electroless deposition at 45 °C for 30 min under "seeded" conditions with adenine in the bath. The optical and SEM images indicate that copper layers formed only in the -COOH terminated SAM areas (the "bar" areas), and no copper deposited in the -CH_3 terminated SAM areas (the "square" areas). In the TOF SIMS images, $^{63}Cu^+$ ions were only observed in the -COOH terminated regions, indicating that copper only deposited on these areas.

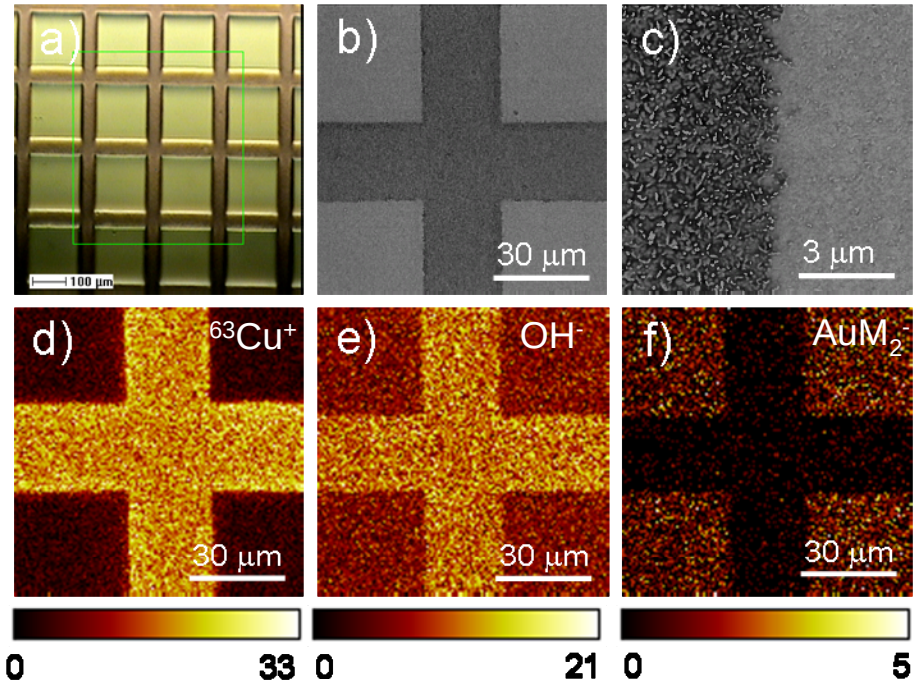

Figure 6.15 (a) Optical; (b, c) SEM; TOF SIMS images centered at (d) $^{63}Cu^{+}$ (*m/z* 63), (e) OH^{-} (*m/z* 17), (f) $-CH_3$ SAM molecular ion AuM_2^{-} (*m/z* 711, M = $S(CH_2)_{15}CH_3$) after copper electroless deposition on a patterned -COOH/$-CH_3$ SAM surface at 45 °C for 30 min. The sample was sonicated in deionized water for 3 min before SEM and TOF SIMS characterization. The lined pattern in the optical image shows that copper has formed a film on the -COOH terminated areas. OH^{-} ion is a characteristic ion of the -COOH terminated SAM and AuM_2^{-} ion is a characteristic ion of the $-CH_3$ terminated SAM. The intensity of the $^{63}Cu^{+}$ ion indicates that copper has selectively deposited on -COOH terminated areas. The dark gray areas in the SEM images indicate that copper crystallites have formed only on -COOH terminated areas. Parameters of TOF SIMS analysis: primary ion, Bi^{+}; kinetic energy = 25 keV; area of analysis = (100 × 100) μm^2, (128 × 128) $pixels^2$. Intensity scale represents maximum ion count.

6.4 Conclusions

Selective electroless copper deposition can be achieved using seeding and by the addition of adenine to the bath. Seeding enhanced the formation of Cu^{2+}-carboxylate complexes, which were the nucleation sites for copper deposition, so improved copper deposition rates on -COOH terminated SAMs. The deposited copper strongly adhered to the SAM surface. On $-CH_3$ terminated SAMs, more Cu^{2+} ions adsorbed on the SAMs during seeding and so the copper deposition rate also increased. However, in contrast to -COOH terminated SAMs, the deposited copper only loosely adhered to -CH3 terminated SAMs and could be easily removed using sonication.

Copper penetration through -COOH terminated SAMs was greatly reduced by adding adenine or guanine to the plating solution. The adenine and guanine surface complexes mediated the Cu^{2+}-SAM interaction. Adenine formed a large number of surface complexes, and so was more effective at preventing copper penetration. No copper penetration was observed if adenine was added to the bath.

The data clearly show that on organic surfaces, the reaction pathways involved in electroless deposition are strongly dependent on the formation of surface complexes. These complexes not only serve as nucleation sites for the metal deposition, but also mediate surface interactions.

Appendix: Positive ions TOF SIMS spectra (*m/z* 2-200) of -COOH and $-CH_3$ terminated SAMs prior to and after Cu electroless deposition under both seeded and unseeded

conditions; Positive ions TOF SIMS spectra (*m/z* 2-200) of -COOH terminated SAMs prior to and after Cu electroless deposition with adenine or guanine as additive: These figures can be found in Appendix Figures A6.1-A6.3.

6.5 References

1. Lu, P.; Walker, A. V., Investigation of the Mechanism of Electroless Deposition of Copper on Functionalized Alkanethiolate Self-Assembled Monolayers Adsorbed on Gold. *Langmuir* **2007,** 23, (25), 12577-12582.

2. Opila, R. L.; Eng, J., Jr., Thin Films and Interfaces in Microelectronics: Composition and Chemistry as Function of Depth. *Prog. Surf. Sci.* **2002,** 69, 125-163.

3. Zaporojtchenko, V.; Strunksus, T.; Behnke, K.; von Bechtolsheim, C.; Kiene, M.; Faupel, F., Metal/Polymer Interfaces with Designed Morphologies *J. Adhes. Sci. Technol.* **2000,** 14, 467-490.

4. Czanderna, A. W.; King, D. E.; Spaulding, D., Metal Overlayer on Organic Functional Group of Self-Organized Molecular Assemblies. 1. X-ray Photoelectron Spectroscopy of Interaction of Cu/COOH on 11-Mercaptoundecanoic Acid. *J. Vac. Sci. Technol., A* **1991,** 9, 2607-2613.

5. Dake, L. S.; King, D. E.; Czanderna, A. W., Ion Scattering and X-Ray Photoelectron Spectroscopy of Copper Overlayers Vacuum Deposited onto Mercaptohexadecanoic Acid Self-Assembled Monolayers. *Solid State Sci.* **2002,** 2, 781-789.

6. Paunovic, M., Ligand Effects in Eiectroless Copper Deposition. *J. Electrochem. Soc*

1977, 124, (3), 349-354.

7. Schoenberg, L. N., The Structure of the Complexed Copper Species in Electroless Copper Plating Solutions. *J. Electrochem. Soc* **1971,** 118, (10), 1571-1576.

8. Shacham-Diamand, Y.; Dubin, V.; Angyal, M., Electroless Copper Deposition for ULSI. *Thin Solid Films* **1995,** 262, (1995), 93-103.

9. Cohen, R. L.; Meek, R. L., The Chemistry of Palladium - Tin Colloid Sensitizing Processes. *J. Colloid Interface Sci.* **1976,** 55, 156-162.

10. Dressick, W. J.; Dulcey, C. S.; Georger, J. H., Jr.; Calvert, J. M., Photopatterning and Selective Electroless Metallization of Surface-Attached Ligands. *Chem. Mater.* **1993,** 5, 148-150.

11. Dressick, W. J.; Dulcey, C. S.; Georger, J. H.; Jr., G. S. C.; Calvert, J. M., Covalent Binding of Pd Catalysts to Ligating Self-Assembled Monolayer Films for Selective Electroless Metal Deposition. *J. Electrochem. Soc* **1994,** 141, 210-220.

12. Osaka, T.; Nagasaka, H.; Goto, F., An Electron Diffraction Study on Mixed $PdCl_2/SnCl_2$ Catalysts for Electroless Plating. *J. Electrochem. Soc* **1980,** 127, 2343-2346.

13. Lin, Y.-M.; Yen, S.-C., Effects of Additives and Chelating Agents on Electroless Copper Deposition. *Appl. Surf. Sci.* **2001,** 178, 116-126.

14. Paunovic, M.; Arndt, R., The Effect of Some Additives on Electroless Copper Deposition. *J. Electrochem. Soc* **1983,** 130, (4), 794-799.

15. Schoenberg, L. N., The Use of Organic Additives to Stabilize and Enhance the Deposition Rate of Electroless Copper Plating. *J. Electrochem. Soc* **1972,** 119, (11),

1491-1493.

16. Chandrasekhar, V.; Athimoolam, A.; Srivatsan, S. G.; Sundaram, P. S.; Verma, S.; Steiner, A.; Zacchini, S.; Butcher, R., Pyrazolylcyclotriphosphazene Containing Pendant polymers: Synthesis, Characterization, and Phosphate Ester Hydrolysis using a Cu(II)-Metalated Cross-Linked Polymeric Catalyst *Inorg. Chem.* **2002,** 41, 5162-5173.

17. Chen, U. S.; Hsieh, W. J.; Shih, H. C.; Chang, Y. S.; Weng, K. W.; Wang, D. Y., Nanostructure and Adhesion of Electroless-Plated Cu film on the Self-Catalyzed Cu using Metal-Plasma Ion Implanter. *Nuc. Instru. Meth. Phys. Res. B* **2005,** 237, 470-476.

18. Inoue, Y.; Matyjaszewski, K., A Dual Catalyst System for Atom Transfer Radical Polymerization Based on a Halogen-Free Neutral Cu(I) Complex. *Macromolecules* **2003,** 36, 7432-7438.

19. Liu, C. F.; Moon, D. K.; Maruyama, T.; Yamamoto, T., Preparation of Polymer Blend Colloids Containing Polyaniline or Polypyrrole by Fe(II)-, Fe(III)-, and Cu(II)-H_2O_2 Catalyst System. *Polym. J.* **1993,** 25, 775-779.

20. Fisher, G. L.; Hooper, A. E.; Opila, R. L.; Allara, D. L.; Winograd, N., The Interaction of Vapor-Deposited Al Atoms with CO2H Groups at the Surface of a Self-Assembled Alkanethiolate Monolayer on Gold. *J. Phys. Chem. B* **2000,** 104, 3267-3273.

21. Fisher, G. L.; Walker, A. V.; Hooper, A. E.; Tighe, T. B.; Bahnck, K. B.; Skriba, H. T.; Reinard, M. D.; Haynie, B. C.; Opila, R. L.; Winograd, N.; Allara, D. L., Bond Insertion, Complexation, and Penetration Pathways of Vapor-Deposited Aluminum Atoms with

HO- and CH_3O-Terminated Organic Monolayers. *J. Am. Chem. Soc.* **2002,** 124, 5528-5541.

22. Nuzzo, R. G.; Allara, D. L., Adsorption of Bifunctional Organic Disulfides on Gold Surface. *J. Am. Chem. Soc.* **1983,** 105, 4481.

23. Nuzzo, R. G.; Dubios, L. H.; L., A. D., Fundamental Studies of Microscopic Wetting on Organic Surfaces. 1. Formation and Structural Characterization of a Self-Consistent Series of Polyfunctional Organic Monolayers. *J. Am. Chem. Soc.* **1990,** 112, 558-569.

24. Zhou, C.; Walker, A. V., Dependence of Patterned Binary Alkanethiolate Self-Assembled Monolayers on "UV-Photopatterning" Conditions and Evolution with Time, Terminal Group, and Methylene Chain Length. *Langmuir* **2006,** 22, 11420-11425.

25. Zhou, C.; Walker, A. V., UV Photooxidation and Photopatterning of Alkanethiolate Self-Assembled Monolayers Adsorbed on GaAs (001). *Langmuir* **2007,** 23, 8876-8881.

26. Zhou, C.; Walker, A. V., UV Photooxidation of a Homologous Series of n-Alkanethiolate Monolayers on GaAs(001): A Static SIMS Investigation. *J. Phys. Chem. C* **2008,** 112, 797-805.

27. Vickerman, J. C., *ToF SIMS: Surface Analysis by Mass Spectrometry*. IM Publications and Surface Spectra Limited: Chichester and Manchester, UK, 2001; p 1-40.

28. Zangmeister, C. D.; van Zee, R. D., Electroless Deposition of Copper onto 4-Mercaptobenzoic Acid Self-Assembled on Gold. *Langmuir* **2003,** 19, 8065-8068.

29. Bruston, F.; Vergne, J.; Grajcar, L.; Drahi, B.; Calvayrac, R.; Baron, M.-H.; Maurel, M.-C., Copper-Adenine Catalyst for O_2 Production from H_2O_2. *Biochem. Biophys. Res.*

Comm. **1999,** 263, 672-677.

30. Pavelka, M.; Shukla, M. K.; Leszczynski, J.; Burda, J. V., Theoretical Study of Hydrated Copper(II) Interactions with Guanine: A Computational Density Functional Theory Study. *J. Phys. Chem. A* **2008,** 112, 256-267.

31. Santos, M. M. C. d.; Lopes, C. M. L. F.; Goncalves, M. L. S., Voltammetric Studies of Purine Bases and Purine Nucleosides with Copper. *Bioelectrochemistry and Bioenergetics* **1996,** 39, 55-60.

32. Smith, R. M.; Martell, A. E.; Chen, Y., Critical Evaluation of Stability Constants for Nucleotide Complexes with Proton and Metal Ions and the Accompanying Enthalpy Changes. *Pure & Appl. Chem.* **1991,** 63, 1015-1080.

Chapter 7

Chemical Bath Deposition of ZnS on Functionalized Alkanethiolate Self-Assembled Monolayers Adsorbed on Gold

[Portions of this work have been published previously by Peng Lu and Amy V. Walker, *ACS Nano*, **2009**, *3*, 370-378]

Abstract: The reaction pathways involved in ZnS chemical bath deposition (CBD) on functionalized alkanethiolate self-assembled monolayers (SAMs) were studied with time-of-flight secondary ion mass spectrometry (TOF SIMS) and scanning electron microscopy (SEM). The reaction mechanism involves both cluster-by-cluster and ion-by-ion growth. The dominant reaction pathway is dependent on both the SAM terminal functionality and the experimental conditions. On -COOH terminated SAMs, two types of ZnS crystallites were observed after CBD: small ~ 500 nm nanoflowers formed *via* ion-by-ion growth and large ~ 2 μm crystallites formed by cluster-by-cluster deposition. On -OH and -CH_3 terminated SAMs, only ~ 2 μm crystallites formed *via* cluster-by-cluster deposition were observed. With CBD, ZnS nanoflowers was selectively deposited in the -COOH terminated SAM regions of a patterned -COOH/-CH_3 SAM, forming “nanoflowerbeds”.

7.1 Introduction

Nanoscale semiconductor materials have attracted extensive research interests over the past 20 years.[1] As a II-VI semiconductor, Zinc sulfide has many superior properties, such as a wide direct band gap (3.65 eV, bulk),[2] high transmittance in the visible range,[3] and a high reflective index.[3] ZnS thin films and nanostructures have many applications. The application of ZnS in optoelectronic devices, such as blue light-emitting diodes[4-8] and photovoltaics[9, 10], is well known. ZnS can also be used in electroluminescent devices,[11, 12] photocatalysts,[13-15] dielectric filters[16] and planar waveguides.[3] Since ZnS is less toxic and has a larger band gap than CdS, there is also interest in replacing CdS with ZnS as the "buffer layer" in solar cells.[9, 10] In addition, studies of using ZnS-polymer nanocomposites in photonic materials[17] and polymer light-emitting diodes[18] are also promising.

Understanding and controlling the interface of the ZnS layer and the organic component is important in many of the applications. However, it is difficult to study the interaction between ZnS and most organic substrates because the substrate properties can not be systematically controlled. Self-assembled monolayers (SAMs) (SAMs) can be employed to overcome these difficulties. SAMs are highly organized structures with a uniform density of terminal groups,[19, 20] and, thus, they provide a controllable platform to study the ZnS/organic layer interactions.

To date, various methods have been employed to fabricate ZnS films, including spray pyrolysis,[21, 22] thermal evaporation,[23, 24] molecular beam epitaxy (MBE),[25] H_2

plasma chemical sputtering,[26] chemical vapor deposition (CVD),[27-29] pulsed laser deposition,[30] atomic layer deposition (ALD),[31] electrodeposition,[32-34] successive ionic layer adsorption and reaction (SILAR),[35] and chemical bath deposition (CBD).[36-49] Among these techniques, chemical bath deposition is particularly attractive to deposit semiconductors on organic thin films. CBD is compatible with organic materials because it can be performed at low temperature (≤ 50 °C). It is also an easy and inexpensive technique that can be performed at ambient pressure. In addition, as a solution phase technique, CBD can be easily adapted to large area processing.

In this chapter, the reaction pathways involved in the chemical bath deposition of ZnS on functionalized SAM surfaces were studied. On -COOH terminated SAMs, two types of ZnS crystallites were formed *via* different reaction pathways. The ~ 500 nm nanoflowers were formed *via* an ion-by-ion mechanism, and they strongly adhered to the SAM surface. In contrast, the ~ 2 μm crystallites were formed *via* cluster-by-cluster precipitation and only loosely adhered to the SAM surface. On -OH and -CH_3 terminated SAMs, the cluster-by-cluster deposition was operative, leading to the deposition of ~ 2 μm crystallites that weakly adhered to the surface. Finally, selective deposition of ZnS "nanoflowerbeds" on a patterned -COOH/-CH_3 terminated SAM was also demonstrated using CBD.

7.2 Experimental

7.2.1 Materials

The alkanethiols used in this study including hexadecanethiol (HDT) (99%), 16-mercaptohexadecanoic acid (MHA) (99%) were purchased from Asemblon, Inc (Redmond, WA). Mercaptohexadecanol (MHL) was synthesized according to the procedure described by Walker et al.[50] Gold and chromium were purchased from Alfa Aesar Inc. (Ward Hill, MA) and were of 99.995% purity. Native silicon oxide wafers (<111> orientation) were purchased from Addison Technologies, Inc. (Pottstown, PA) and were cleaned with piranha etch (H_2SO_4 : H_2O_2 = 3 : 1) before use. Anhydrous ethanol (A.C.S. grade) was obtained from Aaper Alchohol (Shelbyville, KY). Zinc chloride (≥ 98%), hydrazine hydrate ($N_2H_4 \cdot xH_2O$, x ~ 1.5, N_2H_4 ~ 50% - 60%), thiourea (≥ 99%) and ammonia hydroxide solution (NH_4OH, 28% in H_2O) were purchased from Sigma Aldrich (Saint Louis, MO). All chemicals were used without further purification.

7.2.2 SAM Preparation

The preparation and characterization of alkanethiolate SAMs adsorbed on gold substrates have been described in details previously.[50-53] Briefly, first Cr (~5 nm) and then Au (~100 nm) were thermally deposited onto clean Si native oxide wafers. Then the prepared Au substrates were immersed into a 1 mM ethanolic solution of the relevant alkanethiolate molecule for 24 h at ambient temperature (21 ± 2 °C) to prepare well-organized SAMs. In order to ensure that the SAMs are well-ordered and free of significant chemical contamination, for each batch, one sample (~1 cm × 1 cm) was taken and characterized

using single-wavelength ellipsometry (Gaertner Scientific Corp., Skokie, IL) and TOF SIMS (ION TOF Inc., Chestnut Hill, NY) prior to chemical bath deposition.

7.2.3 ZnS Chemical Bath Deposition

The ZnS plating solution consisted of 7 mM $ZnCl_2$ as zinc ion source, 250 mM hydrazine (NH_2NH_2) and 100 mM ammonia hydroxide (NH_4OH) as complexing agent, and 7 mM thiourea (NH_2CSNH_2) as sulfur ion source. The plating solution was prepared as follows: first $ZnCl_2$ was dissolved in deionized water, then hydrazine and ammonia hydroxide solution were added dropwise into the $ZnCl_2$ solution. After adding hydrazine, the solution turned white and cloudy. After adding ammonia hydroxide, the cloudy solution became clear and colorless.

SAMs samples (~ 1 cm × 1 cm) were kept in the prepared solution for 15 min before the addition of thiourea to assist Zn^{2+} complexation with SAMs. This process is called “seeding”. After the seeding period, thiourea was added into the solution to initiate ZnS chemical bath deposition. In contrast, to investigate how Zn^{2+} complexation with the -COOH terminated SAMs can impact the ZnS deposition process, thiourea was added to the bath solution prior to immersion of the MHA SAM in a set of “unseeded” conditions.

The pH of the bath solution was 10.5 and remained constant during the deposition process. Deposition was performed at 22 °C and 45 °C from 1 min up to 2 h. After chemical bath deposition, samples were rinsed thoroughly first with copious amounts of deionized water then anhydrous ethanol, dried using nitrogen gas and immediately transferred to the TOF SIMS or SEM for analysis.

7.2.4 UV Photopatterning of SAMs

The patterned -COOH/-CH_3 terminated SAM was prepared with the following UV photopatterning procedure. First, a copper TEM grid (Electron Microscopy Inc., Hatfield, PA) was placed on top of the -COOH terminated SAM (MHA) as a mask. The sample was then placed ~ 50mm away from a 500W Hg arc lamp which is equipped with a dichroic mirror to remove IR light and a narrow-band-pass filter (280-440 nm) (Thermal Oriel, Spectra Physics Inc., Stratford, CT). After 2h exposure to UV light, the -COOH terminated SAM was then immersed in a freshly made 1mM -CH_3 terminated alkanethiol (HDT) ethanolic solution for 24 h. During the immersion, HDT was adsorbed in the areas exposed to UV light and resulted in a patterned -COOH/-CH_3 terminated SAM surface. The patterned SAM was rinsed with copious degassed ethanol and dried with N_2 before use.

7.2.5 Time-of-Flight Secondary Ion Mass Spectrometry (TOF SIMS)

An ION TOF IV spectrometer equipped with a Bi liquid metal ion gun (ION TOF Inc., Chestnut Hill, NY) was employed to perform the TOF SIMS analyses. Briefly, this apparatus consists of a load lock for sample introduction, a preparation chamber and an analysis chamber, separated by gate valves. The pressure of the preparation and analysis chambers were maintained at $< 3.8 \times 10^{-9}$ mbar. In a standard analysis process, the primary Bi^+ ions were accelerated to 25 keV and contained within a ~100 nm diameter probe beam, and the beam was rastered over the sample for spectra and image acquisition. Typically, the raster area was (100 × 100) μm^2 during spectra acquisition and (500 × 500)

μm^2 during image acquisition. All spectra were acquired within the static regime[54] using a total ion dose less than 10^{11} ions cm^{-2}. The secondary ions were extracted into a time-of-flight mass spectrometer with a 2000V potential and were reaccelerated to 10 keV before reaching the detector.

In this study, the mass spectra peak intensities were reproducible within to ± 10% from scan to scan and from sample to sample. For each experiment, at least two samples were employed and three areas on each sample were analyzed. The ion intensity data presented represent an average of these measurements.

A video camera (ExwaveHAD, Sony) mounted in the TOF SIMS analysis chamber was used to capture optical images of the samples.

7.2.6 Scanning Electron Microscopy (SEM)

A Field Emission Scanning Electron Microscope (Hitachi s-4500) was employed for the SEM measurements. This apparatus is equipped with a NORAN Instruments energy dispersive x-ray (EDX) microanalysis system, a back scattering detector and a mechanical straining stage. The diameters of the deposited ZnS crystallites were measured from the scanned high resolution SEM images. For each deposition condition, 150 - 200 crystallites were measured to obtain the size distribution.

7.3 Results

7.3.1 ZnS Deposition on -COOH terminated SAMs

After 2 h deposition, ZnS nanocrystallites were observed to deposit on -COOH

terminated SAMs. SEM images indicate that two types of ZnS structures were formed: an overlayer of smaller flowerlike ZnS nanocrystallites (570 ± 80 nm) covered the entire MHA surface, and larger flower-like crystallites (2100 ± 390 nm) scattered on the surface (Figure 7.1). More crystallites of both types formed at a bath temperature of 45 °C than at 22 °C. EDX analysis confirmed that the nanoflowers contained only Zn and S in an approximately 1:1 ratio. No molecular or cluster ions of mercaptohexadecanoic acid (MHA) monolayer were observed in the TOF SIMS spectra, indicating that MHA SAM was covered by a ZnS overlayer (Figure 7.2).

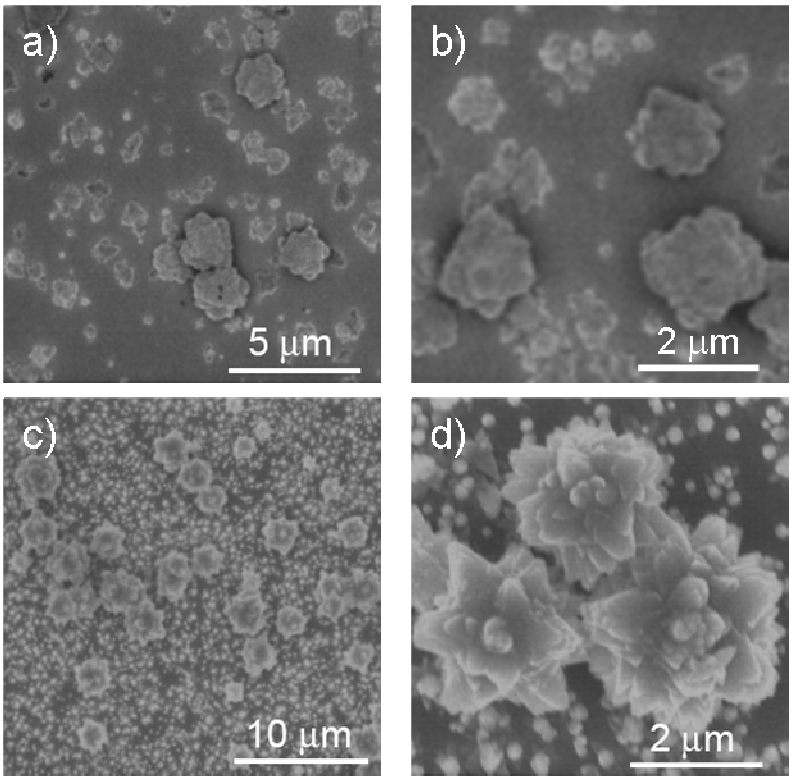

Figure 7.1 SEM images after ZnS chemical bath deposition for 2h on -COOH terminated SAMs at (a, b) 22 °C, (c, d) 45 °C.

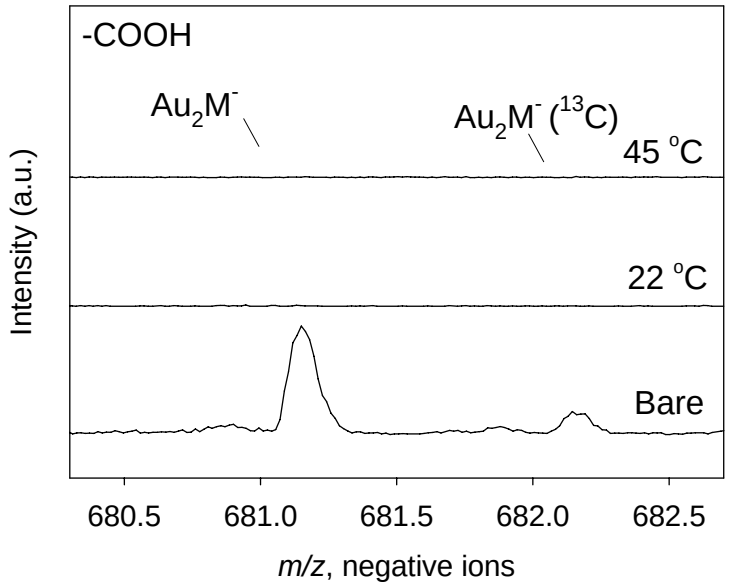

Figure 7.2 High mass resolution negative ion TOF SIMS spectra of the molecular cluster ion, Au_2M^- (M = $-S(CH_2)_{15}COOH$), for -COOH terminated SAM prior to and after ZnS chemical bath deposition for 2 h at 22 °C and at 45 °C.

TOF SIMS data show that Zn^{2+} ions interacted with -COOH terminated SAM. In the positive ion TOF SIMS spectra, a series of $Zn(COO)_2(CH_2)_x(CH)_y^+$ ions were observed, suggesting that Zn^{2+} complexed with two surface -COOH terminal groups (Figure 7.3). The surface Zn^{2+}-carboxylate complexes provided nucleation sites for the subsequent ZnS nanocrystallites growth. No $Au_xZn_yS_z^-$ ions formation was observed in the negative ion TOF SIMS spectra, indicating that Zn or ZnS did not penetrate through the MHA SAM to the Au/S interface.

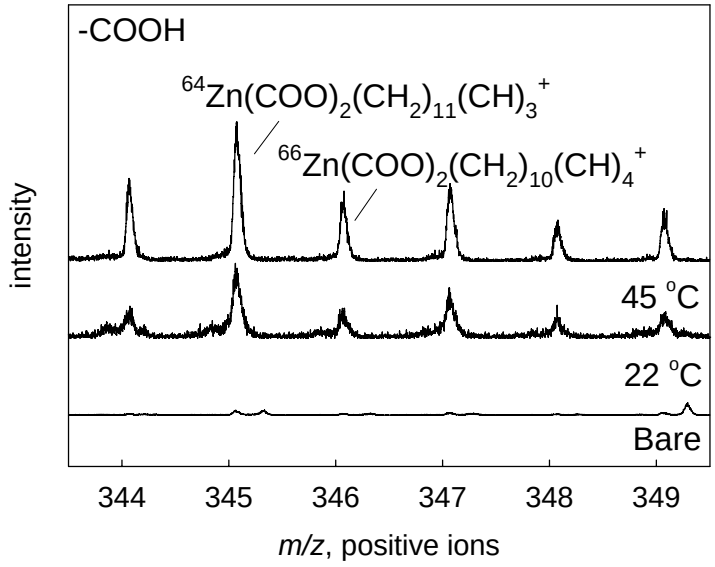

Figure 7.3 High mass resolution positive ion TOF SIMS spectra of $Zn(COO)_2(CH_2)_x(CH)_y^+$ ions (x = 11, y = 3 and x = 10, y = 4) of -COOH terminated SAM prior to and after ZnS chemical bath deposition for 2 h at 22 °C and 45 °C. The ions were assigned based on accurate mass and were not structurally characterized.

ZnS CBD was also performed under "unseeded" conditions in which the MHA SAM was directly immersed in a plating solution containing both Zn^{2+} and thiourea. Under "unseeded" conditions, many large ~ 2 μm flower-like crystallites and only a few scattered ~ 500 nm nanoflowers were observed to form on -COOH terminated SAMs (Figure 7.4c). In contrast, under "seeded" conditions a densely packed layer of ~ 500 nm nanoflowers with a few scattered ~ 2 μm flower-like crystallites were observed (Figure 7.4a). The large flower-like crystallites formed under both conditions could be removed from the MHA surface by sonication, but the small nanoflowers could not be removed, indicating they were strongly adhered to the MHA SAM surface (Figure 7.4b, d).

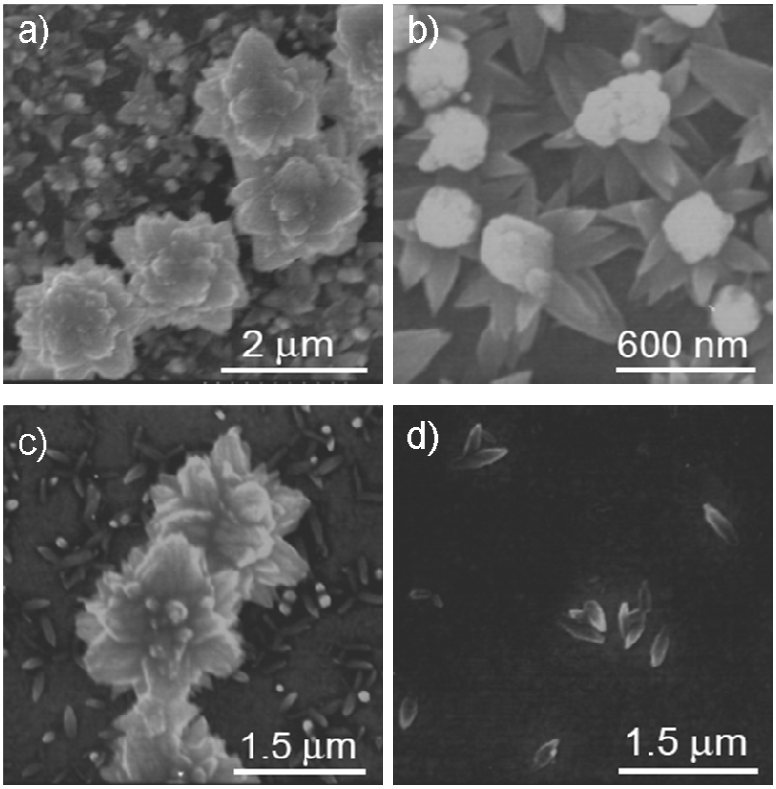

Figure 7.4 SEM images after ZnS chemical bath deposition at 45 °C for 2 h on -COOH terminated SAMs under the following experimental conditions: (a) seeded deposition prior to ultrasonication; (b) seeded deposition after 5 min ultrasonication; (c) unseeded deposition prior to ultrasonication; (d) unseeded deposition after 5 min ultrasonication. The nanoflowers in (b) are of the same sizes as the smaller flowers in (a).

ZnS nanocrystallites growth with time under both “seeded” and “unseeded” conditions was also investigated. Under “seeded” conditions, in the SEM image scattered crystallites were observed to form on -COOH terminated SAMs after 1 min in the bath, and these crystallites formed a densely packed layer after 30 min. Large crystallites were observed to form after 5 min in the bath, and the number of these crystallites increased with time (Figure 7.5). Under “unseeded” conditions, the number of large flower-like crystallites increased with time, but the sizes of these crystallites only increased slightly (Figure 7.6). Table 7.1 summarizes the average diameter of large flower-like crystallites under “seeded” and “unseeded” conditions from 1 min to 120 min bath.

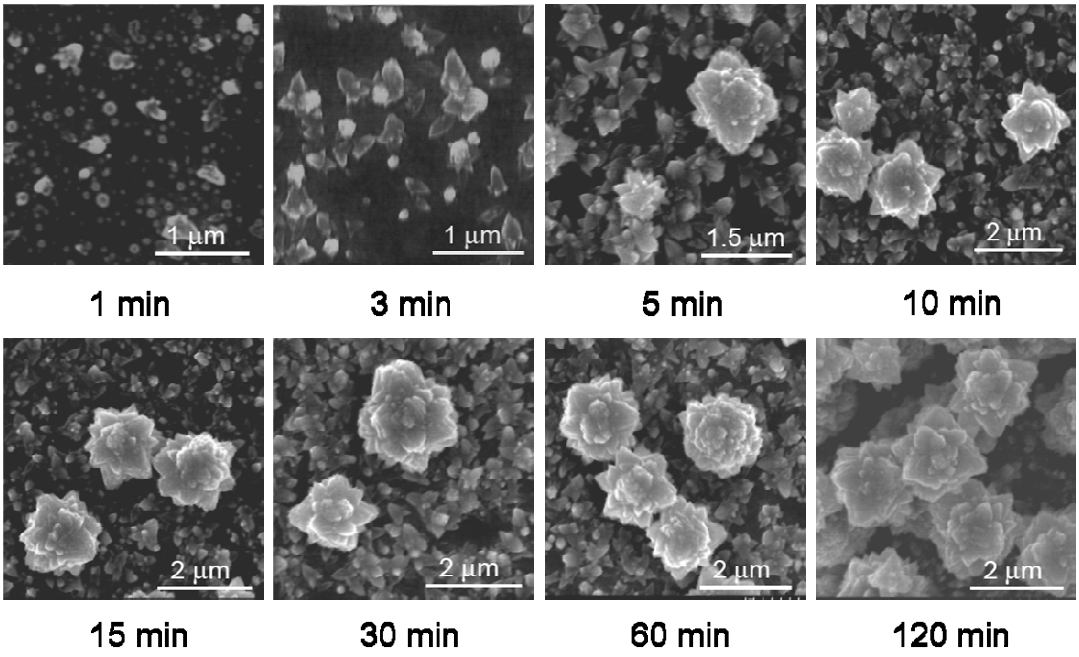

Figure 7.5 SEM images after ZnS chemical bath deposition under "seeded" conditions on -COOH terminated SAMs at 45 °C from 1 min to 120 min.

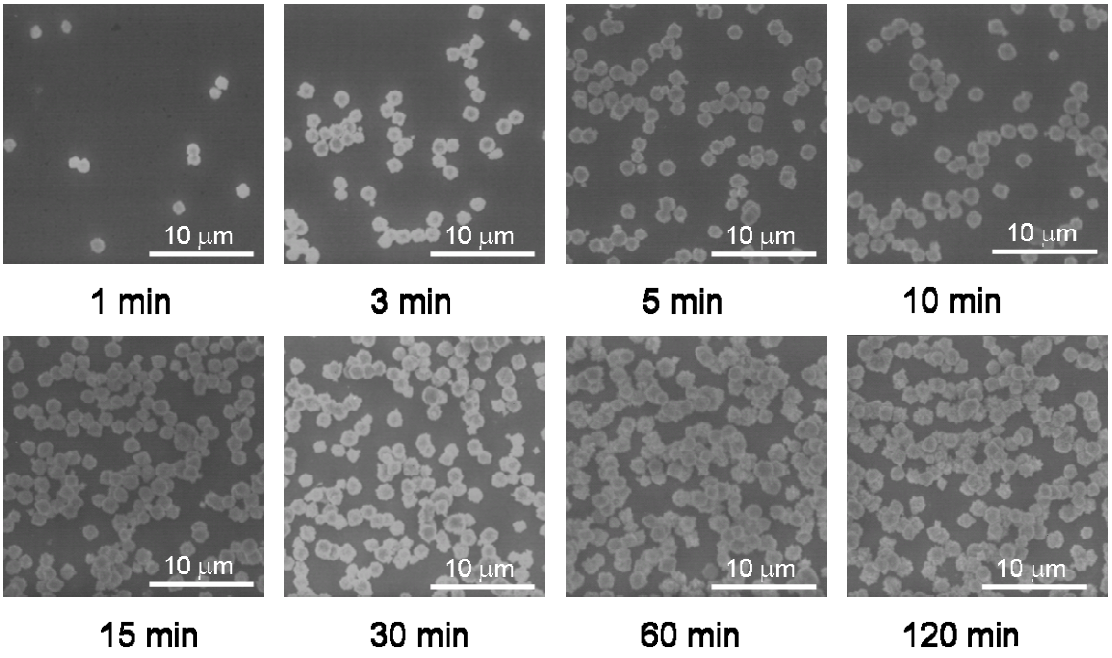

Figure 7.6 SEM images after ZnS chemical bath deposition under "unseeded" conditions on -COOH terminated SAMs at 45 °C from 1 min to 120 min

Immersion Time (min)	Average Diameter (μm)	
	Seeded	**Unseeded**
1	0.15 ± 0.07	1.40 ± 0.24
3	1.37 ± 0.49	1.57 ± 0.16
5	1.37 ± 0.49	1.47 ± 0.17
10	1.38 ± 0.38	1.51 ± 0.21
15	1.63 ± 0.43	1.48 ± 0.21
30	1.74 ± 0.43	1.58 ± 0.20
60	1.79 ± 0.46	1.58 ± 0.22
120	2.10 ± 0.39	1.69 ± 0.19

Table 7.1 Average diameters of large flower-like crystallites for ZnS CBD under unseeded and seeded experimental conditions on -COOH terminated SAM at 45 °C for immersion time from 1 min to 120 min.

The size distribution and number density of the large ZnS crystallites as a function of deposition time under both "seeded" and "unseeded" conditions were also obtained (Figure 7.7 and Appendix A7.7, A7.8). Under both "seeded" and "unseeded" conditions, the number of large flower-like crystallites increased with deposition time (Figure 7.7 a). In addition, the number of large flower-like crystallites under "unseeded" conditions was approximately twice as under "seeded" conditions. Size distributions of the large crystallites were also different (Figure 7.7 b and Appendix A7.7, A7.8). Under "seeded" conditions, the size of the crystallites increased from 0.15 ± 0.07 μm (1 min immersion) to 2.10 ± 0.39 μm (120 min immersion), and the size distribution was relatively broad. In contrast, under unseeded conditions, the size of the crystallites increased very slowly with time (from 1.40 ± 0.24 μm after 1 min immersion to 1.69 ± 0.19 μm after 120 min immersion), and the crystallites size distribution was relatively narrow (Figure 7.7 b).

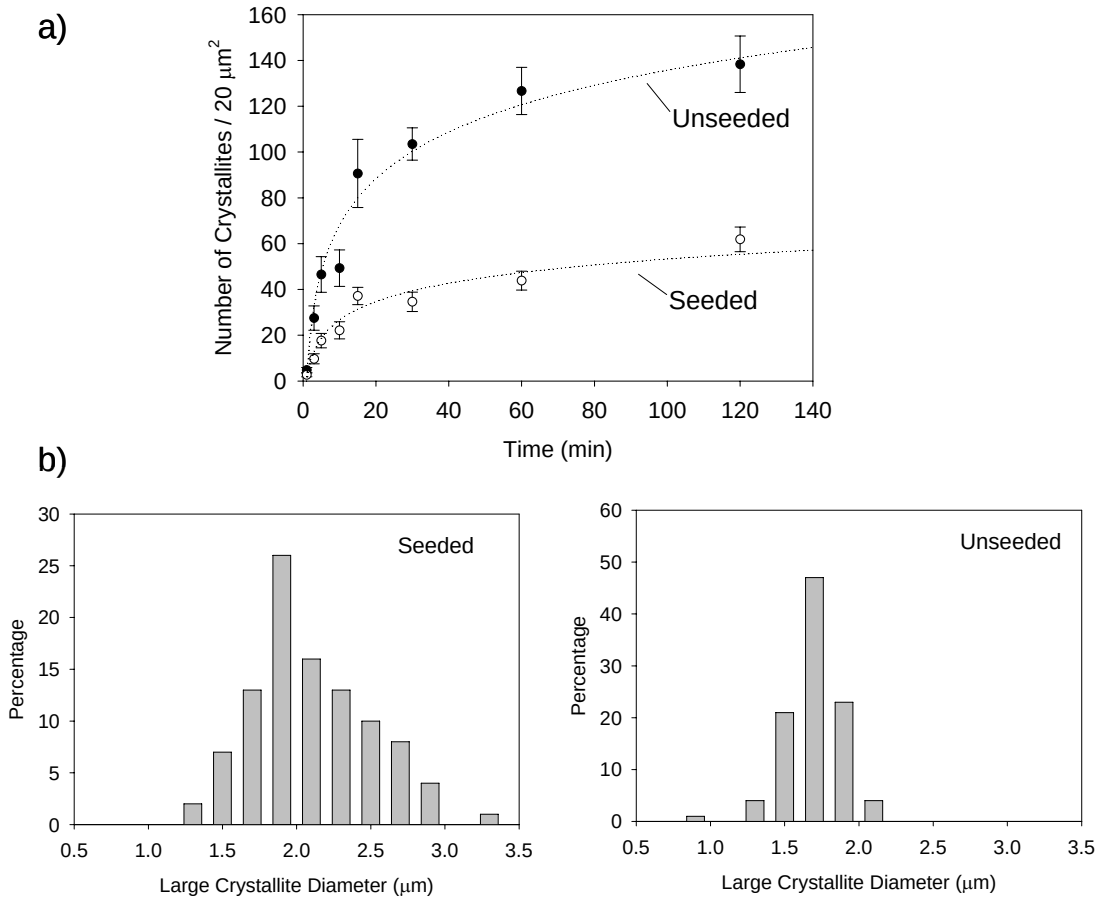

Figure 7.7 (a) Number of large scattered flower-like ZnS crystallites with immersion time. The dotted lines are drawn to guide the eye. (b) Size distribution of large flower-like ZnS crystallites after 120 min CBD bath. The width of the bar is ± 0.10 μm. Average diameters of the large ZnS crystallites are 2.10 ± 0.39 μm under seeded conditions and 1.69 ± 0.19 μm under unseeded conditions after 120 min bath.

7.3.2 ZnS Deposition on -OH and -CH_3 terminated SAMs

Unlike on -COOH terminated SAM, SEM images show that on -OH and -CH_3 terminated SAMs only a few ZnS crystallites were formed at 45 °C, and no ZnS crystallites was observed at 22 °C. No overlayer consisting of ~ 500 nm nanoflowers was observed either (Figure 7.8). Further, these ZnS crystallites loosely adhered to -OH and -CH_3 terminated SAMs, and could be easily removed using sonication (Figure 7.8 c, f).

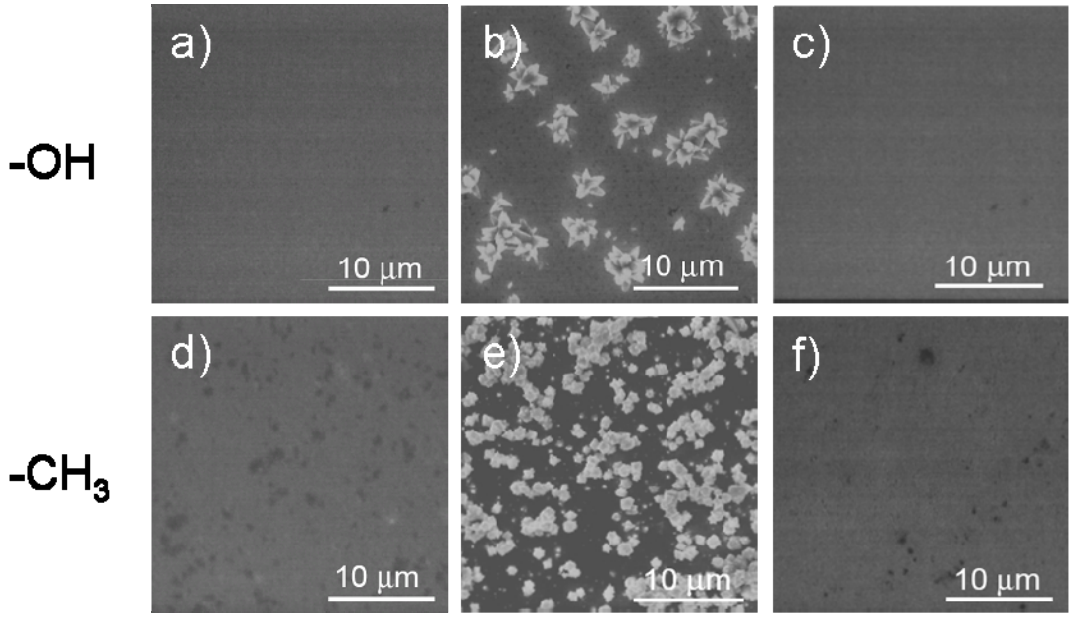

Figure 7.8 SEM images after ZnS chemical bath deposition for 2 h on -OH and -CH_3 terminated SAMs at (a, d) 22 °C, (b, e) 45 °C, and (c, f) 45 °C after ultrasonication in deionized water for 5 min.

TOF SIMS spectra are consistent with SEM data. In the negative ion TOF SIMS spectra, molecular cluster ions (Au_2M^-) of -OH and -CH_3 terminated SAMs were observed after ZnS CBD (Figure 7.9 and Appendix A7.3-A7.6). These ions are characteristic of the SAMs and indicate that ZnS did not form an overlayer on either the -OH or the -CH_3 terminated SAMs. No evidence of Zn^{2+}-SAM complex was observed in the mass spectra (data not shown), suggesting that Zn^{2+} ions did not complex with -OH or -CH_3 terminated SAMs. Cluster ions $Au_xZn_yS_z^-$ were also observed in the negative ion mass spectra, indicating that Zn penetrated through -OH and -CH_3 terminated SAMs to the Au/S interface (Figure 7.10). However, no definite conclusion can be drawn whether the observation of $Au_xZn_yS_z^-$ clusters was caused by Zn^{2+} ions penetration or small ZnS clusters penetration.

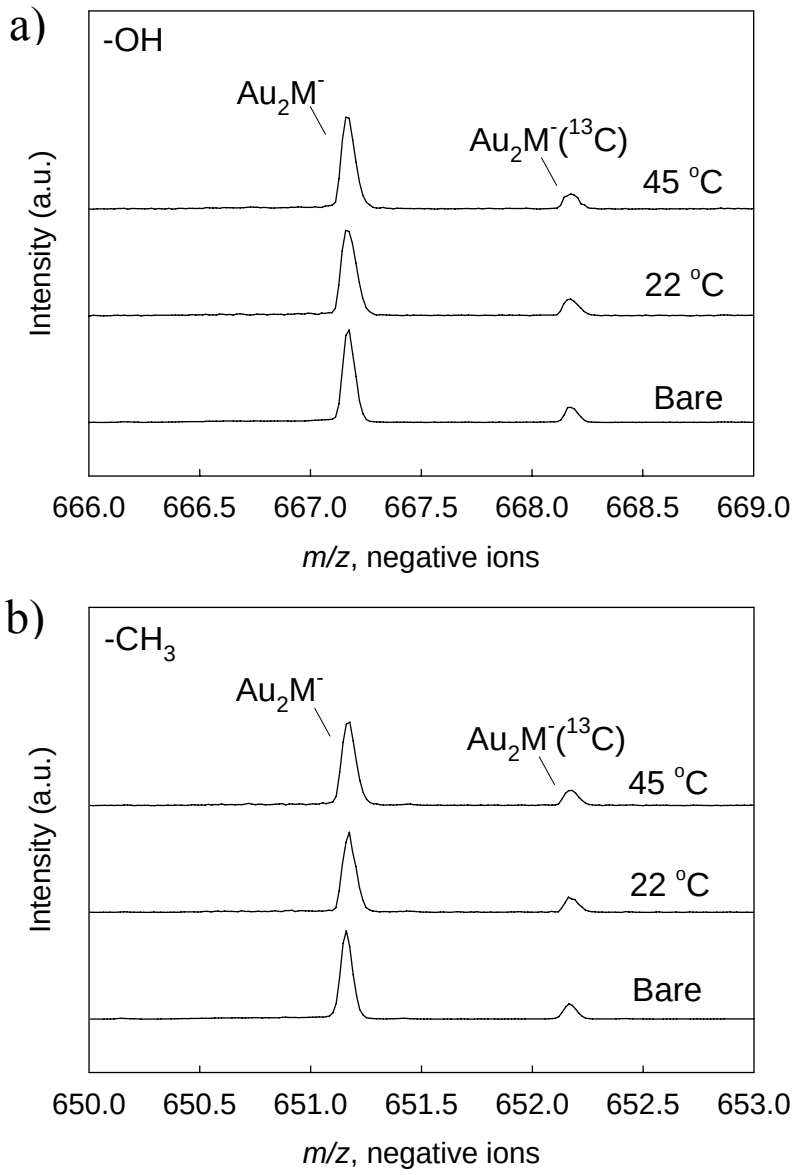

Figure 7.9 High mass resolution negative ion TOF SIMS spectra of (a) the molecular cluster ion, Au_2M^- (M = $-S(CH_2)_{15}CH_2OH$), for -OH terminated SAM; (b) the molecular cluster ion, Au_2M^- (M = $-S(CH_2)_{15}CH_3$), for $-CH_3$ terminated SAM prior to and after ZnS chemical bath deposition for 2 h at 22 °C and at 45 °C

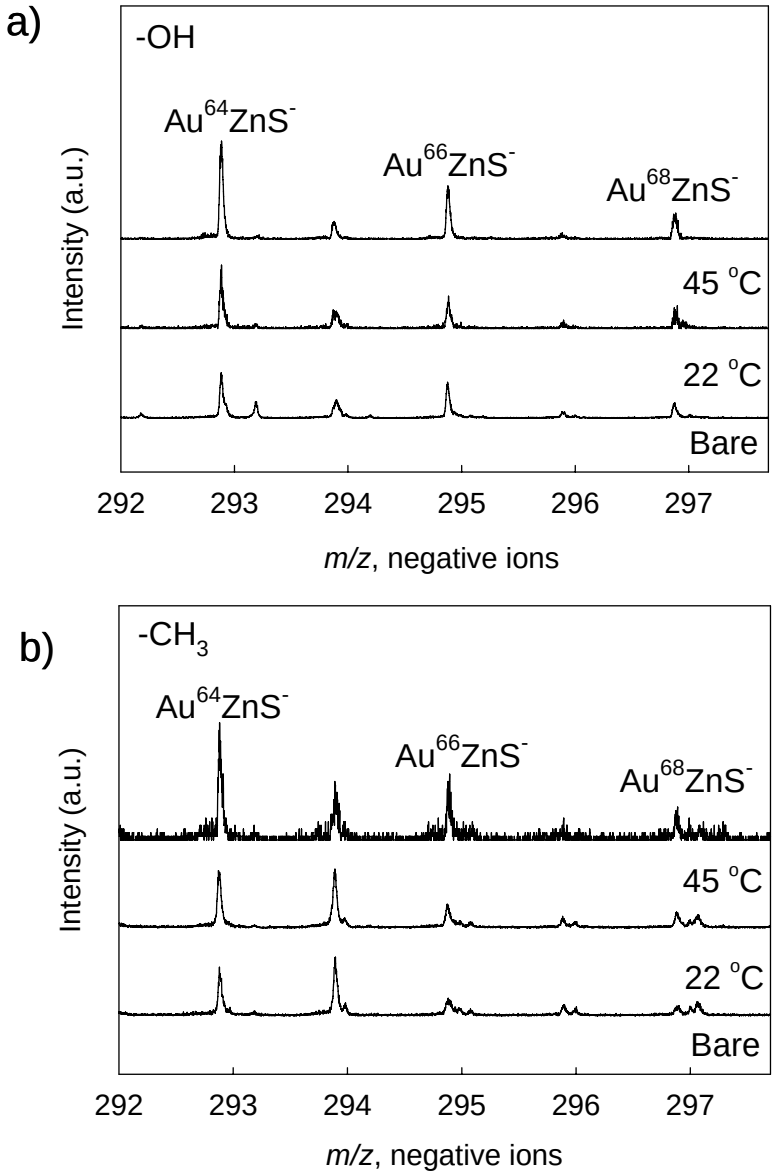

Figure 7.10 High-resolution negative ion TOF SIMS spectra of $AuZnS^-$ for (a) -OH and (b) $-CH_3$ terminated SAMs prior to and after ZnS chemical bath deposition for 2 h at 22 °C and 45 °C.

7.4 Discussion

7.4.1 Reaction Pathways of ZnS Nanoflowers Deposition on -COOH, -OH and -CH_3 terminated SAMs

In general, a chemical bath deposition employs a controlled ion-exchange reaction to deposit a thin film on a substrate in solution.[45, 49, 55] For ZnS CBD, a chalcongenide, normally thiourea, is used as a sulfur source to produce ZnS films. The chalcongenide decomposes in an alkaline solution containing a zinc salt and a suitable complexing agent, such as hydrazine and ammonia, and releases S^{2-} to form ZnS. The overall reaction can be given by:

$$Zn^{2+} + nL \rightleftharpoons ZnL_n^{2+} \quad (1)$$

$$SC(NH_2)_2 + 2OH^- \rightleftharpoons S^{2-} + H_2CN_2 + 2H_2O \quad (2)$$

$$Zn^{2+} + S^{2-} \rightleftharpoons ZnS \quad (3)$$

where L is the complexing agent and ZnL_n^{2+} is a complex Zn(II) ion. In this study, the complexing agent is hydrazine or ammonia.

There have been many studies on ZnS CBD, but the reaction pathways involved are not well understood, and no definite mechanism has been established.[36-49] Dona and Herrero[55] suggested an ion-by-ion mechanism where ZnS deposition occurs *via* the slow release and condensation of Zn^{2+} and S^{2-} ions at the surface. In contrast, based on the observation that the deposited ZnS films appeared to consist of an aggregation of spherical particles, Froment and Lincot[56] suggested a cluster-by-cluster deposition mechanism that ZnS forms colloidal particles in solution, and these then deposit on the

surface.

Based on the experimental observations, we propose the following reaction pathways for ZnS nanoflowers formation. Upon immersion in the plating solution, Zn^{2+} ions form Zn^{2+}-carboxylate on -COOH terminated SAMs, but do not with -OH or -CH_3 terminated SAMs. Since the pK_a of hexadecanoic (palmitic) acid film (~ 8.5-8.8)[57] is lower than the pH of the plating solution (10.5), many of the -COOH terminal groups on -COOH terminated SAMs are deprotonated, promoting formation of Zn^{2+}-carboxylate complexes. The observation of $Zn(COO)_2(CH_2)_x(CH)_y^+$ ions in the positive ion TOF SIMS spectra supports this hypotesis, suggesting that zinc ions complex with two carboxylate groups (Figure 7.3). Once formed, the Zn^{2+}-carboxylate complex can react with S^{2-} from the hydrolysis of thiourea to form ZnS.

This mechanism explains two experimental findings. First, well-separated ZnS nanocrystallites were formed on -COOH terminated SAMs because the nuclei Zn^{2+}-carboxylate complexes were sparsely distributed on the surface. Compared with the binding constants of Zn^{2+} with ammonia ($Zn^{2+} + 4NH_3 \rightleftharpoons Zn(NH_3)_4^{2+}$, $K = 7.9 \times 10^8$) and hydrazine ($Zn^{2+} + 3N_2H_4 \rightleftharpoons Zn(N_2H_4)_3^{2+}$, $K = 3.2 \times 10^5$),[58] the equilibrium constant for Zn^{2+} and carboxylic acid complexation is very low ($K < 100$)[59]. Given the large concentration of ammonia hydroxide and hydrazine in the plating solution, few Zn^{2+}-carboxylate complexes are likely to form and distribute sparsely on -COOH terminated SAMs. These complexes provide nucleation sites for ZnS deposition, and thus discrete ZnS crystallites rather than a smooth ZnS film were observed. Second, when the

temperature of the reaction increased from 22 °C to 45 °C, the ZnS deposition rate on -COOH terminated SAMs did not substantially increase (Figure 7.1). One of previously identified characteristics of ion-by-ion growth is that the deposition rate does not increase significantly with higher bath temperature,[55] and thus the temperature dependence is consistent with the proposed mechanism.

The large micron-size crystallites on -COOH, -OH and -CH_3 terminated SAMs were formed *via* a cluster-by-cluster mechanism. In this pathway, ZnS colloids formed in solution, aggregated, and adsorbed to the SAM surface. These crystallites did not strongly adhere to the SAMs, and could be easily removed using sonication. TOF SIMS data suggest that there was no interaction between Zn^{2+} ions and the -OH and -CH_3 terminal groups. Deposition rate increased with temperature in a typical cluster-by-cluster deposition.[55, 60] This explains the temperature dependence of deposition on -OH and -CH_3 terminated SAMs: significant deposition was only observed at 45 °C but not at 22 °C.

Finally, a combination of ion-by-ion growth and cluster-by-cluster deposition explains the observed behaviors of micro-sized crystallites during "seeded" and "unseeded" growth on -COOH terminated SAMs. Under the "unseeded" conditions, the cluster-by-cluster growth dominated owing to the lack of nucleating complexes at the surface. Under the "seeded" conditions, the ion-by-ion growth of nanoflowers was competitive with the cluster-by-cluster deposition because preformed Zn^{2+}-carboxylate complexes acted as nuclei. Seeding also substantially affected the size and distribution of the larger crystallites, suggesting that other growth mechanisms, such as ripening of the

large flower-like crystallites, were also operative (Table 7.1, Figure 7.7, and Appendix A7.7, A7.8).

7.4.2 Selective Deposition of ZnS on Patterned SAM Surfaces: Formation of Nanoflowerbeds

Under appropriate experimental conditions, ZnS nanoflowers can be selectively deposited on patterned SAM using chemical bath deposition, forming "nanoflowerbeds". As a demonstration, ZnS CBD was carried out on a UV photopatterned -COOH/-CH_3 SAM at 45 °C for 15 min. After the deposition, SAM was sonicated in deionized water for 5 min and then imaged using SEM and TOF SIMS. The optical and SEM images clearly show that ZnS nanoflowers were only observed in the -COOH terminated SAM regions (the "bar" areas), while no ZnS was deposited in the -CH_3 terminated SAM regions (the "square" areas) (Figure 7.11 a, b). In addition, $^{64}Zn^{+}$ positive ions (*m/z* 64), which is characteristic of the ZnS nanoflowers, were only observed in the -COOH terminated SAM areas, suggesting that ZnS nanoflowers only formed in these regions (Figure 7.11 c).

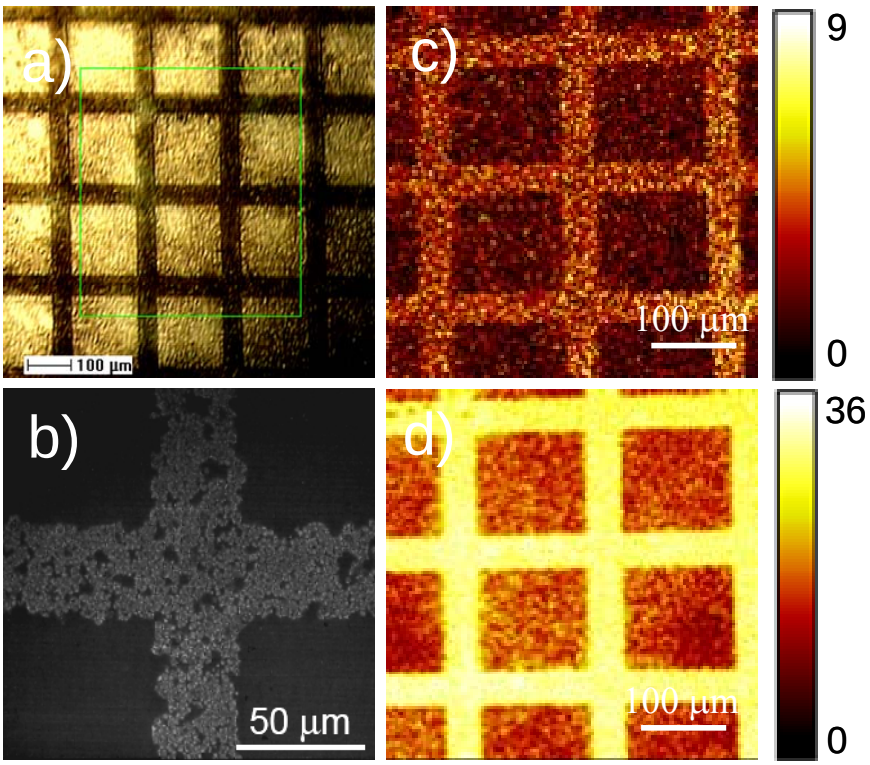

Figure 7.11 (a) Optical, (b) SEM, (c) TOF SIMS image centered at $^{64}Zn^{+}$ (*m/z* 64), (d) TOF SIMS image centered at OH^{-} (*m/z* 17) after ZnS chemical bath deposition on a patterned -COOH/-CH_3 terminated SAM surface at 45 °C for 15 min. The light gray crystallites in the SEM image indicate that ZnS nanoflowers were deposited only in the -COOH terminated SAM regions. The OH^{-} ion intensity is indicative of the -COOH terminated SAM areas. The intensity of the $^{64}Zn^{+}$ ion indicates that ZnS has been selectively deposited in the -COOH terminated SAM areas. Parameters of TOF SIMS analysis: primary ion, Bi^{+}; kinetic energy = 25 keV; area of analysis = (500 × 500) μm^2, (128 × 128) $pixels^2$. Intensity scale represent maximum ion count.

7.5 Conclusions

Chemical bath deposition of ZnS on functionalized SAMs proceeds *via* both ion-by-ion and cluster-by-cluster mechanism. On -COOH terminated SAMs, both ~ 500 nm nanoflowers and ~ 2 μm flower-like crystallites were observed. The nanoflowers grew *via* an ion-by-ion pathway from the Zn^{2+}-carboxylate complexes on the surface and strongly adhered to the -COOH terminated SAM surface. In contrast, the large crystallites formed *via* cluster-by-cluster deposition and did not strongly adhere to SAM surface.

On -OH and $-CH_3$ terminated SAMs, cluster-by-cluster deposition is the dominant mechanism, leading to the formation of ~ 2 μm flower-like crystallites which did not strongly adhere to the SAM surfaces.

Using CBD, ZnS can be selectively deposited in the -COOH terminated SAM regions of a patterned -COOH/$-CH_3$ SAM, forming "nanoflowerbeds".

In summary, CBD can be employed to deposit selectively semiconductor overlayers on organic thin films, and the size and morphology of the deposited semiconductor can be controlled by altering the substrate surface chemistry and deposition conditions. To obtain stable overlayers on organic films, it is important to form surface complexes which act as nucleation sites for further film growth.

Appendix: Positive and negative TOF SIMS spectra of -COOH, -OH, and $-CH_3$ terminated SAMs prior to and after ZnS chemical bath deposition at 22°C and 45 °C for 2 h; Size distribution of large flower-like ZnS crystallites under seeded and unseeded

condition as a function of time on -COOH terminated SAMs: These data can be found in the Appendix Figures A7.1-A7.8.

7.6 References

1. Hu, J.; Odom, T. W.; Lieber, C. M., Chemistry and Physics in One Dimension: Synthesis and Properties of Nanowires and Nanotubes. *Acc. Chem. Res* **1999,** 32, 435-445.

2. Gao, X. D.; Li, X. M.; Yu, W. D., Morphology and Optical Properties of Amorphous ZnS films Deposited by Ultrasonic-Assisted Successive Ionic Layer Adsorption and Reaction Method. *Thin Solid Films* **2004,** 468, 43-47.

3. Ruffner, J. A.; Himel, M. D.; Mizrahi, V.; Stegeman, G. l.; Gibson, U. J., Effects of Low Substrate Temperature and Ion Assisted Deposition on Composition, Optical Properties, and Stress of ZnS Thin Films. *Appl. Opt* **1989,** 28, 5209-5214.

4. Taguchi, T.; Yokogawa, T., Effects of Oxygen Impurity on the Surface in ZnS Crystals and Blue Light-Emitting Diodes. *J. Phys. D: Appl. Phys.* **1984,** 17, 1067-1082.

5. Yamaga, S., Epitaxial ZnS MπS Blue Light Emitting Diode Fabricated on n+-GaAs by Low-Pressure Metalorganic Vapor Phase Epitaxy. *Jpn. J. Appl. Phys.* **1991,** 30, 437.

6. Katayama, H.; Oda, S.; Kukimoto, H., ZnS Blue-Light-Emitting Diodes with an External Quantum Efficiency of 5 X 10^{-4}. *Appl. Phys. Lett.* **1975,** 27, 697-699.

7. Lawther, C.; Fujita, T.; Takagi, T., Blue-Emitting S^{+} - Implanted An-ZnS Schottky Barrier Diodes. *Jpn. J. Appl. Phys* **1980,** 19, 939-947.

8. Ohno, T.; Kurisu, K.; Taguchi, T., Growth of High-Quality Cubic ZnS Crystals and Their Application to MIS Blue Light-Emitting Diodes. *J. Cryst. Growth* **1990,** 99, 737-742.

9. Nakada, T.; Mizutani, M., 18% Efficiency Cd-Free Cu(In,Ga)Se_2 Thin-Film Solar Cells Fabricated Using Chemical Bath Deposition (CBD)-ZnS Buffer Layers. *Jpn. J. Appl. Phys.* **2002,** 41, L165-L 167.

10. Nasr, T. B.; Kamoun, N.; Kanzari, M.; Bennaceur, R., Effect of pH on the Properties of ZnS Thin Films Grown by Chemical Bath Deposition. *Thin Solid Films* **2006,** 500, (2006), 4-8.

11. Horii, Y.; Kitagawa, M.; Taneoka, H.; Kusano, H.; Murakami, T.; Hino, Y.; Kobayashi, H., Electroluminescence Properties of PVCz Electroluminescent Devices Doped with Nano-Crystalline Particles. *Mater. Sci. Eng. B* **2001,** 85, 92-95.

12. Que, W.; Zhou, Y.; Lam, Y. L.; Chan, Y. C.; Kam, C. H.; Liu, B. W.; Gan, L. M.; Chew, C. H.; Xu, G. Q.; Chua, S. J.; al., e., Photoluminescence and Electroluminescence from Copper Doped Zinc Sulphide Nanocrystals/Polymer Composite. *Appl. Phys. Lett.* **1998,** 73, 2727-2729.

13. Kakuta, N.; Park, K. H.; Finlayson, M. F.; Ueno, A.; Bard, A. J.; Campion, A.; Fox, M. A.; Webber, S. E.; White, J. M., Photoassisted Hydrogen Production Using Visible Light and Coprecipitated ZnS · CdS Without a Noble Metal. *J. Phys. Chem.* **1985,** 89, 732-734.

14. Hu, J.-S.; Ren, L.-L.; Guo, Y.-G.; Liang, H.-P.; Cao, A.-M.; Wan, L.-J.; Bai, C.-L.,

Mass Production and High Photocatalytic Activity of ZnS Nanoporous Particles. *Angew. Chem., Int. Ed.* **2005,** 44, 1269-1273.

15. Johne, P.; Kisch, H., Photoreduction of Carbon Dioxide Catalysed by Free and Supported Zinc and Cadmium Sulphide Powders. *J. Photochem. Photobiol., A* **1997,** 111, 223-228.

16. Ledger, A. M., Inhomogeneous Interface Laser Mirror Coatings. *Appl. Opt.* **1979,** 18, 2979-2989.

17. Huang, K. J.; Rajendran, P.; Liddell, C. M., Chemical Bath Deposition Synthesis of Sub-Micron ZnS-Coated Polystyrene. *J. Colloid Interface Sci.* **2007,** 308, 112-120.

18. Huang, J. M.; Yang, Y.; Yang, B.; Liu, S. Y.; Shen, J. C., Assembly and Applications of the Inorganic Nanocrystals in Polymer Networks. *Thin Solid Films* **198,** 327-329, 536-540.

19. Schreiber, F., Structure and Growth of Self-Assembling Monolayers. *Prog. Surf. Sci.* **2000,** 65, 151-256.

20. Ulman, A., Formation and Structure of Self-Assembled Monolayers. *Chem. Rev.* **1996,** 96, 1533-1554.

21. Afifi, H. H.; Mahmoud, S. A.; Ashour, A., Structural Study of ZnS Thin Films Prepared by Spray Pyrolysis. *Thin Solid Films* **1995,** 263, 248-251.

22. Elidrissi, B.; Addoua, M.; Regraguia, M.; Bougrinea, A.; Kachouanea, A.; Berne`de, J. C., Structure, Composition and Optical Properties of ZnS Thin Films Prepared by Spray Pyrolysis. *Mater. Chem. Phys.* **2001,** 68, 175-179.

23. Wang, Y.; Zhang, L.; Liang, C.; Wang, G.; Peng, X., Catalytic Growth and Photoluminescence Properties of Semiconductor Single-Crystal ZnS Nanowires. *Chem. Phys. Lett.* **2002,** 357, 314-318.

24. Zhu, Y.-C.; Bando, Y.; Xue, D.-F., Spontaneous Growth and Luminescence of Zinc Sulfide Nanobelts. *Appl. Phys. Lett.* **2003,** 82, 1769-1771.

25. Yoneta, M.; Ohishi, M.; Saito, H.; Hamasaki, T., Low Temperature Molecular Beam Epitaxial Growth of ZnS/GaAs(001) by Using Elemental Sulfur Source. *J. Cryst. Growth* **1993,** 127, 314-317.

26. Tonouchi, M.; Sun, Y.; Miyasato, T.; Sakama, H.; Ohmura, M., Room-Temperature Synthesis of ZnS:Mn Films by H2 Plasma Chemical Sputtering. *Jpn. J. Appl. Phys.* **1990,** 29, L2453-L2456.

27. Dean, P. J.; Pitt, A. D.; Skolnick, M. S.; Wright, P. J.; Cockayne, B., Optical Properties of Undoped Organometallic Grown ZnSe and ZnS. *J. Cryst. Growth* **1982,** 59, 301-306.

28. Nakamura, S.; Yamada, Y.; Taguchi, T., Room-Temperature 340 nm Ultraviolet Electroluminescence from ZnS-Based Light-Emitting Diodes. *J. Cryst. Growth* **2000,** 214/215, 1091-1095.

29. Abounadi, A.; Di Blasio, M.; Bouchara, D.; Calas, J.; Averous, M.; Briot, O.; Briot, N.; Cloitre, T.; Aulombard, R. L.; Gil, B., Reflectivity and Photoluminescence Measurements in ZnS Epilayers Grown by Metal-Organic Chemical-Vapor Deposition. *Phys. Rev. B* **1994,** 50, 11677-11683.

30. Hillie, K. T.; Curren, C.; Swart, H. C., ZnS Thin Films Grown on Si(100) by XeCl Pulsed Laser Ablation. *Appl. Surf. Sci.* **2001,** 177, 73-77.

31. Tammenmaa, M.; Koskinen, T.; Hiltunen, L.; Niinisto , L.; Leskela, M., Zinc Chalcogenide Thin Films Grown by the Atomic Layer Epitaxy Technique Using Zinc Acetate as Source Material. *Thin Solid Films* **1985,** 124, 125-128.

32. Fathy, N.; Kobayashi, R.; Ichimura, M., Preparation of ZnS Thin Films by the Pulsed Electrochemical Deposition. *Mater. Sci. Eng. B* **2004,** 107, 271-276.

33. Lokhande, C. D.; Jadhav, M. S.; Pawar, S. H., Electrodeposition of ZnS Films from an Alkaline Bath. *J. Electrochem. Soc.* **1989,** 136, 2756-2757.

34. Sanders, B. W.; Kitai, A. H., The Electrodeposition of Thin Film Zinc Sulphide from Thiosulphate Solution. *J. Cryst. Growth* **1990,** 100, 405-410.

35. Meldrum, F. C.; Flatha, J.; Knoll, W., Formation of Patterned PbS and ZnS Films on Self-Assembled Monolayers. *Thin Solid Films* **1999,** 348, 188-195.

36. Arenas, O. L.; Nair, M. T. S.; Nair, P. K., Chemical Bath Deposition of ZnS Thin Films and Modification by Air Annealing. *Semicond. Sci. Technol.* **1997,** 12, 1323-1330.

37. Bayer, A.; Boyle, D. S.; O'Brien, P., In Situ Studies of the Chemical Bath Deposition of Zinc Sulfide from Acidic Solutions. *J. Mater. Chem.* **2002,** 12, 2940-2944.

38. Cheng, J.; Fan, D.; Wang, H.; Liu, B.; Zhang, Y.; Yan, H., Chemical Bath Deposition of Crystalline ZnS Thin Films. *Semicond. Sci. Technol.* **2003,** 18, 676-679.

39. Cruz-vazquez, C.; Rocha-alonzo, F.; Burruel-ibarra, S. E.; Barboza-flores, M.; Bernal, R.; Inoue, M., A New Chemical Bath Deposition Method for Fabricating ZnS, $Zn(OH)_2$,

and ZnO Thin Films, and the Optical and Structural Characterization of These Materials. *Appl. Phys. A* **2004,** 79, 1941-1945.

40. Dona, J. M.; Herrero, J., Chemical Bath Codeposited CdS-ZnS Film Characterization. *Thin Solid Films* **1995,** 268, 5-12.

41. Gangopadhyay, U.; Kim, K.; Mangalaraj, D.; Yi, J., Low Cost CBD ZnS Antireflection Coating on Large Area Commercial Mono-Crystalline Silicon Solar Cells. *Applied Surface Science* **2004,** 230, 364-370.

42. Gode, F.; Gumus, C.; Zor, M., Influence of the Thickness on Physical Properties of Chemical Bath Depositied Hexagonal ZnS Thin Films. *J. Optoelectron. Adv. Mater.* **2007,** 9, 2186-2191.

43. Ladar, M.; Popovici, E.-J.; Baldea, I.; Grecu, R.; Indrea, E., Studies on Chemical Bath Deposited Zinc Sulphide Thin Films with Special Optical Properties. *Journal of Alloys and Compounds* **2007,** 434-435, 697-700.

44. Lee, J.; Lee, S. H.; Cho, S.; Kim, S.; Park, I. Y.; Choi, Y. D., Role of Growth Parameters on Structural and Optical Properties of ZnS Nanocluster Thin Films Grown By Solution Growth Techniques. *Mater. Chem. Phys.* **2002,** 77, 254-260.

45. O'Brien, P.; McAleese, J., Developing and Understanding of the Processes Controlling the Chemical Bath Deposition of ZnS and CdS. *J. Mater. Chem.* **1998,** 8, (11), 2309-2314.

46. O'Brien, P.; Otway, D. J.; Smyth-Boyle, D., The Importance of Ternary Complexes in Defining Basic Conditions for the Deposition of ZnS by Aqueous Chemical Bath

Deposition. *Thin Solid Films* **2000,** 361-362, 17-21.

47. Roy, P.; Ota, J. R.; Srivastava, S. K., Crystalline ZnS Thin Films by Chemical Bath Deposition Method and Its Characterization. *Thin Solid Films* **2006,** 515, 1912–1917.

48. Sartale, S. D.; Sankapal, B. R.; Lux-Steiner, M.; Ennaoui, A., Preparation of Nanocrystalline ZnS by a New Chemical Bath Deposition Route. *Thin Solid Films* **2005,** 480-481, 168-172.

49. Yamaguchi, K.; Yoshida, T.; Lincot, D.; Minoura, H., Mechanistic Study of Chemical Deposition of ZnS Thin Films from Aqueous Solutions Containing Zinc Acetate and Thioacetamide by Comparison with Homogeneous Precipitation. *J. Phys. Chem. B* **2003,** 107, 387-397.

50. Fisher, G. L.; Walker, A. V.; Hooper, A. E.; Tighe, T. B.; Bahnck, K. B.; Skriba, H. T.; Reinard, M. D.; Haynie, B. C.; Opila, R. L.; Winograd, N.; Allara, D. L., Bond Insertion, Complexation, and Penetration Pathways of Vapor-Deposited Aluminum Atoms with HO- and CH3O-Terminated Organic Monolayers. *J. Am. Chem. Soc.* **2002,** 124, 5528-5541.

51. Fisher, G. L.; Hooper, A. E.; Opila, R. L.; Allara, D. L.; Winograd, N., The Interaction of Vapor-Deposited Al Atoms with CO_2H Groups at the Surface of a Self-Assembled Alkanethiolate Monolayer on Gold. *J. Phys. Chem. B* **2000,** 104, 3267-3273.

52. Hooper, A. E.; Fisher, G. L.; Konstadinidis, K.; Jung, D. R.; Nguyen, H.; Opila, R. L.; Collins, R. W.; Winograd, N.; Allara, D. L., Chemical Effects of Methyl and Methyl Ester

Groups on the Nucleation and Growth of Vapor-Deposited Aluminum Films. *J. Am. Chem. Soc.* **1999,** 121, (35), 8052–8064.

53. Nuzzo, R. G.; Dubios, L. H.; L., A. D., Fundamental Studies of Microscopic Wetting on Organic Surfaces. 1. Formation and Structural Characterization of a Self-Consistent Series of Polyfunctional Organic Monolayers. *J. Am. Chem. Soc.* **1990,** 112, 558-569.

54. Vickerman, J. C., *ToF SIMS: Surface Analysis by Mass Spectrometry.* IM Publications and Surface Spectra Limited: Chichester and Manchester, UK, 2001; p 1-40.

55. Dona, J. M.; Herrero, J., Process and Film Characterization of Chemical-Bath-Deposited ZnS Thin Films. *J. Electrochem. Soc.* **1994,** 141, (1), 205-210.

56. Froment, M.; Lincot, L., Electrochim. Acta. *Phase Formation Processes in Solution at the Atomic Level: Metal Chalcogenide Semiconductors* **1995,** 40, 1293-1303.

57. Kanicky, J. R.; Shah, D. O., Effect of Degree, Type, and Position of Unsaturation on the pKa of Long-Chain Fatty Acids. *J. Colloid Interface Sci.* **2002,** 256, 201-207.

58. Smith, R. M.; Martell, A. E., Critical Stability Constants. In Plenum Press: New York, 1976; Vol. 4, pp 40-43.

59. Martell, A. E.; Smith, R. M., *Critical Stability Constants*. Plenum Press: New York, 1974; Vol. 4.

60. Dona, J. M.; Herrero, J., Chemical Bath Deposition of CdS Thin Films: Electrochemical In Situ Kinetic Studies. *J. Electrochem. Soc.* **1992,** 139, 2810-2814.

Chapter 8

Chemical Bath Deposition of CdSe on Functionalized Alkanethiolate Self-Assembled Monolayers Adsorbed on Gold

Abstract: Chemical bath deposition of CdSe on functionalized alkanethiolate self-assembled monolayers (SAMs) was investigated using time-of-flight secondary ion mass spectrometry (TOF SIMS) and scanning electron microscopy (SEM). On all SAM surfaces, the CdSe deposited as nanoparticles with a very narrow size distribution. On -COOH terminated SAMs, the deposition of CdSe was a mixture of ion-by-ion and cluster-by-cluster mechanisms. Initially, Cd^{2+} ions formed Cd^{2+}-carboxylate complexes with the -COOH terminal groups, and these complexes then reacted with Se^{2-} ions to form CdSe *via* an ion-by-ion mechanism. After sufficient Se^{2-} ions were generated in the plating bath, CdSe colloids formed in solution and deposited on -COOH terminated SAMs. At this point, cluster-by-cluster deposition became the dominant process. On -OH and $-CH_3$ terminated SAMs, CdSe nanoparticles formed *via* a cluster-by-cluster deposition only. Finally, selective deposition of CdSe on -COOH terminated regions of -COOH/$-CH_3$ patterned SAMs was demonstrated.

8.1 Introduction

As a member of the II-VI group semiconductors, CdSe has many applications in nanotechnology, energy and biotechnology. CdSe nanocrystals have been employed in light emitting diodes[1-5], photodetectors,[6] laser sources,[7, 8] sensors,[9, 10] and photovoltaics.[11-16] In many of these applications, the structure of the interface between the organic component and Cdse layer is critical. To elucidate these interactions, we employed self-assembled monolayer (SAMs). This is because SAMs have highly organized structures with a uniform density of terminal groups, whose chemistry can be systematically varied.[17-19]

CdSe thin films and nanostructures have been fabricated with a variety of methods, including thermal evaporation,[20, 21] electrodeposition,[22, 23] spray pyrolysis,[24, 25] successive ionic layer adsorption and reaction (SILAR),[26, 27] chemical vapor deposition (CVD),[28, 29] and chemical bath deposition (CBD).[30-38] CBD is an attractive method to deposit CdSe on organic substrates because it can be used at low deposition temperatures. On inorganic substrates it has been demonstrated that the CdSe CBD process is influenced by many reaction parameters, including the plating solution composition,[31, 34, 37, 39] pH,[33, 35, 40] reaction temperature,[31, 33] as well as illumination during the CBD process.[41] It was also shown that CdSe deposition can occur either *via* an ion-by-ion growth on the substrate (successive anion and cation adsorption on the growing crystal) or *via* a cluster-by-cluster mechanism (solution phase colloids adsorption and coagulate on the substrate), depending on the experimental conditions.[31, 34, 35, 39, 42]

In the research described in this chapter, CdSe nanoparticles were deposited on functionalized SAMs using chemical bath deposition and the reaction pathways studied. On all surfaces studied, the CdSe nanoparticles deposited had a very narrow size distribution (≤ ±10%). On -COOH terminated SAMs, CdSe nanoparticles growth involved both ion-by-ion and cluster-by-cluster mechanisms. At the beginning of the CBD, Cd^{2+} ions formed Cd^{2+}-carboxylate complexes with the -COOH terminal groups. These complexes reacted with Se^{2-} ions to form CdSe and served as the nucleation sites for ion-by-ion growth. After a sufficient Se^{2-} ion concentration had built up in the plating solution, CdSe colloids formed in solution and cluster-by-cluster deposition became the dominant process. On -OH and -CH_3 terminated SAMs, Cd^{2+} ions did not complex with the terminal groups, and the deposition followed a cluster-by-cluster mechanism. Under appropriate conditions, CdSe nanoparticles could be selectively deposited on the -COOH regions of -COOH/-CH_3 patterned SAMs using chemical bath deposition.

8.2 Experimental

8.2.1 Materials

Gold and chromium (99.995% purity) were obtained from Alfa Aesar Inc. (Ward Hill, MA). Cadmium sulfate (≥ 99%), selenium (powder, 99.99%), sodium sulfite (≥ 98%) and nitrilotriacetic acid trisodium salt (NTA, ≥ 98%) were purchased from Sigma Aldrich (Saint Louis, MO). Silicon native oxide wafers (<111> orientation) were purchased from Addison Technologies, Inc. (Pottstown, PA) and were cleaned with piranha etch

(H_2SO_4:H_2O_2 = 3:1) before use. Anhydrous ethanol (A.C.S. grade) was obtained from Aaper Alchohol (Shelbyville, KY). 16-mercaptohexadecanoic acid (99%) (MHA), hexadecanethiol (99%) (HDT), and mercaptohexadecanol (99%) (MHL) were obtained from Asemblon, Inc (Redmond, WA). All chemicals were used without further purification.

8.2.2 SAM Preparation

Alkanethiolate SAMs adsorbed on gold substrates were prepared and characterized according to previously published procedures.[17, 43-45] Briefly, first Cr (~5 nm) then Au (~100 nm) were thermally deposited onto clean Si native oxide wafers. The deposited Au substrates were then immersed into a 1 mM ethanolic solution of the relevant hexadecanethiol molecule (with -COOH, -OH and -CH_3 terminal functional groups) for 24 h at ambient temperature (21 ± 2 °C) to prepare well-organized SAMs. For each batch one SAM sample (~ 1 cm × 1 cm) was taken and characterized using single-wavelength ellipsometry (Gaertner Scientific Corp., Skokie, IL) and TOF SIMS (ION TOF Inc., Chestnut Hill, NY) prior to chemical bath deposition. The results showed that the prepared SAMs were well-ordered and free from significant chemical contamination.

8.2.3 CdSe Chemical Bath Deposition

The standard plating solution employed in this study was composed of 40 mM cadmium sulfate ($CdSO_4$), 80mM sodium selenosulphate (Na_2SeSO_3), and 120 mM sodium nitrilotriacetate (NTA). Other concentrations (20 mM, 40 mM) of Na_2SeSO_3 were also employed to investigate the influence of solution composition on CdSe particle formation.

Na_2SeSO_3 was diluted from a 200 mM stock solution, which was made by dissolving 200 mM Se into 400 mM Na_2SO_3 aqueous solution at 60 °C for 2 hour.

To make the plating solution, cadmium sulfate was first dissolved in deionized water, and then sodium nitrilotriacetate was added into the solution. SAM samples (~ 1 cm × 1 cm) were kept in this solution for 15 min before the addition of Na_2SeSO_3 to allow Cd^{2+} complexation with the SAMs. This process is called "seeding". After the seeding process, Na_2SeSO_3 was added into the solution to initiate the deposition. CdSe CBD was also performed under "unseeded" conditions on -COOH terminated SAMs, where Na_2SeSO_3 was added to the bath prior to immersion of the sample.

Deposition was performed in a still solution at 22 °C and 45 °C for times from 1 min to 2 hour. The pH of the plating solution was 8.0 before the addition of Na_2SeSO_3. Immediately after adding Na_2SeSO_3, the plating solution pH increased to 9.5. During deposition, the pH of the solution gradually increased and reached 10.5 after 2 hour. After the deposition, samples were rinsed thoroughly with copious amounts of deionized water and absolute ethanol, dried using nitrogen gas and immediately transferred to the TOF SIMS or SEM for analysis.

8.2.4 UV Photopatterning of SAMs

Patterned -COOH/-CH_3 terminated SAMs were prepared using UV photopatterning following the procedures described by Zhou and Walker.[46-48] First a mask (copper TEM grid, Electron Microscopy, Inc. Hatfield, PA) was placed on top of a MHA SAM (-COOH terminated SAM) placed approximately 50 mm away from a 500 W Hg arc

lamp equipped with a dichroic mirror and a narrow-band-pass filter (280-400 nm) (Thermal Oriel, Spectra Physics Inc., Stratford, CT). The sample was then exposed to the UV light for 2 h. After light exposure, the MHA SAM was immersed into a freshly made 1 mM -CH_3 terminated alkanethiol (HDT) ethanolic solution for 24 h. In the areas exposed to UV light, a -CH_3 terminated SAM was adsorbed, creating a HDT/MHA patterned surface. The patterned SAM was rinsed extensively with degassed ethanol and dried with nitrogen before use.

8.2.5 Time-of-Flight Secondary Ion Mass Spectrometry (TOF SIMS)

TOF SIMS analyses were conducted using an ION TOF IV spectrometer (ION TOF Inc., Chestnut Hill, NY) equipped with a Bi liquid metal ion gun. This instrument consists of an air lock, a preparation chamber and an analysis chamber separated by gate valves. The preparation and analysis chambers were maintained at a pressure $\leq 3.8 \times 10^{-9}$ mbar. The Bi^+ primary ions were accelerated to 25 keV and contained within a ~100 nm diameter probe beam. The beam was rastered over a (100 × 100) μm^2 area for high resolution spectra acquisition and (500 × 500) μm^2 area for image acquisition. Total accumulated ion dose was less than 10^{11} ions cm^{-2}, which is within the static regime.[49] The secondary ions were extracted into a time-of-flight mass spectrometer using 2000V and were reaccelerated to 10 keV before reaching the detector. Peak intensities were reproducible to within ± 10% from scan to scan and from sample to sample. For each CdSe deposition, at least three samples were prepared and three areas on each sample were examined. The ion intensity data presented is therefore an average over at least six

measurements, and the uncertainty shown is standard deviation.

Optical images of the samples were captured using a video camera (ExwaveHAD, Sony) mounted in the TOF SIMS analysis chamber.

8.2.6 Scanning Electron Microscopy (SEM)

SEM measurements were conducted on a Field Emission Scanning Electron Microscope (Hitachi s-4500). This instrument is equipped with a NORAN Instruments energy dispersive x-ray (EDX) microanalysis system, a back scattering detector and a mechanical straining stage. The diameters of the deposited CdSe nanoparticles were measured from the scanned high resolution SEM images. For each deposition condition, 150 - 200 CdSe nanoparticles were measured to obtain the size distribution.

8.3 Results & Discussion

8.3.1 CdSe Deposition on -COOH terminated SAMs

After 2 h chemical bath deposition at 22 °C and 45 °C, CdSe nanoparticles were observed on -COOH terminated SAMs (Figure 8.1). Using EDX, it was observed that the deposited nanoparticles contained only Cd and Se in an approximately 1:1 ratio. The number and average diameter of the CdSe nanoparticles formed at 45 °C were larger than those formed at 22 °C. The average diameter of CdSe nanoparticles formed at 45 °C was 142 ± 11 nm, while nanoparticles formed at 22 °C had an average diameter of 56 ± 7 nm (Figure 8.2). In the TOF SIMS spectra, the SAM molecular ion (AuM_2^-, M = $-S(CH_2)_{15}COOH$) signal intensity decreased to zero after deposition at 22 °C and 45 °C,

suggesting that the SAM has been completely covered by the CdSe overlayer (Figure 8.3). Together with the SEM data, these observations suggest that a layer of smaller CdSe nanoparticles, which could not be detected by SEM, was formed on the -COOH terminated SAM surface at 22 °C.

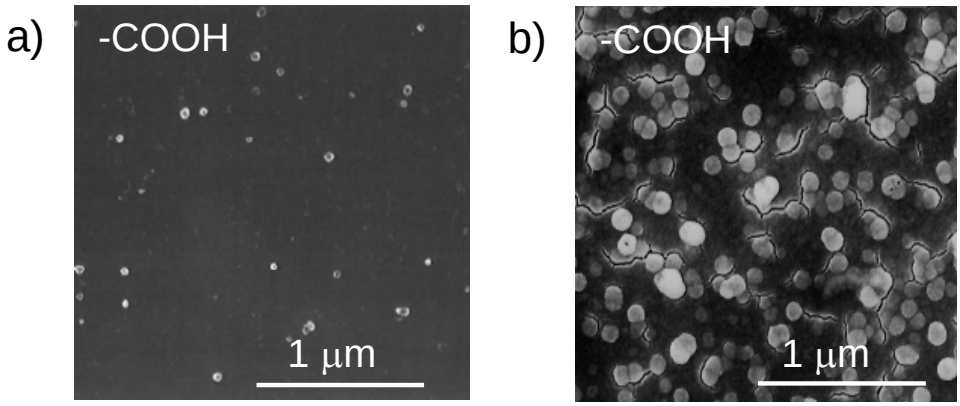

Figure 8.1 SEM images of -COOH terminated SAMs after 2 h chemical bath deposition at (a) 22 °C, (b) 45 °C

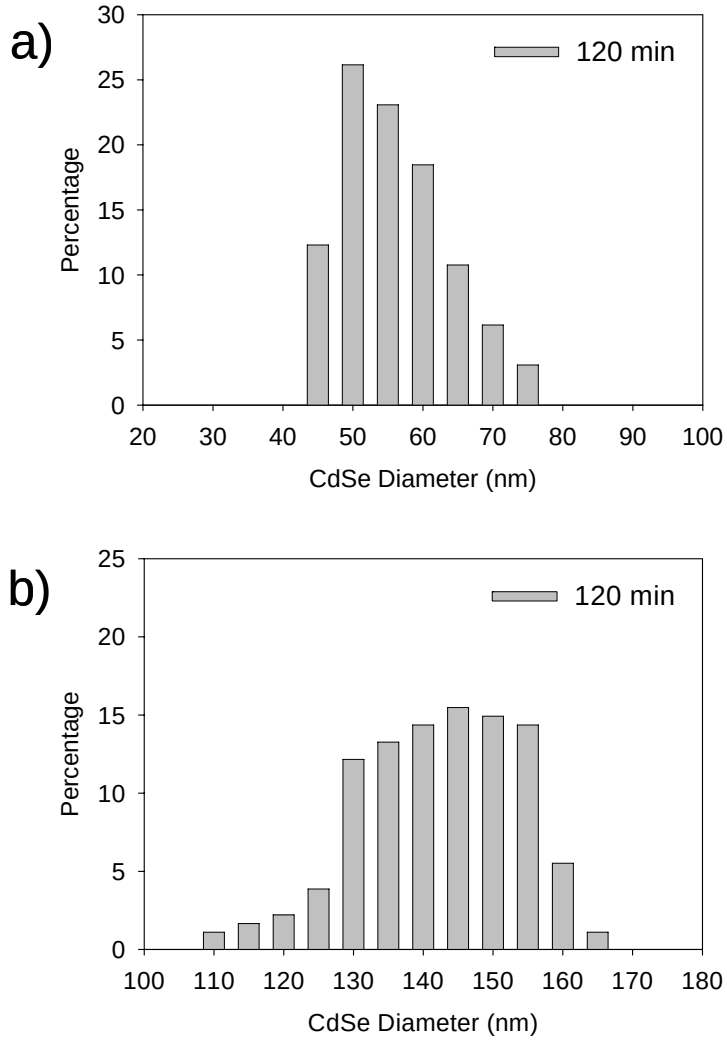

Figure 8.2 Size distribution of CdSe nanoparticles after 2 h chemical bath deposition on -COOH terminated SAMs at (a) 22 °C, (b) 45 °C. Average nanoparticle diameter is in (a) 56 ± 7 nm and in (b) 142 ± 11 nm. The width of the bar is ± 2.5 nm.

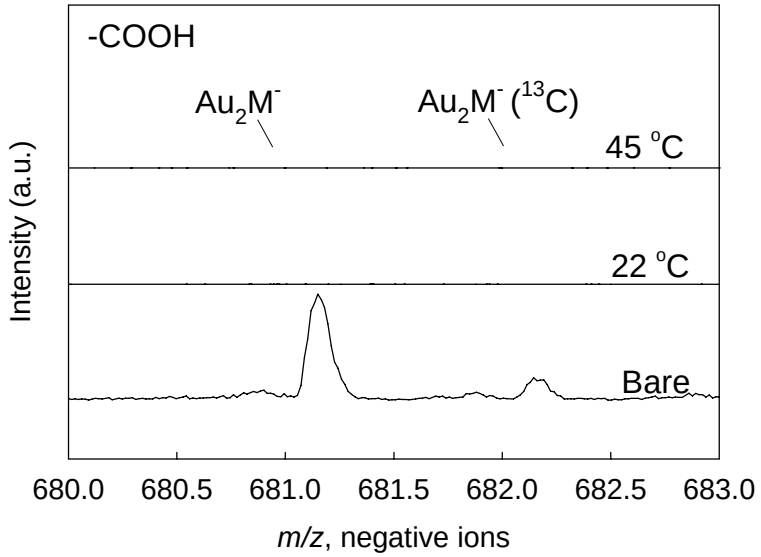

Figure 8.3 High mass resolution negative ion TOF SIMS spectra of the molecular cluster ion, Au_2M^- (M = $-S(CH_2)_{15}COOH$), for -COOH terminated SAM prior to and after CdSe chemical bath deposition for 2 h at 22 °C and at 45 °C.

The growth of CdSe nanoparticles was also investigated with immersion time in the deposition bath (Figure 8.4). Under standard deposition conditions ("seeded" conditions, 80 mM Na_2SeO_3), scattered CdSe crystallites were observed to form on -COOH terminated SAMs after 5 min deposition. The average diameter of the CdSe nanocrystallites increased from 34 ± 3 nm after 5 min to 142 ± 11 nm after 2 h deposition (Table 8.1). The number of CdSe nanocrystallites per unit area also increased and remained approximately constant after 15 min deposition (Figure 8.5).

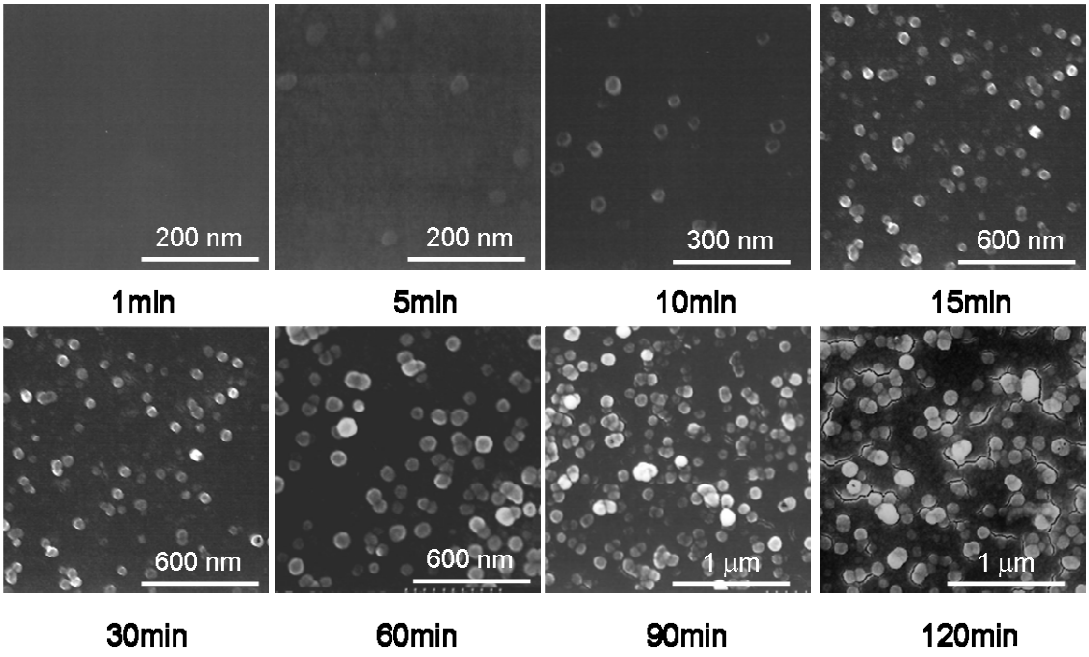

Figure 8.4 SEM images after CdSe chemical bath deposition under seeded conditions on -COOH terminated SAMs at 45 °C from 1 min to 120 min.

Dep. Time (min)	Average Diameter (nm)		
	20 mM Na_2SeSO_3	**40 mM Na_2SeSO_3**	**80 mM Na_2SeSO_3**
1	-.	-.	-
5	-	-	34 ± 3
10	-	-	33 ± 3
15	-	55 ± 3	45 ± 3
30	-	78 ± 7	66 ± 4
60	55 ± 12	115 ± 13	96 ± 7
90	92 ± 10	131 ± 15	124 ± 10
120	120 ± 8	143 ± 16	142 ± 11

Table 8.1 Average diameter of CdSe nanoparticles on -COOH terminated SAMs after chemical bath deposition at 45 °C from 1 min to 120 min under different Na_2SeSO_3 concentrations (20 mM, 40 mM and 80 mM).

The composition of the plating solution also affected the CdSe nanoparticle formation and growth. The size distribution and number of CdSe nanoparticles per unit area under different Na_2SeSO_3 concentrations are shown in Figure 8.5, and Appendix A8.1-A8.3. In agreement with previous studies,[31, 35] the CdSe nanoparticle growth rate was higher at larger Na_2SeSO_3 concentrations. The induction time (delay time for CdSe nanoparticles to form on the MHA surface after adding Na_2SeO_3) increased from 5 min to

60 min when the Na_2SeSO_3 concentration decreased from 80 mM to 20 mM. To form CdSe nanoparticles, Cd^{2+} ions react with Se^{2-} ions formed by the hydrolysis of $SeSO_3^{2-}$. So the most likely reason for the observed increase in induction time is that a sufficient concentration of Se^{2-} ions must be built up in the bath before CdSe colloids form. At higher Na_2SeSO_3 concentrations, a higher density of CdSe nanoparticles was also observed (Figure 8.5 b).

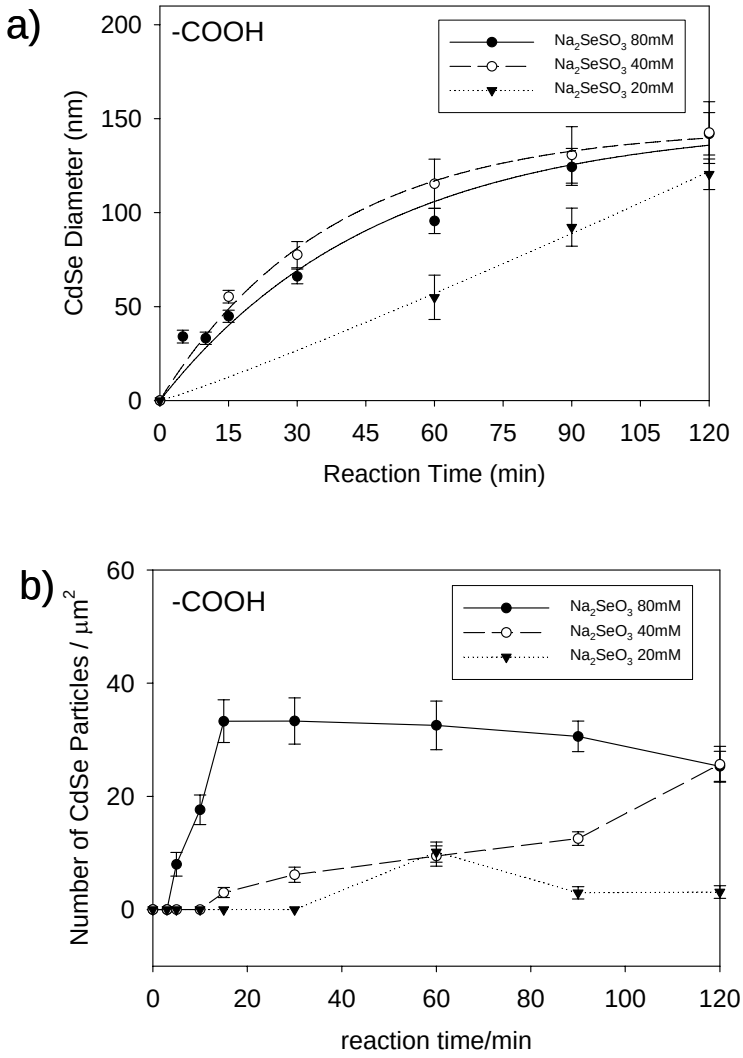

Figure 8.5 (a) Average CdSe nanoparticle diameter as a function of immersion time under different Na_2SeSO_3 concentrations; (b) Number of CdSe nanoparticles per μm^2 as a function of immersion time under different Na_2SeSO_3 concentrations. The lines are drawn to guide the eye. The error bars represent the standard deviation.

The TOF SIMS data also indicate that Cd^{2+} ions interacted with -COOH terminated SAMs and formed Cd^{2+}-carboxylate complexes (Figure 8.6). In the positive ion spectra, ions of the form $Cd(COO)_2(CH_2)_x(CH)_y^+$ were observed, indicating that Cd^{2+} complexed with two surface -COOH terminal groups. Once formed, these surface complexes reacted with Se^{2-} ions to form CdSe, and provided nucleation sites for subsequent CdSe nanoparticle growth. In the negative ion TOF SIMS spectra no $Au_xCd_yS_z^-$ or $Au_xSe_yS_z^-$ cluster ions were observed, indicating that no CdSe, Cd^{2+} or Se^{2-} penetrated through the -COOH terminated SAMs to the Au/S interface.

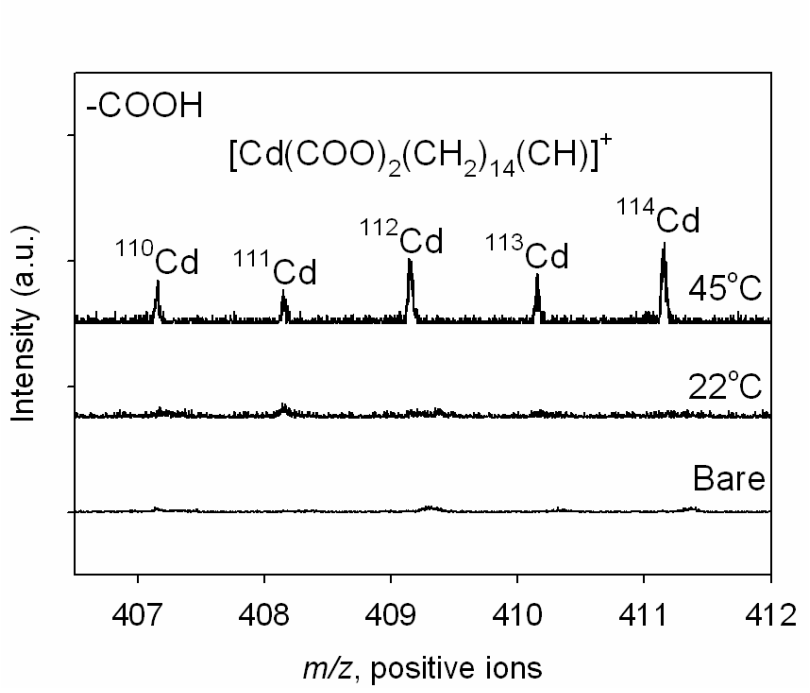

Figure 8.6 High mass resolution positive ion TOF SIMS spectra of $Cd(COO)_2(CH_2)_x(CH)_y^+$ ions (x = 14, y = 1) of -COOH terminated SAMs prior to and after CdSe chemical bath deposition for 2 h at 22 °C and 45 °C. The ions were assigned based on accurate mass and were not structurally characterized.

Similar to previous studies on ZnS chemical bath deposition,[50] the standard CdSe CBD process consisted of a "seeding" step in which the -COOH terminated SAMs were placed in a solution containing only Cd^{2+} ions and NTA for 15 min prior to addition of Na_2SeSO_3. The "seeding' step is designed to assist Cd^{2+} ions in complexing with deprotonated carboxylate groups on -COOH terminated SAMs. CdSe chemical bath deposition was also performed under "unseeded" conditions in which -COOH terminated SAMs were immersed directly into a plating solution containing both Cd^{2+} and $SeSO_3^{2-}$. Unlike ZnS CBD where the seeding process significantly impacted both the size and morphology of ZnS nanocrystallites,[50] CdSe nanoparticles of similar sizes and morphologies were observed to form under both conditions (Figure 8.7 a, c). After 2 h deposition at 45 °C, the average diameter of the CdSe nanoparticles was 138 ± 14 nm under "unseeded" conditions and 142 ± 11 nm under "seeded" conditions. The CdSe nanoparticles formed under both conditions strongly adhered to the MHA surface and could not be removed using sonication (Figure 8.7 b, d).

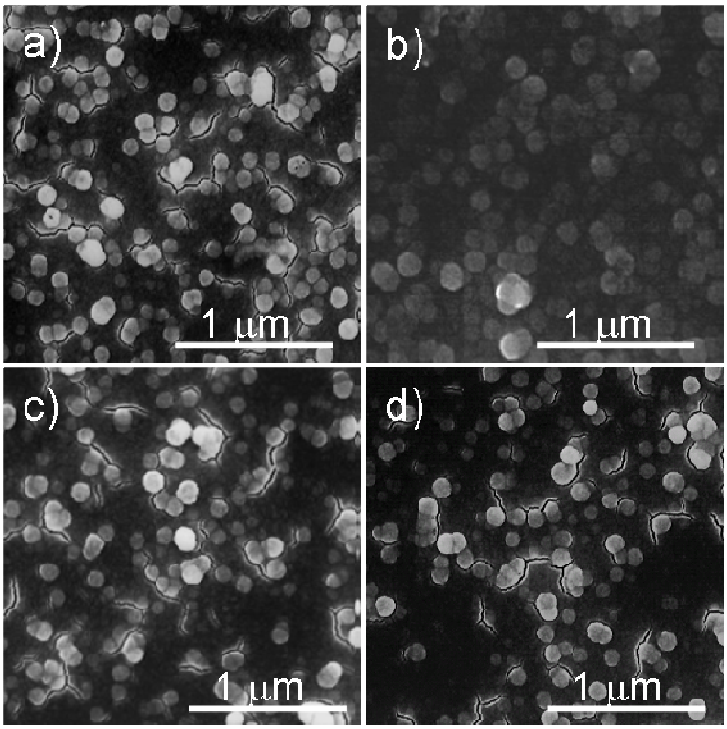

Figure 8.7 SEM images after CdSe chemical bath deposition at 45 °C for 2 h on -COOH terminated SAMs under the following experimental conditions: (a) “seeded” deposition prior to ultrasonication; (b) “seeded” deposition after 5 min ultrasonication; (c) “unseeded” deposition prior to ultrasonication; (d) “unseeded” deposition after 5 min ultrasonication.

8.3.2 CdSe Deposition on -OH and -CH_3 terminated SAMs

In contrast to -COOH terminated SAMs, on -OH and -CH_3 terminated SAMs no CdSe nanoparticles were observed to form after 2 h deposition at 22 °C (Figure 8.8 a, d). At 45 °C, CdSe nanoparticles deposited on both -OH and -CH_3 terminated SAMs (Figure 8.8 b, e). The size distributions and density of CdSe nanoparticles formed on -OH and -CH_3 terminated SAMs were very similar. The average diameter of the particles was 76 ± 7 nm, while the densities of the CdSe nanoparticles were 18.3 ± 3.2 and 15.3 ± 2.5 per μm^2 for -OH and -CH_3 terminated SAMs, respectively (Figure 8.9). These similarities suggest that the different surface properties of -OH (a hydrophilic surface) and -CH_3 terminated (a hydrophobic surface) SAMs did not affect the CdSe nanoparticle growth process, and that the surfaces did not actively participate in the CBD process. Further, on -OH and -CH_3 terminated SAMs, CdSe nanoparticles did not strongly adhere to the surfaces and can be removed after 5 min sonication (Figure 8.8 c, f).

The TOF SIMS spectra indicate that Cd^{2+} ions did not complex with -OH or -CH_3 terminated SAMs. No $Cd(CH)_x(CH_2)_y^{\pm}$, $Cd(O)_x(CH)_y(CH_2)_z^{\pm}$, or similar characteristic ions of a Cd^{2+}-surface interaction were observed. The data also indicate that Cd^{2+}, Se^{2-} or CdSe did not penetrate to the Au/S interface: in the negative ion mass spectra cluster ions such as $Au_xCd_yS_z^-$ or $Au_xSe_yS_z^-$ were not observed. Finally, after deposition at 22 °C and 45 °C, the molecular ions of -OH and -CH_3 terminated SAMs (Au_2M^-) were observed, suggesting that CdSe nanoparticles did not form an overlayer on either SAM surface (Figure 8.10).

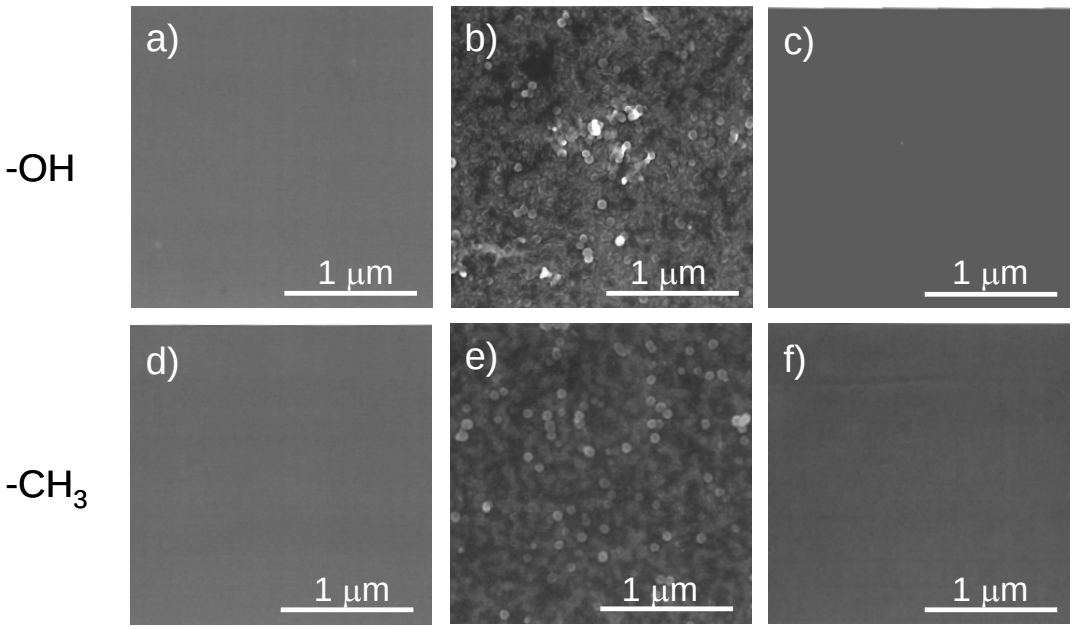

Figure 8.8 SEM images after CdSe chemical bath deposition for 2 h on -OH and -CH_3 terminated SAMs at (a, d) 22 °C, (b, e) 45 °C, and (c, f) 45 °C after ultrasonication in deionized water for 5 min.

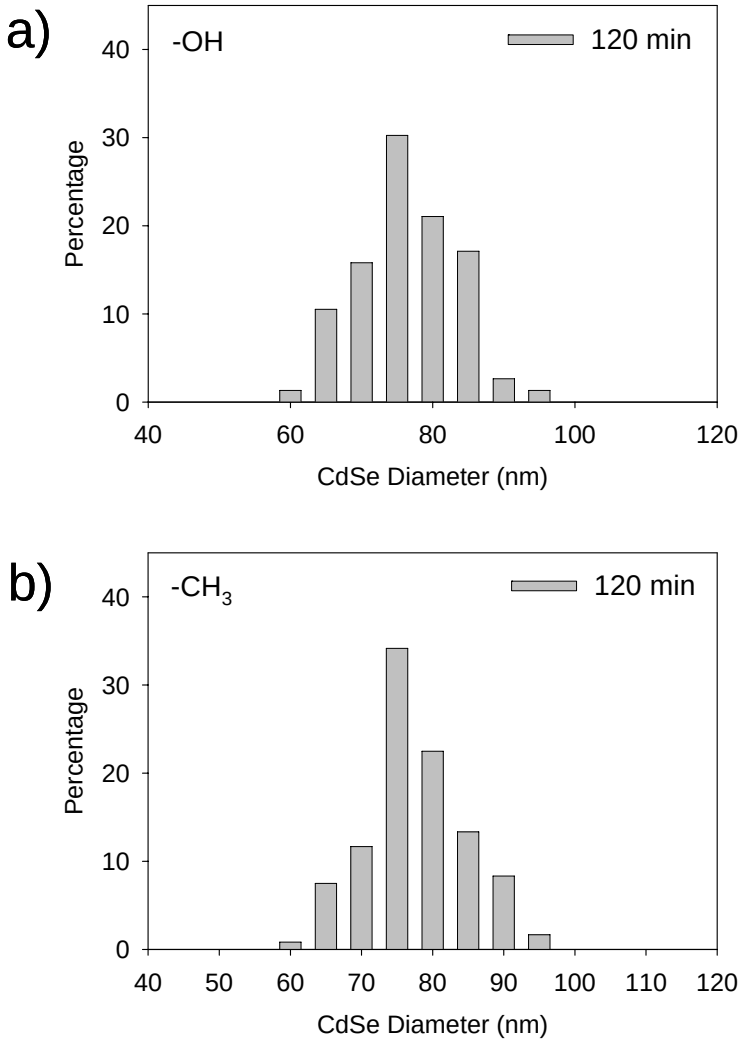

Figure 8.9 The size distributions of CdSe nanoparticles on (a) -OH terminated SAMs, (b) -CH_3 terminated SAMs after 120 min deposition at 45 °C. The width of the bar is ± 2.5 nm. Average diameter of the CdSe nanoparticles is 76 ± 7 nm on -OH terminated SAMs and -CH_3 terminated SAMs.

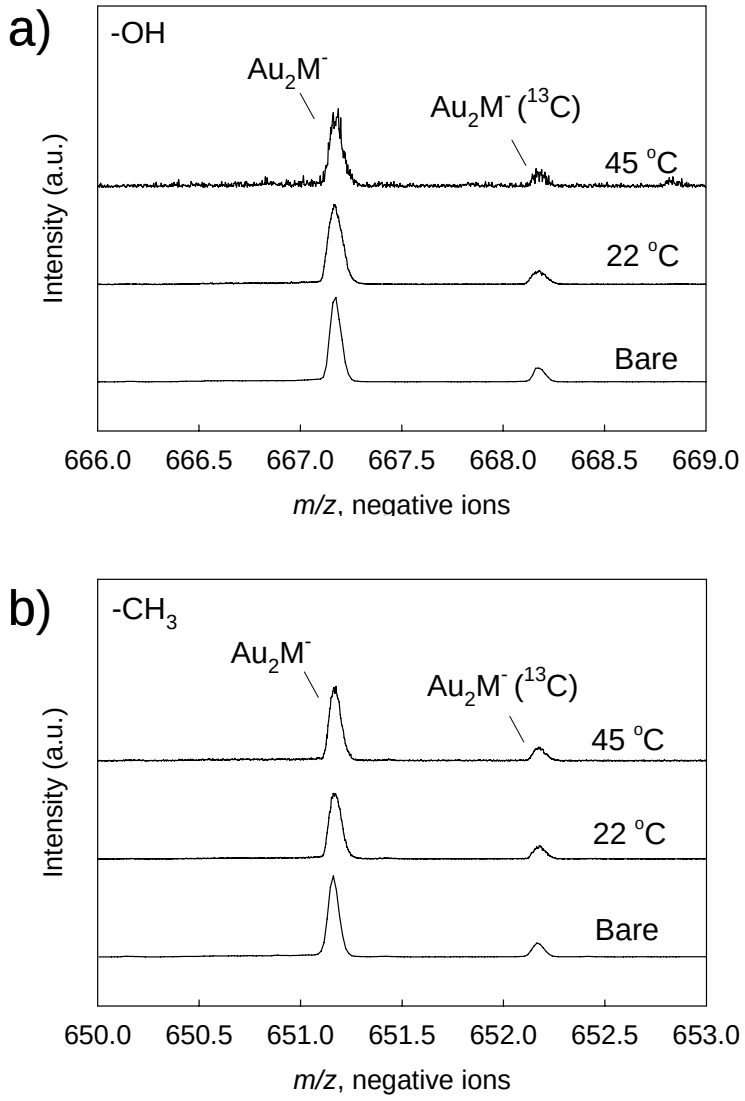

Figure 8.10 High mass resolution negative ion TOF SIMS spectra of the molecular cluster ion, Au_2M^- for (a) -OH terminated SAMs (M = $-S(CH_2)_{15}CH_2OH$); (b) $-CH_3$ terminated SAM (M = $-S(CH_2)_{15}CH_3$) prior to and after CdSe chemical bath deposition for 2 h at 22 °C and at 45 °C.

8.3.3 Reaction Pathways of CdSe CBD on -COOH terminated SAMs

In a chemical bath deposition, a controlled chemical reaction is used to deposit thin films on substrates placed in the plating solution bath.[30-36, 42, 51-55] For CdSe chemical bath deposition, the bath usually contains a cadmium salt as the source of Cd^{2+} ions, a complexing agent such as sodium nitrilotriacetate (NTA) for the slow release of Cd^{2+} ions (reaction 1), and a selenosulphate salt which slowly hydrolyzes to generate Se^{2-} ions (reaction 2). CdSe is formed by Se^{2-} ions reaction with Cd^{2+} ions on the substrate or in the plating solution (reaction 3). In this study, the overall CBD process can be described using the following simplified reactions:

$$Cd^{2+}(aq) \xrightleftharpoons{NTA^{3-}(aq)} Cd(NTA)^{-}(aq) \xrightleftharpoons{NTA^{3-}(aq)} Cd(NTA)_2^{4-}(aq) \quad (1)$$

$$SeSO_3^{2-}(aq) \xrightleftharpoons{OH^{-}(aq)} HSe^{-}(aq) + SO_4^{2-}(aq) \xrightleftharpoons{OH^{-}(aq)} Se^{2-}(aq) + H_2O \quad (2)$$

$$Cd^{2+}(aq) + Se^{2-}(aq) \rightleftharpoons CdSe(s) \quad (3)$$

The actual reaction pathways involved in the CBD process are more complicated than the above reactions suggest.[30, 32-34, 38, 55-58] Two processes are generally believed to contribute to chemical bath deposition: ion-by-ion crystallite growth on the substrate *via* successive ion exchange reaction, and cluster-by-cluster precipitation where colloidal clusters form homogeneously in the solution and deposit on the substrate.[31, 34, 35, 39, 51] The two mechanisms may coexist or compete, and the dominant mechanism may also change

during the deposition as the experimental conditions change.[39] There have been many studies of CdSe CBD, but the reaction pathways are not generally well understood. Kainthla *et al.* [35] suggested that in basic solutions $Cd(OH)_2$ are the nuclei for CdSe growth, and CdSe grows on the substrate and in the plating solution. In solutions where no $Cd(OH)_2$ exists, ion-by-ion growth of CdSe crystallites on the substrate can occur. Gorer and Hodes[31] observed that when the ratio of NTA to the Cd salt is above a critical value (R_c, critical complex value), the reaction mechanism changes from cluster-by-cluster deposition to ion-by-ion growth.

Although it is difficult to determine whether ion-by-ion or cluster-by-cluster growth is operative, there are several empirical criteria that can be employed to differentiate these mechanisms. For deposition *via* the ion-by-ion growth, several characteristics have been identified. These are: a) the deposited film grows epitaxially, i.e. aligned with the substrate crystallographic directions;[31, 39, 59] b) the film strongly adheres to the substrate; [33, 39, 59] and c) the deposition rate is not strongly affected by the deposition temperature.[35, 60] In contrast, deposition *via* the cluster-by-cluster mechanism usually exhibits the following characteristics: a) non-epitaxial growth, b) poor adherence of the deposited film to the substrate and c) a strong dependence of the deposition rate on the temperature.[52, 60]

Based on these criteria, the chemical bath deposition of CdSe on -COOH terminated SAMs appears to be a mixed ion-by-ion and cluster-by-cluster reaction. The following observations suggest that CdSe CBD follows a cluster-by-cluster mechanism.

First, the CdSe nanoparticles exhibit non-epitaxial growth (Figure 8.4). Second, the CdSe nanoparticle growth was strongly temperature dependent (Figure 8.3). However, there are other features of the deposition that can not be explained by a cluster-by-cluster mechanism alone. First, the formation of $Cd(COO)_2(CH_2)_x(CH)_y^+$ ions was observed in the TOF SIMS spectra, indicating that the SAM has complexed with Cd^{2+} ions (Figure 8.6). Second, the diameters of CdSe nanoparticles formed on -COOH terminated SAMs were about twice as big as those formed on $-CH_3$- and -OH terminated SAMs (Figure 8.2, Figure 8.9). Third, the deposited CdSe nanoparticles strongly adhered to -COOH terminated SAM surface (Figure 8.7). These observations suggest that ion-by-ion growth is also operative.

We therefore propose the following reaction mechanism for CdSe CBD on -COOH terminated SAMs. During the seeding step, the plating solution has a pH of 8.0 which is lower than the pK_a of hexadecanoic acid (pK_a ~ 8.5-8.8),[61] and so the MHA does not deprotonate during seeding. After addition of Na_2SeSO_3, the plating solution pH increases to 9.5, and many -COOH terminal groups become deprotonated. Thus Cd^{2+} ions complex with the carboxylic groups to form Cd^{2+}-carboxyate complexes.[62] Once formed, these complexes react with Se^{2-} ions to form CdSe on the SAM surface *via* an ion-by-ion mechanism. The thin layer of tiny CdSe crystallites that could not be observed using SEM is likely to form *via* this mechanism (Figure 8.3). This process also explains the observation that CdSe CBD deposition is similar under the “seeded” and the “unseeded” conditions: Cd^{2+}-carboxylate complexes can only form after addition of Na_2SeSO_3. Thus

both the “seeded” and “unseeded” samples have a similar number of Cd^{2+}-carboxylate complex nuclei for CdSe deposition. After a sufficient Se^{2-} ion concentration is generated *via* the hydrolysis of Na_2SeSO_3, CdSe colloidal clusters form homogeneously in the plating solution and cluster-by-cluster precipitation becomes the dominant process. Once a critical cluster size has been reached, they precipitate and deposit on the -COOH terminated SAM surface.

8.3.4 Reaction Pathways of CdSe CBD on -OH and -CH_3 terminated SAMs

CdSe chemical bath deposition follows the cluster-by-cluster mechanism on -OH and -CH_3 terminated SAMs for the following reasons: a) CdSe nanoparticles exhibited non-epitaxial growth; b) the deposition was strongly temperature dependent (Figure 8.8); c) CdSe nanoparticles had the same size and number density on -OH (hydrophilic) and -CH_3 terminated SAMs (hydrophobic); and d) the deposited CdSe nanoparticles did not strongly adhere to -OH and -CH_3 terminated SAMs. The following reaction pathway is proposed for these surfaces. During the CBD process, Cd^{2+} ions and Se^{2-} ions form CdSe colloidal clusters in solution. These clusters aggregate to form precipitates and the precipitates deposit and weakly adsorb on -OH and -CH_3 terminated SAMs.

8.3.5 Selective Deposition of CdSe Nanoparticles on Patterned SAM Surfaces

The above data suggest that CdSe can be selectively deposited on patterned SAMs. To demonstrate this, CdSe CBD was performed on a UV photopatterned -COOH/-CH_3 SAM at 45 °C for 15 min, and then the deposited SAM was sonicated in deionized water for 5 min before SEM and TOF SIMS characterization. The optical and SEM images indicate

that CdSe was only deposited on the -COOH terminated regions (red “bar” areas in Figure 8.11 (a) and dark “bar” areas in Figure 8.11 (b)). The TOF SIMS data confirm the SEM and optical microscopy data. Negative ion images indicate that $^{78}Se^-$ ions, which are characteristic of CdSe nanoparticle deposition, were only observed present in the -COOH terminated SAM areas (Figure 8.11 c).

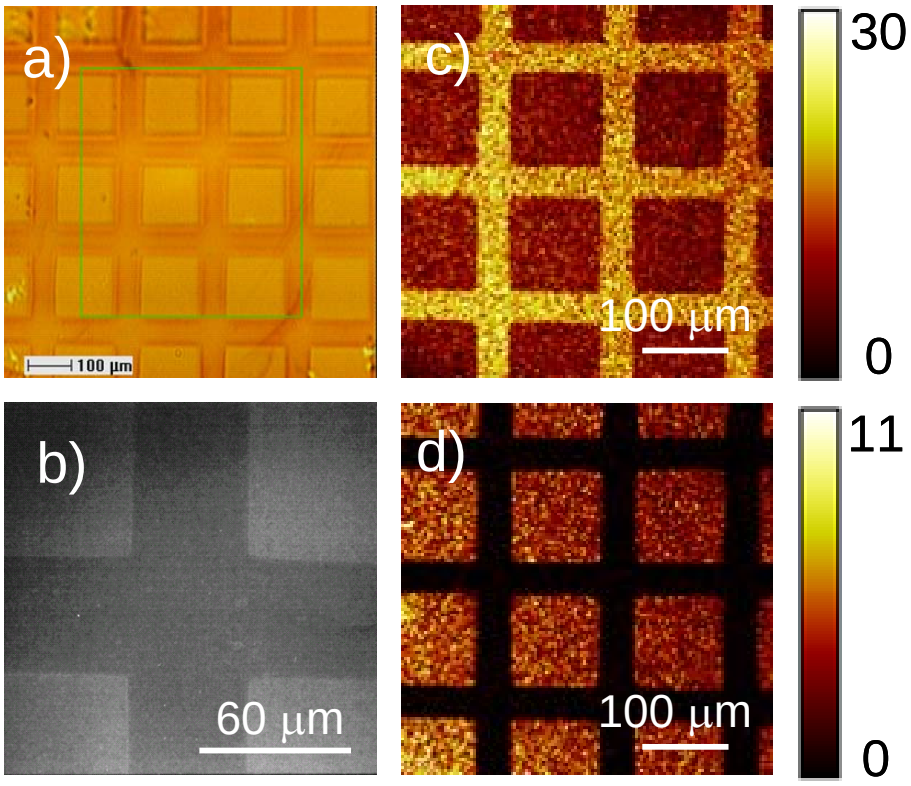

Figure 8.11 (a) Optical, (b) SEM, (c) TOF SIMS image centered at $^{78}Se^-$ (*m/z* = 78), (d) TOF SIMS image centered at -CH_3 terminated SAM molecular ion Au_2M^- (M = $S(CH_2)_{15}CH_3$, *m/z* 651) after CdSe chemical bath deposition on a patterned -COOH/-CH_3 terminated SAM at 45 °C for 15 min. The intensity of the $^{78}Se^-$ ion indicates that CdSe has been selectively deposited on the -COOH terminated SAMs. The Au_2M^- ion is characteristic of -CH_3 terminated SAMs. Parameters of TOF SIMS analysis: primary ion, Bi^+; kinetic energy = 25 keV; area of analysis = (500 × 500) μm^2, (128 × 128) $pixels^2$; intensity scale indicates maximum ion counts.

8.4 Conclusions

In this study, the reaction pathways of CdSe chemical bath deposition on functionalized SAMs have been investigated. On -COOH terminated SAMs, CdSe CBD follows a mixed ion-by-ion and cluster-by-cluster mechanism. Initially, Cd^{2+} ions form Cd^{2+}-carboxylate complexes with the -COOH terminal groups. Once formed, these complexes can react with Se^{2-} to form CdSe and serve as nucleation sites for ion-by-ion growth. After a sufficient Se^{2-} concentration is generated by the hydrolysis of Na_2SeSO_3, Cd^{2+} ions react with Se^{2-} ions to form colloidal clusters in solution and deposit on the SAM surface *via* cluster-by-cluster deposition. On -OH and -CH_3 terminated SAMs, CdSe nanoparticles form *via* a cluster-by-cluster pathway alone, and do not strongly adhere to the SAM surface.

Selective deposition of CdSe on patterned SAMs is also demonstrated using chemical bath deposition. Under appropriate conditions, CdSe is selectively deposited on -COOH terminated areas of -COOH/-CH_3 patterned SAMs by manipulating the surface chemistry of the substrate.

Appendix: Size distribution of CdSe nanoparticles as a function of time on -COOH terminated SAMs when CBD is performed with 20 mM, 40 mM and 80 mM Na_2SeSO_3 at 45 °C: These data can be found in the Appendix Figures A8.1-A8.3.

8.5 References

1. Colvin, V. L.; Schlamp, M. C.; Alivisatos, A. P., Light-Emitting Diodes Made from Cadmium Selenide Nanocrystals and a Semiconducting Polymer. *Nature* **1994,** 370, 354-357.

2. Lee, J.; Sundar, V. C.; Heine, J. R.; Bawendi, M. G.; Jensen, K. F., Full Color Emission from II-VI Semiconductor Quantum Dot-Polymer Composites. *Adv. Mater.* **2000,** 12, 1102-1105.

3. Mueller, A. H.; Petruska, M. A.; Achermann, M.; Werder, D. J.; Akhadov, E. A.; Koleske, D. D.; Hoffbauer, M. A.; Klimov, V. I., Multicolor Light-Emitting Diodes Based on Semiconductor Nanocrystals Encapsulated in GaN Charge Injection Layers. *Nano Lett.* **2005,** 5, 1039-1044.

4. Schlamp, M. C.; Peng, X.; Alivisatos, A. P., Improved Efficiencies in Light Emitting Diodes Made with CdSe(CdS) Core/Shell Type Nanocrystals and a Semiconducting Polymer. *J. Appl. Phys.* **1997,** 82, 5837-5842.

5. Zhao, J.; Bardecker, J. A.; Munro, A. M.; Liu, M. S.; Niu, Y.; Ding, I.; J. Luo; Chen, B.; Jen, A.; Ginger, D. S., Efficient CdSe/CdS Quantum Dot Light-Emitting Diodes Using a Thermally Polymerized Hole Transport Layer. *Nano Lett.* **2006,** 6, 463-467.

6. Rautri, A. K.; Thangraj, R.; Sharma, A. K.; Tripathi, B. B.; Agnivotri, O. P., Structural, Optical and Photoconducting Properties of Sprayed CdSe Films. *Thin Solid Films* **1982,** 91, 55-64.

7. Chan, Y.; Steckel, J. S.; Snee, P. T.; Caruge, J. M.; Hodgkiss, J. M.; Nocera, D. G.;

Bawendi, M. G., Blue Semiconductor Nanocrystal Laser. *Appl. Phys. Lett.* **2005,** 86, 073102.

8. Klimov, V. I.; Tretiak, S.; Anikeeva, P. O.; Bezel, I. V.; Balet, L. P.; Achermann, M.; Piryatinski, A.; Nanda, J.; Ivanov, S. A., Light Amplification Using Inverted Core/Shell Nanocrystals: Towards Lasing in the Single-Exciton Regime. *J. Phys. Chem. B* **2004,** 108, 10625-10630.

9. Smyntyna, V. A.; Gersutenko, V.; Sashulis, S.; Mattogno, G.; Reghini, S., The Causes of Thickness Dependence of CdSe and CdS Gas-Sensor Sensitivity to Oxygen. *Sensors Actuators B* **1994,** 19, 464-465.

10. Somers, R. C.; Bawendi, M. G.; Nocera, D. G., CdSe Nanocrystal Based Chem-/Bio-sensors. *Chem. Soc. Rev.* **2007,** 36, 579-591.

11. Mann, J. R.; Watson, D. F., Adsorption of CdSe Nanoparticles to Thiolated TiO_2 Surfaces: Influence of Intralayer Disulfide Formation on CdSe Surface Coverage. *Langmuir* **2007,** 23, 10924-10928.

12. Huynh, W. U.; Peng, X. G.; Alivisatos, A. P., CdSe Nanocrystal Rods/Poly(3-hexylthiophene) Composite Photovoltaic Devices. *Adv. Mater.* **1999,** 11, 923-927.

13. Greenham, N. C.; Peng, X. G.; Alivisatos, A. P., Charge Separation and Transport in Conjugated-Polymer/Semiconductor-Nanocrystal Composites Studied by Photoluminescence Quenching and Photoconductivity. *Phys. ReV. B* **1996,** 54, 17628-17637.

14. Huynh, W. U.; Dittmer, J. J.; Alivisatos, A. P., Hybrid Nanorod-Polymer Solar Cells. *Science* **2002,** 295, 2425-2427.

15. Dibbell, R. S.; Soja, G. R.; Hoth, R. M.; Watson, D. F., Photocatalytic Patterning of Monolayers for the Site-Selective Deposition of Quantum Dots onto TiO_2 Surfaces. *Langmuir* **2007,** 23, 3432-3439.

16. Robel, I.; Subramanian, V.; Kuno, M.; Kamat, P. V., Quantum Dot Solar Cells. Harvesting Light Energy with CdSe Nanocrystals Molecularly Linked to Mesoscopic TiO_2 Films. *J. Am. Ceram. Soc.* **2006,** 128, 2385-2393.

17. Nuzzo, R. G.; Dubios, L. H.; L., A. D., Fundamental Studies of Microscopic Wetting on Organic Surfaces. 1. Formation and Structural Characterization of a Self-Consistent Series of Polyfunctional Organic Monolayers. *J. Am. Chem. Soc.* **1990,** 112, 558-569.

18. Ulman, A., Formation and Structure of Self-Assembled Monolayers. *Chem. Rev.* **1996,** 96, 1533-1554.

19. Schreiber, F., Structure and Growth of Self-Assembling Monolayers. *Prog. Surf. Sci.* **2000,** 65, 151-256.

20. Samanta, D.; Samanta, B.; Chaudhuri, A. K.; Ghorai, S.; Pal, U., Electrical Characterization of Stable Air-Oxidized CdSe Films Prepared by Thermal Evaporation. *Semicond. Sci. Technol.* **1996,** 11, 548-553.

21. Shreekanthan, K. N.; Rajendra, B. V.; Kasturi, V. B.; Shivakumar, G. K., Growth and Characterization of Semiconducting Cadmium Selenide Thin Films. *Cryst. Res. Technol.* **2003,** 38, 31.

22. Golan, Y.; Margulis, L.; Rubinstein, I.; Hodes, G., Epitaxial Electrodeposition of Cadmium Selenide Nanocrystals on Gold. *Langmuir* **1992,** 8, 749-752.

23. Wynands, H.; Cocivera, M., Hall Effect and Resistivity Characterization of Doped, Electrodeposited CdSe. *J. Electrochem. Soc.* **1992,** 139, 2052-2057.

24. Elango, T.; Subramanian, S.; Murali, K. R., Characteristics of Spray-deposited CdSe Thin Films. *Surf. Coat. Technol.* **2003,** 123, 8.

25. Meteleva, Y. V.; Radychev, N. A.; Novikov, G. F., Properties of CdSe Films Produced via Spray Pyrolysis of $[Cd((NH_2)_2CSe)_2Cl_2]$. *Inorg. Mater.* **2007,** 43, 455-465.

26. Kale, R. B.; Sartale, S. D.; Chougule, B. K.; Lokhande, C. D., Growth and Characterization of Nanocrystalline CdSe Thin Films Deposited by the Successive Ionic Layer Adsorption and Reaction Method. *Semicond. Sci. Technol.* **2004,** 19, 980-986.

27. Pathan, H. M.; Sankapal, B. R.; Desai, J. D.; Lokhande, C. D., Preparation and Characterization of Nanocrystalline CdSe Thin Films Deposited by SILAR Method. *Mater. Chem. Phys.* **2003,** 78, 11-14.

28. Heine, J. R.; Rodriguez-Viejo, J.; Bawendi, M. G.; Jensen, K. F., Synthesis of CdSe Quantum Dot-ZnS matrix Thin Films via Electrospray Organometallic Chemical Vapor Deposition. *J. Cryst. Growth* **1998,** 195, 564-568.

29. Shan, C. X.; Liu, Z.; Ng, C. M.; Hark, S. K., Structure and Luminescence of Pyramid-Shaped CdSe Nanostructures Grown by Metalorganic Chemical Vapor Deposition. *Appl. Phys. Lett.* **2005,** 86, 213106-1.

30. Cachet, H.; Essaaidi, H.; Froment, M.; Maurin, G., Chemical Bath Deposition of

CdSe Layers from Cd(II)-Selenosulfite Solutions. *J. electroanalytical chem.* **1995,** 396, 175-182.

31. Gorer, S.; Hodes, G., Quantum Size Effects in the Study of Chemical Solution Deposition Mechanisms of Semiconductor films. *J. Phys. Chem.* **1994,** 98, 5338-5346.

32. Hankare, P. P.; Bhuse, V. M.; Garadkar, K. M.; Delekar1, S. D.; Mulla, I. S., Chemical Deposition of Cubic CdSe and HgSe Thin Films and Their Characterization. *Semicond. Sci. Technol.* **2004,** 19, 70-75.

33. Hankare, P. P.; Delekar, S. D.; Asabe, M. R.; Chate, P. A.; Bhuse, V. M.; Khomane, A. S.; Garadkar, K. M.; Sarwade, B. D., Synthesis of Cadmium Selenide Thin Films at Low-Temperature by Simple Chemical Route and Their Characterization. *Journal of Physical and Chemistry of Solid* **2006,** 67, 2506-2511.

34. Hodes, G.; Albu-Yaron, A.; Decker, F.; Motisuke, P., Three-Dimensional Quantum-Size Effect in Chemically Deposited Cadmium Selenide Films. *Phys. Rev. (B)* **1987,** 36, 4215-4221.

35. Kainthla, R. C.; Pandya, D. K.; Chopra, K. L., Solution Growth of CdSe and PbSe Films. *J. Electrochem. Soc.* **1980,** 127, 277-283.

36. Lochande, C., Ammonia-free Chemical Bath Method for Deposition of Microcrystalline Cadmium Selenide Films. *Mater. Chem. Phys* **2005,** 91, 200.

37. Vargas-Hernández, C.; Lara, V. C.; Vallejo, J. E.; Jurado, J. F.; Giraldo, O., XPS, SEM and XRD Investigations of CdSe Films Prepared by Chemical Bath Deposition. *Phys. Stat. Sol. (B)* **2005,** 242, 1897-1901.

38. Yamamoto, O.; Sasamoto, T., Preparation of Crystalline CdSe Particles by Chemical Bath Deposition. *J. Mater. Res.* **1998,** 13, 3394-3398.

39. Hodes, G., Mechanisms of Chemical Deposition. In *Chemical Solution Deposition Of Semiconductor Films*, Marcel Dekker, Inc.: New York, 2002.

40. Garuthara, R.; Levine., G., Photoluminescence of Chemically Deposited CdSe Nanocrystallites: Effects of Crystallite Polydispersity. *J. Appl. Phys.* **1996,** 80, 401.

41. Trojanek, F.; Cingolani, R.; Cannoletta, D.; Mikes, D.; Nemec, P.; Uhlirova, E.; Rohovec, J.; Maly, P., Tailoring of Nanocrystal Sizes in CdSe Films Prepared by Chemical Deposition. *Journal of Crystal Growth* **2000,** 209, 695-700.

42. Dona, J. M.; Herrero, J., Chemical Bath Deposition of CdS Thin Films: An Approach to the Chemical Mechanism Through Study of the Film Microstructure. *J. Electrochem. Soc.* **1997,** 144, (11), 4081-4091.

43. Fisher, G. L.; Hooper, A. E.; Opila, R. L.; Allara, D. L.; Winograd, N., The Interaction of Vapor-Deposited Al Atoms with CO_2H Groups at the Surface of a Self-Assembled Alkanethiolate Monolayer on Gold. *J. Phys. Chem. B* **2000,** 104, 3267-3273.

44. Fisher, G. L.; Walker, A. V.; Hooper, A. E.; Tighe, T. B.; Bahnck, K. B.; Skriba, H. T.; Reinard, M. D.; Haynie, B. C.; Opila, R. L.; Winograd, N.; Allara, D. L., Bond Insertion, Complexation, and Penetration Pathways of Vapor-Deposited Aluminum Atoms with HO- and CH_3O-Terminated Organic Monolayers. *J. Am. Chem. Soc.* **2002,** 124, 5528-5541.

45. Hooper, A. E.; Fisher, G. L.; Konstadinidis, K.; Jung, D. R.; Nguyen, H.; Opila, R. L.; Collins, R. W.; Winograd, N.; Allara, D. L., Chemical Effects of Methyl and Methyl Ester Groups on the Nucleation and Growth of Vapor-Deposited Aluminum Films. *J. Am. Chem. Soc.* **1999,** 121, (35), 8052–8064.

46. Zhou, C.; Walker, A. V., Dependence of Patterned Binary Alkanethiolate Self-Assembled Monolayers on "UV-Photopatterning" Conditions and Evolution with Time, Terminal Group, and Methylene Chain Length. *Langmuir* **2006,** 22, 11420-11425.

47. Zhou, C.; Walker, A. V., UV Photooxidation and Photopatterning of Alkanethiolate Self-Assembled Monolayers Adsorbed on GaAs (001). *Langmuir* **2007,** 23, 8876-8881.

48. Zhou, C.; Walker, A. V., UV Photooxidation of a Homologous Series of n-Alkanethiolate Monolayers on GaAs(001): A Static SIMS Investigation. *J. Phys. Chem. C* **2008,** 112, 797-805.

49. Vickerman, J. C., *ToF SIMS: Surface Analysis by Mass Spectrometry.* IM Publications and Surface Spectra Limited: Chichester and Manchester, UK, 2001; p 1-40.

50. Lu, P.; Walker, A. V., Making Nanoflowerbeds: Reaction Pathways Involved in the Selective Chemical Bath Deposition of ZnS on Functionalized Alkanethiolate Self-Assembled Monolayers. *ACS Nano* **2009,** 3, 370-378.

51. Breen, M. L.; Woodward, J. T.; Schwartz, D. K.; Apblett, A. W., Direct Evidence for an Ion-by-Ion Deposition Mechanism in Solution Growth of CdS Thin Films. *Chem. Mater.* **1998,** 10, 710.

52. Dona, J. M.; Herrero, J., Chemical Bath Deposition of CdS Thin Films:

Electrochemical In Situ Kinetic Studies. *J. Electrochem. Soc.* **1992,** 139, 2810-2814.

53. Dona, J. M.; Herrero, J., Chemical Bath Codeposited CdS-ZnS Film Characterization. *Thin Solid Films* **1995,** 268, 5-12.

54. Liu, L.; Peng, Q.; Li, Y., Preparation of CdSe Quantum Dots with Full Color Emission Based on a Room Temperature Injection Technique. *Inorg. Chem.* **2008,** 47, 5022-5028.

55. O'Brien, P.; McAleese, J., Developing an Understanding of the Processes Controlling the Chemical Bath Deposition of ZnS and CdS. *J. Mater. Chem.* **1998,** 8, (11), 2309-2314.

56. Kostoglou, M.; Andritsos, N.; Karabelas, A. J., Progress Towards Modelling the CdS Chemical Bath Deposition Process. *Thin Solid Films* **2001,** 387, 115-117.

57. Simurda, M.; Nemec, P.; Formanek, P.; Nemec, I.; Nemcova, Y.; Maly, P., Morphology of CdSe Films Prepared by Chemical Bath Deposition: The Role of Substrate. *Thin Solid Films* **2006,** 511-512, 71-75.

58. Rieke, P. C.; Bentjen, S. B., Deposition of Cadmium Sulfide Films by Decomposition of Thiourea in Basic Solutions. *Chem. Mater.* **1993,** 5, 43-53.

59. Kaur, I.; Pandya, D. K.; K. L, C., Growth Kinetics and Polymorphism of Chemically Deposited CdS Films. *J. Electrochem. Soc.* **1980,** 127, 943-948.

60. Dona, J. M.; Herrero, J., Process and Film Characterization of Chemical-Bath-Deposited ZnS Thin Films. *J. Electrochem. Soc.* **1994,** 141, (1), 205-210.

61. Kanicky, J. R.; Shah, D. O., Effect of Degree, Type, and Position of Unsaturation on

the pK_a of Long-Chain Fatty Acids. *J. Colloid Interface Sci.* **2002,** 256, 201-207.

62. Martell, A. E.; Smith, R. M., *Critical Stability Constants*. Plenum Press: New York, 1974; Vol. 3, p 1-12.

Chapter 9

Conclusions and Future Work

9.1 Conclusions

Fabricating metal and semiconductor overlayers on organic thin films is of great interest because these structures have many technological applications, including in molecular electronics,[1-7] polymer light emitting diodes,[8-10] photonic materials[11] and electroluminescent devices.[12-14] To develop effective film growth techniques to make high quality devices, it is important to develop an understanding of metal and semiconductor interactions with organic substrates. In this thesis, functionalized self-assembled monolayers (SAMs), which have highly organized structures and a uniform surface density of functional groups, are employed as substrates to investigate the growth of metal and semiconductor overlayers. Several novel techniques, including chemical vapor deposition (CVD), chemical bath deposition (CBD) and electroless deposition, were developed to deposit metal (Al, Cu) and nanoscale semiconductor (ZnS, CdSe) overlayers on functionalized SAMs.

At room temperature, it was demonstrated that alumina and aluminum were deposited on functionalized SAMs using CVD. The reaction was influenced by both the level of H_2O and O_2 pressure in the deposition environment and the terminal functionality of the SAMs. In a nitrogen-purged glovebox, alumina was deposited on -OH, -COOH, and -CH_3 terminated SAMs. The TMA precursor reacted with -OH and -COOH terminal

groups to form dimethyl aluminum complexes, and these complexes reacted with H_2O and O_2 to deposit alumina. For these SAMs, the alumina layer was observed to be strongly adherent. The alumina observed on -CH_3 terminated SAMs was formed by TMA reaction with H_2O and O_2 in the environment, and could be removed from the rinsing with organic solvent. In a deposition chamber where the pressure was less than 10^{-8} Torr, only aluminum was deposited on the -OH and -COOH terminated SAMs, but not on -CH_3 terminated SAMs. UV light can be used to increase the deposition rate of Al on functionalized SAMs using TMA precursor. When a patterned -CH_3/-COOH SAM was exposed to TMA, alumina or aluminum could be selectively deposited on the -COOH terminated areas depending on the reaction conditions.

Compared with vacuum deposition techniques, electroless deposition has several advantages. These include low reaction temperatures, low cost (since no vacuum chamber is required), and suitability for large area processing. Using electroless deposition, copper was deposited on -COOH and -CH_3 terminated SAMs but not on -OH terminated SAMs. On -COOH terminated SAMs, Cu^{2+} ions complexed with the -COOH terminal groups to form Cu^{2+}-carboxylate complexes, which provided the nucleation sites for copper film growth. On -CH_3 terminated SAMs, Cu^{2+} ions only weakly adsorbed on the SAM surface. Thus when the bath temperature increased from 22 °C to 45 °C, copper continued to deposit on -COOH terminated SAMs, but not on -CH_3 terminated SAMs because Cu^{2+} ions could not stably adsorb at the -CH_3/solution interface at this temperature. However, the deposited Cu was not stable on either -COOH or -CH_3 terminated SAMs. Copper

penetration through the monolayer was observed, and penetration continued for at least 48 h after sample removal from the deposition bath. No copper was deposited on -OH terminated SAMs because the -OH groups reacted with formaldehyde to form acetals, which prevented Cu^{2+} ions adsorption.

A new copper electroless deposition method was developed to deposit selectively stable copper overlayers on -COOH terminated SAMs without copper penetration. A "seeding" step, in which the -COOH terminated SAM was immersed in a Cu^{2+}-containing plating solution prior to addition of the reducing agent (formaldehyde), was employed to increase the copper deposition rate. "Seeding" increased copper deposited rate on both $-CH_3$ and -COOH terminated SAMs. However, copper penetration through -COOH terminated SAMs was still observed. By adding the organic additive adenine in the plating solution, copper penetration was prevented. Finally, It was demonstrated that copper was selectively deposited in -COOH terminated SAM areas of a patterned -COOH/$-CH_3$ SAM using electroless deposition by employing the following conditions: 45 °C, seeding and the addition of adenine.

Chemical bath deposition (CBD), another solution-phase technique, was employed to deposit ZnS and CdSe nanostructures on functionalized SAMs. After CBD, flower-like ZnS nanocrystallites and spherical CdSe nanoparticles were formed on the SAMs.

After CBD on -COOH terminated SAMs, two types of ZnS nanocrystallites were observed: small nanoflowers (~ 500 nm diameter) and large crystallites (~ 2 μm

diameter). The small nanoflowers were formed *via* an ion-by-ion mechanism and strongly adhered to the SAM surface. The larger crystallites were deposited on the SAMs *via* a cluster-by-cluster mechanism and could be removed using sonication. On -OH and -CH_3 terminated SAMs, ZnS CBD proceeded *via* cluster-by-cluster precipitation. In this case, only larger crystallites were observed, and these could also be easily removed by sonication. Selective deposition of ZnS was achieved using CBD. When the deposition was performed on a -CH_3/-COOH patterned SAM, ZnS nanoflowers only grew in the -COOH terminated SAM areas, forming "nanoflowerbeds".

Spherical CdSe nanoparticles with narrow size distribution ($\sigma \leq 10\%$) were deposited on -COOH, -OH and -CH_3 terminated SAMs using CBD. On -COOH terminated SAMs, CdSe nanoparticles were formed *via* a mixed ion-by-ion and cluster-by-cluster mechanism. On -CH_3 and -OH terminated SAMs, CdSe nanoparticles were deposited *via* a cluster-by-cluster mechanism. Using CBD, CdSe could also be selectively deposited in the -COOH terminated SAM areas of a patterned -CH_3/-COOH SAM.

In summary, to form a stable metallic or semiconducting contact on an organic thin film, one of the reactants (either the metal ion or a mediating species) must form a stable complex with the SAM surface. In the case of Al CVD, this is the formation of dimethyl aluminum-oxygen complexes. For ZnS and CdSe CBD, it is the formation of Zn^{2+}- and Cd^{2+}-carboxylate complexes. Finally, in Cu electroless deposition, two different stable surface complexes are required: Cu^{2+}-surface complexes and

adenine-carboxylate complexes.

9.2 Future Work

Improvements are still needed to the developed deposition techniques before they can be widely implemented. In CVD, UV-assisted processes will greatly increase deposition rates on SAMs and could be employed to deposit other industrially important metals such as Cu and Ni. Copper- and nickel-containing organic compounds are generally less reactive than TMA, and so their depositions need high substrate temperature, which is not compatible with SAMs. UV light-assisted CVD may aid in lowing the deposition temperatures required, allowing them to be employed on SAMs. Finally, it is also of interest to employ CVD, CBD and electroless deposition to construct 3D complex molecular structures that incorporate metallic and semiconducting layers.

9.3 References

1. Aviram, A., Molecules for Memory, Logic, and Amplification. *J. Am. Chem. Soc.* **1988,** 110, 5687-5692.

2. Chen, J.; Reed, M. A.; Rawlett, A. M.; Tour, J. M., Large On-Off Ratios and Negative Differential Resistance in a Molecular Electronic Device. *Science* **1999,** 286, 1550-1552.

3. Collier, C. P.; Mattersteig, G.; Wong, E. W.; Luo, Y.; Beverly, K.; Sampaio, J.; Raymo, F. M.; Stoddart, J. F.; Heath, J. R., A [2]Catenane-Based Solid State Electronically

Reconfigurable Switch. *Science* **2000,** 289, 1172-1175.

4. Metzger, R. M.; Chen, B.; Hopfner, U.; Lakshmikantham, M. V.; Vuillaume, D.; Kawai, T.; Wu, X.; Tachibana, H.; Hughes, T. V.; Sakurai, H.; Baldwin, J. W.; Hosch, C.; Cava, M. P.; Brehmer, L.; Ashwell, G. J., Unimolecular Electrical Rectification in Hexadecylquinolinium Tricyanoquinodimethanide. *J. Am. Chem. Soc.* **1997,** 119, 10455-10466.

5. Reinerth, W. A.; Jones, L., II.; Burgin, T. P.; Zhou, C.-W.; Muller, C. J.; Deshpande, M. R.; Reed, M. A.; Tour, J. M., Molecular Scale Electronics: Syntheses and Testing *Nanotechnology* **1998,** 9, 246-250.

6. Chen, J.; Lee, T.; Su, J.; Wang, W.; Reed, M. A.; Rawlett, A. M.; Kozaki, M.; Yao, Y.; Jagessar, R. C.; Dirk, S. M., Molecular Electronic Devices. In *Molecular Nanoelectronics*, American Scientific Publishers: Stevenson Ranch, CA, 2003; pp 40-114.

7. Love, J. C.; Estroff, L. A.; Kriebel, J. K.; Nuzzo, R. G.; Whitesides, G. M., Self-Assembled Monolayers of Thiolates on Metals as a Form of Nanotechnology. *Chem. Rev.* **2005,** 105, 1103-1169.

8. Friend, R.; Burroughes, J.; Shimoda, T., Polymer Diodes. *Phys. World* **1999,** June, 35-40.

9. Halls, J. J. M.; Walsh, C. A.; Greenham, N. C.; Marseglia, E. A.; Friend, R. H.; Moratti, S. C.; Holmes, A. B., Electroluminescence in Conjugated Polymers. *Nature* **1995,** 397, 121-128.

10. Huang, J. M.; Yang, Y.; Yang, B.; Liu, S. Y.; Shen, J. C., Assembly and Applications

of the Inorganic Nanocrystals in Polymer Networks. *Thin Solid Films* **1998,** 327-329, 536-540.

11. Huang, K. J.; Rajendran, P.; Liddell, C. M., Chemical Bath Deposition Synthesis of Sub-Micron ZnS-Coated Polystyrene. *J. Colloid Interface Sci.* **2007,** 308, 112-120.

12. Mittal, K. L., *Metallized Plastics: Fundamentals and Applications*. Marcel Dekker: New York, 1997.

13. Sacher, E., *Metallization of Polymers 2*. Kluwer Academic/Plenum Publishers: New York, 2002.

14. Sacher, E.; Pireaux, J.-J.; Kowalczyk, S. P., *Metallization of Polymers*. American Chemical Society: Washington, DC, 1990; Vol. 440.

Appendix

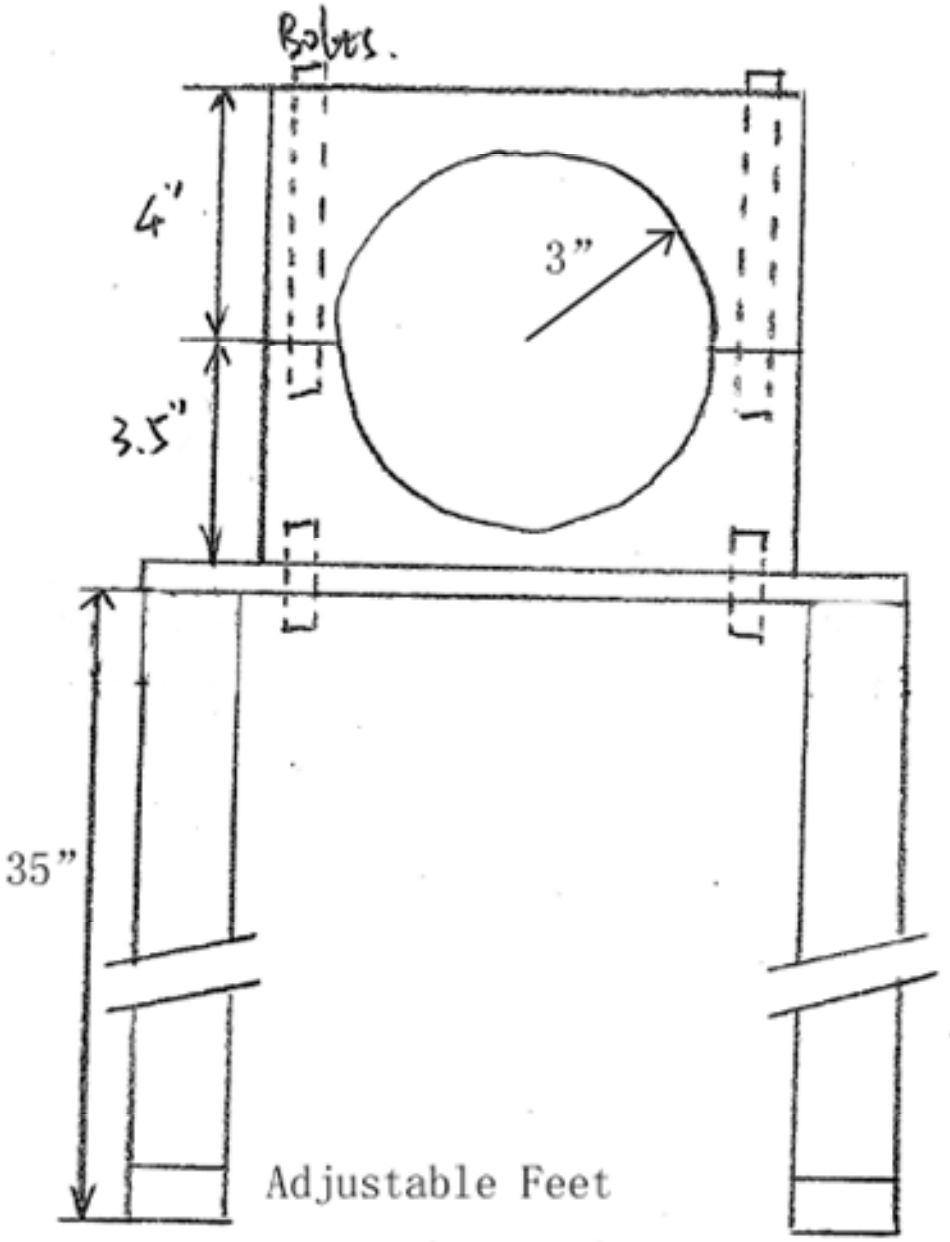

Figure A3.1 A schematic diagram of the CVD chamber holder and stand.

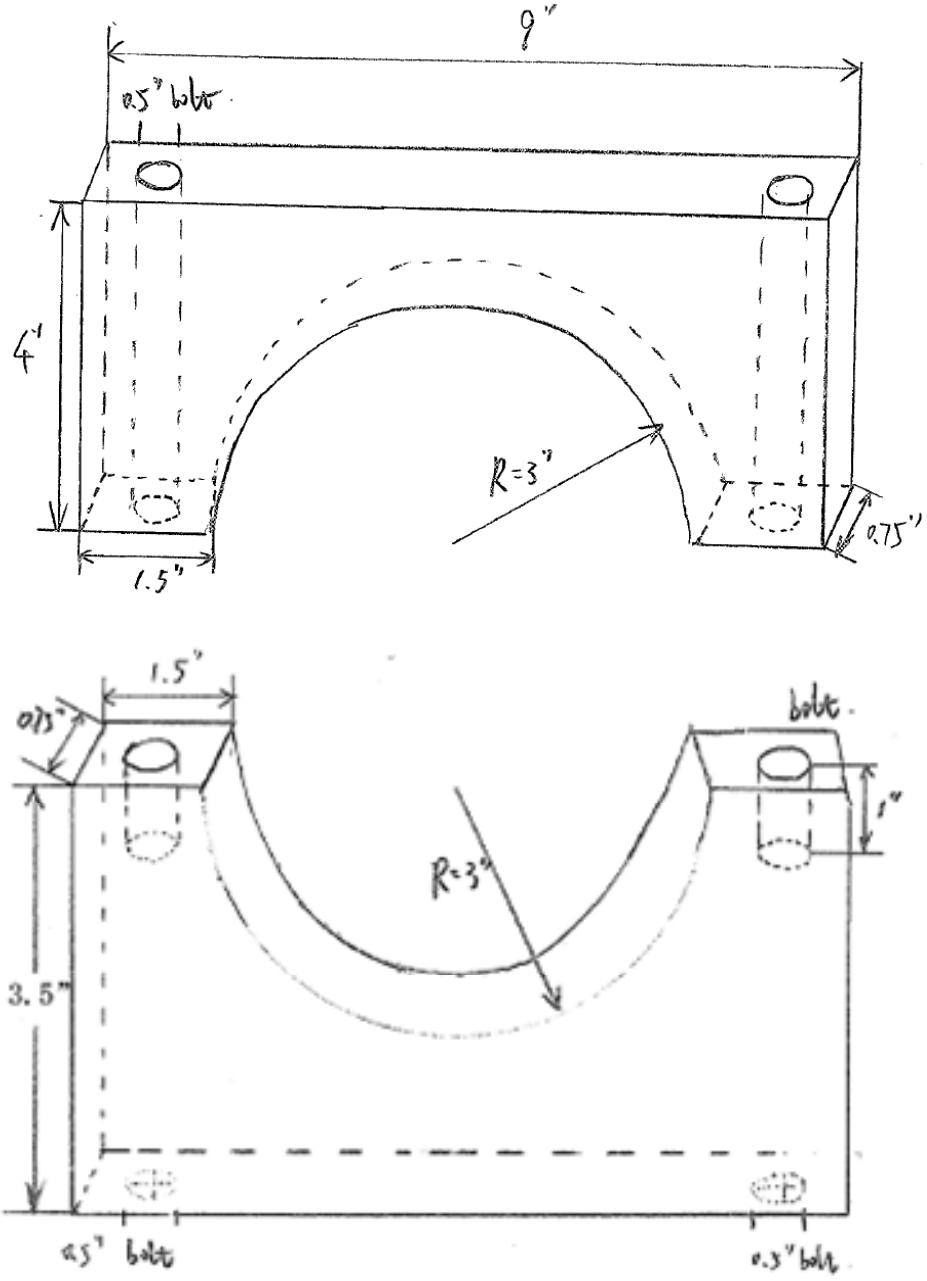

Figure A3.2 A schematic diagram of CVD chamber holder.

a)

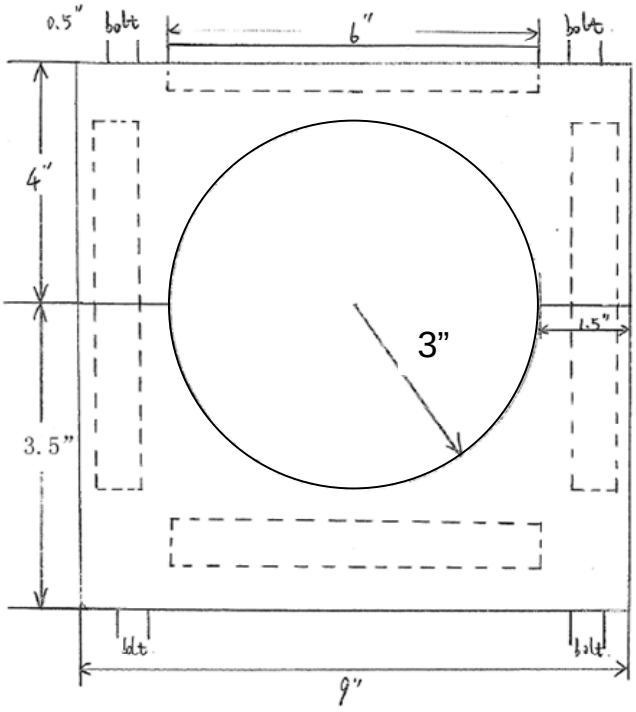

b)

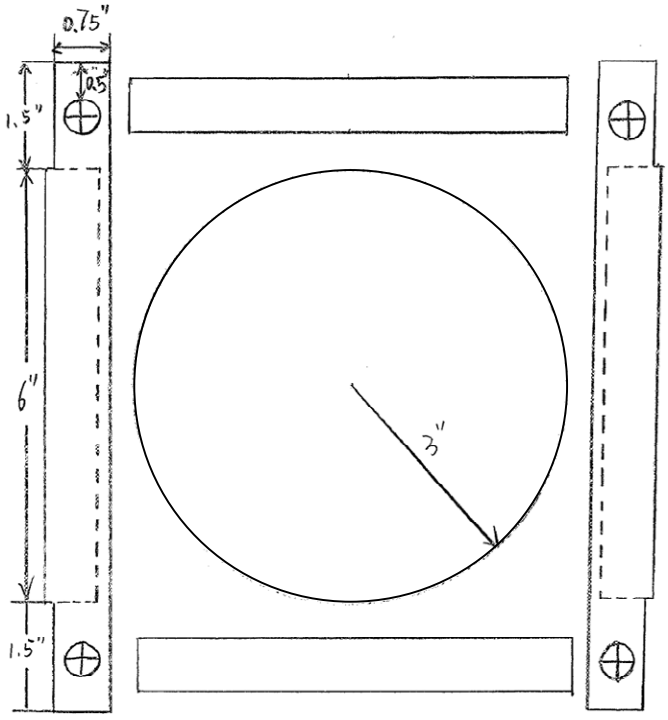

Figure A3.3 Schematic Diagrams of the CVD chamber holder, (a) side view; (b) top view.

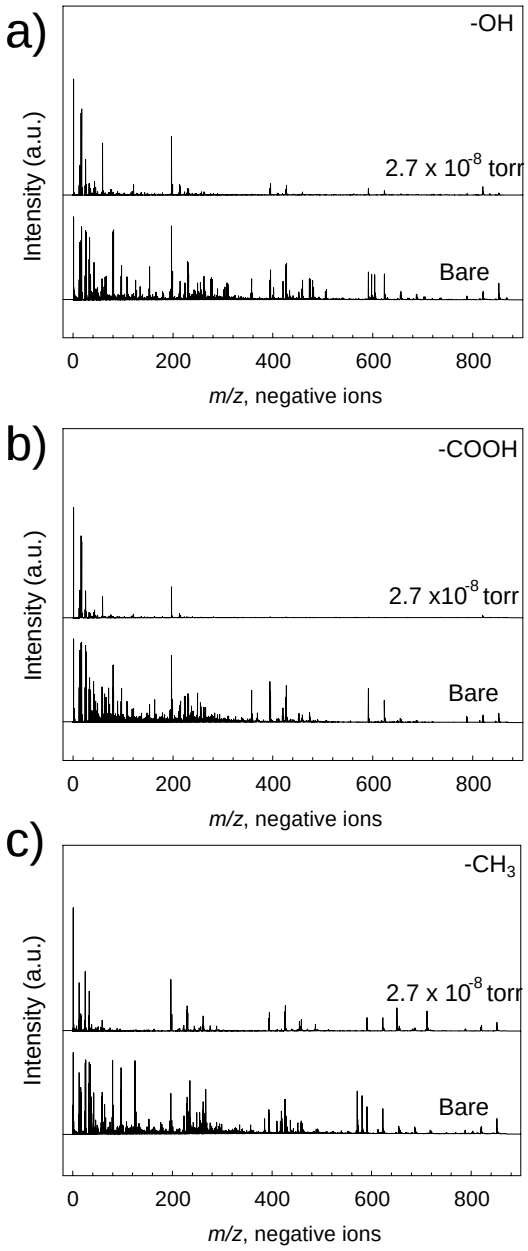

Figure A4.1 High resolution negative ion TOF SIMS spectra *m/z* = 0 - 900 of (a) -OH, (b) -COOH and (c) -CH_3 terminated SAMs before and after exposure to TMA for 15 minutes in a reaction chamber with a base pressure of 2.7×10^{-8} torr.

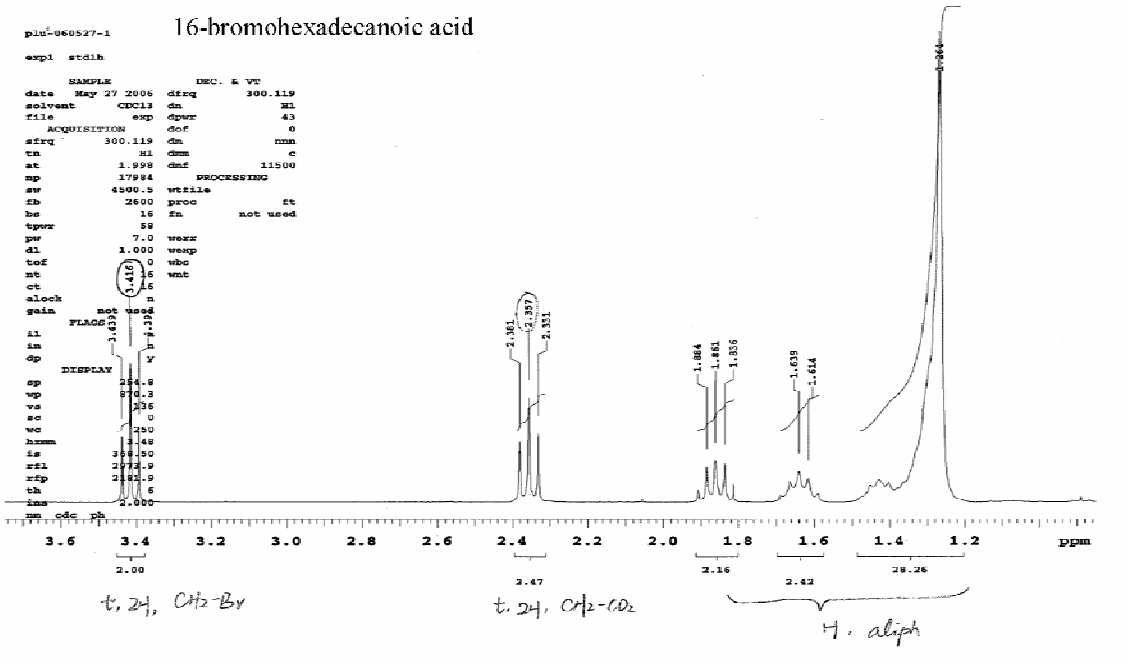

Figure A4.2 NMR spectrum of 16-bromohexadecanoic acid.

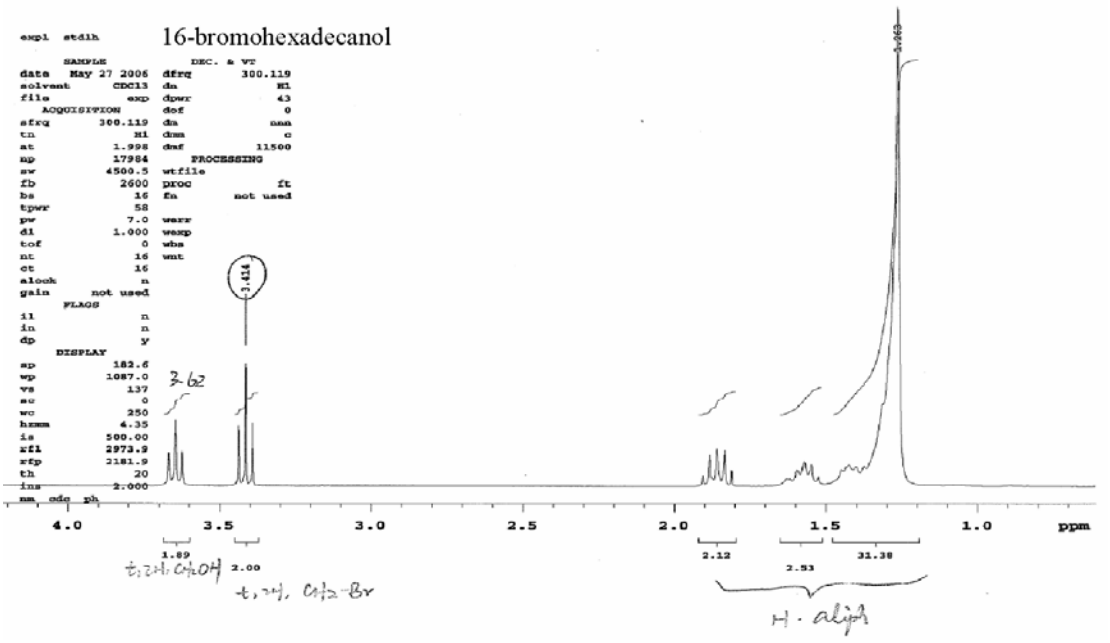

Figure A4.3 NMR spectrum of 16-bromohexadecanol.

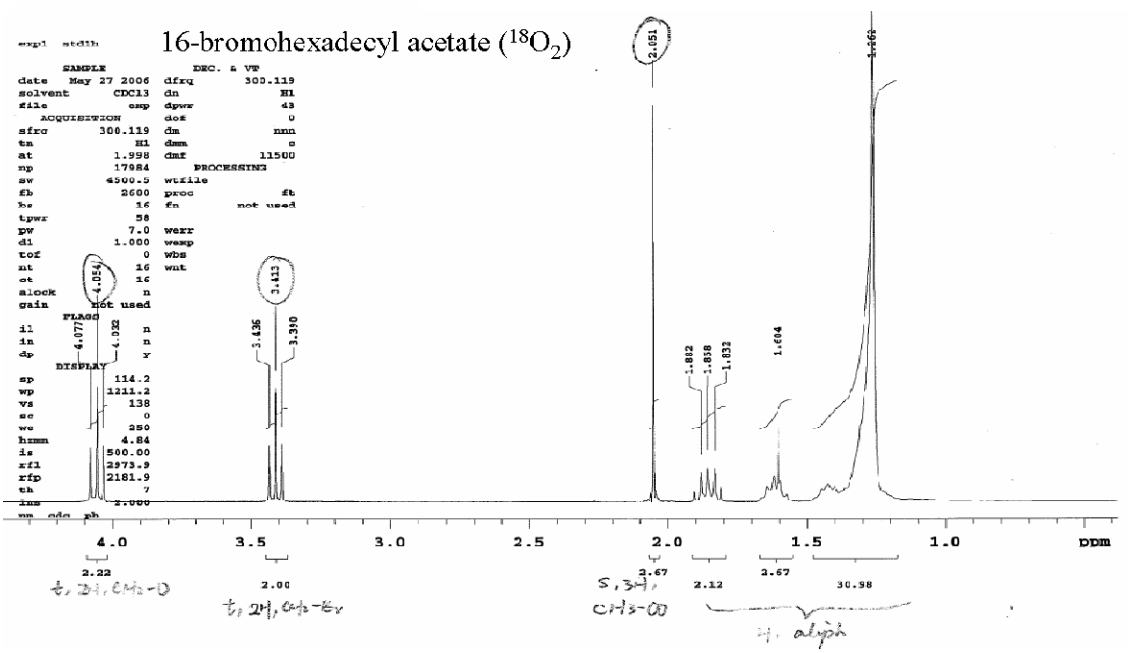

Figure A4.4 NMR spectrum of 16-bromohexadecyl acetate ($^{18}O_2$).

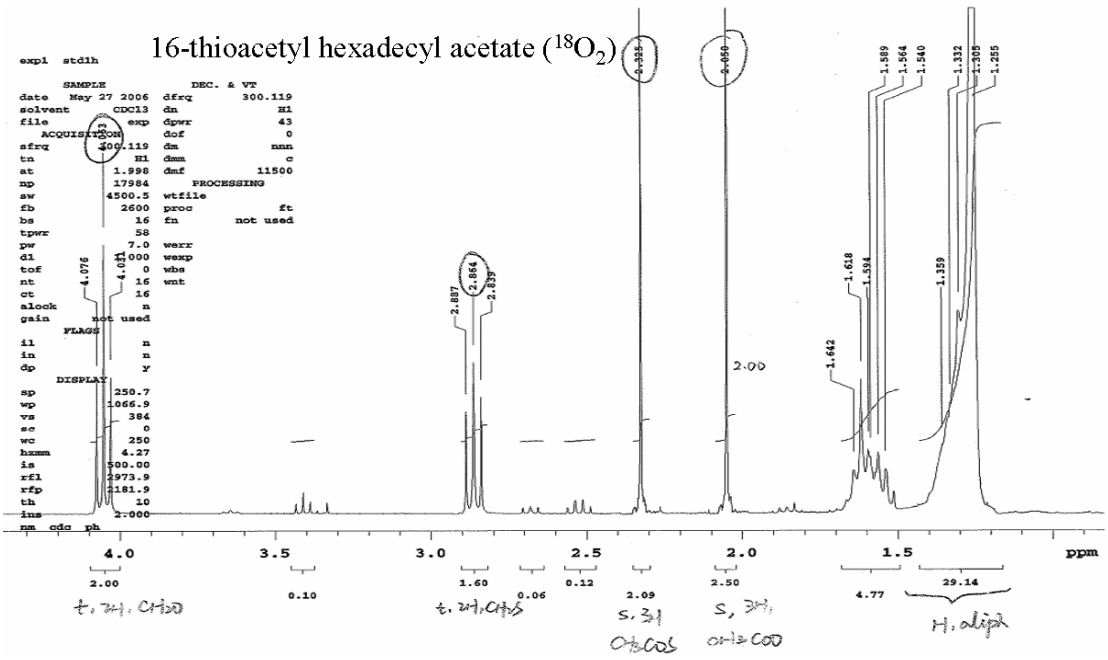

Figure A4.5 NMR spectrum of 16-thioacetyl hexadecyl acetate ($^{18}O_2$).

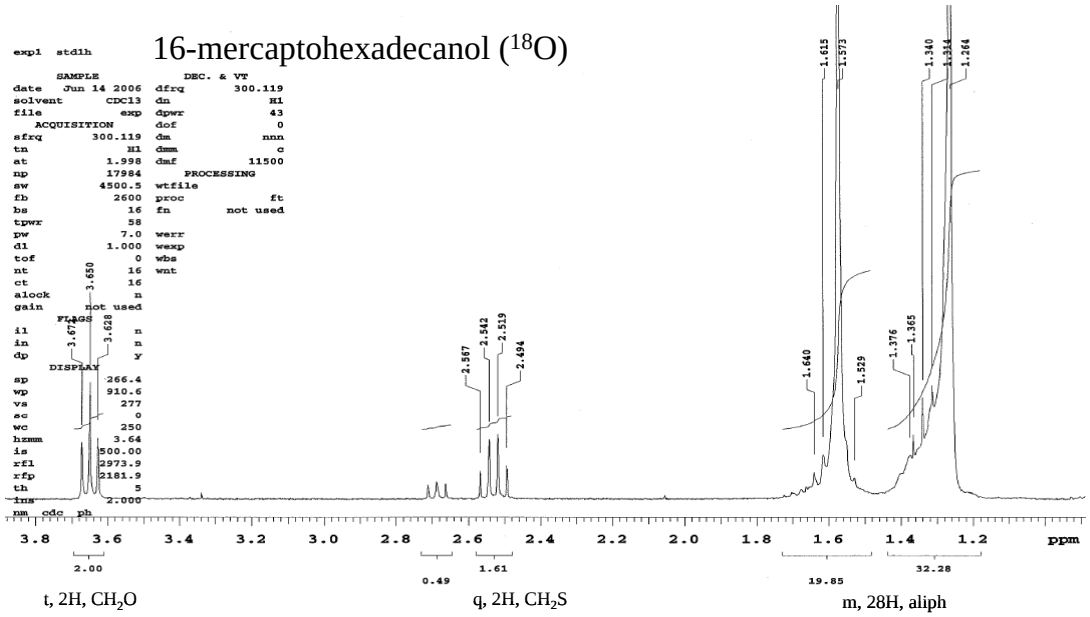

Figure A4.6 NMR spectrum of 16-mercaptohexadecanol (^{18}O).

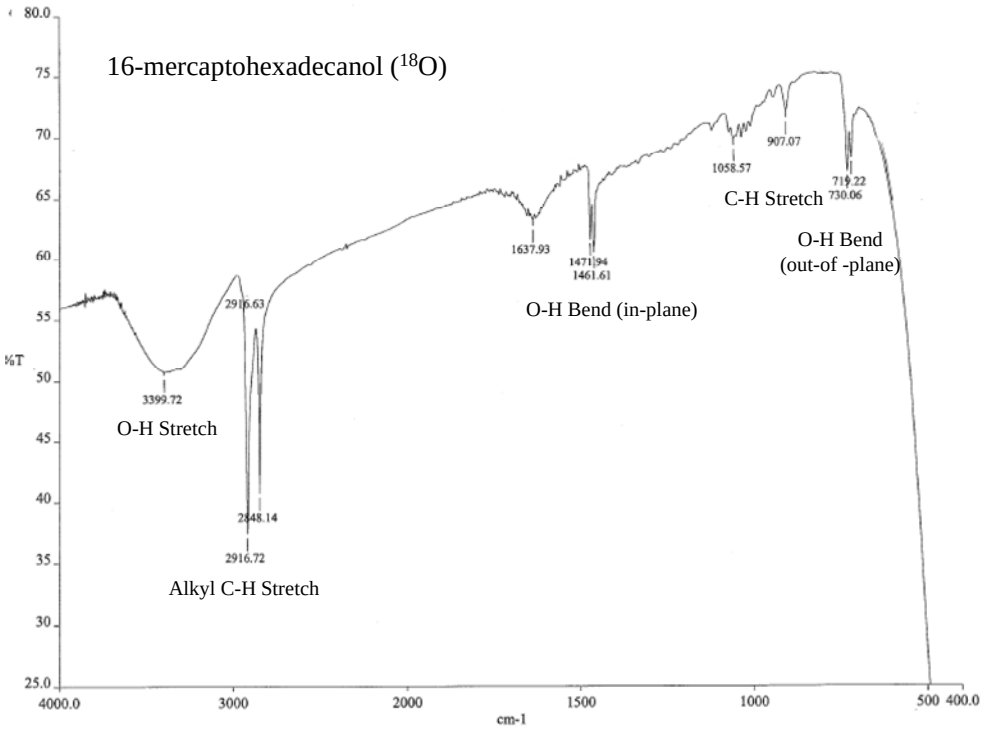

Figure A4.7 IR spectrum of 16-mercaptohexadecanol (^{18}O).

Procedures for Synthesizing ^{18}O Labeled Mercaptohexadecanol (MHL)[1]

BOND INSERTION, COMPLEXATION AND PENETRATION PATHWAYS OF VAPOR-DEPOSITED ALUMINUM ATOMS WITH HO- AND CH_3O-TERMINATED ORGANIC MONOLAYERS

G. L. Fisher, A.V. Walker, A.E Hooper, T.B Tighe, K.B Bahnck, H.T. Skriba, M.D. Reinard, B.C Haynie, R.L. Opila, N. Winograd and D.L. Allara

SUPPORTING INFORMATION SECTION

1. Synthesis of 16-Mercaptohexadecanol (^{18}O)

The syntheses of the ^{18}O-labeled compounds followed the published procedures for the unlabeled analogs.[1-7].

16-Bromohexadecanoic Acid: Hexadecanolide (10.0g, 39.30mmol) was added to 100 mL of a 1:1 solution of glacial acetic acid and 48 % HBr and refluxed for 24 hrs. The maroon solution was poured into a 400 mL beaker containing 100 mL of H_2O. After cooling the solution to 0 °C, the precipitate was filtered and washed with copious amounts of cold water. The crude solid was recrystallized from hexane and dried under vacuum to yield white, iridescent crystals. Yield: 10.54 g (80%) Analysis: mp 69 - 70°C, ^{1}H-NMR ($CDCl_3$) δ[ppm]: 1.2 - 1.9 (m, 26H, aliph.), 2.36 (t, 2H, CH_2-CO_2), 3.42 (t, 2H, CH_2-Br)

16-Bromohexadecanol: A solution of 16-bromohexadecanoic acid (6.50 g, 19.38 mmol) in dry THF (36 mL, 1.26 M) was cooled to 0 °C. Borane (25.78 mmol, 1 M in THF) was added dropwise via an addition funnel, and the mixture was allowed to come to room temperature before refluxing for 2 hrs. Upon completion, the reaction was quenched dropwise with H_2O at 0 °C and the THF was removed by rotoevaporation. The remainder was added to a separatory funnel with 15 mL of water and extracted with ether (3 x 25 mL). The combined ether layers were washed with brine (15 mL), dried over $MgSO_4$ and filtered. The ether was removed and the solid was dried under vacuum to obtain off-white crystals. Yield: 5.55 g (89%) Analysis: mp 53 - 54 °C, ^{1}H-NMR ($CDCl_3$) δ[ppm]: 1.2 - 1.9 (m, 28H, aliph.), 3.42 (t, 2H, CH_2-Br), 3.62 (t, 2H, CH_2-OH)

16-Bromohexadecyl Acetate ($^{18}O_2$): Diisopropyl azodicarboxylate (1.63 g, 8.07 mmol) was added to a solution of cold (0 °C) triphenyl phosphine (2.11 g, 8.07 mmol) in 21 mL of dry THF and stirred for 45 min. A white precipitate formed. A thoroughly stirred solution of 16-bromohexadecanol (1.29 g, 4.03 mmol) and acetic acid ($^{18}O_2$) (0.50 g, 8.07 mmol) in 21 mL of dry THF was then added dropwise at 0 °C. The mixture was stirred at 0 °C for 1 hr, then overnight at 25 °C. Concentrating the mixture and column chromatography (with 10% ethyl acetate/hexane as an eluant) gave a white solid. Yield: 1.14 g (77%) Analysis: mp 33 - 34°C, ^{1}H-NMR ($CDCl_3$) δ[ppm]: 1.2 - 1.9 (m, 28H, aliph.), 2.04 (s, 3H, CH_3-CO), 3.42 (t, 2H, CH_2-Br), 4.05 (t, 2H, CH_2-O)

16-Thioacetyl Hexadecyl Acetate ($^{18}O_2$): Potassium thioacetate (0.342 g, 1.0 eq) was added to a solution of 16-bromohexadecyl acetate ($^{18}O_2$) (1.10 g, 1.0 eq) in 18 mL of dry MeOH. After 24 hrs of reflux, the MeOH was removed by rotoevaporation and the remainder was added to a separatory funnel containing 20 mL of H_2O and 35 mL of ether. The aqueous layer was extracted with ether (3 x 30 mL) and the combined organic extracts were washed with brine (25 mL), dried over $MgSO_4$ and filtered. The solvent was removed and drying the solid in vacuo resulted in brownish-white crystals.

Yield: 0.975 g (90%) Analysis: mp 43 - 44 °C, ^{1}H-NMR ($CDCl_3$) δ[ppm]: 1.2 - 1.6 (m, 28H, aliph.), 2.00 (s, 3H, CH_3-COO), 2.33 (s, 3H, CH_3-COS), 2.87 (t, 2H, CH_2-S), 4.01 (t, 2H, CH_2-O)

16-Mercaptohexadecanol (^{18}O): A solution of 16-thioacetyl hexadecyl acetate ($^{18}O_2$) (0.91 g, 2.51 mmol) and 2.5 mL of NaOH (4 N) in 10 mL of degassed EtOH was heated for 3 - 4 min over a heat gun. The mixture was added to a separatory funnel containing 50 mL of degassed ether and 10 mL of degassed 50 % HCl. The layers were shaken once, and the ether layer was dried over $MgSO_4$. The ether was evaporated in vacuo to give a wet solid that crystallized under vacuum to give white crystals. Yield: 0.64 g (92%) Analysis: mp 56 - 57^{O}C, ^{1}H-NMR ($CDCl_3$) δ[ppm]: 1.2 - 1.7 (m, 28H, aliph.), 2.51 (q, 2H, CH_2-S), 3.62 (t, 2H, CH_2-O)

References:

1. Fisher, G. L.; Walker, A. V.; Hooper, A. E.; Tighe, T. B.; Bahnck, K. B.; Skriba, H. T.; Reinard, M. D.; Haynie, B. C.; Opila, R. L.; Winograd, N.; Allara, D. L., Bond Insertion, Complexation, and Penetration Pathways of Vapor-Deposited Aluminum Atoms with HO- and CH_3O-Terminated Organic Monolayers. *J. Am. Chem. Soc.* **2002,** 124, 5528-5541.

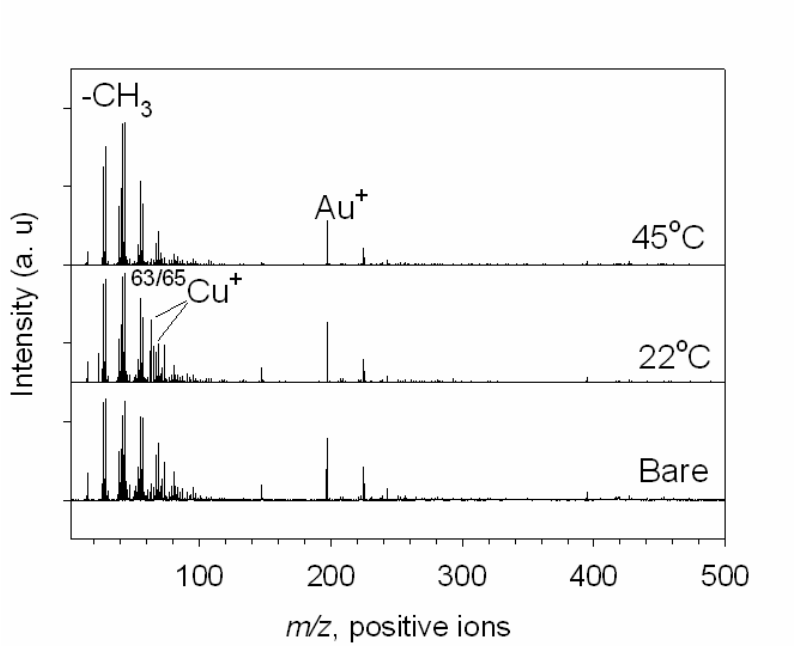

Figure A5.1: Positive ion TOF SIMS spectra (*m/z* 2-500) for -CH_3 terminated SAMs prior to and after Cu electroless depositions at 22 °C and at 45 °C for 1 h.

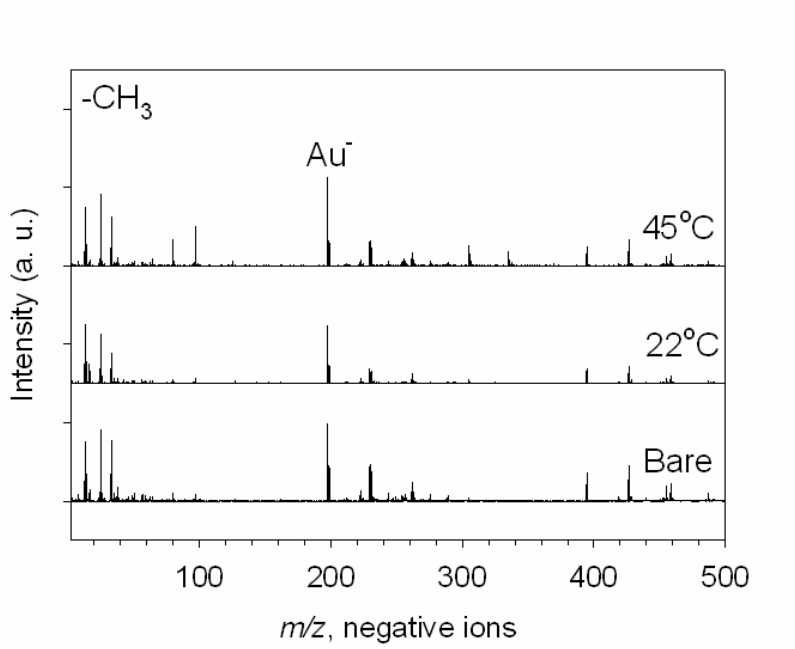

Figure A5.2: Negative ion TOF SIMS spectra (*m/z* 2-500) for -CH_3 terminated SAMs prior to and after Cu electroless depositions at 22 °C and at 45 °C for 1 h.

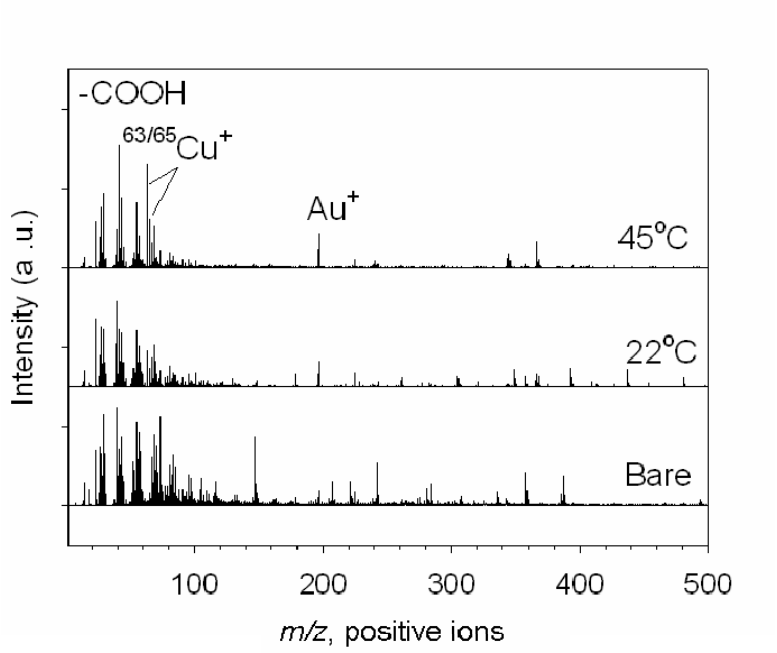

Figure A5.3: Positive ion TOF SIMS spectra (*m/z* = 2-500) for -COOH terminated SAMs prior to and after Cu electroless depositions at 22 °C and at 45 °C for 1 h.

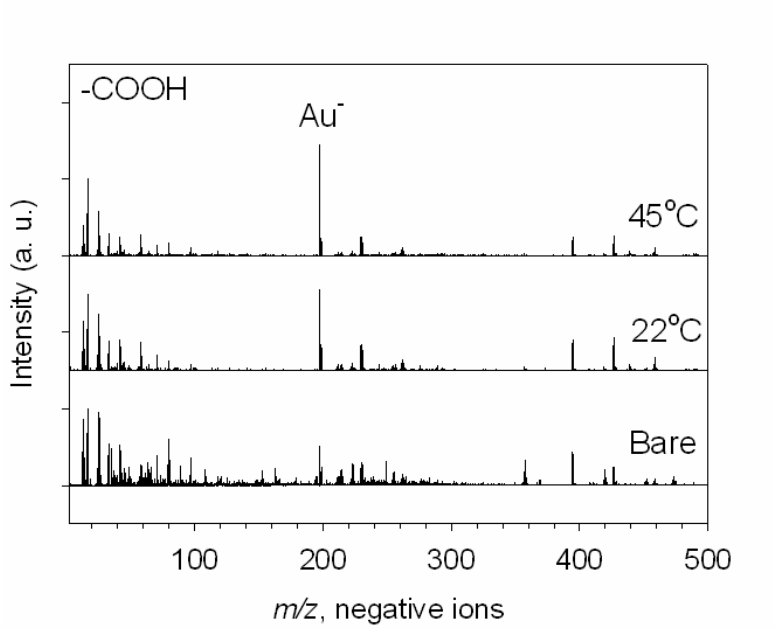

Figure A5.4: Negative ion TOF SIMS spectra (*m/z* 2-500) for -COOH terminated SAMs prior to and after Cu electroless depositions at 22 °C and at 45 °C for 1 h.

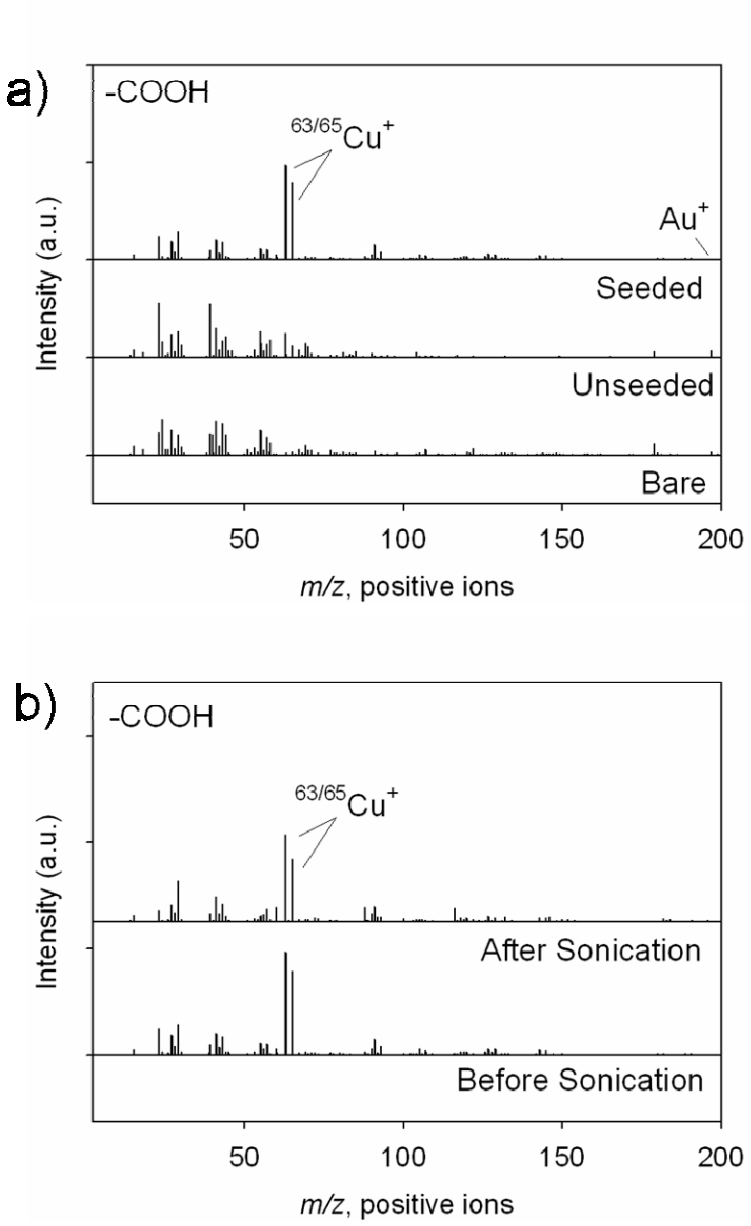

Figure A6.1 Positive ion TOF SIMS spectra (*m/z* 2-200) for -COOH terminated SAMs after 1 h Cu electroless deposition at 45 °C (a) under unseeded and seeded conditions, (b) seeded sample prior to and after sonication in deionized water for 3 min

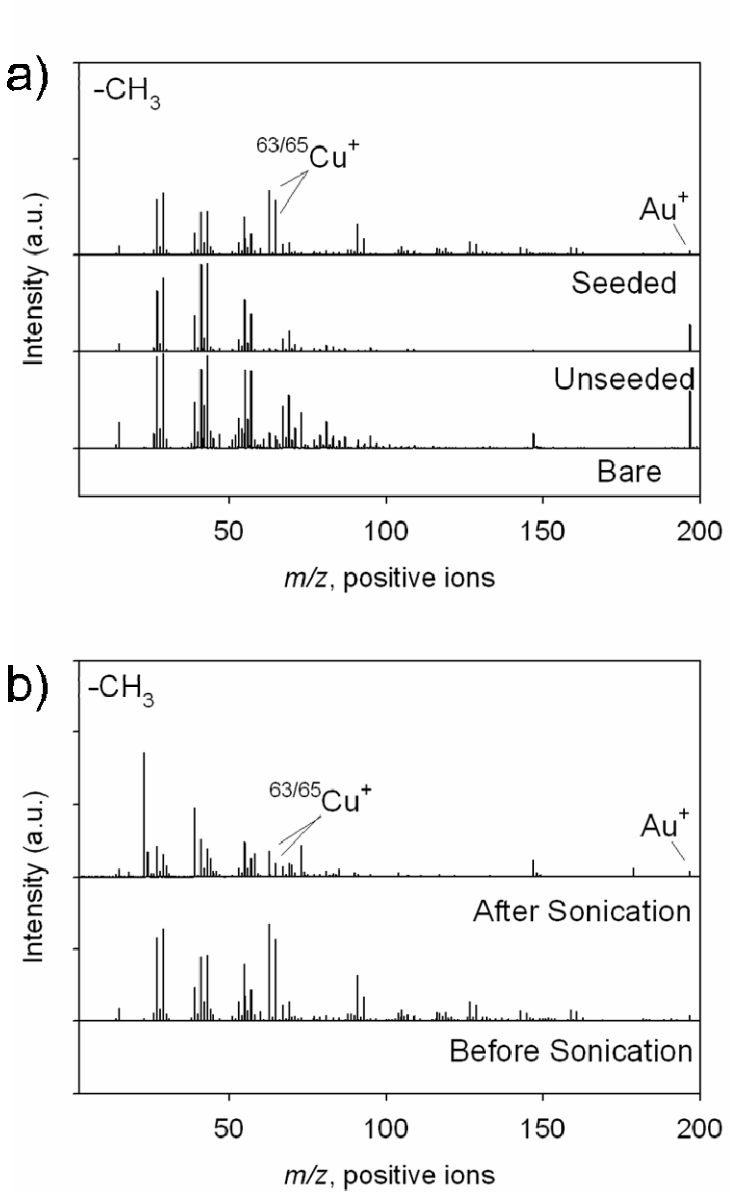

Figure A6.2 Positive ion TOF SIMS spectra (*m/z* 2-200) for -CH_3 terminated SAMs after 1 h Cu electroless deposition at 45 °C (a) under unseeded and seeded conditions, (b) seeded sample prior to and after sonication in deionized water for 3 min

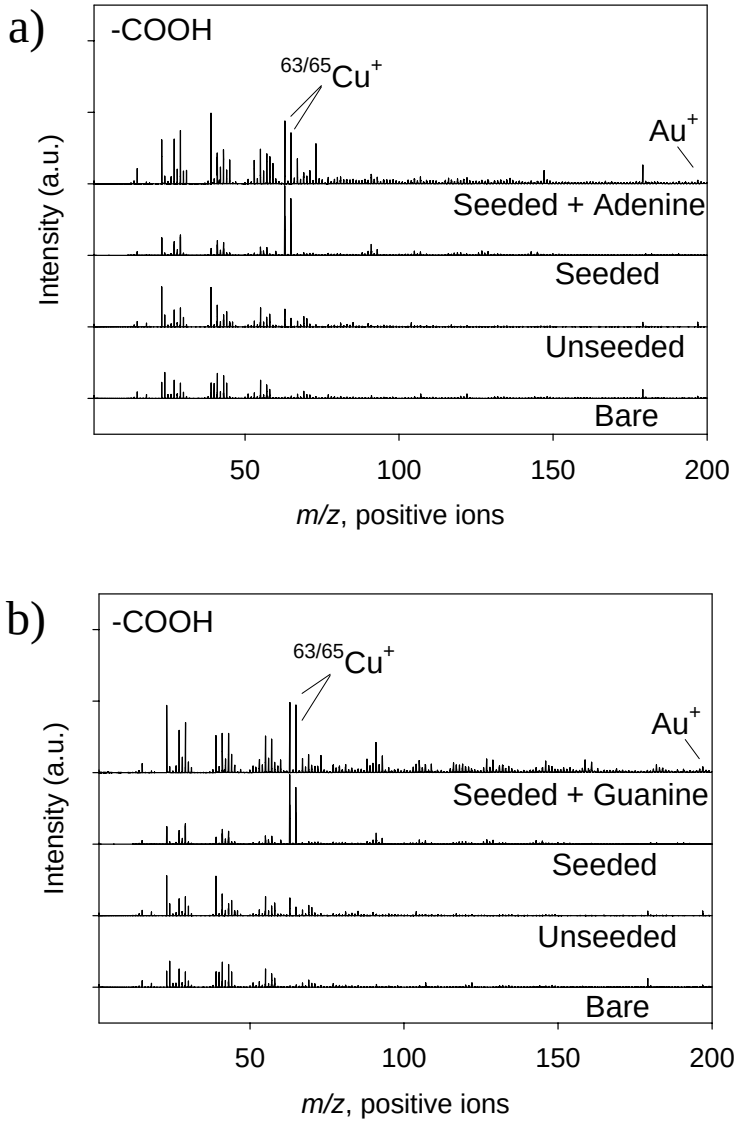

Figure A6.3 Positive ion TOF SIMS mass spectra (*m/z* 2-200) for -COOH terminated SAMs prior to and after Cu electroless depositions with (a) adenine, (b) guanine as additive at 45 °C for 1 h.

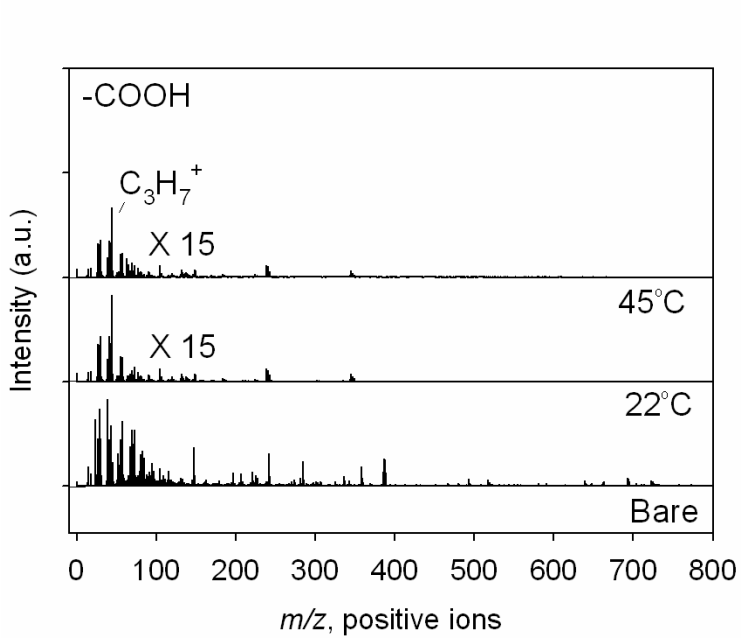

Figure A7.1 Positive ion TOF SIMS spectra (*m/z* 0-800) for -COOH terminated SAM prior to and after ZnS chemical bath deposition for 2h at 22 °C and at 45 °C.

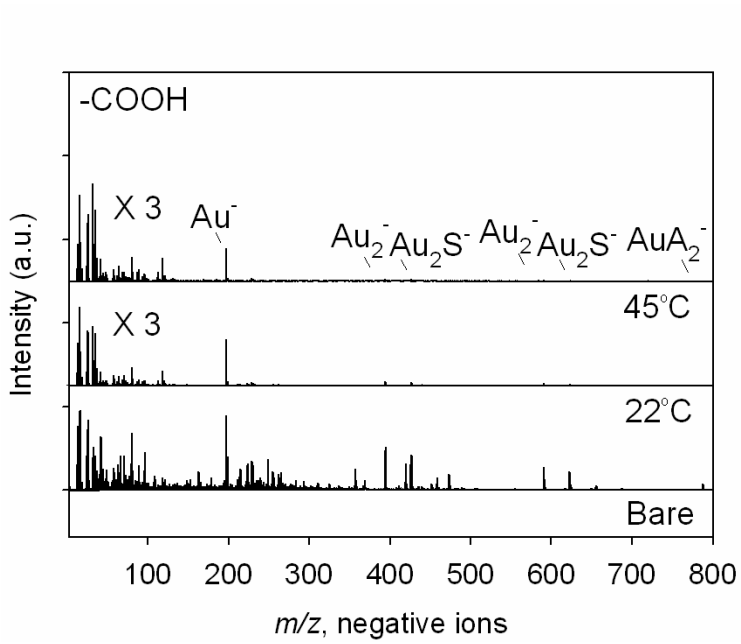

Figure A7.2 Negative ion TOF SIMS spectra (*m/z* 2-800) for -COOH terminated SAM prior to and after ZnS chemical bath deposition for 2h at 22 °C and at 45 °C.

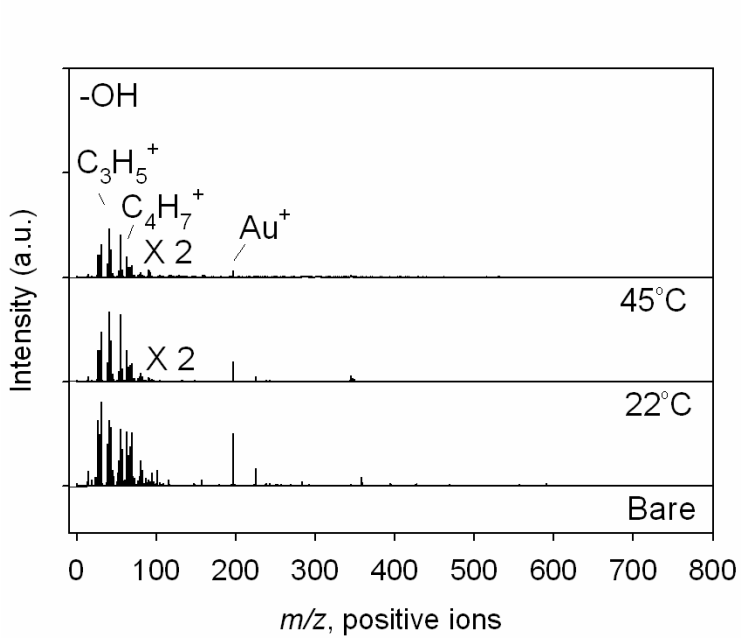

Figure A7.3 Positive ion TOF SIMS spectra (*m/z* 0-800) for -OH terminated SAM prior to and after ZnS chemical bath deposition for 2h at 22 °C and at 45 °C.

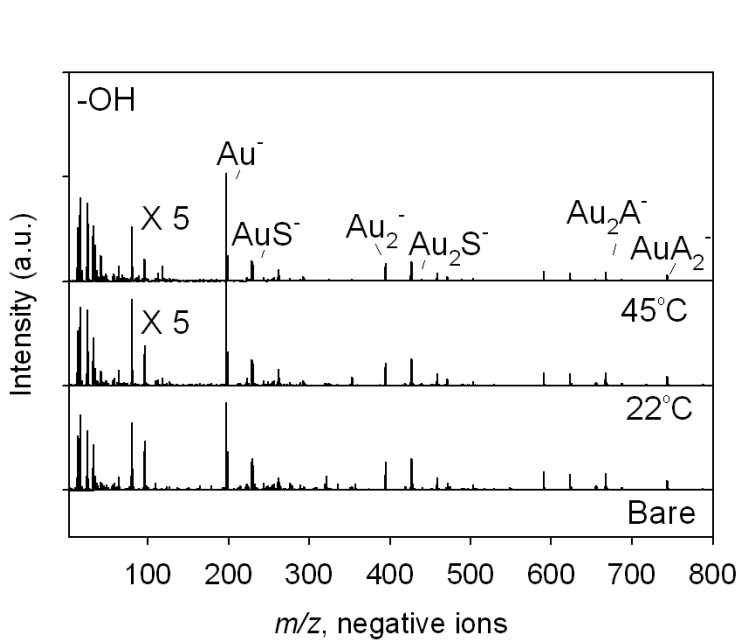

Figure A7.4 Negative ion TOF SIMS spectra (*m/z* 2-800) for -OH terminated SAM prior to and after ZnS chemical bath deposition for 2h at 22 °C and at 45 °C.

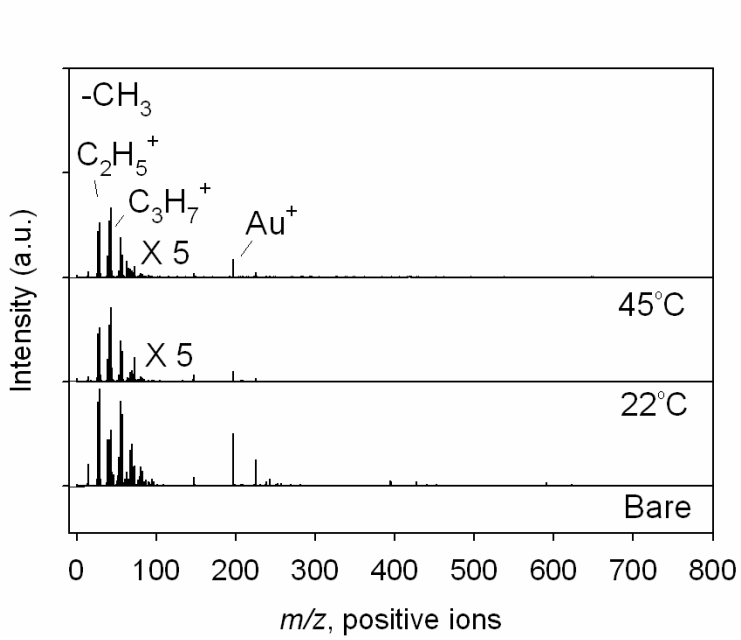

Figure A7.5 Positive ion TOF SIMS spectra (*m/z* 0-800) for -CH_3 terminated SAM prior to and after ZnS chemical bath deposition for 2h at 22 °C and at 45 °C.

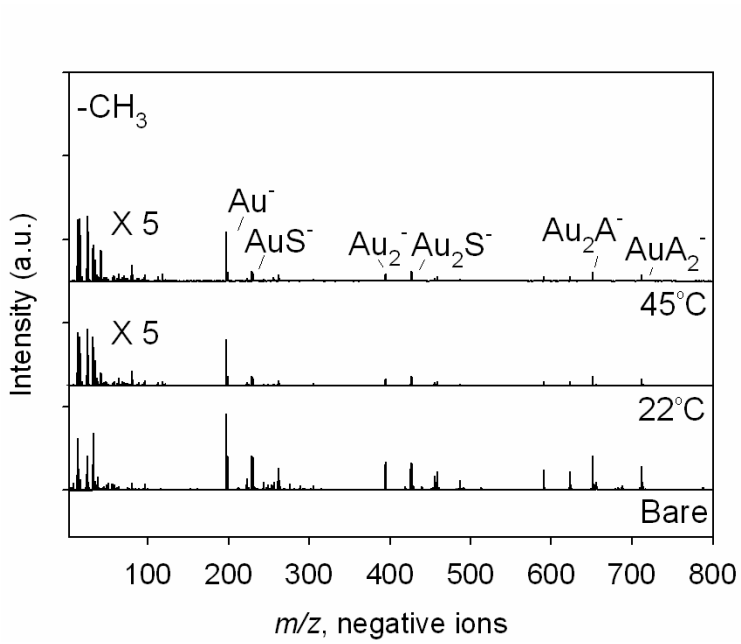

Figure A7.6 Negative ion TOF SIMS spectra (*m/z* 2-800) for -CH_3 terminated SAM prior to and after ZnS chemical bath deposition for 2h at 22 °C and at 45 °C.

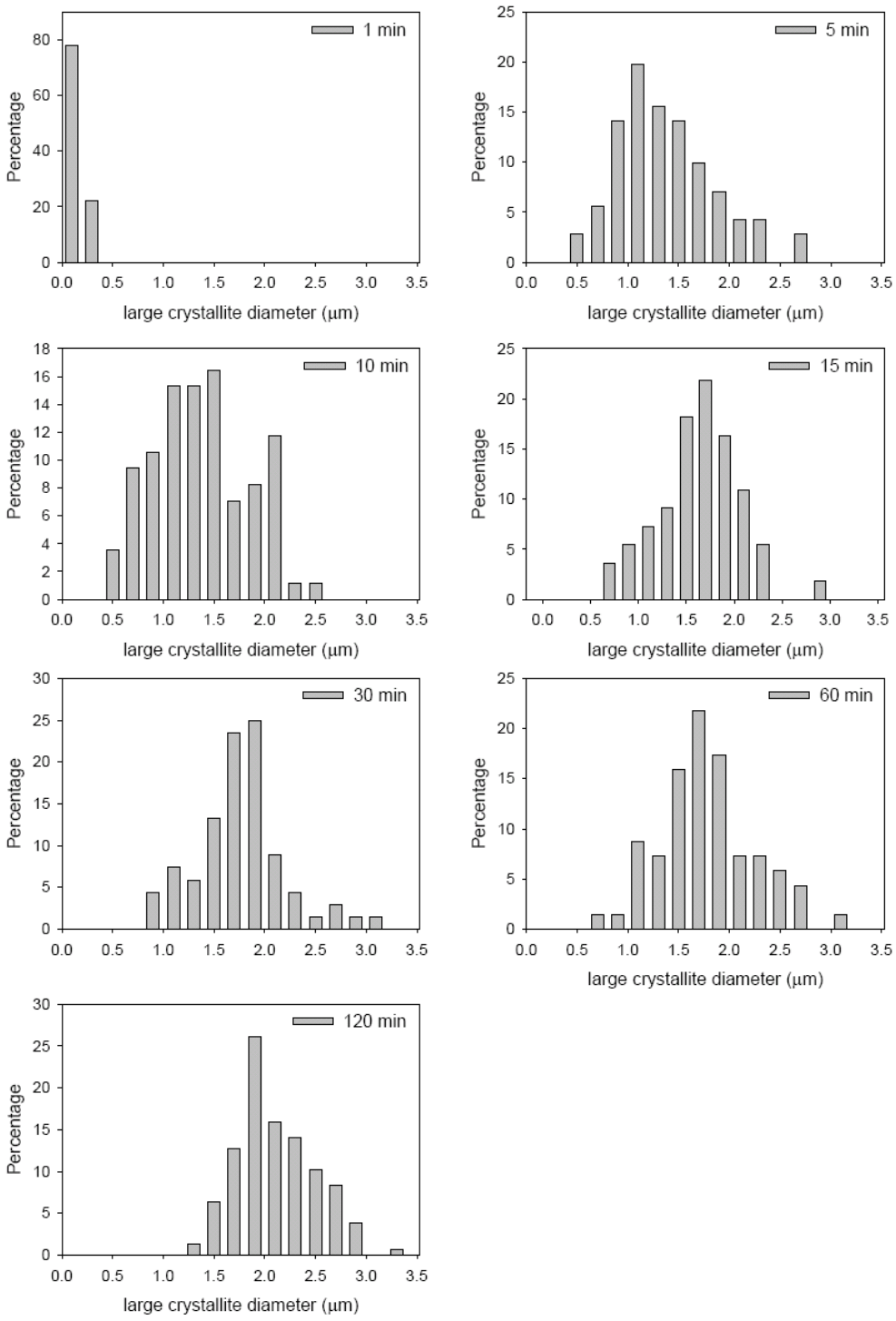

Figure A7.7 The size distribution of large flower-like crystallites as a function of time on –COOH terminated-SAMs at 45 °C under seeded conditions. The width of the bar is ± 0.10 μm. Corresponding SEM images are shown in Figure 5.5.

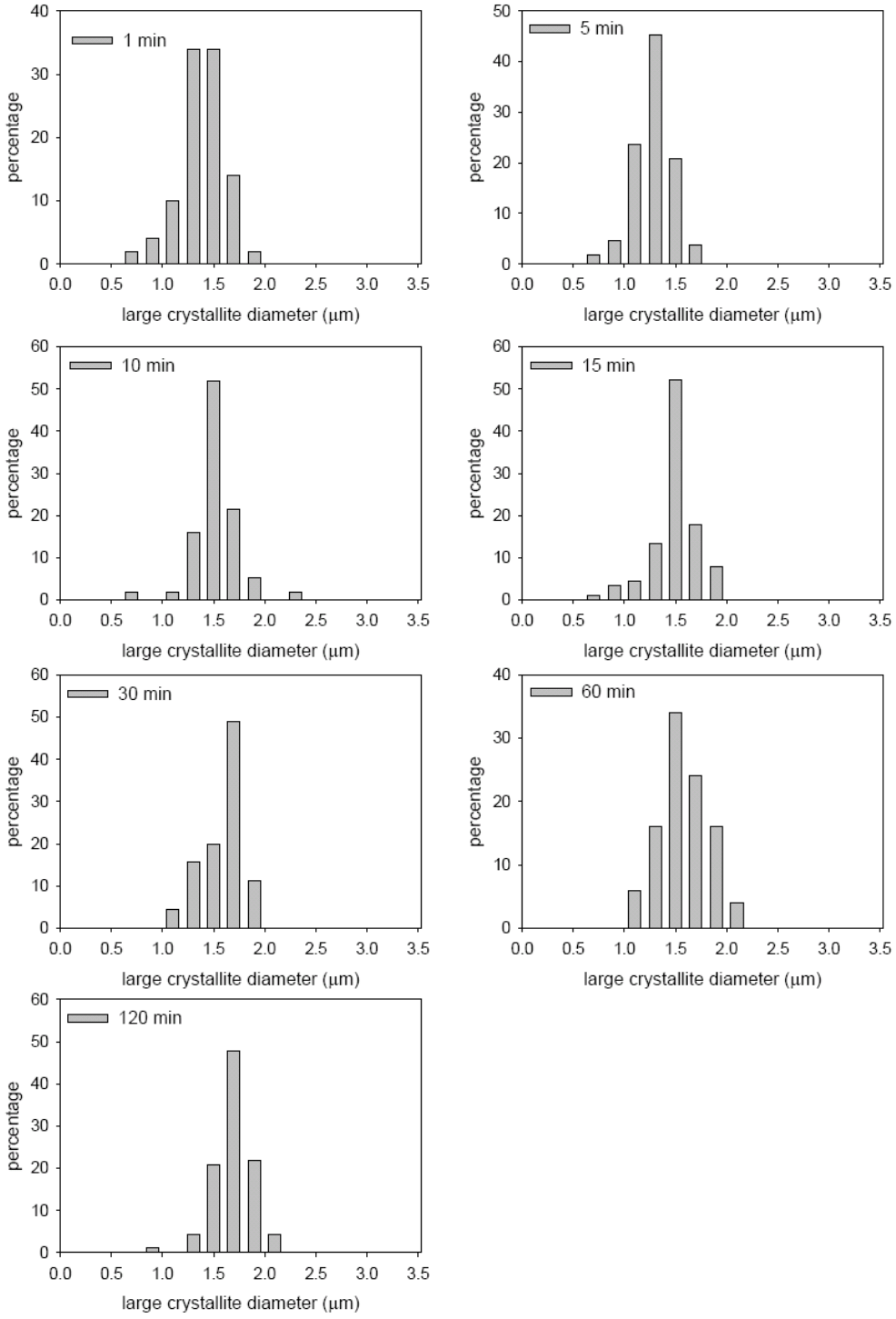

Figure A7.8 The size distribution of large flower-like crystallites as a function of time on –COOH terminated-SAMs at 45 °C under unseeded conditions. The width of the bar is ± 0.10 μm. Corresponding SEM images are shown in Figure 5.6.

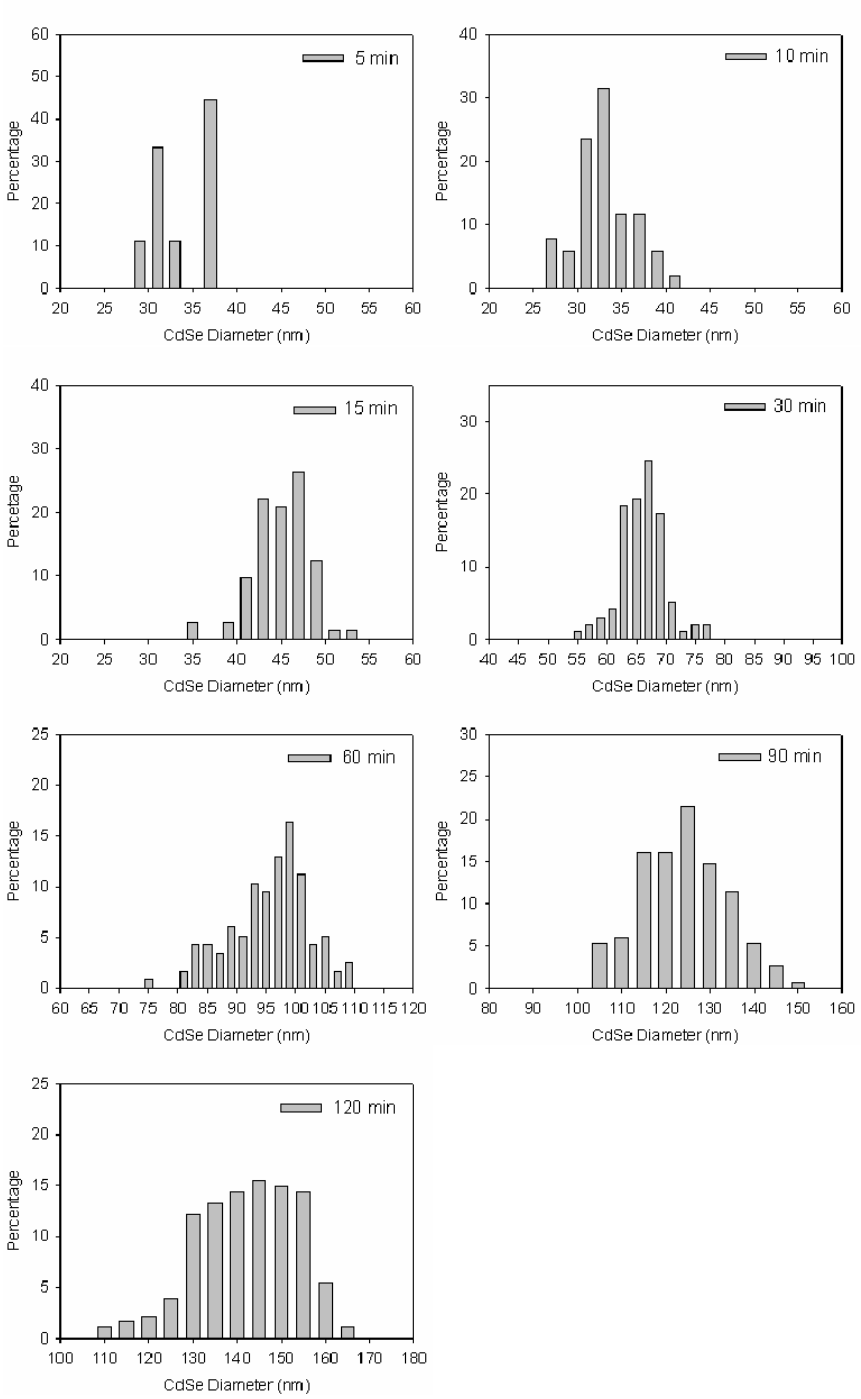

Figure A8.1 The size distribution of CdSe nanoparticles as a function of time on -COOH terminated-SAMs when CBD is performed with 80 mM Na_2SeSO_3 at 45 °C. The width of the bar is ± 1 nm for 5 min, 15 min, 30 min and 60 min deposition, and ± 2.5 nm for 90 min and 120 min deposition.

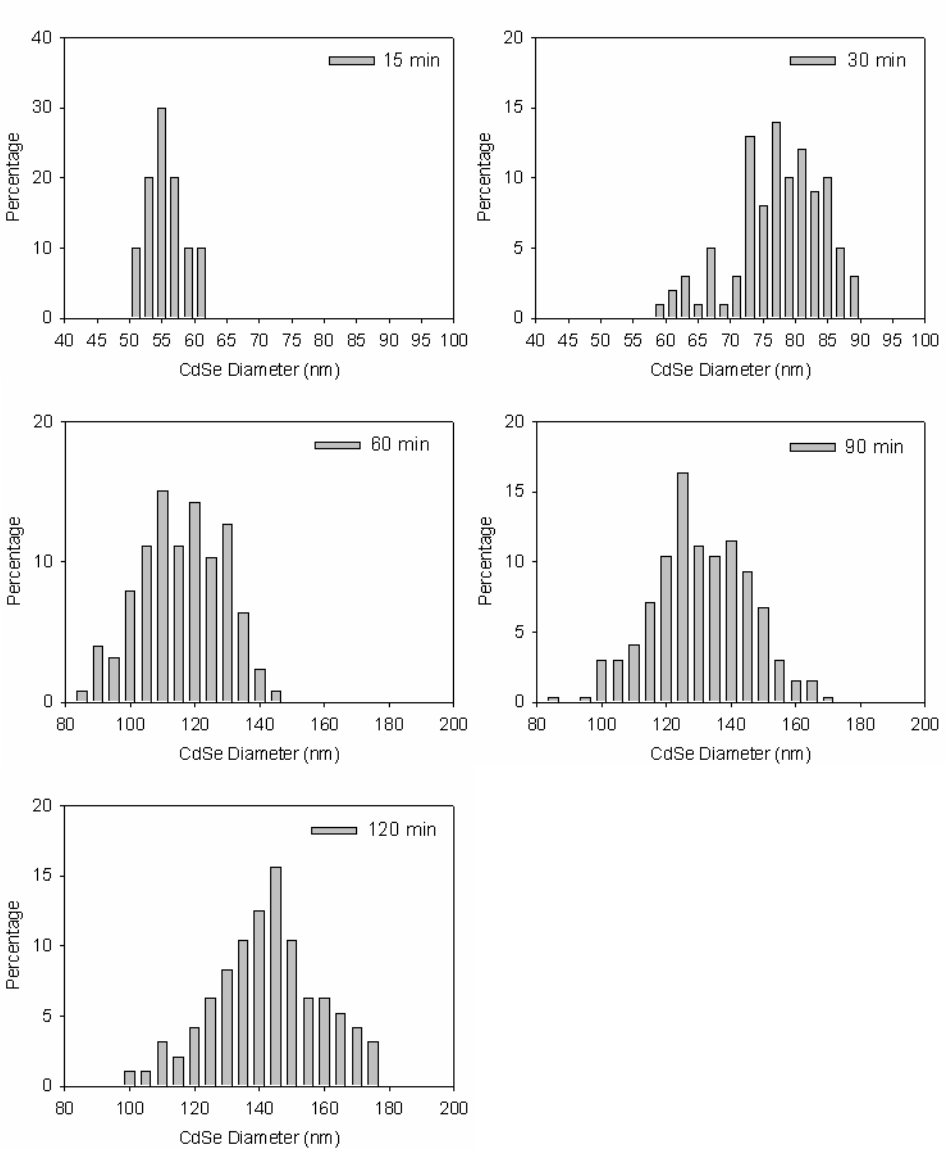

Figure A8.2 The size distribution of CdSe nanoparticles as a function of time on -COOH terminated-SAMs when CBD is performed with 40 mM Na_2SeSO_3 at 45 °C. The width of the bar is ± 1 nm for 15 min and 30 min deposition, and ± 2.5 nm for 60min, 90 min and 120 min deposition.

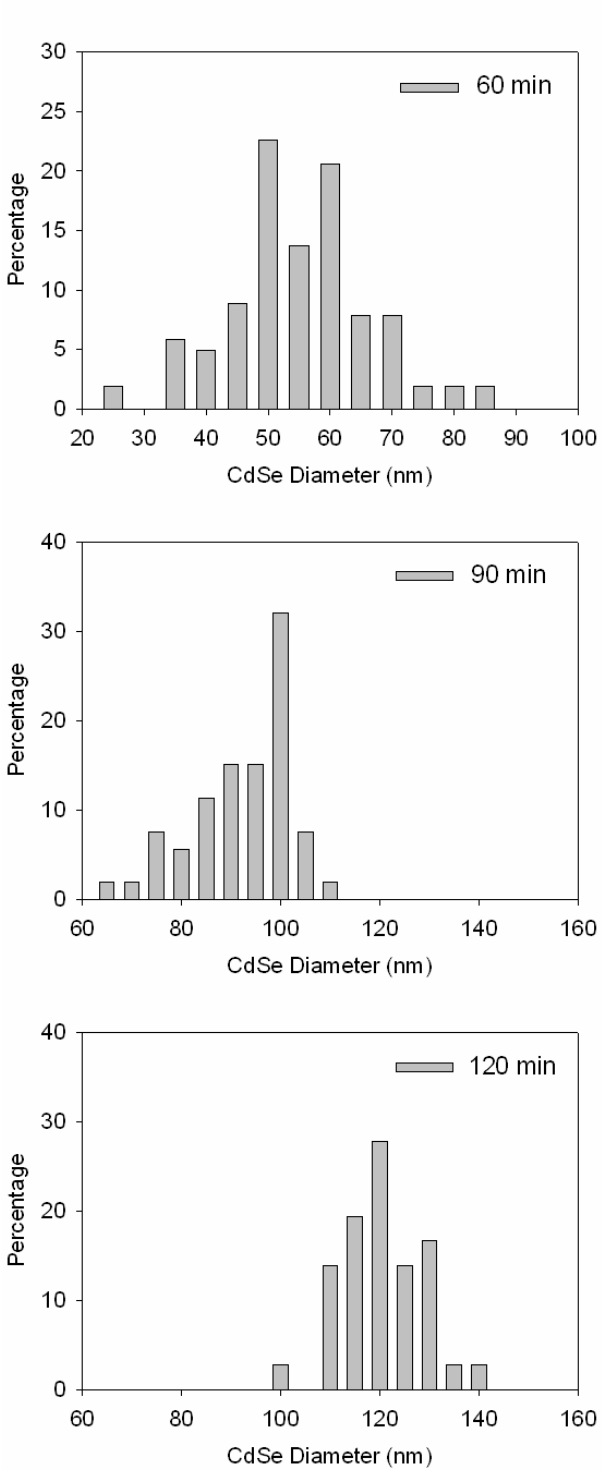

Figure A8.3 The size distribution of CdSe nanoparticles as a function of time on -COOH terminated-SAMs when CBD is performed with 20 mM Na_2SeSO_3 at 45 °C. The width of the bar is ± 2.5 nm.